Template-Directed Synthesis of One-Dimensional Hybrid Nanostructures from Cylindrical Polymer Brushes

DISSERTATION

zur Erlangung des akademischen Grades eines
Doktors der Naturwissenschaften (Dr. rer. nat.)
an der Bayreuther Graduiertenschule für Mathematik und
Naturwissenschaften der Universität Bayreuth

vorgelegt von

Markus Müllner

Geboren in Amberg

Bayreuth, 2012

Die vorliegende Arbeit wurde in der Zeit von Februar 2009 bis Januar 2012 in Bayreuth am Lehrstuhl Makromolekulare Chemie II unter Betreuung von Herrn Prof. Dr. Axel H.E. Müller angefertigt.

Vollständiger Abdruck der von der Bayreuther Graduiertenschule für Mathematik und Naturwissenschaften der Universität Bayreuth genehmigten Dissertation zur Erlangung des akademischen Grades eines Doktors der Naturwissenschaften (Dr. rer. nat.).

Dissertation eingereicht am: 02.02.2012

Zulassung durch die Promotionskommission: 14.02.2012

Wissenschaftliches Kolloquium: 07.05.2012

Amtierender Dekan: Prof. Dr. Beate Lohnert

Prüfungsausschuss:

Prof. Dr. Axel H.E. Müller (Erstgutachter)

Prof. Dr. Josef Breu (Zweitgutachter)

Prof. Dr. Carlo Unverzagt (Vorsitz)

Prof. Dr. Andreas Fery

A day without laughter is a day wasted

Charlie Chaplin

To My Family and Iva

Table of Contents

Chapter 5

Chapter 6

Summary

The thesis deals with the study of cylindrical polymer brushes (CPBs) and their use in template chemistry. Herein, we developed template-directed syntheses of one-dimensional (1D) hybrid nanostructures in which CPBs served as 1D soft templates. So called ‘molecular’ core-shell or core-shell-corona CPBs, as well as CPBs obtained through microphase separation of diblock copolymers, were applied as templates for the preparation of various types of 1D organic-inorganic hybrid nanomaterials.

Well-defined molecular core-shell and core-shell-corona CPBs with a narrow molecular weight distribution in both the backbone and the side chains have been synthesized via the combination of several polymerization techniques. Anionic polymerization has enabled the precise synthesis of polymer backbones, whereas atom transfer radical polymerization and ring-opening polymerization have allowed the sequential growth of side chains via the ‘grafting-from’ approach. Depending upon the desired functional 1D hybrid nanostructures, different combinations of core, shell and corona have been chosen.

Core-shell-corona CPBs with a poly(*tert*-butyl acrylate) (P*t*BA) core, a poly(3-acryloylpropyl trimethoxysilane) (PAPTS) shell and a poly[oligo (ethylene glycol) methyl ether methacrylate] (POEGMA) corona were hydrolyzed by aqueous ammonia to produce water-soluble organo-silica hybrid nanotubes. As the trimethoxysilyl group was directly incorporated into the structure of the CPBs, we avoided the addition of an external inorganic precursor.

Amphiphilic core-shell-corona CPBs with a hydrophobic poly(ε-caprolactone) (PCL) core, a hydrophilic poly(2-(dimethylamino)ethyl methacrylate) (PDMAEMA) shell and a hydrophilic POEGMA corona were used as 1D templates and nanoreactors for the fabrication of titania dioxide (TiO_2) semiconductor nanotubes. The cationic PDMAEMA shell was loaded with a negatively charged titania precursor, namely titanium(IV) bis(ammonium lactate) dihydroxide (TALH). TALH underwent hydrolysis within the CPB shell upon heating above 70 °C. Accordingly, crystalline (that is, anatase) TiO_2 hybrid nanotubes with a very well defined thickness were obtained. Subsequently, the diameter of the hybrid nanotubes was adjusted by modifying the side chain length of the PDMAEMA shell.

Amphiphilic core-shell CPBs with a hydrophobic PCL core and a hydrophilic PDMAEMA shell were employed for the fabrication of silica nanotubes with different aspect ratios. Tetramethyl orthosilicate (TMOS) was used for the deposition of silica into the PDMAEMA shell. Several polymers with different dimensions, with respect to length as well as core and shell diameter, were synthesized and used as templates for the fabrication 1D silica nanostructures. Furthermore, silica nanotubes were obtained after acid treatment or calcination, and catalytically active porous nanomaterials were produced via the embedment of metal nanoparticles within the silica shell.

All the hybrid nanotubes templated by molecular core-shell and core-shell-corona CPBs were uniform in length as well as diameter, due to the narrow molecular weight distribution of the CPB backbone and side chains. Moreover, the POEGMA corona in the core-shell-corona CPBs served as a shielding layer and protected the nanotubes from agglomeration and intermolecular crosslinking during the hybrid formation. Additionally, POEGMA rendered the hybrid nanomaterials soluble in various solvents, including water.

Water-soluble core-shell CPBs were obtained from microphase separated cast films of polystyrene-*b*-poly(allyl methacrylate) (PS-PAMA) diblock copolymers. After UV-crosslinking of the cylindrical PAMA domains, CPBs with a PS shell and a crosslinked PAMA core were obtained. Subsequent sulfonation rendered the PS shell into poly(styrenesulfonic acid) and thereby made it water-soluble. The negatively charged brush templates were infiltrated with oppositely charged TiO_2 nanocrystals to produce crystalline TiO_2 hybrid nanowires. Further, it was possible to adjust the crystal structure of the nanostructures to either a rutile or anatase structure.

The presented novel 1D hybrid nanomaterials based on CPBs have many potential applications due to their electronic, catalytic and semiconducting properties.

Zusammenfassung

Die vorliegende Arbeit beschäftigt sich mit zylindrischen Polymerbürsten und deren Anwendungen in Bereichen der Templatchemie. Mittels templatgesteuerten Syntheseabläufen konnten eindimensionale Hybridstrukturen im Nanometer-Maßstab hergestellt werden. Dazu dienten die während der Doktorarbeit hergestellten Polymerbürsten als eindimensionale Templatstrukturen. Neben sogenannten „molekularen“ Kern-Schale oder Kern-Schale-Korona Polymerbürsten wurden auch Bürsten, die aus mikrophasen-separierten Diblockcopolymeren gewonnen wurden, als Template eingesetzt, um verschiedene eindimensionale organisch-anorganische Hybridmaterialien darzustellen.

Durch die Kombination von unterschiedlichen Polymerisationstechniken konnten wohldefinierte molekulare Kern-Schale und Kern-Schale-Korona Polymerbürsten hergestellt werden, bei denen sowohl das Polymerrückgrat als auch die Seitenketten eine enge Molekulargewichtsverteilung besaßen. Die anionische Polymerisation von funktionalen Methacrylaten ermöglichte ein präzises Herstellen der Polymerrückgrate zur Synthese der molekularen Polymerbürsten. Die ringöffnende Polymerisation und die sogenannte „Atom Transfer Radical Polymerisation“ machten ein sequenzielles Aufpfropfen der Seitenketten möglich. Je nach Art der gewünschten eindimensionalen Hybridstruktur wurden verschiedene Zusammensetzungen der Polymerbürsten ausgewählt.

Zylindrische Kern-Schale-Korona Polymerbürsten mit Poly(*tert*-butylacrylat)-Kern, Poly(3-acryloylpropyl trimethoxysilan)-Schale und Poly(oligoethylenglykol) methacrylat-Korona (POEGMA) konnten mittels Ammoniak-Lösung zu wasserlöslichen Silika-Nanoröhrchen hydrolysiert werden. Da die Trimethoxysilyl-Gruppe kovalent und damit direkt an die Schale der Polymerbürste gebunden war, konnten wir vermeiden, dass man zusätzlich anorganische Siliziumbausteine zugeben musste.

Amphiphile Kern-Schale-Korona Polymerbürsten mit einem Polycaprolactone-Kern (PCL), einer Poly(dimethylaminoethyl)metharcylat-Schale (DMAEMA) und einer POEGMA-Korona wurden als Bausteine und Nanoreaktoren zur Herstellung von Nanoröhrchen aus Halbleitern (TiO_2) verwendet. Die kationische PDMAEMA-Schale wurde mit Titanium(IV) bis(ammoniumlactat) dihydroxid (TALH), einer negativ geladene TiO_2 Vorstufe, beladen. Bei Temperaturen über 70 °C hydrolysierte TALH

innerhalb der Schale der zylindrischen Polymerbürsten. Dadurch konnten kristalline TiO_2 (Anatas) Hybridröhrchen im Nanomaßstab hergestellt werden, die einen sehr definierten Durchmesser aufweisen. Zudem konnte der Durchmesser durch die Länge der Seitenketten der PDMAEMA-Schale eingestellt werden.

Amphiphile Kern-Schale Polymerbürsten mit einem PCL-Kern und einer PDMAEMA-Schale wurden zur Herstellung von Silika-Nanoröhrchen mit unterschiedlichen Aspektverhältnissen eingesetzt. Eine Silikavorstufe namens Tetramethylorthosilikat (TMOS) wurde benutzt, um die PDMAEMA-Schale mit SiO_2 zu beladen. Templatbürsten mit unterschiedlichen Ausmaßen, bezüglich deren Länge als auch deren Durchmessers des Kerns und der Schale, wurden zur Herstellung von eindimensionalen Silikat-Nanostrukturen verwendet. Aus letzteren konnten schließlich durch Hitze- oder Säurebehandlung Silika-Nanoröhrchen hergestellt werden. Alternativ wurden Metal-Nanopartikel in die Silikaschale eingelagert, um katalytisch-aktives poröses Nanomaterial zu erhalten.

Alle diese von molekularen Polymerbürsten stammenden nanoskalierten Hybridröhrchen sind sehr uniform bezüglich ihrer jeweiligen Länge und Durchmesser, was auf die niedrige Molekulargewichtsverteilung des Polymerrückgrats und der Seitenketten zurückzuführen ist. Die POEGMA-Korona diente hauptsächlich als Schutzhülle und schützte die Nanoröhrchen somit vor Agglomeration und intermolekularem Vernetzen während der Hybridbildung. Desweiteren ermöglichte POEGMA, dass die Hybridmaterialien sowohl in organischen Lösungsmitteln als auch in Wasser löslich wurden.

Ferner konnten wasserlösliche Kern-Schale Polymerbürsten aus Mikrophasen-separierten Polymerfilmen von Polystyrol-*b*-Polyallylmethacrylat (PS-PAMA) Diblockcopolymeren gewonnen werden. Nach dem Vernetzen der zylindrischen PAMA Domänen mit UV-Licht und der Redispergierung des Polymerfilms konnten schließlich Polymerbürsten, bestehend aus PS-Schale und PAMA-Kern, erhalten werden. Unmittelbare Sulfonierung machte aus der PS-Schale eine Polyelektrolyt-Schale, bestehend aus Polystyrolsulfonsäure. In die dadurch wasserlöslichen und negativ geladenen zylindrischen Polymerbürsten wurden anschließend gegensätzlich geladene TiO_2 Nanokristalle eingelagert. Folglich konnten kristalline Hybrid-Nanodrähte hergestellt werden, bei denen die Kristallstruktur eindeutig auf entweder Rutil oder Anatas eingestellt werden konnte.

All diese neuartigen, eindimensionalen und auf Polymerbürsten basierenden Hybridstrukturen besitzen faszinierende elektronische, katalytische und halbleitende Eigenschaften und sind somit im Rahmen verschiedenster Anwendungen von Interesse.

Glossary

1D	one-dimensional
^{1}H-NMR	proton nuclear magnetic resonance
AAO	anodized aluminium oxide
AFM	atomic force microscopy
AMA	allyl methacrylate
ATRP	atom transfer radical polymerization
Brij 58	polyoxyethylene(20) cetyl ether
CNT	carbon nanotubes
CPB(s)	cylindrical polymer brush(es)
CRP	controlled radical polymerization
Cryo-TEM	cryogenic transmission electron microscopy
CTAB	hexadecyltrimethylammonium bromide
CuAAC	copper-catalyzed azide-alkyne cycloaddition
D	distance
DCE	dichloroethane
DLS	dynamic light scattering
DMAEMA	2-(dimethylamino)ethyl methacrylate
DP_n	number-average degree of polymerization
EDX	energy dispersive X-ray spectroscopy
FWHM	full width of half maximum
GMA	glycidyl methacrylate
GPC	gel permeation chromatography
GTP	group transfer polymerization
H2SO4	sulfuric acid
HCl	hydrogen chloride
HF	hydrogen fluoride
HR-TEM	high resolution transmission electron microscopy
IPEC	interpolyelectrolyte complex
l_m	length per monomer unit
l_p	persistence length
Lucirin TPO®	[diphenyl(2,4,6-trimethylbenzoyl)phosphine oxide]
MWCNT	multi-walled CNTs
MWD	molecular weight distribution
***n*BA**	*n*-butyl acrylate
NMP	nitroxide mediated polymerization
NP(s)	nanoparticle(s)
OEGMA	oligo(ethylene glycol) methyl ether methacrylate
OsO_4	osmium tetroxide
P2VP	poly(2-vinylpyridine)
PAA	poly(acrlyic acid)

PAMA	poly(allyl methacrylate)
PAPTS	poly(3-acryloylpropyl trimethoxysilane)
PB	polybutadiene
PBIEM	poly(2-bromoisobutyryloxyethyl methacrylate)
PCEMA	poly(2-cinnamoylethyl methacrylate)
PCEVE	poly(chloroethyl vinyl ether)
PCL	poly(ε-caprolactone)
PDADMAC	poly(diallyldimethylammonium)chloride
PDMAEMA	poly(2-(dimethylamino)ethyl methacrylate)
PE	polyethylene
PEG	polyethylene gylcol
PFS	poly(ferrocenyldimethylsilane)
PGMA	poly(glycidyl methacrylate)
PHEMA	poly(hydroxyethyl methacrylate)
PI	polyisoprene
PLA	poly(lactic acid)
PMDETA	N,N,N',N'',N''-pentamethyldiethylenetriamine
PMETAI	poly{[2-(methacryloyloxy)ethyl] trimethylammonium iodide}
PMMA	poly(methyl methacrylate)
PMS	4-(pyrrolmethyl)styrene
P*n*BA	poly(*n*-butyl acrylate)
PNIPAM	poly(*N*-isopropylacrylamide)
POEGMA	poly[oligo (ethylene glycol) methyl ether methacrylate]
POSS	polyhedral oligomeric silsesquioxane
PS	polystyrene
PSS	poly(styrenesulfonate), poly(styrenesulfonic acid)
P*t*BA	poly(*tert*-butyl acrylate)
PTEPM	poly(3-(triethoxysilyl)propyl methacrylate)
PTMS-HEMA	poly(2-(trimethylsiloxy)ethyl methacrylate)
PVP	poly(vinylpyrrolidone)
PXRD	powder X-ray diffractometry
QD	quantum dot
RAFT	reversible addition fragmentation transfer polymerization
RI	refractive index
ROMP	ring-opening metathesis polymerization
ROP	ring-opening poylmerization
SAED	selected area electron diffraction
SDS	sodium dodecyl sulphate
SDV gel	styrenedivinylbenzene gel
SEC	size exclusion chromatography
SEM	scanning electron microscopy
$SiO_{1.5}$	silsesquioxane
SiO_2	silicon dioxide, silica

SLS	static light scattering
$Sn(Oct)_2$	tin(II) 2-ethylhexanoate
TALH	titanium(IV) bis(ammonium lactate) dihydroxide
tBA	*tert*-butyl acrylate
TEM	transmission electron microscopy
TGA	thermogravimetric analysis
THF	tetrahydrofuran
$Ti(OBu)_4$	titanium(IV) butoxide
TiO_2	titanium dioxide, titania
TMOS	tetramethyl orthosilicate
TMS-HEMA	2-(trimethylsilyloxy)ethyl methacrylate
TMV	tobacco mosaic virus
Tween 60	polyoxyethylene sorbitan monostearate

Chapter 1 – Introduction

One-Dimensional Hybrid Nanostructures

The demand for advanced functional materials with novel properties has led to a continually expanding research area that covers not only chemistry, but also biology, physics and materials sciences. Nanostructured materials, which are materials with structural features of at least one-dimension in the range of 1-100 nm, have become one of the hottest topics in the field of materials science.[1] The reason for the increased interest in nanomaterials lies in their unique electrical, optical, magnetic, thermal, mechanical and chemical properties when compared to their bulk parent counterparts.[2-4] It is known that the peculiar physical and chemical properties are deeply connected to the morphology and size in nanoscale of the respective material. Especially one-dimensional (1D) nanomaterials, such as nanowires and nanotubes, have attracted immense interest, as these anisotropic nanostructures are expected to play an important role as building blocks, interconnects and functional units in the fabrication of electronic, optoelectronic, electrochemical and electromechanical nanoscale devices. Therefore, it was necessary to develop straightforward syntheses of these nanostructures and alter their composition. The interest and demand for 1D hybrid nanomaterials increased dramatically after their production became much more feasible through various templating techniques and electrospinning. Template-directed or template-assisted production of 1D hybrid nanomaterials became even more facile when polymeric soft templates were used. The large scale production of well-defined polymers and polymeric templates in all kinds of compositions became rather simple due to the many improvements in controlled/living polymerization techniques. The following chapters describe the synthesis of soft 1D templates and their use in the template-directed synthesis of hybrid materials in more detail.

This thesis is dealing with the application of soft polymeric templates for the production of 1D hybrid nanostructures. Different types of cylindrical polymer brushes with well-defined structures were prepared through different methods. Further, these 1D soft templates were used for the controlled fabrication of 1D hybrid nanomaterials.

1. Cylindrical Polymer Brushes

According to Milner, polymer brushes are “long-chain polymer molecules attached by one end to a surface or interface by some means, with a density of attachment points high enough so that the chains are obliged to stretch away from the interface, sometimes much farther than the typical unstretched size of a chain”.[5] Although, this definition was originally directed at planar polymer brushes two decades ago, the quintessence still holds true today. However, the term ‘polymer brushes’ refers nowadays to assemblies of polymer chains, which are attached by one end to the surface of a planar (2D), a sphere (3D), a linear polymer chain or a thin polymeric or inorganic rod (1D).[6] 3D polymer brushes are commonly referred to as spherical polymer brushes (SPBs) whereas 1D polymer brushes are usually given the name ‘molecular brushes’ or are simply called cylindrical polymer brushes (CPBs).

By definition, CPBs are organic 1D nanostructures consisting of polymer chains that are densely tethered next to each other. The density of chains of polymer molecules (grafting density) is eventually so high that the chains become crowded and are stretched.[7] This stretching of a CPB can be achieved by two major pathways: firstly, the lateral attachment of polymer chains onto a long polymer main chain (backbone) and, secondly, the crosslinking of cylindrical domains in either bulk thin films or cylindrical micelles. Scheme 1-1 shows possible ways to synthesize CPBs. The dense attachment of side chains to a linear polymer backbone can be achieved by three possible pathways: (A) ‘grafting-through’,[8-10] (B) ‘grafting-onto’, and (C) ‘grafting-from’ (see Scheme 1-1A). Besides these three methods, where the side chains are covalently linked to the backbone, there are several non-covalent approaches. Non-covalent interactions, such as coordination,[11] hydrogen bonding[12] and ionic interaction,[13,14] have been successfully used to bond surfactants onto linear polymer chains to form brush-like architectures. Many groups have synthesized CPBs through the crosslinking of cylindrical domains in microphase-separated polymer bulk films (see Scheme 1-1C).[15-18] Researchers have also found ways to obtain cylindrical brushes from worm-like micelles by preserving their shape through crosslinking of the cylindrical inner domain (see Scheme 1-1B).[19-21] Furthermore, crystallization-driven cylindrical polymer micelles were produced by several groups[22-25] through crystallizing one block of linear block copolymers into a cylindrical domain. However, the core of these brush-like micelles is not crosslinked and therefore is less stable regarding fracturing compared to the core-crosslinked analogues. However, it is debatable whether the polymer brushes derived from block copolymers are genuine CPBs or rather "brush-like" cylinders compared to the classic CPBs derived from the abovementioned grafting approaches. Regardless, the stretching of lateral polymer chains lead to many new physical phenomena, which opened many new research areas and increased the interest in anisotropic polymeric material dramatically.

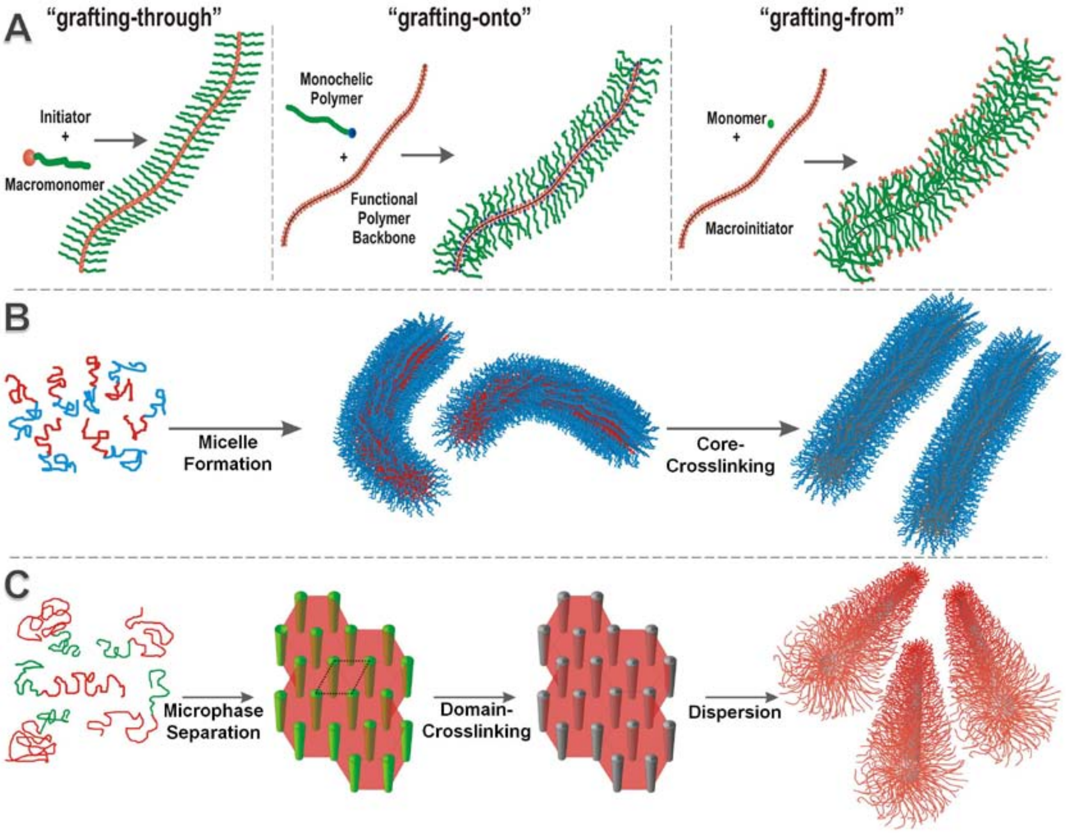

Scheme 1-1. Different approaches to prepare CPBs: (**A**) 'Grafting-through', 'grafting-onto' and 'grafting-from' techniques involving a step-wise build-up of CPBs. (**B**) Core-crosslinking of cylindrical micelles in solution. (**C**) Micro-phase separation of block copolymers in bulk into hexagonally packed cylinders and the subsequent crosslinking of the cylindrical domain to produce CPBs after dispersion.

1.1 Cylindrical Polymer Brushes via Grafting Approaches

As illustrated in Scheme 1-1A, CPBs can be synthesized by three grafting routes, namely 'grafting-through', 'grafting-onto' and 'grafting-from'. One characteristic that all three methods have in common is that polymeric side chains become adhered very closely next to each other and the lateral dimension is relatively small compared to the actual length of the main chain.[26] Efforts in gaining increased control over the polymerization kinetics brought out several living/controlled polymerization techniques with which it became feasible to produce defined CPBs with various compositions by the following grafting methods.

‘**Grafting-through**’ describes the polymerization of macromonomers into polymer brushes. Macromonomers are polymer chains carrying terminal polymerizable groups.[27] Since macromonomers have to be produced separately, it is easier to control length and composition of the side chains. In addition, they can be accurately characterized prior to polymerization. Another clear advantage of this method is the grafting density of 100 %, as every repeating unit carries one side chain. Despite the excellent control of the composition and the well-defined grafting density, the ‘grafting-through’ method bears its limitations. As polymer chains tend to coil, the accessibility of the terminal functionality of macromonomers is hampered. Additionally, sterical hindrance and a low concentration of polymerizable groups decrease the propagation of the main chain and hence limit the actual length of the backbone. Polymerizations often show incomplete conversion and consequently make purification tedious.[28-30] Conventional radical polymerization allowes the use of a wide range of monomers and reaction conditions; however, the relatively poor control over molecular weight and chain end functionality prevents the preparation of well-defined structures.[31] Consequently, many research groups failed to produce poly(macromonomers) with respectable backbone lengths using different kinds of polymerization techniques, such as anionic[32-34] and cationic[35] polymerization, as well as group transfer polymerization (GTP),[29] atom transfer radical polymerization (ATRP),[28] and reversible addition fragmentation transfer (RAFT) polymerization.[36] However, ring-opening metathesis polymerization (ROMP) of norbornene end-functionalized polymers enabled the synthesis of longer polymer backbones. Whereas the so-called ‘Schrock initiator’[37] still did not produce long enough main chains,[30,38] the use of metallocene-catalyzed ROMP allowed high monomer conversion and hence resulted in polymer brushes with passable backbone length [39,40] and acceptable length and molecular weight distribution.[41-44] Next to the significant progress in the ‘grafting-through’ approach, many research groups focused as well on developing ‘grafting-from’ and ‘grafting-onto’ techniques.

The ‘**grafting-onto**’ method involves a polymer main chain that carries functional groups on each monomer unit and end-functional polymer chains. Both backbone and side chain polymers are produced separately and can be characterized prior to the polymer brush formation. The side chains are then grafted onto the backbone by reacting the pendant functional groups of the backbone precursor with end-functionalized polymer chains. A diverse set of techniques has been used so far to produce molecular brushes by the ‘grafting-onto’ approach. Initially, many research groups focused on using living anionic chain ends and quenched them with suitable electrophilic polymer backbones to obtain comb-like polymers or polymer brushes.[45-51] These synthetic routes enabled, already back in the early 1980s, the synthesis of many graft copolymers. With the start of the 21st century, so-called ‘click chemistry’ enabled new possibilities regarding the covalent attachment of polymeric side chains onto a precursor backbone. The outrider of today’s ‘click chemistry’ was the azide-alkyne Huisgen cycloaddition,[52] where azide and alkyne groups react equimolar to form a triazole ring. Today, there exists a number of improved or different click reactions compared to the classic Huisgen model.[53] The most applied version is the copper(I)-catalyzed azide-alkyne cycloaddition (CuAAC).[54,55] The diversity, simplicity and efficiency of many click reactions allowed the preparation of polymer backbones with a high grafting density. Biopolymers or polymeric backbones prepared by controlled radical polymerization (CRP) have been equipped with clickable groups and then employed to synthesize CPBs.[56-58] Another way to produce molecular brushes is to use non-covalent (secondary) interactions, such as hydrogen bonding,[12,59,60] ionic interactions,[14,61,62] or coordination bonding.[11]

Independent on the way side chains are grafted onto a polymer backbone, the ‘grafting-onto’ approach has its limitations regarding grafting efficiency. The limitations arise through issues concerning entropy and sterical hindrance. As both the polymer backbone and the yet unattached polymer side chains exist as random coils in solution, the attachment of more and more side chains to the backbone leads to the stretching of the backbone and accordingly to the stretching of the side chains - both are entropically unfavored. The constantly increasing density of the grafted chains also causes difficulties for the diffusion of further chains to the reactive sites due to sterical hindrance. One can overcome these issues by adding a large excess of the to-be-grafted side chains, however, unreacted chains will remain in solution after the reaction and require further purification steps. Another way to increase grafting efficiency is to decrease the lengths of the to-be-grafted side chains, as this will reduce sterical hindrance.[57] As a result of the limitations faced in the ‘grafting-through’ and ‘grafting-onto’ methods, the ‘grafting-from’ approach became the most utilized method to graft side chains to a polymer backbone.

The '**grafting-from**' method is the most prominent grafting approach and utilizes a polymer backbone carrying initiator groups on each monomer unit. The polymerization of monomers is initiated at the polymer backbone and side chains are grown from the backbone. Through the 'grafting-from' approach, it became feasible to produce very well-defined polymer brushes with high grafting densities. First, the polyinitiator backbone is produced via living/controlled polymerization techniques by either polymerizing monomers with initiation sites (so-called 'inimers') directly[63,64] or by a subsequent functionalization step after the backbone synthesis.[65-67] Backbones are mostly synthesized by anionic polymerization,[68,69] RAFT,[63,70] ATRP,[66,71] nitroxide mediated polymerization (NMP)[72,73] or ring-opening polymerization (ROP).[74,75] As in all grafting approaches, a well-defined long backbone with a narrow molecular weight distribution (MWD) is crucial as the length distribution of the CPBs largely depends on the MWD of the backbone. Depending on the initiating groups, polymer chains have been grafted mostly by ATRP.[6,76-78] Moreover, polymers side chains were also grown using RAFT,[79] NMP[80,81] and ROP.[82-84] CRP techniques imply relatively high tolerance towards functional groups, which allowed the syntheses of polymer brushes bearing functional groups[69,85,86] or brushes consisting out of charged[87] or partially inorganic[78,88] side chains. Moreover, CRP techniques made the sequential grafting of polymer side chains feasible, which enabled straightforward syntheses of di- and tri- block copolymer brushes.[88-90]

Issues regarding purification, like in the previously discussed grafting methods, became negligible in the 'grafting-from' approach, as polymer brushes can be relatively easily separated from residual monomer molecules. Although this method seems to be the most commonly used one, it still bears its drawbacks. Grafting density is a general issue in this approach, since the initiation on the backbone is limited, as well, by sterical hindrance through bulky monomers. Nonetheless, a grafting efficiency of between 50 % and 90 % is mostly reported[85,91,92] – obviously depending on the method used for the growth of the side chains. This is still significantly higher when compared to polymer brushes produced through the 'grafting-onto' approach, where the grafting efficiency rarely exceeds 20-40 %.[57]

Aside from the grafting methods, there has been extensive research to obtain brush-like polymer cylinders and CPBs from block copolymers. Cylindrical structures were obtained both in bulk and solution, by either crosslinking, self-assembly or crystallization processes.

1.1.1 Structural Compositions of Cylindrical Polymer Brushes

In terms of chemical composition, CPBs can be classified into eight different types having linear side chains (see Scheme 1-2). The most commonly synthesized structures are homopolymer and diblock copolymer brushes. By using the previously discussed grafting techniques, many new compositions of CPBs have been realized aimed at creating new materials, properties and applications. Through the combination of different methods it is possible to synthesize structures of brushes that would be unobtainable by a single method. In most cases, CPBs were prepared from flexible backbones. Up to now, the syntheses of core-shell, core-shell-corona, Janus, block-type, statistical, gradient and macrocyclic copolymer brushes, as well as homopolymer brushes, has been reported. Additionally, CPBs can be used as building blocks to synthesize stars and networks. Furthermore, CPBs where the side chains are oligomeric polymer brushes themselves, so called ‘graft-on-grafts’, have been reported.

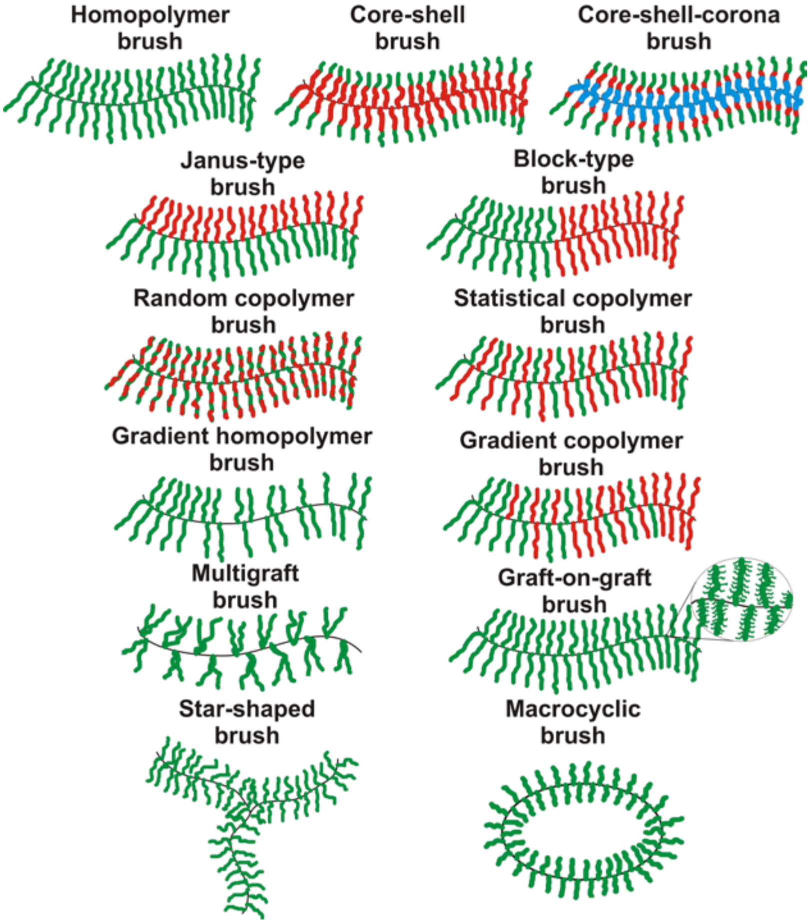

Scheme 1-2. Various branching topologies and chemical compositions of CPBs.

1.1.2 Core-Shell and Core-Shell-Corona Block Copolymer Brushes

If the side chains are diblock copolymers or triblock terpolymers, the CPBs will feature a core-shell or core-shell-corona type structure. Up to now, core-shell CPBs have been synthesized by ‘grafting-through’[8,93,94] and sequential ‘grafting-from’[66,69,71,78,82,90] methods. However, the issues discussed above concerning purification and conversion in the ‘grafting-through’ method resulted in the favoring of the ‘grafting-from’ approach by the scientific community. Very often, side chains were grown via ATRP from a poly(methacrylate)-based backbone, such as poly(2-bromoisobutyryloxyethyl methacrylate) (PBIEM). Almost at the same time, Börner *et al.* and Cheng *et al.* used PBIEM backbones to prepare core-shell CPBs.[66,71] Similar to Cheng, Zhang *et al*. showed the systematic build-up of amphiphilic core-shell CPBs via sequential grafting of *tert*-butyl acrylate (*t*BA) and *n*-butyl-acrylate (*n*BA) from PBIEM and a subsequent deprotection step for poly(*tert*-butyl acrylate) (P*t*BA) (see Figure 1-1A).

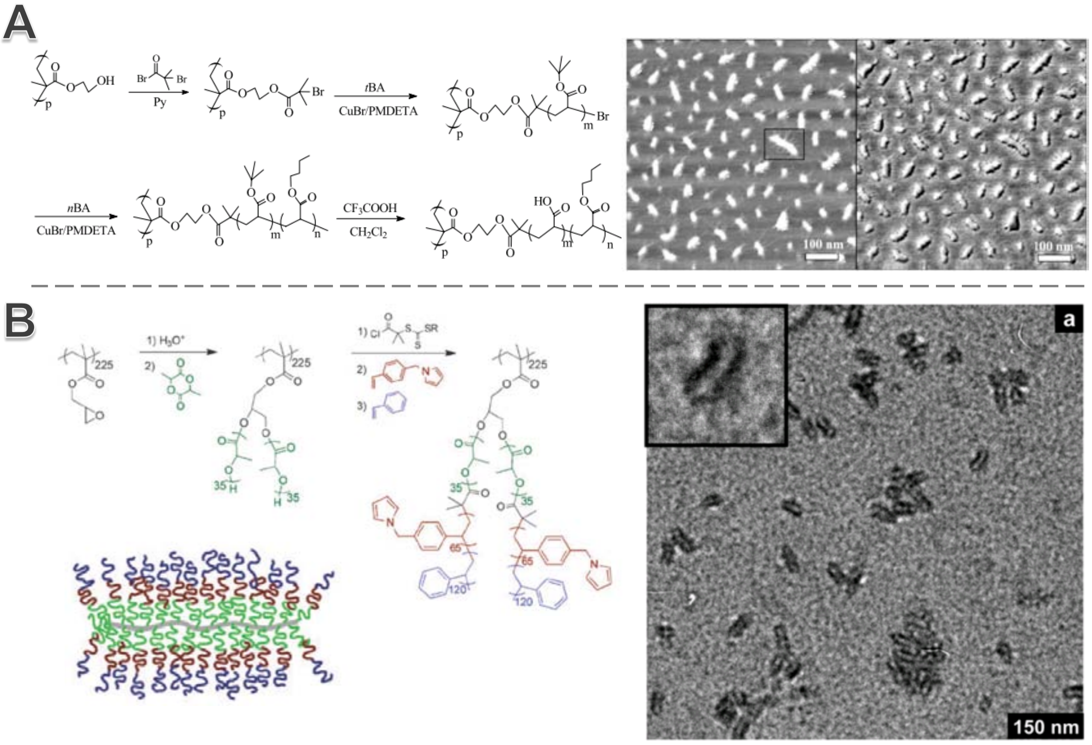

Figure 1-1. (**A**) Core-shell diblock copolymer brushes obtained by the sequential ‘grafting-from’ of *t*BA and *n*BA by ATRP[69] and (**B**) the core-shell-corona triblock terpolymer brushes obtained by the combination of ROP of lactide and sequential RAFT of PMS and styrene.[84]

Core-shell-corona polymer brushes have been obtained by the sequential grafting of different polymer blocks using ATRP[88,95] or a combination of ROP and RAFT.[83,84] Huang *et al*. used poly(glycidyl methacrylate) (PGMA)as a polyinitiator for the ROP of lactide.

After modification with an initiator for RAFT polymerization, poly(lactide) was able to initiate the sequential polymerization of 4-(pyrrolmethyl)styrene (PMS) and styrene. Finally core-shell-corona CPBs were obtained (see Figure 1-1B).

Multiblock side chains do not only increase the number of structural components, but also introduce new morphologies and properties. Side chains may consist of components with different softness, polarity and functionality. The different side chain blocks divide the CPBs into cylinders with different concentric compartments and, therefore, the entire brushes resemble unimolecular cylindrical micelles that can then be used to undertake chemistry in. Matyjaszewski *et al.* highlighted the incompatibility of side chain blocks through atomic force measurement (AFM) studies on CPBs composed of poly(ε-caprolactone)-*b*-poly(*n*-butyl acrylate) (PCL-P*n*BA) side chains. The cylindrical microphase separation of the crystalline PCL core and the amorphous PBA shell resulted in the formation of a spine-like morphology, where fully extended PCL ribs were embedded in a matrix of P*n*BA.[92] By using not only incompatible but also stimuli-responsive polymer blocks as side chains, it is possible to make CPBs respond to environmental changes, such as salt concentration, light, temperature, pH and a solvent environment. Thus, amphiphilic core-shell brushes with a poly(acrylic acid) (PAA) core and a P*n*BA shell are able to complex positively charged ions inside the core. Complexation of bivalent or trivalent ions changed the regular worm-like morphology in a methanol/chloroform solution into a pearl-necklace-like structure due to the insolubility of the polymer/ion chelate complex. Surface minimization led to the formation of ‘pearls’. Even without metal ions, the typical pearl-necklace-like structures were observed in a non-solvent (for instance, toluene) for the core polymer due to the incompatibility of the polar PAA core.

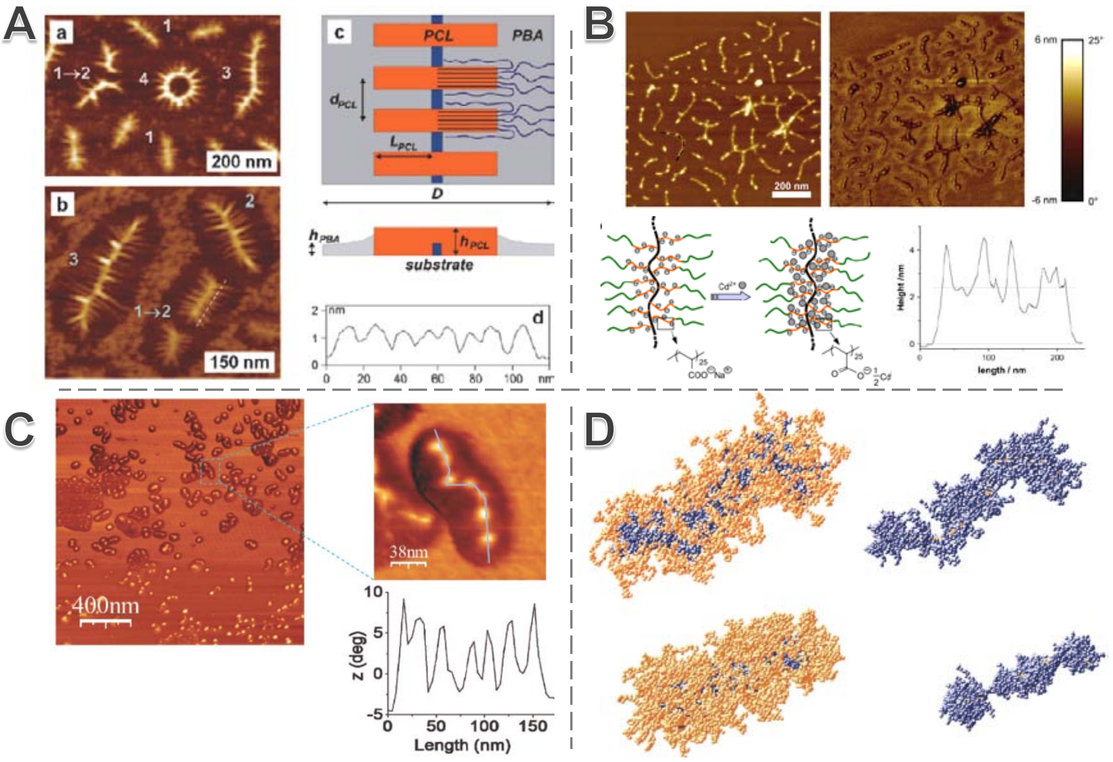

Figure 1-2. (**A**) PCL-PBA core-shell brushes on mica. Due to the crystallization of PCL chains, the worm-like pristine structure is transformed into a spine-like morphology.[92] (**B**) AFM images of PAA-P*n*BA core-shell brushes with a distinct pearl-necklace-like structure due to the polychelate complexes of Cd^{2+} and PAA in the core.[96] (**C**) AFM images of PAA-P*n*BA core-shell brushes on mica from a toluene solution.[97] (**D**) Snapshots of typical conformations of molecular core-shell brushes obtained by Monte Carlo simulations. The upper two images show the conformation in a good solvent for the corona (orange) and the core (blue) blocks, and the lower two images show the conformation in a bad solvent for the core block (blue).[97]

Such incompatibilities based on crystallinity, polarity or other parameters are extremely advantageous in the fabrication of hybrid nanostructures. CPBs can therefore be used as unimolecular and organic templates for the template-directed synthesis of 1D hybrid nanostructures. Section 2 will describe the template-directed synthesis of hybrid nanostructures in further detail.

1.1.3 Statistical, Gradient, Block and Janus-Type Cylindrical Polymer Brushes

Two types of chemically different homopolymer side chains can be attached to the same backbone. Depending on their distribution along the backbone, their interaction parameters and the nature of the solvent, the side chains of these brushes can have a mixed structure or segregate into two different hemicylinders, also called ‘prototype copolymer brush’ or Janus cylinder.[18,98,99]

Statistical CPBs consist out of two different polymer side chains that are statistically tethered to the backbone; for instance, poly(2-vinylpyridine) (P2VP) and poly(methyl methacrylate) (PMMA), where P2VP and PMMA macromonomers were randomly copolymerized by free radical polymerization. [100] Intramolecular phase separation can be induced by quaternization of the P2VP side chains. Due to the increased incompatibility, the statistical CPBs form patchy (meander-like) or Janus-type structures (see Figure 1-3A). So far, Janus brushes have mainly been synthesized via phase separation of triblock terpolymer with a crosslinkable middle block in the bulk.[18] However, triblock terpolymers with a crystalline poly(ethylene) (PE) middle block allow the crystallization-induced growth of worm-like micelles with a patchy corona.[101,102]

Block-type CPBs can be considered as a different kind of Janus-type brushes. However, the CPBs are now divided perpendicular to the backbone into two blocks. Ishizu *et al.* were the first to report AB-type brush–*block*–brush amphiphilic copolymers via ATRP.[103] In their work, poly(ethylene glycol) (PEG) methacrylate macromonomers were used to form block A. The PEG brush was then used as a macroinitiator for the subsequent polymerization of hydroxyethyl methacrylate (HEMA). PHEMA was modified into PBIEM by the esterification of ATRP initiator groups. Thereby, it was possible to graft more PHEMA as block B via the ‘grafting-from’ approach. However, Ishizu’s method involved problems concerning purification and backbone length, since ‘grafting-through’ was used to synthesize block A. More recently, Matyjaszewski *et al.* and Rzayev *et al.* developed more promising synthetic strategies by only using the ‘grafting-from’ method and the subsequent combination of two different polymerization techniques for the step-wise growth of two different polymer hemispheres. Both groups used ROP for the polymerization of one block and ATRP for the second block (see Figure 1-3D).[104,105] Only very recently, Rzayev *et al.* synthesized block-type CPBs by combining RAFT and ATRP selectively for the grafting of side chains of each block.[106]

Gradient CPBs have a gradient distribution of side chains along the backbone. Such a gradient grafting was achieved by utilizing the ‘grafting-through’ and ‘grafting-from’ methods.[107-109] A macroinitiator backbone that consists of a gradient copolymer of HEMA and MMA, where HEMA is modified with ATRP initiating groups, was used for the grafting of *n*BA. The MMA monomer units are unable to initiate the polymerization of *n*BA and hence only the modified HEMA units grow side chains.[107] Such gradient homopolymer brushes undergo transformation from rod-like into tadpole-like conformations.[110] Heterografted copolymer brushes have been synthesized by Neugebauer *et al.* via the ‘grafting-through’ of macromonomers. The macromonomers had either acrylate or methacrylate groups, which led to reactivity ratios of the macromonomers and therefore to a gradient copolymer brush (see Figure 1-3C).[108,109]

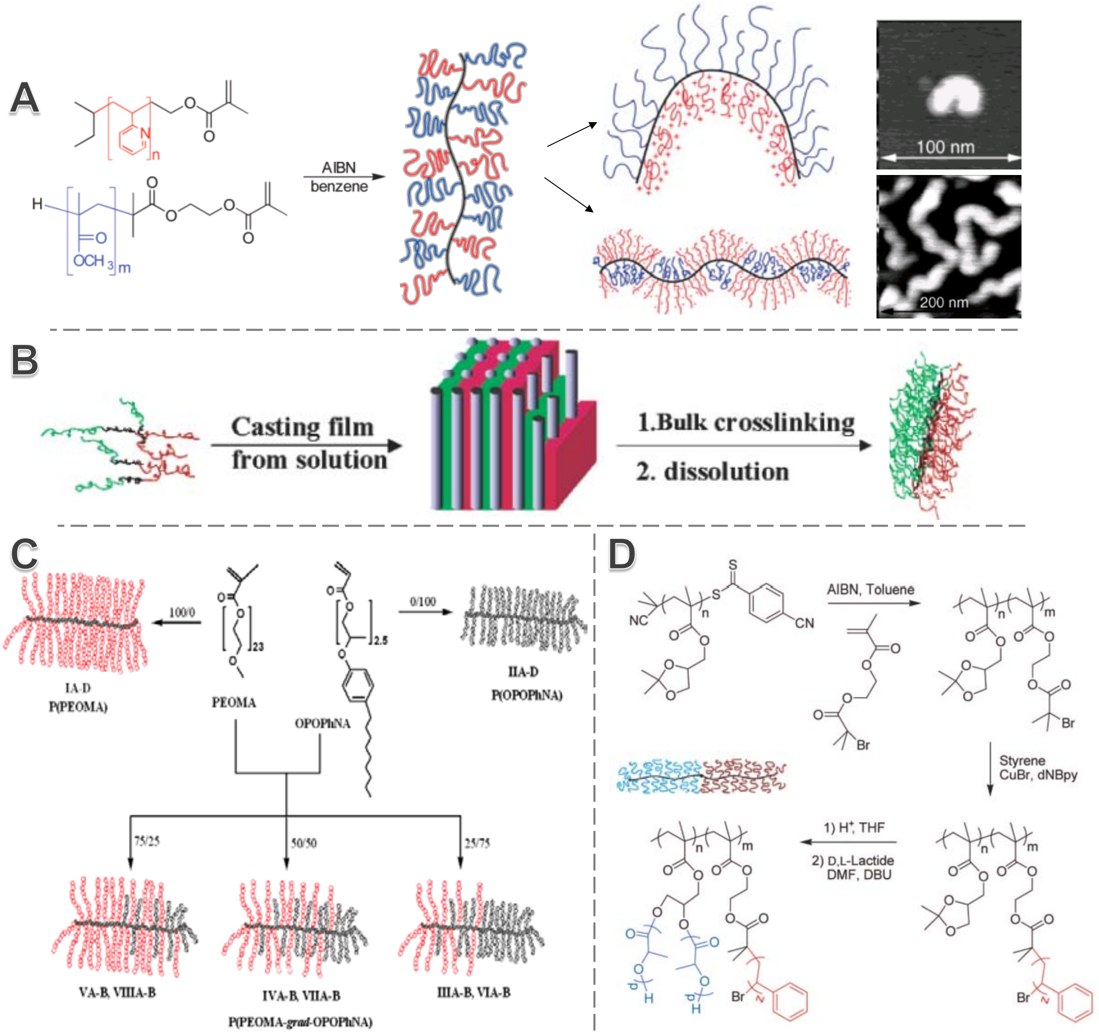

Figure 1-3. (**A**) Statistical copolymer brushes were obtained via the ‘grafting-through’ of macromonomers and formation of Janus-type and patchy brushes after quaternization.[100] (**B**) Microphase separation of triblock terpolymers and subsequent crosslinking was used to obtain Janus-type polymer cylinders.[18] (**C**) Copolymerization of macromonomers of different reactivity was undertaken to obtain heterografted gradient polymer brushes.[108] (**D**) A bifunctional polymer backbone was used for the sequential block growth of poly(lactic acid) (PLA) via ROP and polystyrene (PS) via ATRP to obtain block-type CPBs.[105]

1.1.4 Branched, Macrocyclic and Multigraft Polymer Brushes

CPBs have been used as building blocks to construct more complex polymer architectures, such as double-grafted (graft-on-graft) brushes,[89,111] cylindrical tubes,[112] barbwires[113] and flower-like or dumbbell-like structures.[104,114] Branched polymer brushes, such as dendridic polymer brushes, have been prepared by several groups via all three grafting approaches (see Figure 1-4C).[115-120] Another type of branched brushes are star-shaped brushes. Four or five arm stars were successfully synthesized via a coupling of living anionic PS and star-like poly(chloroethyl vinyl ether) (PCEVE) chains.[121] By producing a three- or four- armed star polymer with ATRP initiator groups as monomer units for the arms, it was possible to prepare very uniform three- or four- armed star molecular brushes (see Figure 1-4A).[122]

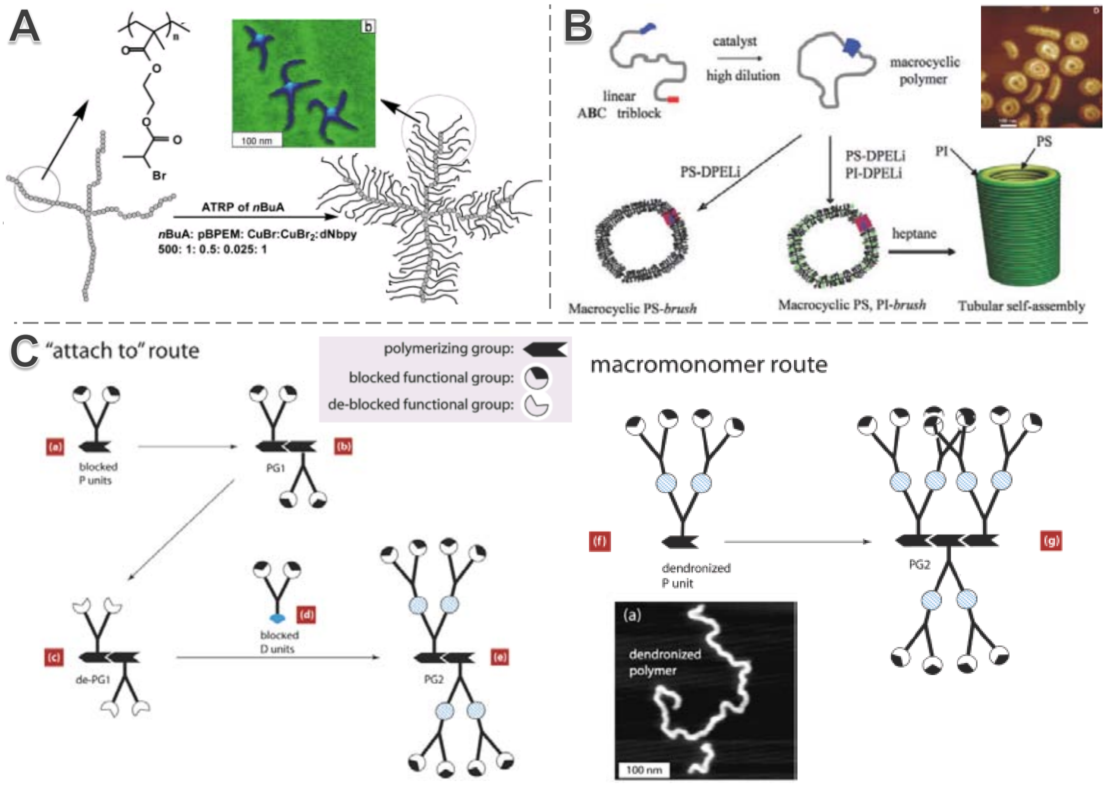

Figure 1-4. (**A**) Star-shaped molecular brushes obtained when star-shaped precursors were used with an ATRP initiator containing arms, and the respective AFM image. [6,122] (**B**) The strategy for the synthesis of macrocyclic copolymer brushes using ABC triblock terpolymers and anionic living chain ends. Macrocyclic brushes (see AFM phase image) formed cylindrical tubes.[112] (**C**) Two strategies towards dendronized polymer brushes using either the 'grafting-onto' ('attach to') route or the 'grafting-through' (macromonomer) route. Dedronized polymer brushes can form long cylinders (see AFM image).[119]

Another special type of polymer brushes are macrocyclic brushes, where the two ends of the brush are connected to each other by a coupling reaction.[123] The preparation of large macrocyclic (co)polymer brushes is limited by several factors. Firstly, it is difficult to obtain only α,ω-difunctional high molar mass precursors and, secondly, there is a drastic decrease in the end-to-end ring closing efficiency when the distance between the chain ends becomes too large. Lastly, the separation from non-closed and still-linear contaminants is difficult, as each consists out of comparable molar mass.[124]

Deffieux *et al*. developed a strategy to synthesize large polymer macrocycles which are based on an ABC triblock terpolymer.[112] The triblock terpolymer has a long central block B, which possesses two short blocks (A and C) on each end. Blocks A and C bear monomer units that react exclusively with each other. The external blocks are then selectively activated under dilute conditions to allow intramolecular coupling between the A and C blocks to form the macrocyclic polymers. Chloroethyl vinyl ether was selected as the monomer for the central block B, because it can be readily derivatized into brushlike polymers by a ‘grafting-onto’ process. The corresponding macrocyclic brushes were decorated with PS or randomly distributed PS and polyisoprene (PI) branches (see Figure 1-4B). In a selective solvent for the PI branches, the macrocyclic brushes self-assemble into cylindrical tubes with a length up to several hundred nanometers.[112]

1.2 Cylindrical Polymer Brushes from Block Copolymers

CPBs or rather brush-like polymer cylinders can also be obtained from diblock copolymers or triblock terpolymers in either solution or bulk. The brush formation in solution can be achieved by producing cylindrical micelles and the subsequent crosslinking of the cylindrical domain.[19,125,126] As an example, Liu *et al*. used the diblock copolymer poly(styrene)-*block*-poly(2-cinnamoylethyl methacrylate) (PS-PCEMA), where PCEMA formed the cylindrical micellar core and could be crosslinked by UV-light.[20] In this case, the PS chains are then the grafts of the PCEMA rod and the whole unit resembles a CPB. Schmalz *et al*.[23] and Winnik *et al*.,[22] as discussed above, used diblock or triblock polymers with a crystallizable block to form CPBs. The crystallizable block formed the cylindrical core upon cooling and therefore preserved the worm-like geometry. Winnik *et al*. used the diblock copolymer poly(ferrocenyldimethylsilane)-*block*-poly(isoprene) (PFS-PI) to induce crystallization of PFS into cylinders with PI grafts (see Figure 5B).

Alternatively, the same type of cylindrical brush can also be prepared by the crosslinking of cylindrical microdomains of microphase-separated block copolymers in bulk. In this way, CPBs from bulk thin films were achieved by choosing the composition of AB diblock copolymers or ABC triblock terpolymers in a way that the block B would microphase-separate into a cylindrical morphology.[15,16,18] For example, it was again Liu *et al*. who used the photo-crosslinkable polymer PCEMA, but this time they yielded cylinders of PCEMA dispersed in the continuous phase of PS in bulk. The dissolution of the crosslinked cylinders resulted in isolated polymer brushes with crosslinked PCEMA cores and PS grafts (see Figure 1-5A).[17]

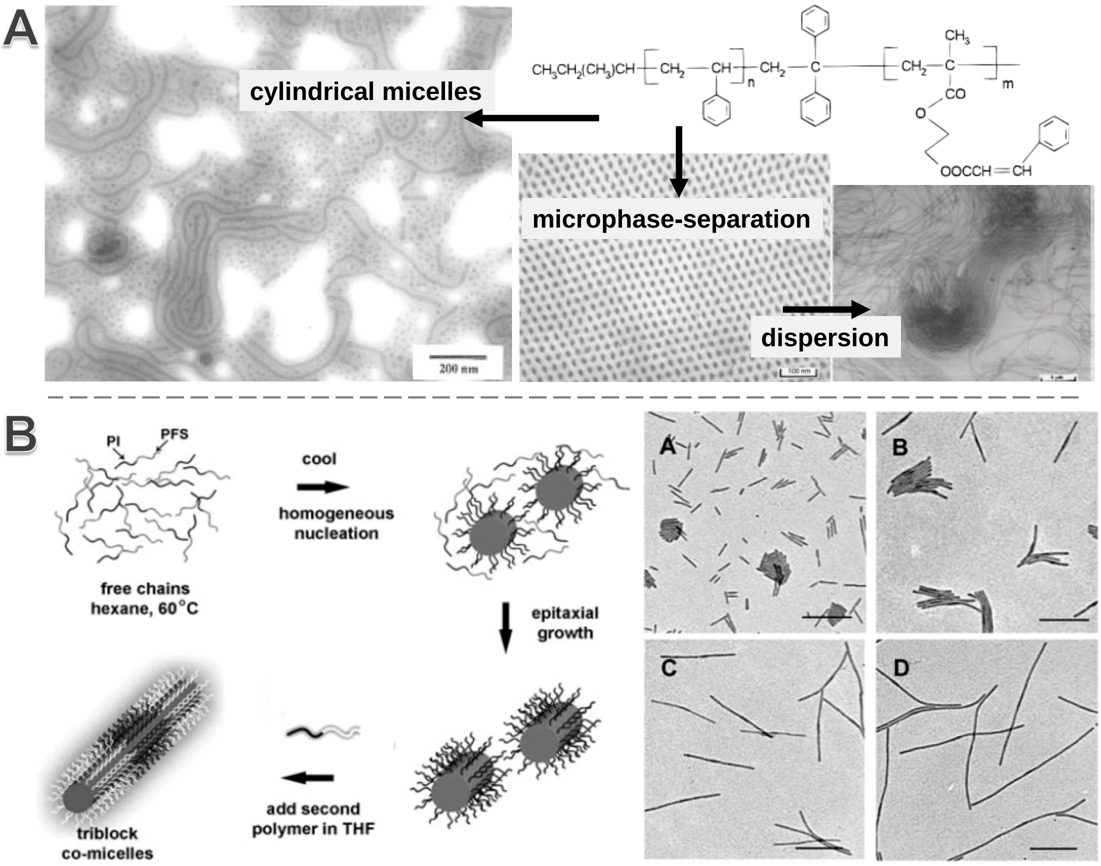

Figure 1-5. (**A**) PS-PCEMA diblock copolymer can be used for either forming cylindrical micelles in solution or PCEMA cylinders in a PS matrix in bulk. In each case, PCEMA can be crosslinked by UV-light and yield PCEMA cylinders with PS grafts.[15,20] (**B**) PFS-PI diblock copolymers were used to undergo crystallization. Thereby, PFS formed cylinders whereas the PI block produced the grafts.[22]

1.3 Properties of Cylindrical Polymer Brushes

The conformation of CPBs is a result of competing forces between the backbone and the grafts. The densely grafted side chains repel each other, but their ability to move apart is hampered by the backbone, which locally confines the side chains to a cylindrical volume. Consequently, cylindrical brushes may exhibit different conformations on different length scales.[127,128]

Intensive research has been performed to highlight the unique properties of CPBs. CPBs are structurally more compact when compared to the corresponding linear polymers of the same molecular weight. This compactness derives from a higher density of chain segments. The steric repulsion of densely grafted side chains results in an extended worm-like conformation. The extent of backbone stretching is mostly dependent on the side chain length and the nature of the solvent used. The extended worm-like conformation makes it difficult to characterize CPBs with conventional characterization techniques, such as size exclusion chromatography (SEC), dynamic or static light scattering (DLS and SLS) or viscometry. Characterization becomes even more problematic when the composition of CPBs is heterogeneous. Therefore, several types of scanning probe microscopies have been established and are nowadays frequently used in the characterization of CPBs. The most frequently used type is AFM, as it is a powerful tool and allows the precise imaging of CPBs and the characterization of their molecular weight, size and conformation.[82,129-131] There have been many scientific studies on the properties of CPBs in solution, on surfaces and in bulk.

1.3.1 Solution Properties

As mentioned above, the cylindrical shape of CPBs derives from the repulsion of side chains that are tethered very densely onto a polymer backbone. In solution, CPBs adopt the conformation of a worm-like object that can be characterized by the length per monomer l_m, the brush diameter D, and the persistence length l_p. Obviously, these parameters, and hence the cylindrical dimensions, depend on grafting density, side chain length and solvent nature. Many theoretical,[61,132-134] simulation[135-141] and experimental[31,142-146] studies have been performed to learn about side chain effects, solvent effects and main chain conformations. However, opinions and results differ as to how much chain side length is crucial for l_p and the overall brush structure. For example, for flexible side chains, it is theoretically predicted that a stiffening of the backbone is not sufficient to cause ordering of CPBs,[128] but experiments show hexagonal ordering of cylinders that stiffened with increasing side chain length.[147,148]

A further property of CPBs is that they can act as liquid crystals and, therefore, form a lyotropic phase when concentrated in solution (see Figure 1-6A).[78,149] When a threshold concentration is exceeded, the polymer side chains will interpenetrate and hence show ordering. Threshold concentrations depend strongly on the length of the side chains.

Another interesting solution property of CPBs is that they can respond easily to environmental changes and change their morphology accordingly. Their morphology, as well as their flexibility, is mainly directed by solvent quality, which in water depends on salt concentration, surfactants, temperature and pH. It is possible to trigger sharp transitions in the morphology of CPBs. This makes them an interesting material for various applications, such as membranes or sensors. CPBs consisting of thermo-responsive polymers, such as poly(2-(dimethylamino)ethyl methacrylate) (PDMAEMA) or poly(*N*-isopropylacrylamide) (PNIPAM) are classical examples where the cylindrical shape will collapse upon heating above a certain temperature.[77,150,151] Further, PDMAEMA polymer brushes are responsive to pH[151,152] and salt (see Figure 1-6C).[152] PDMAEMA loses its responsiveness to pH and temperature upon quaternization due to the permanent charge; however, it stays sensitive to salts. Charged CPBs like poly{[2-(methacryloyloxy)ethyl] trimethylammonium iodide} (PMETAI) can also be used for the formation of interpolyelectrolyte complexes (IPECs) with oppositely charged polyions, such as poly(styrenesulfonate) (PSS).[153]

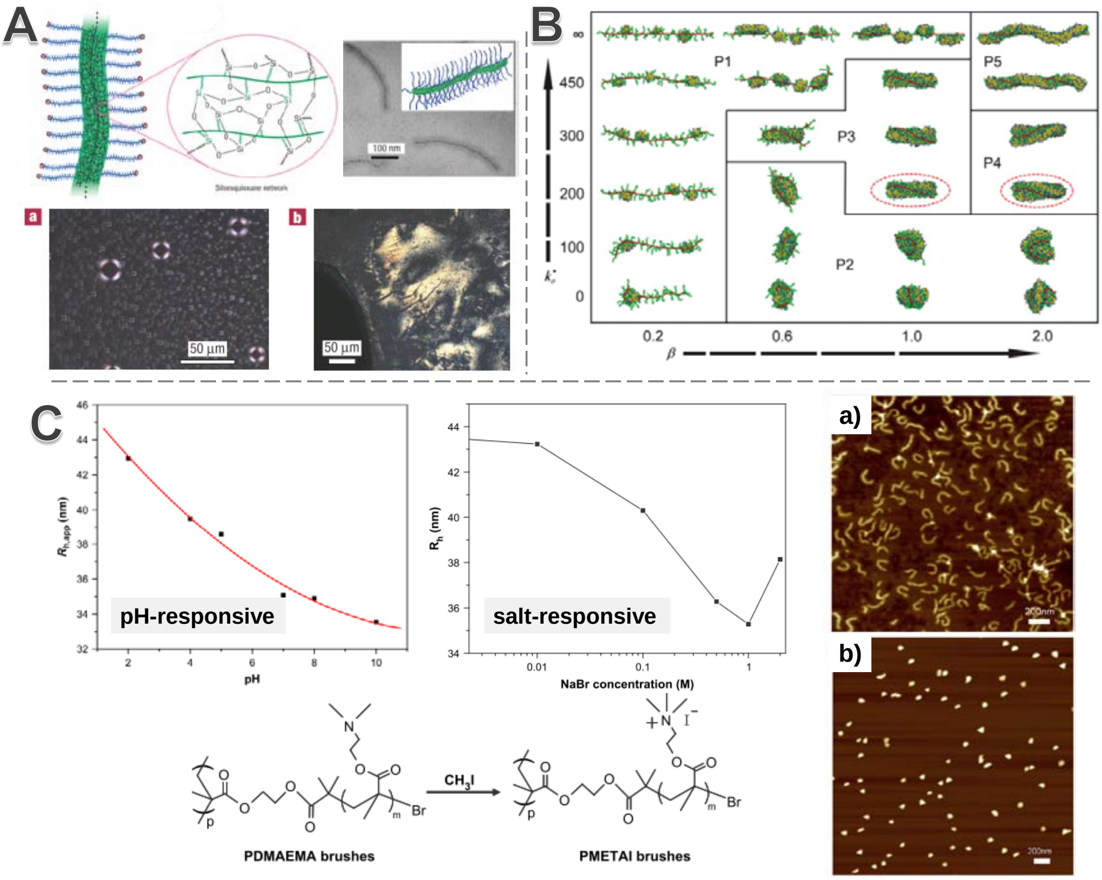

Figure 1-6. (**A**) $[(SiO)_{1.5}\text{-OEGMA}]_{3200}$ core-shell CPBs with a partially inorganic core are rather stiff in solution (see cryo-TEM) and form (**a**) isotropic and (**b**) lyotropic phases upon concentrating.[78] (**B**) Simulated results for the interaction of charged CPBs and surfactants. Depending on the stiffness of the backbone, the main chain can adopt various conformations from stiff cylinders to spheres.[140] (**C**) DLS demonstrates that PDMAEMA brushes show pH-responsiveness and are salt-responsive after quaternization. AFM studies highlight the collapsed spherical structures after the increase of salt concentration of sodium bromide (NaBr).[152]

The solution properties of heterogeneous brushes, such as core-shell brushes are considerably more complicated. Borisov *et al.* have reported that the shape of core-shell brushes can be very different depending on the solvent quality for the core and the shell (see Figure 1-2D).[97]

1.3.2 Cylindrical Polymer Brushes on Surfaces and in the Bulk

Similar to the solution properties, where the brushes behave according to the environment and changes therein, polymer brushes tend to behave differently according to the interaction between the individual blocks, the underlying substrate and the surrounding environment.[127] Figure 1-7A shows possible morphologies of core-shell CPBs on a substrate. Depending on the strength of the adsorption and the brush architecture, it is possible that molecular brushes undergo association and dissociation during their adsorption on the substrate.[154] P*n*BA brushes associate due to the crystallization of the linear poly(octadecyl methacrylate) chains on both ends of the brush backbone. A more intriguing phenomenon is the scission of polymer brushes on substrates. Long CPBs with long side chains may undergo scission of the backbone upon the adsorption onto a substrate, such as graphite or mica.[155] Different incubation times verified the proceeding scission of polymer brushes into sphere-like brush fragments (see Figure 1-7C). The macromolecular destruction originated from side-chain-induced stretching of the polymer backbone to maximize the number of contacts with the substrate. Moreover, CPBs can be used to study the motion and flow of molecules.[156,157] It is further possible to order molecular brushes during spreading. Flow-enhanced diffusion of macromolecules resulted in epitaxial alignment of macromolecules, where the orientation was independent of the flow direction.[158]

In bulk, CPBs behave differently as compared to linear polymer chains. CPBs can be used to produce new materials with unusual mechanical properties. Molecular brush backbones are less entangled in bulk due to the large fraction of densely grafted side chains. This self-disentanglement results in unique viscoelastic properties, which depend on both the length of the main chain (backbone) and the side chains. Transformation of the brush films into crosslinked networks produced a high local mobility and sufficient macroscopic mechanical stability.[111,159-161] The resulting class of materials are termed (super-) soft elastomers. Rzayev *et al.*further reported the phase-separation of block-type PS-PLA polymer brushes analogue to linear block copolymers.[105,162] Consequently, it was possible to obtain a cylindrical bulk morphology from CPBs for the first time. After degradation of the cylinder-forming PLA block, a nanoporous polymer network was produced (see Figure 1-7B). The same PS-PLA polymer brush was used for controlled evaporative self-assembly of hierarchically structured bottlebrush block copolymers (see Figure 1-7D).[163] In a special evaporation process, a toluene solution of the PS-PLA block copolymer brushes was aligned in gradient stripes with internal lamellar nanodomains.

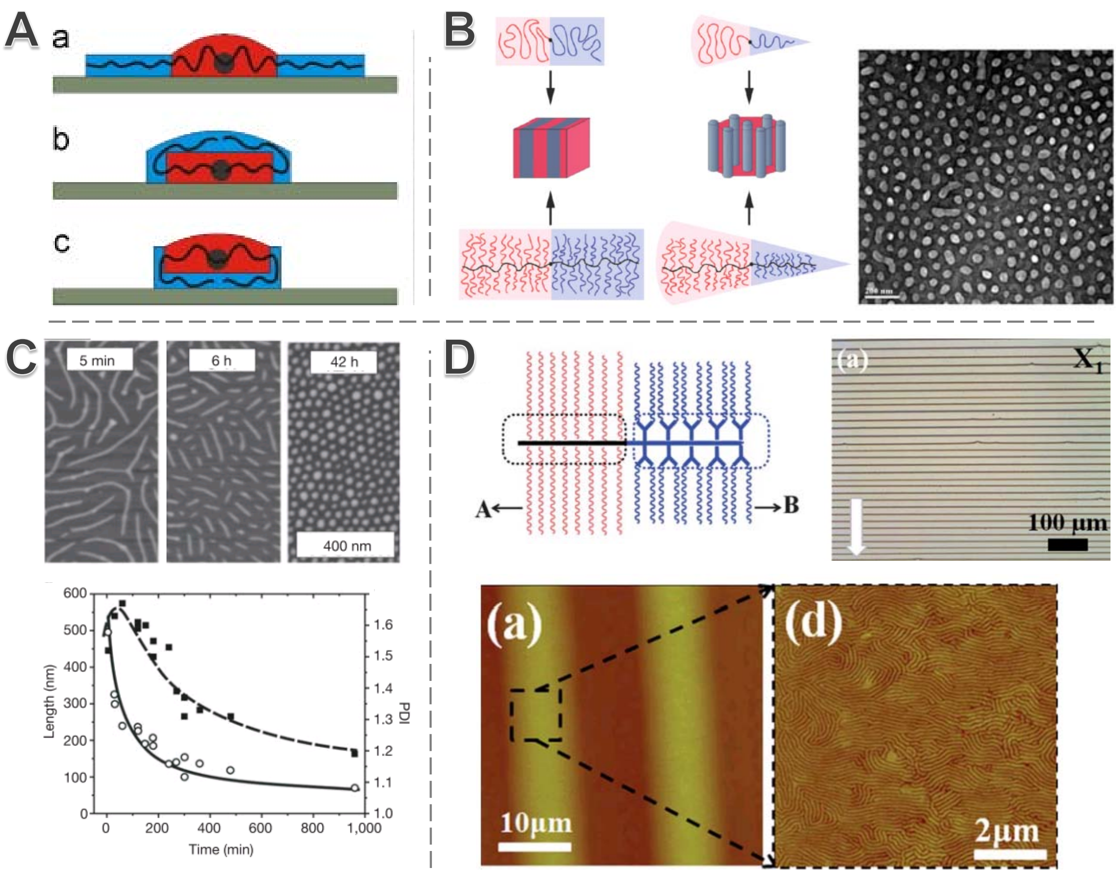

Figure 1-7. (**A**) Possible morphologies adopted by core-shell CPBs on different substrates.[127] (**B**) Phase-separated PS-PLA block-type CPBs, which form a nanoporous network after PLA cylinder degradation.[162] (**C**) Scission of long polymer brush backbones with long side chains.[155] (**D**) Hierarchical structuring of block-type CPBs into gradient lines with internal lamellar phase-separation.[163]

1.4 Applications of Cylindrical Polymer Brushes

The many different properties and high functionalities, together with the often straightforward syntheses, render CPBs useful tools for a plethora of applications in all kinds of fields of physics, chemistry, biology and material sciences. The 1D shape and the multiple, concentric and individually separated compartments make CPBs suitable to be used as delivery vehicles or templates. The following sections highlight the versatile applications of CPBs and their use as nanosized building blocks for the fabrication of hierarchically structured 1D materials.

Not only can CPBs be used to visualize and demonstrate molecular processes,[155,164] but more so, they can be used in medical and biological applications, such as potential drug delivery vehicles or gene transfection. Cell entry is dependent on the shape of the delivery vehicles.[165] It is reported that the cell entry of 1D nanomaterials occurs by tip recognition and rotation,[166] and that a cylindrical shape is advantageous regarding the retention time in the body.[167] Accordingly, Grubbs *et al.* recently reported the synthesis of drug loaded CPBs, where the drug can be released upon degradation of a linking group (see Figure 1-8).[42,168]

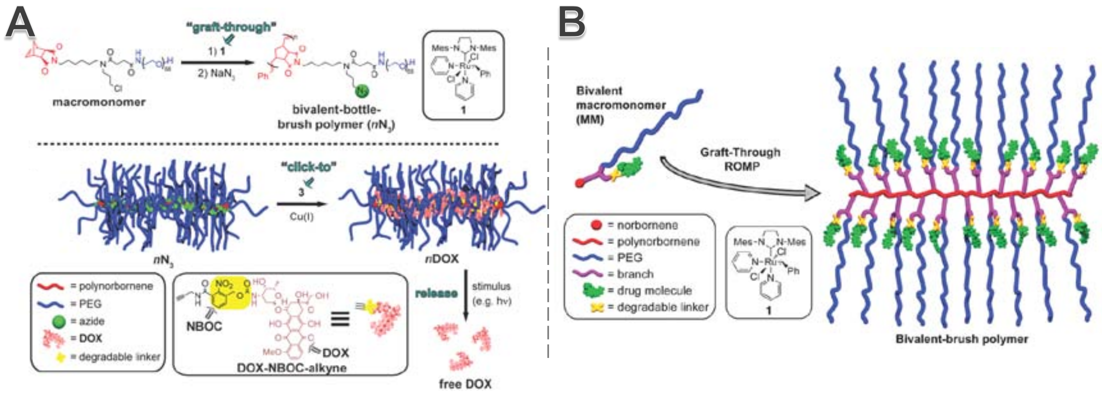

Figure 1-8. (**A/B**) Novel 1D drug delivery vehicles developed via the 'grafting-through' of functional and drug-containing bivalent macromonomers.[42,168]

Aside from the biological applications, CPBs often find use as template materials for the preparation of organic/inorganic hybrid nanomaterials. Among the different structures, core–shell CPBs are of special interest because they can be utilized in the synthesis of cylindrical hybrid nanostructures, such as nanowires and nanotubes, with interesting properties after metallization or other modification. The following section focuses on template-directed syntheses of 1D hybrid nanostructures, in which CPBs play an significant role in the bottom-up processes.

2. One-Dimensional Hybrid Organic-Inorganic Nanostructures

Polymeric-inorganic hybrid materials are a group of materials described as polymers in which a certain amount of inorganic nanoparticles are homogeneously distributed. The fact that one part is still organic material brings several advantages regarding the stability and flexibility of the hybrids. The formed hybrid material consequently holds a combination of properties from both material classes.

The combination of inorganic and organic components to form 1D nanostructures at the nanosize level led the way to the development of an immense new area of materials science, which is expected to have tremendous effects on the development of multi-functional materials.[124] 1D nanostructures are considered to have superior properties according to their size and geometry.[169-171] These functional hybrid materials are considered as innovative and advanced materials that hold promising applications in multiple fields, such as optics, electronics, energy storage and conversion, mechanics, membranes, catalysis, sensors and biology.[172] Research on such promising nanostructures is mainly guided by three motives: (A) utilizing the unique properties of nanostructures for applications; (B) defining the size- and shape- dependent physical properties of nanostructures; and (C) producing large quantities of nanostructures with controllable sizes and shapes.[169]

Within the past several years, the research dealing with 1D hybrid nanomaterials, such as wires, rods and tubes, has developed rapidly (see Figure 1-9). Many different nanostructures ranging from homogenous to core-shell and scattered-type to even block-type composition have been reported (see Figure 1-9C).[173] One of the most promising methods to obtain 1D nanomaterials is through template-directed or template-assisted synthesis routes, which often allow the precise tuning of the composition and build-up of such nanomaterials. An important class of organic templates used for the synthesis of composite materials derives from 1D templates, in particular CPBs.[13,174,175]

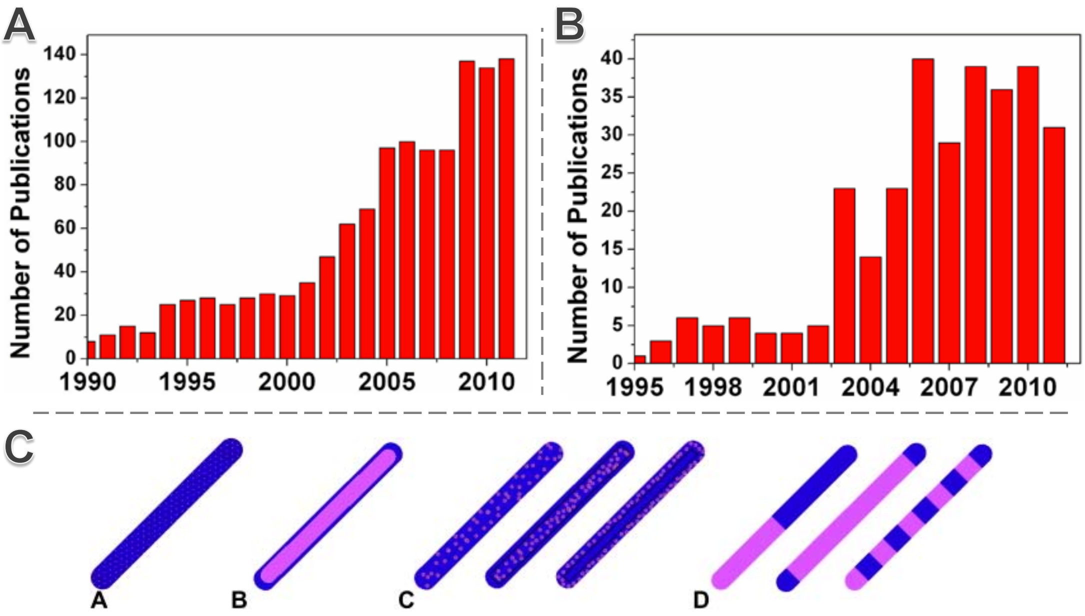

Figure 1-9. (**A**) Number of publications dealing with 1D hybrid nanomaterials.[176] (**B**) Number of publications dealing with the template-directed synthesis of 1D nanomaterials.[176] (**C**) Illustration of possible compositions of 1D organic-inorganic hybrid nanostructures.[173]

Pioneering works of Lieber *et al.*, Xia *et al.* and Yang *et al.* pushed the field of 1D hybrid materials immensely.[177-181] Whereas initial efforts were mainly aimed towards controlling the preparation steps and exploring the unique properties of the hybrid material, efforts are nowadays aimed at using the established preparation techniques to produce large amounts (upscaling) of interesting materials and using them in novel nanodevices. The most promising and frequently used methods to prepare 1D hybrid nanostructures are elucidated in the following sections.

2.1 Template-Directed Approaches Toward One-Dimensional Hybrid Materials

Template-directed or template-assisted preparation methods are the most facile and mainly used methods to produce 1D hybrid materials. They allow a direct translation of a desired topology of the template into the hybrid material. This direct transfer is often simple, intuitive, versatile and straightforward. The template materials can be divided into two groups: soft and hard templates. Both bear advantages and disadvantages. Soft templates are usually organic materials, including polymers; whereas hard templates are made up of rigid inorganic materials. Classic organic templates are surfactants, block copolymers, CPBs and biological superstructures, such as DNA and viruses. Most soft template (except, DNA and viruses) can be produced in large numbers and are relatively cheap and easy to produce. Hard templates, on the other hand, are quite difficult and expensive to produce; however, they exhibit a superior uniformity and small feature sizes. Hard templates are mainly porous inorganic materials, such as anodized aluminium oxide (AAO).

2.1.1 Cylindrical Polymer Brushes as Soft Templates for Fabrication of One-Dimensional Hybrid Nanomaterials

One of the first examples for the template-directed synthesis of nanowires was reported by Schmidt *et al.*.[182] There, linear arrays of gold nanoclusters and nanowires were obtained by loading $AuCl_4^-$ ions into the hydrophilic core of core-shell PS-P2VP CPBs. A subsequent reduction generated gold nanoparticles *in-situ* and aligned them linearly within the CPB. Highly conductive nanowires were produced by polymerizing pyrrole within a P2VP core.[183] In both of the mentioned examples, the template brushes were synthesized via the ‘grafting-through’ approach. As discussed above, this method has some issues regarding the uniformity and purity of the obtained polymer brushes. This plays a significant role here again, as both criteria influence the quality of the produced hybrid materials.

In order to obtain more uniform nanomaterials, Müller *et al.* synthesized uniform core-shell CPBs via ‘grafting-from’ with ATRP, where the backbones were synthesized via anionic polymerization and had low PDIs. Through the incompatibility of each side chain block, the polymer brush can be divided into different 1D interior domains, with lengths up to several hundred nanometers, which can then be considered as ideal 1D nanoreactors for the synthesis of anisotropic hybrid and inorganic nanostructures. Many different template brushes were used as unimolecular soft templates for the fabrication of well-defined anisotropic nanomaterials. The prinicple is mostly the same: the core is able to coordinate or attach metal precursors, whereas the shell shields the nanoreactor core, protects the fabricated nanoparticles from agglomeration and guarantees sufficient solubility of the hybrid cylinders in various media. Accordingly, CPBs with a hydrophilic PAA core and a hydrophobic P*n*BA shell were used to obtain wire-like assemblies of semiconducting CdS[184], CdSe[185] and superparamagnetic iron oxide[186] nanoparticles (see Figure 1-10B). When the core was built up from a polyol like PHEMA, it was possible to fix a titania precursor ($Ti(OBu)_4$) via transalcoholysis. Subsequent condensation and calcination steps yielded crystalline TiO_2 (anatase) nanowires (see Figure 1-10A).[85] An elegant way of synthesizing silica nanowires was to use a monomer that already carried the inorganic components. Consequently, water-soluble core-shell CPBs were synthesized where the core consisted of poly(3-acryloylpropyl trimethoxysilane) (PAPTS) and the shell of poly[oligo(ethylene glycol) methyl ether methacrylate] (POEGMA).[187] After basic hydrolysis and condensation, the PAPTS core was transformed into a silsequioxane network, which resulted in water-soluble $SiO_{1.5}$ nanowires.

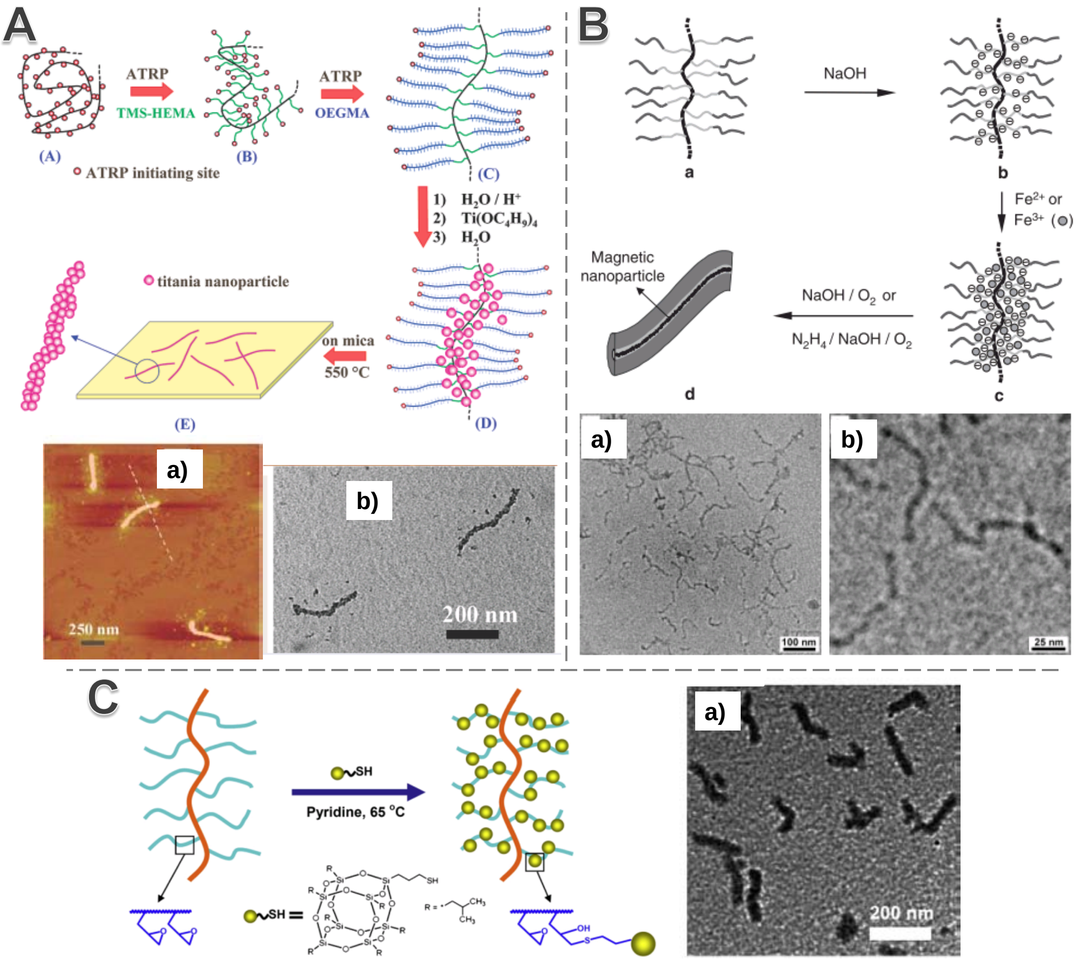

Figure 1-10. (**A**) The synthesis route towards anatase nanowires via PHEMA-POEGMA core-shell CPBs as templates. (**a**) AFM and (**b**) TEM images of hybrid titania CPBs after hydrolysis of the titania precursor within the core.[85] (**B**) PAA-PBA core-shell CPBs were used for the synthesis of superparamagnetic nanowires.[186] (**C**) PGMA homopolymer CPBs react with mono-functionalized POSS to result in POSS loaded CPBs.[86]

Analogous to block copolymer brushes, homopolymer brushes with functional groups can be uitilized for the synthesis of nanowires. Due to the missing shielding shell, it is more challenging to avoid intermolecular crosslinking. A way to bypass the issue of crosslinking was reported by Müller *et al.*, where they used poly(glycidyl methacrylate)

(PGMA) homopolymer brushes and mono-functionalized polyhedral oligomeric silsesquioxane (POSS).[86] Each POSS cage was equipped with only one thiol group. One thiol group reacted only with one glyicidyl group and convalently bonded upon ring opening. PGMA cannot react with itself and thus crosslinking was avoided (see Figure 1-10C).

2.1.2 Self-Assembled One-Dimensional Templates from Solution

The self-assembly of organic molecules and macromolecules can be used to form 1D templates, which can be used for the fabrication of hybrid materials. Solution-based self-assembly of surfactants and block copolymers may result in anisotropic micelles. Surfactants can organize into rod-like micelles when their concentration reaches a critical value.[188] Anisotropic micelles can be used for the synthesis of metal and metal oxide nanostructures, such as rods, wires and tubes. Murphy *et al.* reported the synthesis of gold nanorods using cylindrical micelles of hexadecyltrimethylammonium bromide (CTAB).[189,190] Cylindrical micelles of sodium dodecyl sulphate (SDS) were used for the synthesis of porous α-Fe_2O_3 nanorods.[191] With non-ionic surfactants, like nona(ethylenglycol) monododecyl ether ($C_{12}EO_9$) and polyoxyethylene sorbitan monostearate (Tween 60), it was possible to synthesize platinum, palladium and silver nanotubes from liquid-crystalline phases of cylindrical micelles.[192] Polyoxyethylene(20) cetyl ether (Brij 58) produced reverse micelles in cyclohexane, where the hydrophilic PEG core was then used as a nanoreactor for the synthesis of nickel nanorods. The nanorods themselves served as templates for the fabrication of uniform silica nanotubes (see Figure 1-11A).[193]

Similar to surfactants, linear block copolymers are also able to form cylindrical micelles in solution. The formation of cylindrical micelles is dependent on the block copolymer composition and the concentration. It further depends on external stimuli such as temperature or solvent-selectivity. Block copolymers can self-assemble into various morphologies in solution, such as micelles, vesicles and worm-like structures.[194,195] The worm-like micelles can be used as soft templates for the formation of 1D hybrid nanostructures. Eisenberg *et al.* produced a loose necklace of quantum dots (QDs) within PEO-PS-PAA triblock terpolymer cylindrical micelles.[196] The cylindrical morphology was obtained by the self-assembly of the triblock terpolymer in the presence of Cd^{2+} ions, which were complexed by the PAA block. Consequently, the PAA core of the micelles was ‘ionically crosslinked’. Conversion of the Cd^{2+} ions into CdS via H_2S gas led to the 1D alignment of CdS QDs.

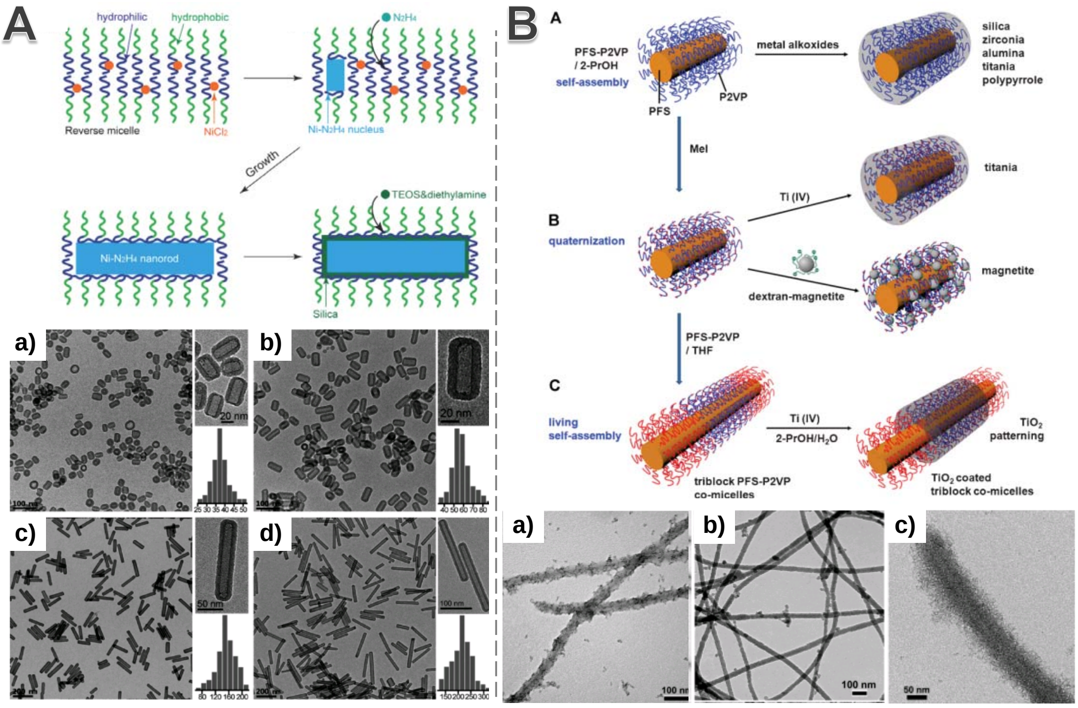

Figure 1-11. (**A**) Reverse cylindrical surfactant micelles of Brij 58 were used for the synthesis of nickel nanorods, which were used as a template to produce uniform silica nanotubes with different aspect ratios (see TEM micrographs).[193] (**B**) Cylindrical diblock copolymer micelles from PFS-P2VP diblock copolymers and the possible hybrid formation of inorganic material within the P2VP shell. The TEM micrographs show hybrid cylinders with (**a**) a titania and (**b**) a silica shell. Further, (**c**) dextran-covered magnetite nanoparticles were infiltrated into the shell after quaternization.[198]

Most micelles obtained from surfactants lack a distinct shell around the core, whereas cylindrical micelles are built up of a core and a shell. Accordingly, it is possible to also use the shell of cylindrical polymer micelles to form hybrid materials, and not only the core segment. Winnik and Manners *et al.* carried out pioneering research in polymerizing various iron-containing monomers, such as ferrocenyldimethylsilane.[22,197-202] The common characteristic of the corresponding polymers is their ability to crystallize into rod-like objects. For example, cylindrical micelles from the diblock copolymer poly(ferrocenyldimethylsilane)-*b*-poly(2-vinylpyridine) (PFS-P2VP) were used to form tubular metal oxide nanostructures.[198] Since PFS was forming the core of the micelle and P2VP was forming the shell of the micelle, it was possible to use the P2VP shell for sol-gel chemistry to form silica, zirconia, alumina and titania shells. Dextran covered magnetite nanoparticles were also complexed into the quaternized P2VPq shell (see Figure 1-11B). This crystallization-induced cylindrical template formation displays the characteristics of a living process.[24,203] Hence, it was possible to grow block-type cylindrical micelles where only a certain block were hybridized in a controlled way.[24]

2.1.3 Self-Assembled One-Dimensional Templates from Bulk

As illustrated above, block copolymers can be used as soft templates as they can form 1D nanostructures in solution due to their different or incompatible blocks. The incompatibility of blocks is a necessity for the micro-phase separation of block copolymers in thin films. Phase-separated block copolymers have been studied extensively for the fabrication of hybrid and inorganic materials.[204-207] Diblock copolymers can phase-separate into a cylindrical morphology, as illustrated in Scheme 1-1C, and can be used as 1D soft templates after crosslinking of the cylindrical domain. Template CPBs from PB-P2VP were used to produce polyoxometalate nanostructures after loading the P2VP corona with oppositely charged $[SiMo_{12}O_{40}]^{4-}$ Keggin ions (see Figure 1-12A).[175] Chen *et al.* used silicon containing and gel-able monomers to synthesize block copolymers where the crosslinked silsesquioxane ($SiO_{1.5}$) products themselves can be considered as hybrid materials. $SiO_{1.5}$ nanowires and tubes have been prepared from bulk thin films.[208-210] Poly(3-(triethoxysilyl)propyl methacrylate)-*block*-poly(2-vinylpyridine) (PTEPM-P2VP) was used for the synthesis of $SiO_{1.5}$ nanowires with a P2VP shell, which were used in a subsequent step to immobilize gold nanoparticles within the shell.[210] $SiO_{1.5}$ nanotubes were obtained in the case of an ABC triblock terpolymer where the middle block B consisted out of PTEPM.[208] Depending on the preparation of the bulk film, block A (PS) could be the outer corona and block C (P2VP) could be in the core, or vice versa (see Figure 1-12B). P2VP was again used for further immobilization of nanoparticles.[208]

The concept of ABC triblock terpolymers phase separation was also applied by Liu *et al.* to obtain polymeric nanotubes where the tube-forming block B (PCEMA) was photo-crosslinkable .[211-215] Depending on the core-forming polymer block, various 1D hybrid nanostructures were synthesized. In the case of a PAA core, Yan *et al.* produced water-dispersible polymer/Pd/Ni hybrid magnetic nanofibers by sequential filling of the core with Pd and Ni.[213] They further reported γ-Fe_2O_3 hybrid magnetic nanofibers following a similar procedure.[211]

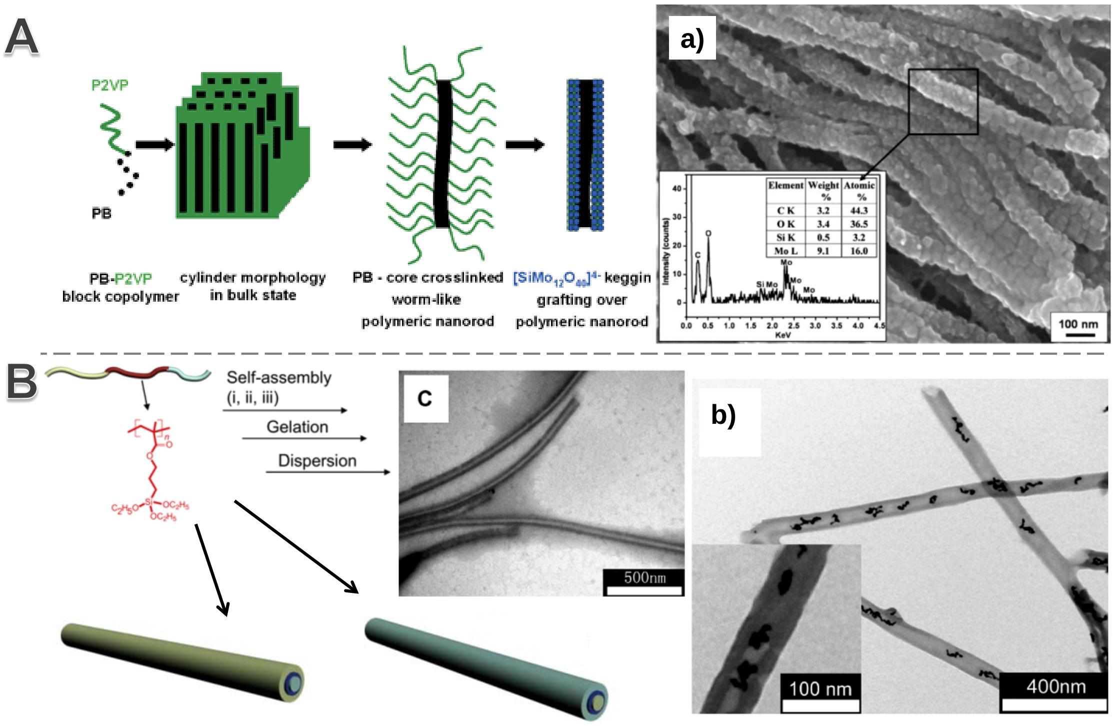

Element	Weight %	Atomic %
C K	3.2	44.3
O K	3.4	36.5
Si K	0.5	3.2
Mo L	9.1	16.0

Figure 1-12. (**A**) The synthetic strategy for the fabrication of Keggin ion nanostructures, including a SEM image of the hybrid nanofibers.[175] (**B**) The self-assembly of ABC triblock terpolymers that contain a gel-able middle block can form (**a**) nanotubes in bulk thin films. (**b**) Nanotubes with a P2VP core were filled with gold nanoparticles.[208]

2.1.4 Biological and Other One-Dimensional Templates

Polymeric soft templates need to be shaped into 1D morphology by experimental efforts. However, nature provides already pre-existing 1D nanostructures that can be used for template chemistries. Typical examples of biological nanostructures that consist of building blocks that are aligned one-dimensionally are cellulose,[216] collagen,[217] DNA[218-222] and various viruses.[223-227] The most famous soft template is the tobacco mosaic virus (TMV), which is very uniform in length and diameter. TMV was, for example, used to synthesize CdS, SiO_2 and TiO_2 nanowires (see Figure 1-13A).[225,227] Next to TMV, DNA often finds use as a template material. Co nanowires were grown on Pd nanoparticles seeded DNA.[228]

Similar to biological systems, there are other 1D nanostructures that can be applied in template-assisted and template-directed hybridization reactions. Currently existing inorganic, organic and even hybrid 1D objects are useful as templates in their unmodified states. The most frequently used among the many available 1D structures are carbon nanotubes (CNTs). Their straightforward functionalization led to numerous works on polymer-coated CNTs.[229-231] These polymer coatings can then again be used for hybridization. For example, gold nanoparticles were attached to poly(diallyl-dimethylammonium)chloride (PDADMAC) covered CNTs (see Figure 1-13B).[232] PDMAEMA-covered multi-walled CNTs (MWCNTs) were able to be used for the synthesis of worm-like silica nanotubes.[233] Other 1D objects, such as nickel nanorods, were applied in several strategies to obtain hybrid materials.[193,234]

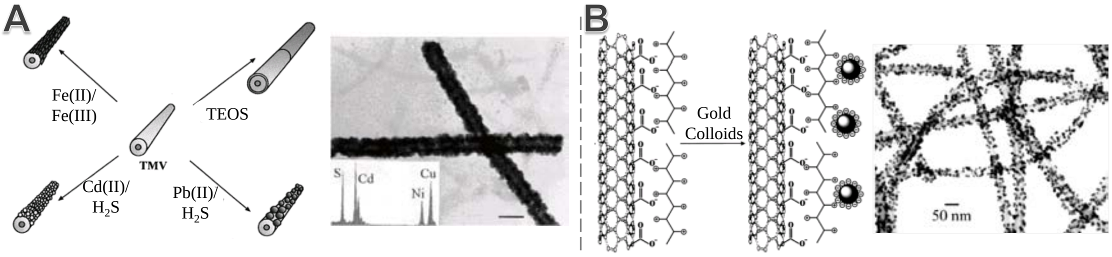

Figure 1-13. (**A**) TMV was used to produce various 1D hybrid material, such as CdS nanowires (see TEM micrograph).[225] (**B**) PDADMAC-covered CNTs were used to align gold nanoparticles into a 1D manner (see TEM micrograph).[232]

2.2 Porous Membrane-Based Templates

The use of porous membranes, such as AAO, track-etched polycarbonate membranes or mesoporous silica, gave rise to simple and straightforward methods for the preparation of 1D nanomaterials. The main advantage of such porous templates with cylindrical pores is the superior uniformity of pore diameters, which can be adjusted during the preparation method. Many 1D materials have been synthesized, including metals,[235] oxides,[236] semiconductors[237] and polymers.[235] The process of filling the pores is highly variable and can be easily controlled, which consequently allows the synthesis of very complex nanostructures. However, when compared to the abovementioned soft templating techniques, it is quite difficult to obtain large amounts of materials from such approaches.

2.3 Electrospinning

Electrospinning is not a templating technique per se; however, it should be mentioned as it is a highly versatile method for the production of 1D hybrid materials. With electrospinning, it became possible to synthesize ultra-thin nanowires or nanofibers. From many polymer melts or solutions, fibers have been produced via electrospinning processes. By adding inorganic materials or precursors into the melts and mixtures, hybrid nanomaterials of defined thickness have been obtained, either directly or after a subsequent step. Combined with sol-gel chemistry, many polymer-metal oxide hybrid fibers have been synthesized by electrospinning, such as poly(vinylpyrrolidone)/TiO_2 (PVP/TiO_2) or PVP/ZrO_2 hybrids.[238] Furthermore, inorganic materials, like ZnO[239,240] or CdS[241], have been blended into polymeric nanofibers. Greiner *et al.* used electrospun PLA fibers as templates for the fabrication of TiO_2 and Pd tubes [242,243]

3. Aim of the Thesis

The motivation of this work was to broaden the application range of CPBs as templates for the preparation of novel 1D polymer-inorganic hybrid nanomaterials. It was intended that molecular core-shell or core-shell-corona CPBs, plus CPBs obtained through microphase separation of diblock copolymers, be used for the synthesis of new 1D hybrid materials.

Core-shell-corona CPBs containing a gelable shell block were to be synthesized in order to directly incorporate the inorganic part into the polymer brush structure. This would be a novel way of synthesizing uniform hybrid nanotubes.

Core-shell(-corona) CPBs with a degradable core were to be synthesized for the production of hollow inorganic nanomaterials with high aspect ratios. Hollow/porous nanostructures from silica or titania were of particular interest, as they can be used as carrier systems (SiO_2) or in photovoltaic applications and catalysis (TiO_2).

Mesoscopic polyelectrolyte core-shell CPBs were to be designed for the hierarchical 1D structuring of metal oxide nanoparticles. It was intended that these new materials, which are interesting for photovoltaic applications and catalysis, be achieved by the synthesis of anisotropic crystalline TiO_2 nanostructures.

References

(1) Liang, H.-W.; Liu, S.; Yu, S.-H. *Adv. Mater.* **2010**, *22*, 3925-3937.

(2) Peng, X.; Manna, L.; Yang, W.; Wickham, J.; Scher, E.; Kadavanich, A.; Alivisatos, A. P. *Nature* **2000**, *404*, 59-61.

(3) Buhro, W. E.; Colvin, V. L. *Nat. Mater.* **2003**, *2*, 138-139.

(4) Burda, C.; Chen, X.; Narayanan, R.; El-Sayed, M. A. *Chem. Rev.* **2005**, *105*, 1025-1102.

(5) Milner, S. T. *Science* **1991**, *251*, 905-914.

(6) Zhang, M.; Müller, A. H. E. *J. Polym. Sci. Part A: Polym. Chem.* **2005**, *43*, 3461-3481.

(7) Advincula, R. C.; Brittain, W. J.; Kenneth, C. C.; Rühe, J. *Polymer Brushes*; Wiley-VCH Verlag Weinheim, 2004.

(8) Djalali, R.; Hugenberg, N.; Fischer, K.; Schmidt, M. *Macromol. Rapid Commun.* **1999**, *20*, 444-449.

(9) Tsukahara, Y.; Mizuno, K.; Segawa, A.; Yamashita, Y. *Macromolecules* **1989**, *22*, 1546-1552.

(10) Tsukahara, Y.; Tsutsumi, K.; Yamashita, Y.; Shimada, S. *Macromolecules* **1990**, *23*, 5201-5208.

(11) Ruokolainen, J.; Tanner, J.; ten Brinke, G.; Ikkala, O.; Torkkeli, M.; Serimaa, R. *Macromolecules* **1995**, *28*, 7779-7784.

(12) Ruokolainen, J.; Torkkeli, M.; Serimaa, R.; Komanschek, E.; ten Brinke, G.; Ikkala, O. *Macromolecules* **1997**, *30*, 2002-2007.

(13) Antonietti, M.; Conrad, J.; Thuenemann, A. *Macromolecules* **1994**, *27*, 6007-6011.

(14) Ikkala, O.; Ruokolainen, J.; ten Brinke, G.; Torkkeli, M.; Serimaa, R. *Macromolecules* **1995**, *28*, 7088-7094.

(15) Liu, G. *Adv. Mater.* **1997**, *9*, 437-439.

(16) Ishizu, K.; Ikemoto, T.; Ichimura, A. *Polymer* **1999**, *40*, 3147-3151.

(17) Liu, G.; Qiao, L.; Guo, A. *Macromolecules* **1996**, *29*, 5508-5510.

(18) Liu, Y.; Abetz, V.; Müller, A. H. E. *Macromolecules* **2003**, *36*, 7894-7898.

(19) Won, Y. Y.; Davis, H. T.; Bates, F. S. *Science* **1999**, *283*, 960-963.

(20) Tao, J.; Stewart, S.; Liu, G. J.; Yang, M. L. *Macromolecules* **1997**, *30*, 2738-2745.

(21) Ishizu, K.; Tsubaki, K.; Mori, A.; Uchida, S. *Prog. Polym. Sci.* **2003**, *28*, 27-54.

(22) Wang, X.; Guerin, G.; Wang, H.; Wang, Y.; Manners, I.; Winnik, M. A. *Science* **2007**, *317*, 644-647.

(23) Schmalz, H.; Schmelz, J.; Drechsler, M.; Yuan, J.; Walther, A.; Schweimer, K.; Mihut, A. M. *Macromolecules* **2008**, *41*, 3235-3242.

(24) Gadt, T.; Ieong, N. S.; Cambridge, G.; Winnik, M. A.; Manners, I. *Nat. Mater.* **2009**, *8*, 144-150.

(25) Qian, J.; Zhang, M.; Manners, I.; Winnik, M. A. *Trends Biotechnol.* **2010**, *28*, 84-92.

(26) Matyjaszewski, K.; Xia, J. *Chem. Rev.* **2001**, *101*, 2921-2990.

(27) Rempp, P.; Franta, E. *Macromonomers: Synthesis, characterization and applications* Springer Berlin / Heidelberg, 1984; Vol. 58.

(28) Yamada, K.; Miyazaki, M.; Ohno, K.; Fukuda, T.; Minoda, M. *Macromolecules* **1998**, *32*, 290-293.

(29) Asami, R.; Takaki, M.; Moriyama, Y. *Polym. Bull.* **1986**, *16*, 125-130.

(30) Heroguez, V.; Gnanou, Y.; Fontanille, M. *Macromolecules* **1997**, *30*, 4791-4798.

(31) Wintermantel, M.; Gerle, M.; Fischer, K.; Schmidt, M.; Wataoka, I.; Urakawa, H.; Kajiwara, K.; Tsukahara, Y. *Macromolecules* **1996**, *29*, 978-983.

(32) Rempp, P.; Lutz, P.; Masson, P.; Chaumont, P. *Die Makromolekulare Chemie* **1985**, *13*, 47-66.

(33) Tsukahara, Y.; Inoue, J.; Ohta, Y.; Kohjiya, S.; Okamoto, Y. *Polym. J.* **1994**, *26*, 1013-1018.

(34) Pantazis, D.; Chalari, I.; Hadjichristidis, N. *Macromolecules* **2003**, *36*, 3783-3785.

(35) Kanaoka, S.; Sueoka, M.; Sawamoto, M.; Higashimura, T. *J. Polym Sci Part A: Polym Chem* **1993**, *31*, 2513-2521.

(36) Li, Z.; Zhang, K.; Ma, J.; Cheng, C.; Wooley, K. L. *J. Polym. Sci. Part A: Polym. Chem.* **2009**, *47*, 5557-5563.

(37) Dubois, P.; Coulembier, O.; Raquez, J.-M. *Handbook of Ring-Opening Polymerization*; Wiley-VCH Verlag Weinheim, 2009.

(38) Heroguez, V. r.; Breunig, S.; Gnanou, Y.; Fontanille, M. *Macromolecules* **1996**, *29*, 4459-4464.

(39) Neiser, M. W.; Okuda, J.; Schmidt, M. *Macromolecules* **2003**, *36*, 5437-5439.

(40) Mecerreyes, D.; Dahan, D.; Lecomte, P.; Dubois, P.; Demonceau, A.; Noels, A. F.; Jérôme, R. *J. Polym. Sci. Part A: Polym. Chem.* **1999**, *37*, 2447-2455.

(41) Xia, Y.; Kornfield, J. A.; Grubbs, R. H. *Macromolecules* **2009**, *42*, 3761-3766.

(42) Johnson, J. A.; Lu, Y. Y.; Burts, A. O.; Lim, Y.-H.; Finn, M. G.; Koberstein, J. T.; Turro, N. J.; Tirrell, D. A.; Grubbs, R. H. *J. Am. Chem. Soc.* **2011**, *133*, 559-566.

(43) Jha, S.; Dutta, S.; Bowden, N. B. *Macromolecules* **2004**, *37*, 4365-4374.

(44) Cheng, C.; Yang, N.-L. *Macromolecules* **2010**, *43*, 3153-3155.

(45) Pitsikalis, M.; Sioula, S.; Pispas, S.; Hadjichristidis, N.; Cook, D. C.; Li, J.; Mays, J. W. *J. Polym. Sci. Part A: Polym. Chem.* **1999**, *37*, 4337-4350.

(46) Hirao, A.; Kawano, H.; Ryu, S. W. *Polym. Adv. Technol.* **2002**, *13*, 275-284.

(47) Hadjichristidis, N.; Pitsikalis, M.; Pispas, S.; Iatrou, H. *Chem. Rev.* **2001**, *101*, 3747-3792.

(48) George, M. H.; Majid, M. A.; Barrie, J. A.; Rezaian, I. *Polymer* **1987**, *28*, 1217-1220.

(49) Watanabe, H.; Amemiya, T.; Shimura, T.; Kotaka, T. *Macromolecules* **1994**, *27*, 2336-2338.

(50) Selb, J.; Gallot, Y. *Polymer* **1979**, *20*, 1273-1280.

(51) Gromadzki, D.; Jigounov, A.; Stepánek, P.; Makuska, R. *Eur. Polym. J.* **2010**, *46*, 804-813.

(52) Huisgen, R. *Proceed. Chem. Soc.* **1961**, 357-396.

(53) Kolb, H. C.; Finn, M. G.; Sharpless, K. B. *Angew. Chem. Int. Ed.* **2001**, *40*, 2004-2021.

(54) Tornoe, C. W.; Christensen, C.; Meldal, M. *J. Org. Chem.* **2002**, *67*, 3057-3064.

(55) Rostovtsev, V. V.; Green, L. G.; Fokin, V. V.; Sharpless, K. B. *Angew. Chem. Int. Ed.* **2002**, *41*, 2596-2599.

(56) Engler, A. C.; Lee, H.-i.; Hammond, P. T. *Angew. Chem. Int. Ed.* **2009**, *48*, 9334-9338.

(57) Gao, H.; Matyjaszewski, K. *J. Am. Chem. Soc.* **2007**, *129*, 6633-6639.

(58) Jiang, X.; Lok, M. C.; Hennink, W. E. *Bioconjug. Chem.* **2007**, *18*, 2077-2084.

(59) Tal'roze, R. V.; Kuptsov, S. A.; Sycheva, T. I.; Bezborodov, V. S.; Plate, N. A. *Macromolecules* **1995**, *28*, 8689-8691.

(60) Huh, J.; Ikkala, O.; ten Brinke, G. *Macromolecules* **1997**, *30*, 1828-1835.

(61) Fredrickson, G. H. *Macromolecules* **1993**, *26*, 2825-2831.

(62) Bazuin, C. G.; Tork, A. *Macromolecules* **1995**, *28*, 8877-8880.

(63) Venkatesh, R.; Yajjou, L.; Koning, C. E.; Klumperman, B. *Macromol. Chem. Phys.* **2004**, *205*, 2161-2168.

(64) Beers, K. L.; Gaynor, S. G.; Matyjaszewski, K.; Sheiko, S. S.; Möller, M. *Macromolecules* **1998**, *31*, 9413-9415.

(65) Lian, X.; Wu, D.; Song, X.; Zhao, H. *Macromolecules* **2010**, *43*, 7434-7445.

(66) Cheng, G.; Böker, A.; Zhang, M.; Krausch, G.; Müller, A. H. E. *Macromolecules* **2001**, *34*, 6883-6888.

(67) Wu, D.; Song, X.; Tang, T.; Zhao, H. *J. Polym. Sci. Part A: Polym. Chem.* **2010**, *48*, 443-453.

(68) Mori, H.; Wakisaka, O.; Hirao, A.; Nakahama, S. *Macromol. Chem. Phys.* **1994**, *195*, 3213-3224.

(69) Zhang, M.; Breiner, T.; Mori, H.; Müller, A. H. E. *Polymer* **2003**, *44*, 1449-1458.

(70) Fleet, R.; van den Dungen, E. T. A.; Klumperman, B. *S. Afr. J. Sci.* **2011**, *107*.

(71) Börner, H. G.; Beers, K.; Matyjaszewski, K.; Sheiko, S. S.; Müller, M. *Macromolecules* **2001**, *34*, 4375-4383.

(72) Gromadzki, D.; Filippov, S.; Netopilik, M.; Makuska, R.; Jigounov, A.; Plestil, J.; Horsky, J.; Stepanek, P. *Eur. Polym. J.* **2009**, *45*, 1748-1758.

(73) Gromadzki, D.; Makuska, R.; Netopilik, M.; Holler, P.; Lokaj, J.; Janata, M.; Stepanek, P. *Eur. Polym. J.* **2008**, *44*, 59-71.

(74) Nomura, K.; Abdellatif, M. M. *Polymer* **2010**, *51*, 1861-1881.

(75) Guo, S.; Wang, W.; Deng, L.; Xing, J.; Dong, A. *Macromol. Chem. Phys.* **2010**, *211*, 1572-1578.

(76) Pietrasik, J.; Sumerlin, B. S.; Lee, R. Y.; Matyjaszewski, K. *Macromol. Chem. Phys.* **2007**, *208*, 30-36.

(77) Lee, H.-i.; Pietrasik, J.; Matyjaszewski, K. *Macromolecules* **2006**, *39*, 3914-3920.

(78) Yuan, J.; Xu, Y.; Walther, A.; Bolisetty, S.; Schumacher, M.; Schmalz, H.; Ballauff, M.; Müller, A. H. E. *Nat. Mater.* **2008**, *7*, 718-722.

(79) Cheng, C.; Khoshdel, E.; Wooley, K. L. *Macromolecules* **2007**, *40*, 2289-2292.

(80) Cheng, C.; Qi, K.; Khoshdel, E.; Wooley, K. L. *J. Am. Chem. Soc.* **2006**, *128*, 6808-6809.

(81) Fan, X.; Wang, G.; Zhang, Z.; Huang, J. *J. Polym. Sci. Part A: Polym. Chem.* **2011**, *49*, 4146-4153.

(82) Lee, H.-i.; Jakubowski, W.; Matyjaszewski, K.; Yu, S.; Sheiko, S. S. *Macromolecules* **2006**, *39*, 4983-4989.

(83) Huang, K.; Rzayev, J. *J. Am. Chem. Soc.* **2009**, *131*, 6880-6885.

(84) Huang, K.; Canterbury, D. P.; Rzayev, J. *Chem. Commun.* **2010**, *46*, 6326-6328.

(85) Yuan, J.; Lu, Y.; Schacher, F.; Lunkenbein, T.; Weiss, S.; Schmalz, H.; Müller, A. H. E. *Chem. Mater.* **2009**, *21*, 4146-4154.

(86) Xu, Y.; Yuan, J.; Müller, A. H. E. *Polymer* **2009**, *50*, 5933-5939.

(87) Xu, Y.; Walther, A.; Müller, A. H. E. *Macromol. Rapid Commun.* **2010**, *31*, 1462-1466.

(88) Müllner, M.; Yuan, J.; Weiss, S.; Walther, A.; Förtsch, M.; Drechsler, M.; Müller, A. H. E. *J. Am. Chem. Soc.* **2010**, *132*, 16587-16592.

(89) Xu, Y.; Becker, H.; Yuan, J.; Burkhardt, M.; Zhang, Y.; Walther, A.; Bolisetty, S.; Ballauff, M.; Müller, A. H. E. *Macromol. Chem. Phys.* **2007**, *208*, 1666-1675.

(90) Xu, Y.; Yuan, J.; Fang, B.; Drechsler, M.; Müllner, M.; Bolisetty, S.; Ballauff, M.; Müller, A. H. E. *Adv. Funct. Mater.* **2010**, *20*, 4182-4189.

(91) Neugebauer, D.; Sumerlin, B. S.; Matyjaszewski, K.; Goodhart, B.; Sheiko, S. S. *Polymer* **2004**, *45*, 8173-8179.

(92) Yu-Su, S. Y.; Sheiko, S. S.; Lee, H.-i.; Jakubowski, W.; Nese, A.; Matyjaszewski, K.; Anokhin, D.; Ivanov, D. A. *Macromolecules* **2009**, *42*, 9008-9017.

(93) Tsubaki, K.; Ishizu, K. *Polymer* **2001**, *42*, 8387-8393.

(94) Ishizu, K.; Tsubaki, K.-i.; Ono, T. *Polymer* **1998**, *39*, 2935-2939.

(95) Tang, C.; Dufour, B.; Kowalewski, T.; Matyjaszewski, K. *Macromolecules* **2007**, *40*, 6199-6205.

(96) Yuan, J.; Drechsler, M.; Xu, Y.; Zhang, M.; Müller, A. H. E. *Polymer* **2008**, *49*, 1547-1554.

(97) Polotsky, A.; Charlaganov, M.; Xu, Y.; Leermakers, F. A. M.; Daoud, M.; Müller, A. H. E.; Dotera, T.; Borisov, O. *Macromolecules* **2008**, *41*, 4020-4028.

(98) Ishizu, K.; Toyoda, K.; Furukawa, T.; Sogabe, A. *Macromolecules* **2004**, *37*, 3954-3957.

(99) Ishizu, K.; Sawada, N.; Satoh, J.; Sogabe, A. *J. Mater. Sci. Lett.* **2003**, *22*, 1219-1222.

(100) Stephan, T.; Muth, S.; Schmidt, M. *Macromolecules* **2002**, *35*, 9857-9860.

(101) Schmelz, J.; Drechsler, M.; Yuan, J.; Walther, A.; Schmalz, H. *PMSE Prepr.* **2008**, *99*, 680-681.

(102) Schmelz, J.; Karg, M.; Hellweg, T.; Schmalz, H. *ACS Nano* **2011**, *5*, 9523-9534.

(103) Ishizu, K.; Satoh, J.; Sogabe, A. *J. Colloid Interface Sci.* **2004**, *274*, 472-479.

(104) Lee, H.-i.; Matyjaszewski, K.; Yu-Su, S.; Sheiko, S. S. *Macromolecules* **2008**, *41*, 6073-6080.

(105) Rzayev, J. *Macromolecules* **2009**, *42*, 2135-2141.

(106) Bolton, J.; Rzayev, J. *ACS Macro Letters* **2012**, *1*, 15-18.

(107) Börner, H. G.; Duran, D.; Matyjaszewski, K.; da Silva, M.; Sheiko, S. S. *Macromolecules* **2002**, *35*, 3387-3394.

(108) Neugebauer, D. *Polymer* **2007**, *48*, 4966-4973.

(109) Neugebauer, D.; Theis, M.; Pakula, T.; Wegner, G.; Matyjaszewski, K. *Macromolecules* **2005**, *39*, 584-593.

(110) Lord, S. J.; Sheiko, S. S.; LaRue, I.; Lee, H.-I.; Matyjaszewski, K. *Macromolecules* **2004**, *37*, 4235-4240.

(111) Neugebauer, D.; Zhang, Y.; Pakula, T.; Sheiko, S. S.; Matyjaszewski, K. *Macromolecules* **2003**, *36*, 6746-6755.

(112) Schappacher, M.; Deffieux, A. *Science* **2008**, *319*, 1512-1515.

(113) Mijovic, J.; Sun, M.; Pejanovic, S.; Mays, J. W. *Macromolecules* **2003**, *36*, 7640-7651.

(114) Zhao, L.; Byun, M.; Rzayev, J.; Lin, Z. *Macromolecules* **2009**, *42*, 9027-9033.

(115) Kaneko, T.; Horie, T.; Asano, M.; Aoki, T.; Oikawa, E. *Macromolecules* **1997**, *30*, 3118-3121.

(116) Percec, V.; Ahn, C. H.; Barboiu, B. *J. Am. Chem. Soc.* **1997**, *119*, 12978-12979.

(117) Schlüter, A. D.; Rabe, J. P. *Angew. Chem. Int. Ed.* **2000**, *39*, 864-883.

(118) Ouali, N.; Méry, S.; Skoulios, A.; Noirez, L. *Macromolecules* **2000**, *33*, 6185-6193.

(119) Guo, Y.; van Beek, J. D.; Zhang, B.; Colussi, M.; Walde, P.; Zhang, A.; Kröger, M.; Halperin, A.; Dieter Schlüter, A. *J. Am. Chem. Soc.* **2009**, *131*, 11841-11854.

(120) Roeser, J.; Moingeon, F.; Heinrich, B.; Masson, P.; Arnaud-Neu, F.; Rawiso, M.; Méry, S. *Macromolecules* **2011**, *44*, 8925-8935.

(121) Schappacher, M.; Deffieux, A. *Macromolecules* **2000**, *33*, 7371-7377.

(122) Matyjaszewski, K.; Qin, S.; Boyce, J. R.; Shirvanyants, D.; Sheiko, S. S. *Macromolecules* **2003**, *36*, 1843-1849.

(123) Lahasky, S. H.; Serem, W. K.; Guo, L.; Garno, J. C.; Zhang, D. *Macromolecules* **2011**, ASAP.

(124) Yuan, J., Universität Bayreuth, 2008.

(125) Liu, G. J.; Li, Z.; Yan, X. H. *Polymer* **2003**, *44*, 7721-7727.

(126) Liu, G. *Macromolecular Symposia* **1997**, *113*, 233-248.

(127) Sheiko, S. S.; Sumerlin, B. S.; Matyjaszewski, K. *Prog. Polym. Sci.* **2008**, *33*, 759-785.

(128) Saariaho, M.; Ikkala, O.; Szleifer, I.; Erukhimovich, I.; Ten Brinke, G. *J. Chem. Phys.* **1997**, *107*, 3267.

(129) Sheiko, S. S.; da Silva, M.; Shirvaniants, D.; LaRue, I.; Prokhorova, S.; Moeller, M.; Beers, K.; Matyjaszewski, K. *J. Am. Chem. Soc.* **2003**, *125*, 6725-6728.

(130) Gunari, N.; Schmidt, M.; Janshoff, A. *Macromolecules* **2006**, *39*, 2219-2224.

(131) Boyce, J. R.; Shirvanyants, D.; Sheiko, S. S.; Ivanov, D. A.; Qin, S.; Börner, H.; Matyjaszewski, K. *Langmuir* **2004**, *20*, 6005-6011.

(132) Subbotin, A.; Saariaho, M.; Stepanyan, R.; Ikkala, O.; ten Brinke, G. *Macromolecules* **2000**, *33*, 6168-6173.

(133) Terao, K.; Farmer, B. S.; Nakamura, Y.; Iatrou, H.; Hong, K.; Mays, J. W. *Macromolecules* **2005**, *38*, 1447-1450.

(134) Subbotin, A.; Saariaho, M.; Ikkala, O.; ten Brinke, G. *Macromolecules* **2000**, *33*, 3447-3452.

(135) Rathgeber, S.; Pakula, T.; Wilk, A.; Matyjaszewski, K.; Lee, H.-i.; Beers, K. L. *Polymer* **2006**, *47*, 7318-7327.

(136) Feuz, L.; Leermakers, F. A. M.; Textor, M.; Borisov, O. *Macromolecules* **2005**, *38*, 8891-8901.

(137) Murat, M.; Grest, G. S. *Macromolecules* **1991**, *24*, 704-708.

(138) Rouault, Y.; Borisov, O. V. *Macromolecules* **1996**, *29*, 2605-2611.

(139) Saariaho, M.; Subbotin, A.; Szleifer, I.; Ikkala, O.; ten Brinke, G. *Macromolecules* **1999**, *32*, 4439-4443.

(140) Cao, Q.; Zuo, C.; Li, L.; He, H. *Soft Matter* **2011**, *7*, 6522-6528.

(141) Theodorakis, P. E.; Paul, W.; Binder, K. *Macromolecules* **2010**, *43*, 5137-5148.

(142) Wataoka, I.; Urakawa, H.; Kajiwara, K.; Schmidt, M.; Wintermantel, M. *Polym. Internat.* **1997**, *44*, 365-370.

(143) Fischer, K.; Schmidt, M. *Macromol. Rapid Commun.* **2001**, *22*, 787-791.

(144) Gerle, M.; Fischer, K.; Roos, S.; Müller, A. H. E.; Schmidt, M.; Sheiko, S. S.; Prokhorova, S.; Möller, M. *Macromolecules* **1999**, *32*, 2629-2637.

(145) Terao, K.; Nakamura, Y.; Norisuye, T. *Macromolecules* **1999**, *32*, 711-716.

(146) Lecommandoux, S.; Chécot, F.; Borsali, R.; Schappacher, M.; Deffieux, A.; Brûlet, A.; Cotton, J. P. *Macromolecules* **2002**, *35*, 8878-8881.

(147) Zhang, B.; Gröhn, F.; Pedersen, J. S.; Fischer, K.; Schmidt, M. *Macromolecules* **2006**, *39*, 8440-8450.

(148) Schoot, P. *J. Chem. Phys.* **1996**, *104*, 1130.

(149) Wintermantel, M.; Fischer, K.; Gerle, M.; Ries, R.; Schmidt, M.; Kajiwara, K.; Urakawa, H.; Wataoka, I. *Angew. Chem. Int. Ed.* **1995**, *34*, 1472-1474.

(150) Li, C.; Gunari, N.; Fischer, K.; Janshoff, A.; Schmidt, M. *Angew. Chem. Int. Ed.* **2004**, *43*, 1101-1104.

(151) Yamamoto, S.-i.; Pietrasik, J.; Matyjaszewski, K. *Macromolecules* **2008**, *41*, 7013-7020.

(152) Xu, Y.; Bolisetty, S.; Drechsler, M.; Fang, B.; Yuan, J.; Ballauff, M.; Müller, A. H. E. *Polymer* **2008**, *49*, 3957-3964.

(153) Larin, S. V.; Pergushov, D. V.; Xu, Y.; Darinskii, A. A.; Zezin, A. B.; Müller, A. H. E.; Borisov, O. V. *Soft Matter* **2009**, *5*, 4938-4943.

(154) Qin, S.; Matyjaszewski, K.; Xu, H.; Sheiko, S. S. *Macromolecules* **2003**, *36*, 605-612.

(155) Sheiko, S. S.; Sun, F. C.; Randall, A.; Shirvanyants, D.; Rubinstein, M.; Lee, H.-i.; Matyjaszewski, K. *Nature* **2006**, *440*, 191-194.

(156) Xu, H.; Shirvanyants, D.; Beers, K.; Matyjaszewski, K.; Rubinstein, M.; Sheiko, S. S. *Phys. Rev. Lett.* **2004**, *93*, 206103.

(157) Gallyamov, M. O.; Tartsch, B.; Mela, P.; Borner, H.; Matyjaszewski, K.; Sheiko, S.; Khokhlov, A.; Möller, M. *Phys. Chem. Chem. Phys.* **2007**, *9*, 346-352.

(158) Xu, H.; Sheiko, S. S.; Shirvanyants, D.; Rubinstein, M.; Beers, K. L.; Matyjaszewski, K. *Langmuir* **2005**, *22*, 1254-1259.

(159) Tsukahara, Y.; Namba, S.-i.; Iwasa, J.; Nakano, Y.; Kaeriyama, K.; Takahashi, M. *Macromolecules* **2001**, *34*, 2624-2629.

(160) Pakula, T.; Zhang, Y.; Matyjaszewski, K.; Lee, H.-i.; Börner, H.; Qin, S.; Berry, G. C. *Polymer* **2006**, *47*, 7198-7206.

(161) Zhang, Y.; Costantini, N.; Mierzwa, M.; Pakula, T.; Neugebauer, D.; Matyjaszewski, K. *Polymer* **2004**, *45*, 6333-6339.

(162) Bolton, J.; Bailey, T. S.; Rzayev, J. *Nano Lett.* **2011**, *11*, 998-1001.

(163) Han, W.; Byun, M.; Zhao, L.; Rzayev, J.; Lin, Z. *J. Mater. Chem.* **2011**, *21*, 14248-14253.

(164) Li, Y.; Nese, A.; Lebedeva, N. V.; Davis, T.; Matyjaszewski, K.; Sheiko, S. S. *J. Am. Chem. Soc.* **2011**, *133*, 17479-17484.

(165) Decuzzi, P.; Pasqualini, R.; Arap, W.; Ferrari, M. *Pharmaceut. Res.* **2009**, *26*, 235-243.

(166) Shi, X.; von dem Bussche, A.; Hurt, R. H.; Kane, A. B.; Gao, H. *Nat. Nano.* **2011**, *6*, 714-719.

(167) Geng, Y.; Dalhaimer, P.; Cai, S.; Tsai, R.; Tewari, M.; Minko, T.; Discher, D. E. *Nat Nano* **2007**, *2*, 249-255.

(168) Johnson, J. A.; Lu, Y. Y.; Burts, A. O.; Xia, Y.; Durrell, A. C.; Tirrell, D. A.; Grubbs, R. H. *Macromolecules* **2010**, *43*, 10326-10335.

(169) Chen, J.; Wiley, B. J.; Xia, Y. *Langmuir* **2007**, *23*, 4120-4129.

(170) Cui, S.; Liu, H.; Gan, L.; Li, Y.; Zhu, D. *Adv. Mater.* **2008**, *20*, 2918-2925.

(171) Zhao, Y. S.; Fu, H.; Peng, A.; Ma, Y.; Xiao, D.; Yao, J. *Adv. Mater.* **2008**, *20*, 2859-2876.

(172) Greiner, A.; Wendorff, J. H. *Angew. Chem. Int. Ed.* **2007**, *46*, 5670-5703.

(173) Yuan, J.; Müller, A. H. E. *Polymer* **2010**, *51*, 4015-4036.

(174) Yuan, J.; Müller, A. H. E. *Polymer*, *51*, 4015-4036.

(175) Yelamanchili, R. S.; Walther, A.; Müller, A. H. E.; Breu, J. *Chem. Commun.* **2008**, 489-491.

(176) SciFinder: 15 November 2011.

(177) Xia, Y.; Yang, P.; Sun, Y.; Wu, Y.; Mayers, B.; Gates, B.; Yin, Y.; Kim, F.; Yan, H. *Adv. Mater.* **2003**, *15*, 353-389.

(178) Law, M.; Goldberger, J.; Yang, P. *Annu. Rev. Mater. Res.* **2004**, *34*, 83-122.

(179) Hu, J.; Odom, T. W.; Lieber, C. M. *Acc. Chem. Res.* **1999**, *32*, 435-445.

(180) Law, M.; Sirbuly, D. J.; Johnson, J. C.; Goldberger, J.; Saykally, R. J.; Yang, P. *Science* **2004**, *305*, 1269-1273.

(181) Johnson, J. C.; Choi, H.-J.; Knutsen, K. P.; Schaller, R. D.; Yang, P.; Saykally, R. J. *Nat Mater* **2002**, *1*, 106-110.

(182) Djalali, R.; Li, S.-Y.; Schmidt, M. *Macromolecules* **2002**, *35*, 4282-4288.

(183) Ishizu, K.; Tsubaki, K.; Uchida, S. *Macromolecules* **2002**, *35*, 10193-10197.

(184) Zhang, M.; Drechsler, M.; Müller, A. H. E. *Chem. Mater.* **2004**, *16*, 537-543.

(185) Yuan, J.; Drechsler, M.; Xu, Y.; Zhang, M.; Müller, A. H. E. *Polymer* **2008**, *49*, 1547-1554.

(186) Zhang, M.; Estournès, C.; Bietsch, W.; Müller, A. H. E. *Adv. Funct. Mater.* **2004**, *14*, 871-882.

(187) Yuan, J.; Xu, Y.; Walther, A.; Bolisetty, S.; Schumacher, M.; Schmalz, H.; Ballauff, M.; Müller, A. H. E. *Nature Mater.* **2008**, *7*, 718-722.

(188) Kresge, C. T.; Leonowicz, M. E.; Roth, W. J.; Vartuli, J. C.; Beck, J. S. *Nature* **1992**, *359*, 710-712.

(189) Jana, N. R.; Gearheart, L.; Murphy, C. J. *Adv. Mater.* **2001**, *13*, 1389-1393.

(190) Murphy, C. J.; Jana, N. R. *Adv. Mater.* **2002**, *14*, 80-82.

(191) Mandal, S.; Müller, A. H. E. *Mater. Chem. Phys.* **2008**, *111*, 438-443.

(192) Kijima, T.; Yoshimura, T.; Uota, M.; Ikeda, T.; Fujikawa, D.; Mouri, S.; Uoyama, S. *Angew. Chem. Int. Ed.* **2004**, *43*, 228-232.

(193) Gao, C.; Lu, Z.; Yin, Y. *Langmuir* **2011**, *27*, 12201-12208.

(194) Zhang, L.; Eisenberg, A. *Polym. Adv. Technol.* **1998**, *9*, 677-699.

(195) Yu, Y.; Zhang, L.; Eisenberg, A. *Macromolecules* **1998**, *31*, 1144-1154.

(196) Duxin, N.; Liu, F.; Vali, H.; Eisenberg, A. *J. Am. Chem. Soc.* **2005**, *127*, 10063-10069.

(197) Raez, J.; Manners, I.; Winnik, M. A. *J. Am. Chem. Soc.* **2002**, *124*, 10381-10395.

(198) Wang, H.; Patil, A. J.; Liu, K.; Petrov, S.; Mann, S.; Winnik, M. A.; Manners, I. *Adv. Mater.* **2009**, *21*, 1805-1808.

(199) Wang, H.; Wang, X.; Winnik, M. A.; Manners, I. *J. Am. Chem. Soc.* **2008**, *130*, 12921-12930.

(200) Cao, L.; Manners, I.; Winnik, M. A. *Macromolecules* **2002**, *35*, 8258-8260.

(201) Wang, X.-S.; Winnik, M. A.; Manners, I. *Angew. Chem. Int. Ed.* **2004**, *43*, 3703-3707.

(202) Massey, J. A.; Temple, K.; Cao, L.; Rharbi, Y.; Raez, J.; Winnik, M. A.; Manners, I. *J. Am. Chem. Soc.* **2000**, *122*, 11577-11584.

(203) Presa Soto, A.; Gilroy, J. B.; Winnik, M. A.; Manners, I. *Angew. Chem. Int. Ed.* **2010**, *122*, 8396-8399.

(204) Nagarajan, S.; Russell, T. P.; Watkins, J. J. *Adv. Funct. Mater.* **2009**, *19*, 2728-2734.

(205) Park, S.; Kim, B.; Cirpan, A.; Russell, T. P. *Small* **2009**, *5*, 1343-1348.

(206) Park, S.; Wang, J.-Y.; Kim, B.; Russell, T. P. *Nano Lett.* **2008**, *8*, 1667-1672.

(207) Park, S.; Kim, B.; Wang, J. Y.; Russell, T. P. *Adv. Mater.* **2008**, *20*, 681-685.

(208) Zhang, K.; Gao, L.; Chen, Y. *Polymer* **2010**, *51*, 2809-2817.

(209) Zhang, K.; Gao, L.; Chen, Y. *Macromolecules* **2008**, *41*, 1800-1807.

(210) Zhang, K.; Gao, L.; Chen, Y. *Macromolecules* **2007**, *40*, 5916-5922.

(211) Yan, X.; Liu, G.; Liu, F.; Tang, B. Z.; Peng, H.; Pakhomov, A. B.; Wong, C. Y. *Angew. Chem. Int. Ed.* **2001**, *40*, 3593-3596.

(212) Yan, X.; Liu, G.; Li, Z. *J. Am. Chem. Soc.* **2004**, *126*, 10059-10066.

(213) Yan, X.; Liu, G.; Haeussler, M.; Tang, B. Z. *Chem. Mater.* **2005**, *17*, 6053-6059.

(214) Liu, G.; Shimizu, T.; Springer Berlin / Heidelberg: 2008; Vol. 220, p 29-64.

(215) Yan, X.; Liu, F.; Li, Z.; Liu, G. *Macromolecules* **2001**, *34*, 9112-9116.

(216) Zollfrank, C.; Scheel, H.; Greil, P. *Adv. Mater.* **2007**, *19*, 984-987.

(217) Bai, H.; Xu, K.; Xu, Y.; Matsui, H. *Angew. Chem. Int. Ed.* **2007**, *46*, 3319-3322.

(218) Nguyen, K.; Monteverde, M.; Filoramo, A.; Goux-Capes, L.; Lyonnais, S.; Jegou, P.; Viel, P.; Goffman, M.; Bourgoin, J.-P. *Adv. Mater.* **2008**, *20*, 1099-1104.

(219) Jan, R.; Michael, M.; Wolfgang, P.; Ingolf, M.; Hans, K. S. *Appl. Phys. Lett.* **2001**, *78*, 536-538.

(220) Kodama, T.; Jain, A.; Goodson, K. E. *Nano Lett.* **2009**, *9*, 2005-2009.

(221) Pruneanu, S.; Olenic, L.; Farha Al-Said, S.; Borodi, G.; Houlton, A.; Horrocks, B. *J. Mater. Sci.* **2010**, *45*, 3151-3159.

(222) Monson, C. F.; Woolley, A. T. *Nano Lett.* **2003**, *3*, 359-363.

(223) Mao, C.; Solis, D. J.; Reiss, B. D.; Kottmann, S. T.; Sweeney, R. Y.; Hayhurst, A.; Georgiou, G.; Iverson, B.; Belcher, A. M. *Science* **2004**, *303*, 213-217.

(224) Fonoberov, V. A.; Balandin, A. A. *Nano Lett.* **2005**, *5*, 1920-1923.

(225) Shenton, W.; Douglas, T.; Young, M.; Stubbs, G.; Mann, S. *Adv. Mater.* **1999**, *11*, 253-256.

(226) Dang, X.; Yi, H.; Ham, M.-H.; Qi, J.; Yun, D. S.; Ladewski, R.; Strano, M. S.; Hammond, P. T.; Belcher, A. M. *Nat. Nano.* **2011**, *6*, 377-384.

(227) Rong, J.; Oberbeck, F.; Wang, X.; Li, X.; Oxsher, J.; Niu, Z.; Wang, Q. *J. Mater. Chem.* **2009**, *19*, 2841-2845.

(228) Gu, Q.; Haynie, D. T. *Mater. Lett.* **2008**, *62*, 3047-3050.

(229) Gao, C.; Muthukrishnan, S.; Li, W.; Yuan, J.; Xu, Y.; Müller, A. H. E. *Macromolecules* **2007**, *40*, 1803-1815.

(230) Petrov, P.; Stassin, F.; Pagnoulle, C.; Jerome, R. *Chem. Commun.* **2003**, 2904-2905.

(231) Qin, S.; Qin, D.; Ford, W. T.; Zhang, Y.; Kotov, N. A. *Chem. Mater.* **2005**, *17*, 2131-2135.

(232) Jiang, K.; Eitan, A.; Schadler, L. S.; Ajayan, P. M.; Siegel, R. W.; Grobert, N.; Mayne, M.; Reyes-Reyes, M.; Terrones, H.; Terrones, M. *Nano Lett.* **2003**, *3*, 275-277.

(233) Yang, L.-P.; Zou, P.; Pan, C.-Y. *J. Mater. Chem.* **2009**, *19*, 1843-1849.

(234) Mayya, K. S.; Gittins, D. I.; Dibaj, A. M.; Caruso, F. *Nano Lett.* **2001**, *1*, 727-730.

(235) Martin, C. R. *Chem. Mater.* **1996**, *8*, 1739-1746.

(236) C. Hulteen, J.; Martin, C. R. *J. Mater. Chem.* **1997**, *7*, 1075-1087.

(237) Routkevitch, D.; Bigioni, T.; Moskovits, M.; Xu, J. M. *J. Phys. Chem.* **1996**, *100*, 14037-14047.

(238) Li, D.; Wang, Y.; Xia, Y. *Nano Lett.* **2003**, *3*, 1167-1171.

(239) Chen, W.-S.; Huang, D.-A.; Chen, H.-C.; Shie, T.-Y.; Hsieh, C.-H.; Liao, J.-D.; Kuo, C. *Crystal Growth & Design* **2009**, *9*, 4070-4077.

(240) Viswanathamurthi, P.; Bhattarai, N.; Kim, H. Y.; Lee, D. R. *Nanotechnol.* **2004**, *15*, 320.

(241) Lu, X.; Zhao, Y.; Wang, C.; Wei, Y. *Macromol. Rapid Commun.* **2005**, *26*, 1325-1329.

(242) Caruso, R. A.; Schattka, J. H.; Greiner, A. *Adv. Mater.* **2001**, *13*, 1577-1579.

(243) Hou, H.; Jun, Z.; Reuning, A.; Schaper, A.; Wendorff, J. H.; Greiner, A. *Macromolecules* **2002**, *35*, 2429-2431.

Chapter 2 – Overview of the Thesis

This thesis consists of six chapters including four publications, which are presented in Chapters 3 to 6.

The study of cylindrical polymer brushes (CPBs) and their use in template chemistry is the common theme that connects the thesis. My research efforts have focused on (i) developing new preparation pathways to obtain negatively charged anisotropic templates, (ii) the preparation of novel molecular template brushes, and (iii) the application of these synthesized soft templates in template-directed synthesis pathways for the preparation of one-dimensional (1D) organic/inorganic hybrid nanostructures.

Our new molecular CPBs proved to be excellent unimolecular soft templates for the fabrication of hybrid nanotubes. In particular, core-shell-corona CPBs proved to be suitable templates, as the corona helped to avoid intermolecular crosslinking during the hybrid formation. At the same time it made no difference whether the inorganic precursor was already internally integrated within the template brush (in case of $SiO_{1.5}$, **Chapter 3**) or was brought into the template brush by a subsequent loading step (in case of TiO_2, **Chapter 4**). In some cases, a shielding corona was not even necessary and therefore, simply core-shell CPBs were applied in the template-directed synthesis of SiO_2 nanotubes (**Chapter 5**).

Aside the molecular CPBs, we also produced cylindrical template brushes from diblock copolymers phase-separated in the bulk and transformed their polystyrene shell into poly(styrenesulfonic acid) via sulfonation. The resulting water-soluble and negatively charged shell of the core-shell CPBs was then infiltrated by oppositely charged TiO_2 nanocrystals, which were produced separately. In addition, their crystal structure conferred the crystallinity of the later hybrid material (**Chapter 6**).

In the following, an overview of the main results detailed in the thesis is presented.

2.1 Organo-Silica Hybrid Nanotubes

Uniform and selective loading of different compartments of cylindrical nanostructures remains a challenging task. The construction of CPBs where one compartment is covalently carrying an inorganic precursor is an elegant way to produce homogenous hybrid nanostructures, as the inorganic part is confined within only one compartment. In this chapter, we describe the synthesis of water-soluble organo-silica hybrid nanotubes (see Scheme 2-1).

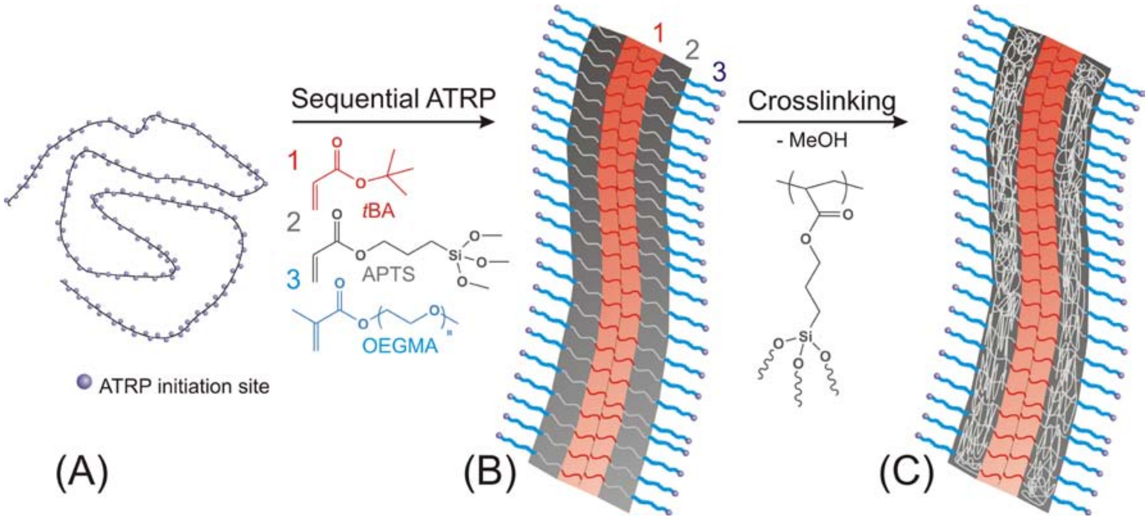

Scheme 2-1. Synthetic route to obtain 1D water-soluble organo-silica hybrid nanotubes templated from core-shell-corona structured CPBs. (**A**) ATRP polyinitiator backbone (PBIEM) with a DP_n of ~3200; (**B**) core-shell-corona structured CPB $[t\mathrm{BA}_{75}\text{-}b\text{-}\mathrm{APTS}_x\text{-}b\text{-}\mathrm{OEGMA}_y]_{3200}$; and (**C**) water-soluble organo-silica hybrid nanotubes $[t\mathrm{BA}_{75}\text{-}b\text{-}(\mathrm{SiO}_{1.5})_x\text{-}b\text{-}\mathrm{OEGMA}_y]_{3200}$.

The synthesis involved anionic polymerization and atom transfer radical polymerization (ATRP). Firstly, a poly(2-bromoisobutyryloxyethyl methacrylate) (PBIEM) backbone with a number-average degree of polymerization (DP_n) of 3200 was obtained by anionic polymerization of 2-(trimethylsilyloxy)ethyl methacrylate (TMS-HEMA). ATRP initiating groups were then attached along the backbone. The PBIEM polyinitiator backbone was used to sequentially grow triblock terpolymer side chains via the 'grafting-from' approach (see Chapter 1). Through sequential grafting, it became facile to adjust the length of each side chain block, and consequently the dimension of the respective compartment. Various core-shell-corona CPBs with different dimensions of the shell and corona were produced, which were then transferred into the corresponding hybrid nanostructure (see Table 2-1). The core consisted of poly(*tert*-butyl acrylate) (P*t*BA), whereas the shell and the corona were built up from poly(3-acryloylpropyl trimethoxysilane) (PAPTS) and poly[oligo(ethylene glycol) methyl ether methacrylate] (POEGMA), respectively. The successful synthesis was verified by molecular visualization with atomic force microscopy (AFM) of the products at each stage. In all cases, AFM revealed individual worm-like structures lying flat on mica (see Figure 2-1).

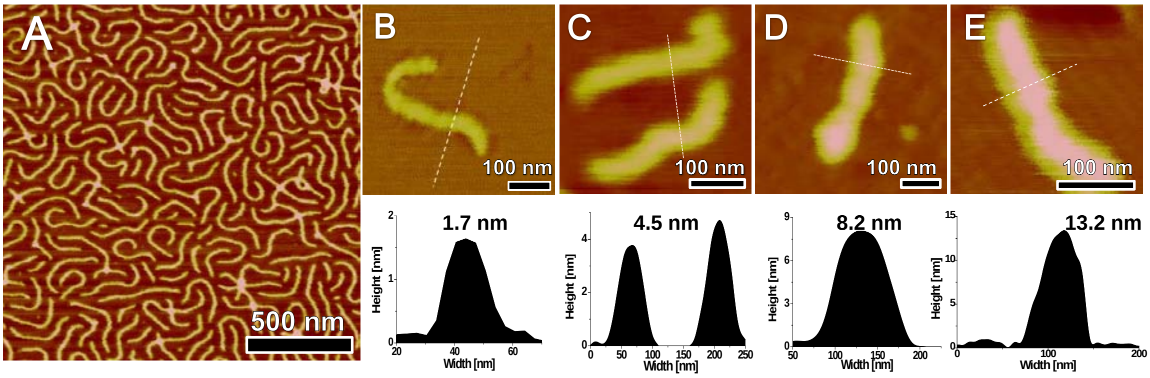

Figure 2-1. (**A**) Tapping-mode AFM overview height image of $[t\mathrm{BA}_{75}]_{3200}$ and (B-E) AFM close view height images and the corresponding height cross-section analysis of (**B**) $[t\mathrm{BA}_{75}]_{3200}$, (**C**) $[t\mathrm{BA}_{75}\text{-}b\text{-}\mathrm{APTS}_{115}]_{3200}$, (**D**) $[t\mathrm{BA}_{75}\text{-}b\text{-}\mathrm{APTS}_{115}\text{-}b\text{-}\mathrm{OEGMA}_{150}]_{3200}$ and (**E**) $[t\mathrm{BA}_{75}\text{-}b\text{-}(\mathrm{SiO}_{1,5})_{115}\text{-}b\text{-}\mathrm{OEGMA}_{150}]_{3200}$.

AFM verified that the height of CPBs increased with increasing length of the side chains, in particular after adding each block. In addition, the increasing length of the side chains causes them to more and more repel each other, which led to an increased stretching of the backbone and resulted in rather stiff CPBs.

The formation of the hybrid nanotubes occurred through an intramolecular sol-gel reaction. PAPTS underwent hydrolysis in basic media to form a silsesquioxane ($\mathrm{SiO}_{1.5}$) network, which formed the partially inorganic shell of the hybrid nanotubes. Due to the inorganic network, the spreading of the CPBs on mica was hindered, which led to a further height increase, as verified via AFM (see Figure 2-1 E). At the same time, the CPBs shrunk as the shell network formed. The longitudinal size contraction and horizontal size expansion resulted from the intramolecular crosslinking of the side chains. Table 2-1 summarizes the produced hybrid nanotubes and their dimensions in water after intramolecular crosslinking.

Table 2-1. Organo-silica hybrid nanotubes with different dimensions[a] (in nm)

Nanotube composition[b]	Length[c]	Tube diameter[c]	Shell thickness[c,d]
$t\mathrm{BA}_{75}\text{-}b\text{-}(\mathrm{SiO}_{1.5})_{50}\text{-}b\text{-}\mathrm{OEGMA}_{300}$	460 ± 120	18 ± 2	~4
$t\mathrm{BA}_{75}\text{-}b\text{-}(\mathrm{SiO}_{1.5})_{115}\text{-}b\text{-}\mathrm{OEGMA}_{150}$	330 ± 70	27 ± 3	~10
$t\mathrm{BA}_{75}\text{-}b\text{-}(\mathrm{SiO}_{1.5})_{170}\text{-}b\text{-}\mathrm{OEGMA}_{400}$	285 ± 55	33 ± 3	~14

[a] Polymethacrylate backbone with 3200 repeating units. [b] Nanotube composition after crosslinking. [c] Length as evaluated from cryo-TEM measurements, [d] taking into account that the P*t*BA core is always around 8 ± 1 nm.

The absolute dimensions of the organo-silica hybrid nanowires in dry state and in solution were determined by transmission electron microscopy (TEM) and cryogenic transmission electron microscopy (cryo-TEM), respectively. The non-stained TEM micrograph of non-crosslinked core-shell-corona CPBs clearly revealed a tubular morphology (see Figure 2-2 A and a). A grey POEGMA corona is visible in cryo-TEM (see Figure 2-2 B). Cryo-TEM further identified the structure of the hybrid nanowires in water (see Figures 2-2 B - D). A grey-scale analysis highlights the tubular structure, as the core and the corona have significantly lower contrast as compared to the silicon containing shell. Treatment with hydrofluoric acid (HF) reopened the $\mathrm{SiO}_{1.5}$ networks. Due to the missing crosslinks, the backbone was then able to stretch again.

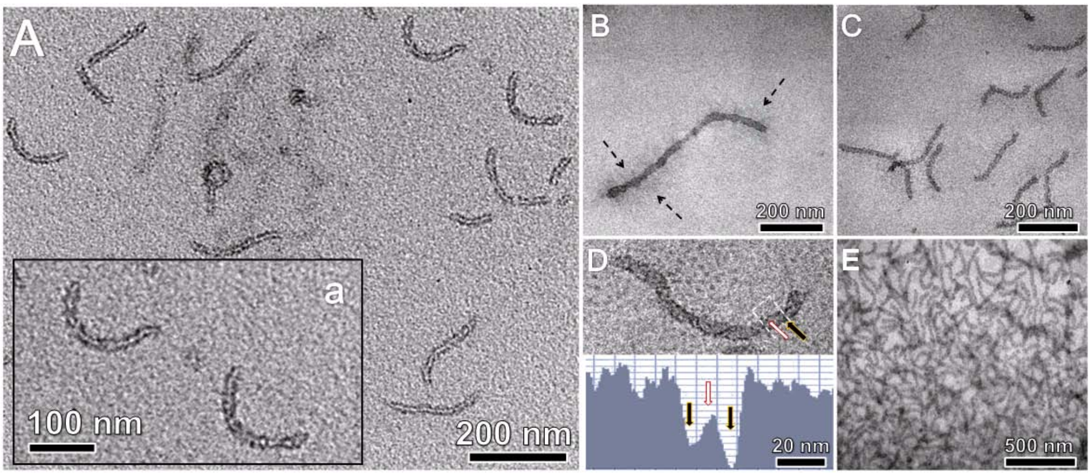

Figure 2-2. TEM characterization of organo-silica nanotubes: (**A/a**) TEM micrograph of non-crosslinked $[t\mathrm{BA}_{75}\text{-}b\text{-}\mathrm{APTS}_{170}\text{-}b\text{-}\mathrm{OEGMA})_{400}]_{3200}$; (**B/C**) cryo-TEM micrographs of the hybrid nanotube $[t\mathrm{BA}_{75}\text{-}b\text{-}(\mathrm{SiO}_{1.5})_{50}\text{-}b\text{-}\mathrm{OEGMA}_{300}]_{3200}$ and hybrid nanotubes $[t\mathrm{BA}_{75}\text{-}b\text{-}(\mathrm{SiO}_{1.5})_{170}\text{-}b\text{-}\mathrm{OEGMA}_{400}]_{3200}$ in water, respectively; (**D**) a single hybrid nanotube in aqueous solution (the insert is a gray scale analysis of the area shown in image D); and (**E**) TEM images of HF treated $[t\mathrm{BA}_{75}\text{-}b\text{-}(\mathrm{SiO}_{1.5})_{170}\text{-}b\text{-}\mathrm{OEGMA}_{400}]_{3200}$.

2.2 Anatase Hybrid Nanotubes

Titanium dioxide (titania) nanomaterials have tremendous practical applications in many different fields such as photocatalysis, gas sensors, dye-sensitized solar cells and optics. They are usually synthesized from templates assembled from small surfactants or amphiphilic block copolymers. This chapter describes the template-directed synthesis of anatase nanotubes within cylindrical core-shell-corona brushes.

To gain more control over the deposition of titania into the respective brush compartment, we utilized electrostatic interaction for the infiltration of titania precursor molecules into the brush templates. The brush templates consisted of poly(*ε*-caprolactone) (PCL) as the core, poly(2-(dimethylamino)ethyl methacrylate) (PDMAEMA) as the shell and POEGMA as the corona. The templates were synthesized via the combination of three polymerization techniques, namely anionic polymerization, ring-opening polymerization (ROP) and ATRP (see Scheme 2-2).

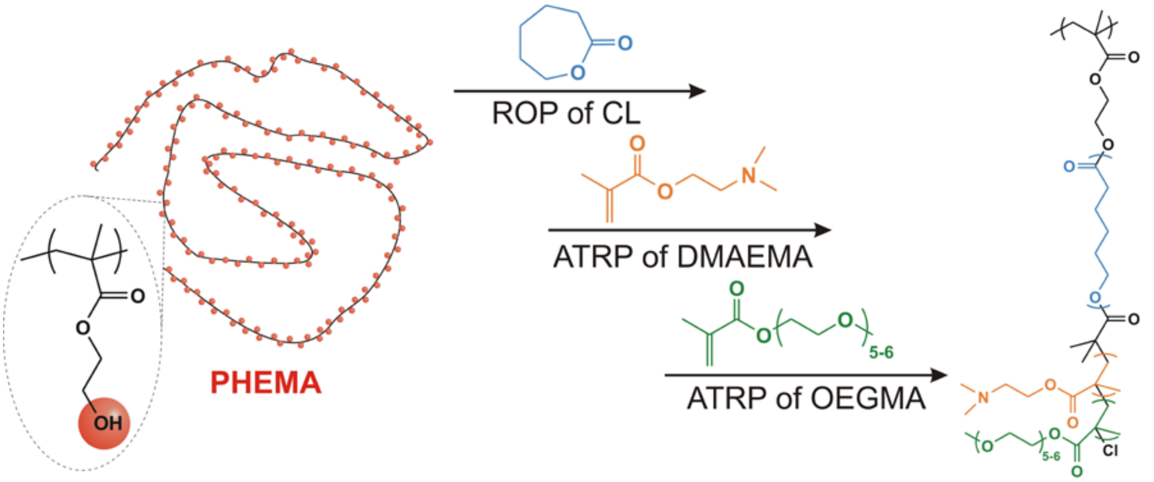

Scheme 2-2. Synthetic route to obtaining 1D water-soluble polymeric templates. The core-shell-corona structured CPBs were built up from a PHEMA backbone by grafting PCL, PDMAEMA and POEGMA from the backbone.

First, PCL homopolymer brushes were synthesized by 'grafting-from' the poly(hydroxyethyl methacrylate) (PHEMA) backbone. After the terminal hydroxyl groups were esterified with an ATRP initiator, PDMAEMA and POEGMA side chains were grafted sequentially (see Scheme 2-2). Two different polymer brushes (template brush 1 and 2) with different lengths of the PDMAEMA shell compartment were produced (see Table 2-2).

Table 2-2. Template core-shell-corona CPBs with different dimensions.

Name	Composition[a]	Shell diameter[b]
Template brush 1	$[CL_{14}\text{-}b\text{-}DMAEMA_{40}\text{-}b\text{-}OEGMA_{65}]_{7500}$	23 ± 2 nm
Template brush 2	$[CL_{14}\text{-}b\text{-}DMAEMA_{150}\text{-}b\text{-}OEGMA_{240}]_{7500}$	39 ± 2 nm

[a] Composition as determined by ^{1}H-NMR. [b] Shell diameter after TALH infiltration.

The loading of the PDMAEMA shell was performed in a water/ethanol mixture by the drop-wise addition of titanium(IV) bis(ammonium lactate) dihydroxide (TALH). TALH is negatively charged and therefore immobilizes only into the PDMAEMA shell compartment, whereas the POEGMA corona cannot complex TALH and remained unloaded. The negatively charged titania precursor complexed exclusively with the amino groups of PDMAEMA, forming concentric TALH nanotubes. Furthermore, TALH shows superior stability in aqueous solution at room temperature, compared to other titania precursors, like titanium(IV) butoxide, which hydrolyze rather rapidly in the presence of water and hence can also deposit in undesired regions, such as the corona. The filling of the template brush with inorganic material was documented by AFM measurements. Filled and hydrolyzed template brushes showed a significant increase in height as compared to the unfilled and pristine CPBs (see Figure 2-3).

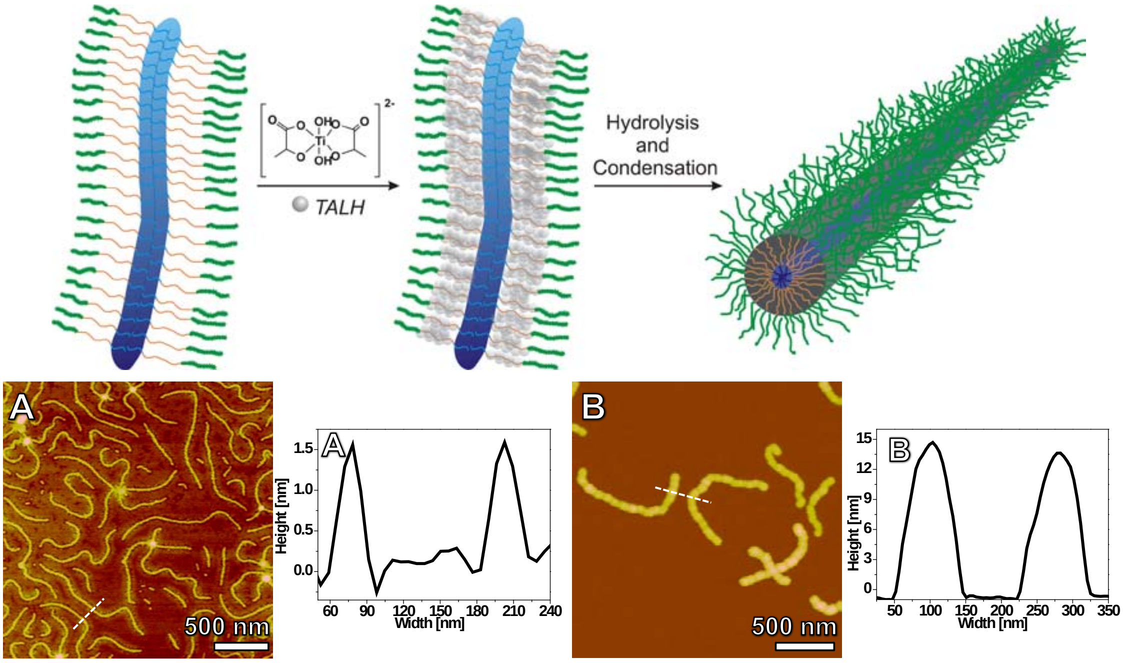

Figure 2-3. (**A**) $[CL_{14}\text{-}b\text{-}DMAEMA_{40}\text{-}b\text{-}OEGMA_{65}]_{7500}$ core-shell-corona CPBs were infiltrated with TALH and produced (**B**) anatase nanotubes after hydrolysis and condensation. The height of pristine CPBs was 1.5 nm and increased to 15 nm for the anatase nanotubes.

The filling of the template brushes resulted in very defined TiO_2 hybrid nanotubes after hydrolysis and condensation. TALH guaranteed stability upon hydrolysis during the loading of the template at ambient temperatures. Only above 70 °C, TALH hydrolyzed thermally and crystallized into anatase. Cryo-TEM and grey-scale analysis illustrated the tubular morphology of the hybrid nanostructures. TEM micrographs highlighted the uniform thickness of the nanotubes, which could be adjusted by the length of the PDMAEMA side chains (see Figures 2-4 B and C). The amount of TiO_2 within the hybrid nanotubes was determined by thermogravimetric analysis (TGA). TGA revealed that longer PDMAEMA side chains increased the loading capacity of the template (see Figure 2-4 F). High resolution TEM (HR-TEM) and powder X-ray diffractometry (PXRD) verified the high crystallinity of the anatase hybrid nanotubes (see Figures 2-4 D and E). Scanning electron microscopy (SEM) highlighted the uniform diameter of the hybrid nanotubes before and after pyrolysis (see Figure 2-5).

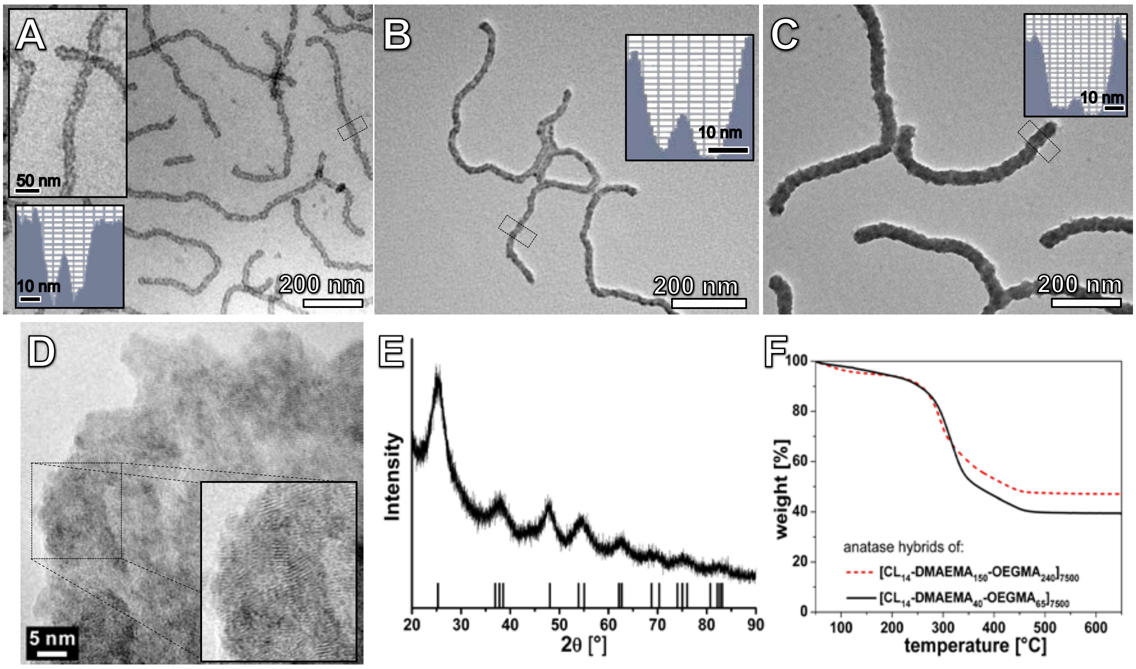

Figure 2-4. (**A**) Cryo-TEM and (**B**) TEM micrographs of anatase nanotubes from template brush 1. (**C**) TEM micrograph of anatase nanotubes from template brush 2. (**D**) HR-TEM micrograph of a highly crystalline anatase nanotube. (**E**) PXRD of anatase nanotubes. (**F**) TGA of the hybrid nanostructures.

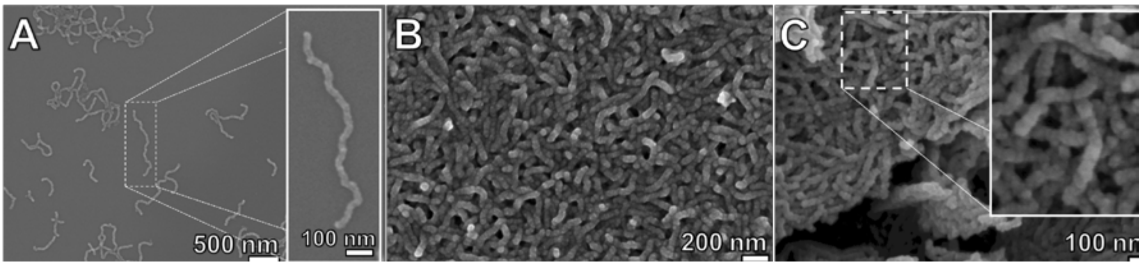

Figure 2-5. SEM images of hybrid nanotubes from (**A**) brush template 1 and (**B**) brush template 2. (**C**) Calcined hybrid nanostructures from template brush 2.

In conclusion, our templating strategy towards crystalline anatase nanotubes has proved to be very effective and versatile in producing well-defined hybrid nanomaterials. The core-shell-corona template brushes provided excellent solubility in various media and prevented crosslinking during hydrolysis and condensation. Highly crystalline 1D TiO_2 nanomaterials were obtained, which may serve useful as catalysts or in photovoltaic applications.

2.3 Silica Nanowires and Nanotubes

Silica-based materials are attractive materials due to their chemical inertness, corrosion resistance, and mechanical and thermal stability. In this chapter, we used core-shell CPBs as unimolecular soft templates for the synthesis of 1D silica hybrid nanostructures (see Scheme 2-3).

Through the combination of anionic polymerization, ROP and ATRP, we produced core-shell CPBs with a degradable core (namely, PCL) and a polyelectrolyte shell (namely, PDMAEMA). The PCL core also acted as a spacer for the initiation sites for ATRP and thereby increased the grafting efficiency of PDMAEMA to 90 % compared to 50-70 % of PBIEM, as reported in literature.[1-3] These unimolecular template brushes were then used for the production of pure hybrid silica (see Scheme 2-3 iv) or nanoparticle-doped hybrid silica nanostructures (see Scheme 2-3 vi). By varying the DP_n of the backbone and the side chains and consequently the dimensions of the template brush (see AFM images in Figure 2-6 A and D), we adjusted the dimensions of the later silica nanostructure, i.e. the thickness of the core and the shell (see Figure 2-6).

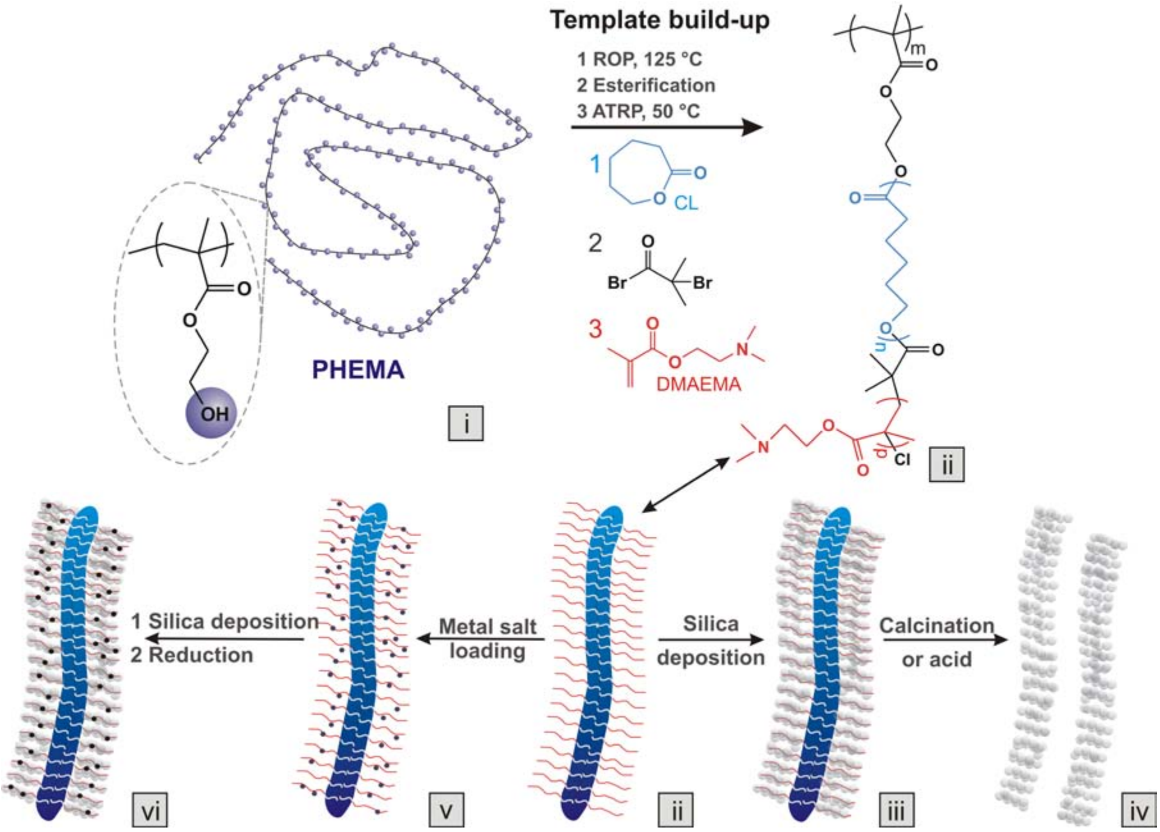

Scheme 2-3. Schematic illustration of the template build-up achieved by combining multiple polymerization techniques. (**i**) PHEMA was 'grafted-from' via ROP of ε-caprolactone and ATRP of DMAEMA to produce a (**ii**) core-shell CPB. The template brush was then infiltrated with (**iii**) silica or (**v**) metal salts (such as $AuCl_4^-$ or $PtCl_4^{2-}$), (**vi**) prior to silica infiltration into the shell. (**iv**) Calcination of acid treatment produced hollow silica nanotubes.

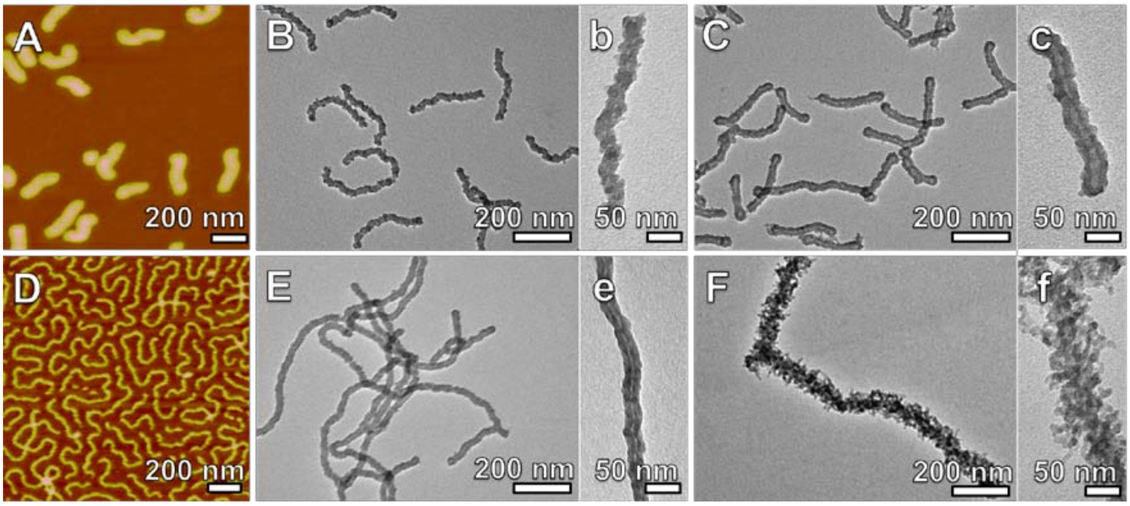

Figure 2-6. AFM height images of template brushes (**A**) $[CL_{25}\text{-}b\text{-}DMAEMA_{76}]_{2700}$ and (**D**) $[CL_{14}\text{-}b\text{-}DMAEMA_{43}]_{7500}$. TEM micrographs of 1D silica hybrid nanostructures from template brushes (**B**, **b**) $[CL_{10}\text{-}b\text{-}DMAEMA_{58}]_{2700}$, (**C**, **c**) $[CL_{25}\text{-}b\text{-}DMAEMA_{76}]_{2700}$, (**E**, **e**) $[CL_{14}\text{-}b\text{-}DMAEMA_{43}]_{7500}$ and (**F**, **f**) $[CL_{14}\text{-}b\text{-}DMAEMA_{342}]_{7500}$.

Consequently, we obtained various 1D silica hybrids for various template brushes (see Table 2-3). Short PDMAEMA side chains gave smooth silica hybrid nanostructures. With increasing length of the PDMAEMA side chains, the hybrid nanostructures became more and more 'hairy', as longer side chains tended to form bundles and threads upon silica deposition (see Figure 2-6 E and F).

Table 2-3. 1D silica hybrids with different dimensions (in nm)

Template composition[a]	Template length[b]	Hybrid length[c]	Core diameter[c]	Silica shell diameter[c]
$[CL_{10}DMAEMA_{58}]_{2700}$	295 ± 20	270 ± 15	5-6	~25
$[CL_{25}DMAEMA_{76}]_{2700}$	265 ± 20	235 ± 20	10-12	~35
$[CL_{14}DMAEMA_{43}]_{7500}$	1250 ± 200	950 ± 350	6-7	~25
$[CL_{14}DMAEMA_{342}]_{7500}$	1250 ± 200	950 ± 350[d]	6-7[e]	~ 85[f]

[a] Determined by ^{1}H-NMR; [b] measured from AFM images of the template brushes; [c] measured from TEM micrographs of the as-synthesized silica hybrids; [d] estimated from TEM micrographs, as it was rather difficult to directly measure the actual length due to the jamming of hairy silica nanostructures; [e] assumed to be the same dimension as with $[CL_{14}DMAEMA_{43}]_{7500}$; [f] taking into account that the core is ~6 nm in diameter.

SEM images highlight the network-like structures of the dried hybrid materials (see Figure 2-7). The 1D nanostructures tended to pack closer as the aspect ratio decreased. The material quite resembled the structure of common filter systems. Calcination or treatment with an acid led to the removal of the core and resulted in hollow silica nanostructures.

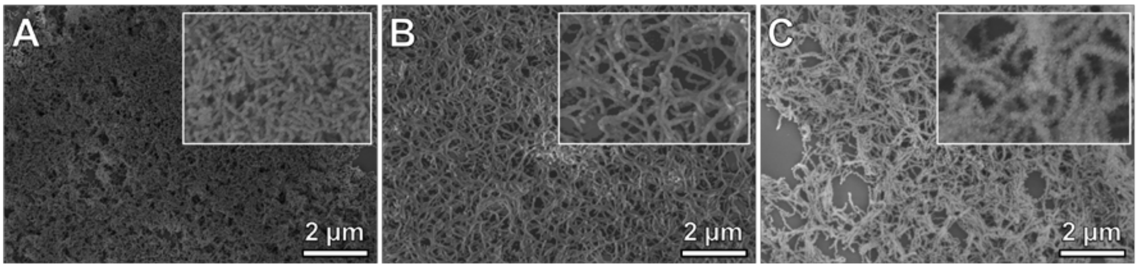

Figure 2-7. SEM images of 1D silica hybrid nanostructures from template brushes (**A**) $[CL_{10}\text{-}b\text{-}DMAEMA_{58}]_{2700}$, (**B**) $[CL_{14}\text{-}b\text{-}DMAEMA_{43}]_{7500}$ and (**C**) $[CL_{14}\text{-}b\text{-}DMAEMA_{342}]_{7500}$.

We further embedded catalytically active metal nanoparticles (NPs) into the shells of the anisotropic nanomaterials to obtain catalytically active nanomaterials. Figure 2-8 shows TEM micrographs of NP-doped nanostructures. Gold and platinum NPs are visible within the silcia shell. The reduction of 4-nitrophenol to 4-aminophenol by $NaBH_4$ in the presence of the metal NP-doped silica nanomaterials was performed to demonstrate the accessibilty and the activity of the catalytically active material. Thus, the incorporation of catalytically active NPs renders very robust carriers for catalysts, which can be easily removed from the system after the reaction. Additionally, the embedment of metallic NPs into silica allows the structures to be used in high temperature applications. This material might also be interesting in the application of catalytically active filter systems.

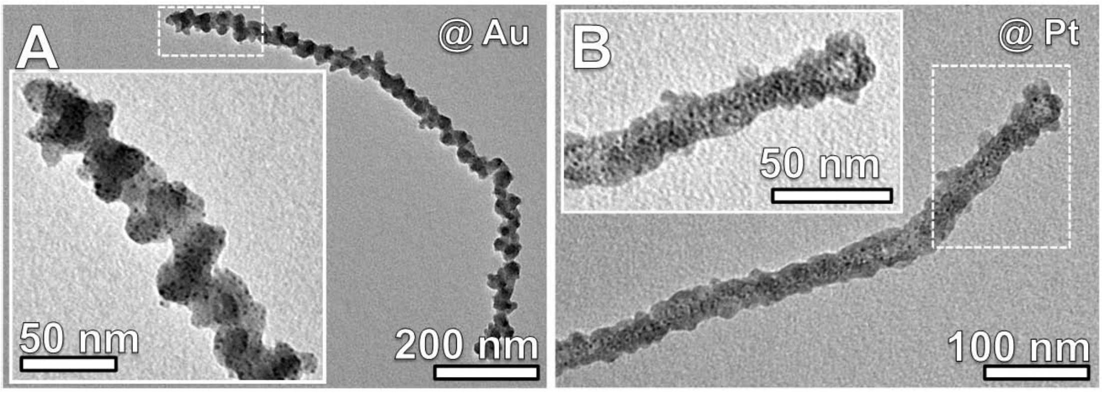

Figure 2-8. TEM micrographs of (**A**) a silica hybrid doped with Au NPs from template brush $[CL_{14}\text{-}b\text{-}DMAEMA_{342}]_{7500}$ and (**B**) a silica hybrid doped with Pt NPs from template brush $[CL_{14}\text{-}b\text{-}DMAEMA_{43}]_{7500}$.

2.4 Mesostructuring of TiO_2 Nanocrystals into One-Dimensional Nanostructures

1D nanostructures of metal oxides have been under close investigation due to their size-dependent optical and electronical properties, which allow them to be used in catalysis, separation or photovoltaic applications. In this chapter, we demonstrate a highly applicable synthesis concept applied for structuring metal oxides into 1D hybrid nanostructures by a template-directed approach. 1D polyelectrolyte template brushes were produced from a polystyrene-*b*-poly(allyl methacrylate) (PS-*b*-PAMA) diblock copolymer, which was obtained by sequential anionic polymerization with narrow molecular weight distribution. Microphase separation of the diblock copolymer in bulk resulted in hexagonally packed PAMA cylinders within a PS matrix. After photo-crosslinking of the PAMA cylinders and re-dispersion of the bulk film in THF, cylindrical polymer brushes were obtained. The PS corona was mildly sulfonated in a subsequent step to transform the PS into poly(styrenesulfonic acid) (PSS) and render the corona water-soluble (see Scheme 2-4 ii and iii).

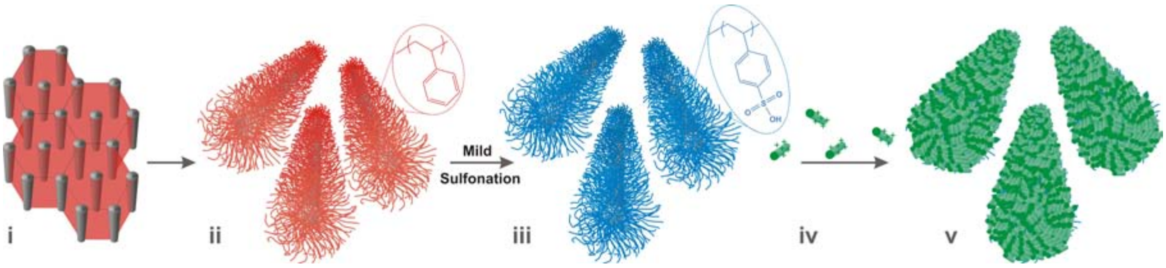

Scheme 2-4. (**i**) Diblock copolymer PS-PAMA microphase-separated into hexagonally packed cylinders. (**ii**) UV-crosslinked PS-PAMA cylindrical polymer brushes are redispersed and (**iii**) sulfonated into polyelectrolyte brushes with a PSS corona. (**iv**) Positively charged and pre-synthesized TiO_2 nanocrystals are infiltrated into the PSS corona to produce (**v**) anisotropic and crystalline TiO_2 nanowires.

The strongly anionic polyelectrolyte brushes (see Figure 2-9 A) were then used as templates for the fabrication of crystalline 1D TiO_2 nanostructures by infiltration of oppositely charged TiO_2 nanocrystals into the polyelectrolyte corona. The nanocrystals were produced separately prior to the formation of the hybrid. We could adjust the crystallinity of the nanocrystals to either rutile or antase by using different acids for the hydrolysis of the titania precursor. Phase purity of the crystalline colloids was confirmed via PXRD. Their apparent hydrodynamic diameter was either 8 nm (rutile) or 14 nm (anatase), as determined by dynamic light scattering.

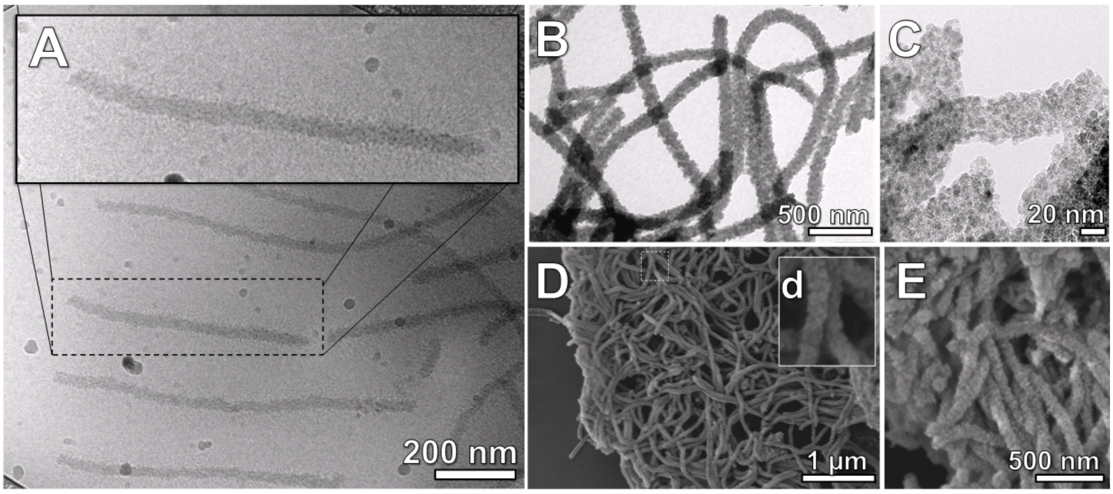

Figure 2-9. (**A**) Cryo-TEM micrograph of PSS-PAMA template brushes in water. (**B**/**C**) TEM micrographs of as-synthesized 1D rutile nanostructures. SEM micrographs of (**D**) as-synthesized rutile nanowires and (**E**) calcined rutile nanowires.

Drop-wise addition of a template brush suspension to a particular amount of the respective nanocrystal suspension at 60 °C and pH 1 resulted in highly crystalline hybrid nanostructures (see Figure 2-9). The hybrid nanowires adopted the same crystallinity as the infiltrated nanocrystals, as confirmed by PXRD (see Figures 2-10 A and D).

Furthermore, HR-TEM highlights the high crystallinity of the hybrid nanostructures (see Figures 2-10 B and E).

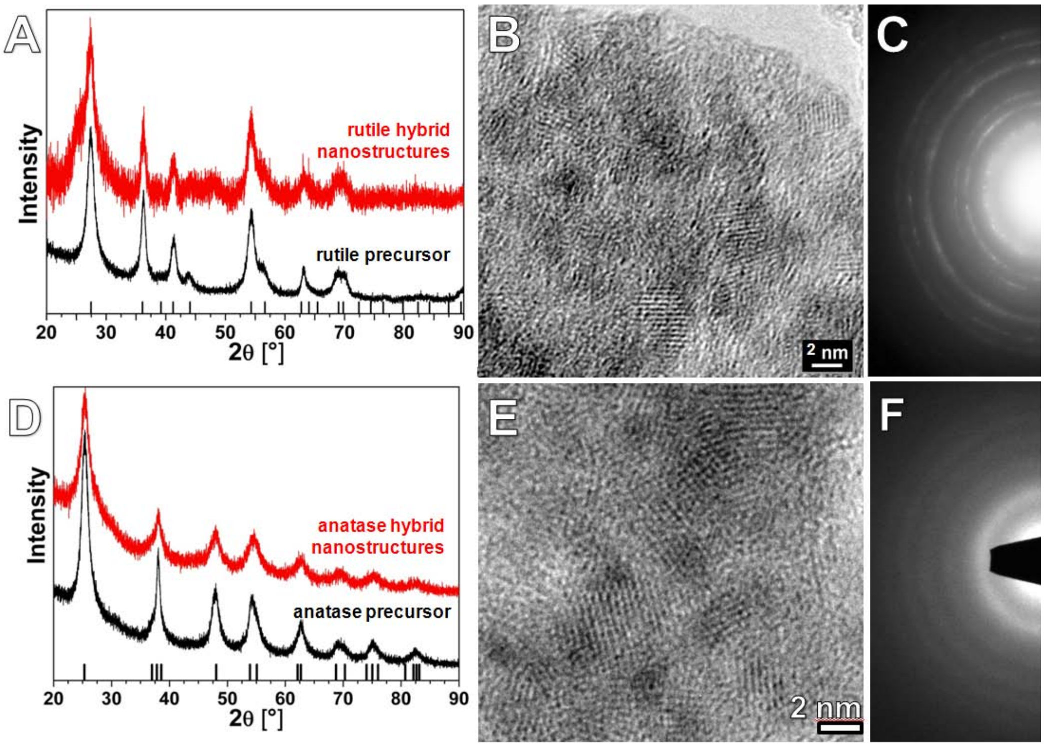

Figure 2-10. (**A and D**) PXRD patterns of crystalline TiO_2 precursors (red pattern) and as-synthesized TiO_2 hybird nanomaterials (black pattern). HR-TEM micrographs and SAED pattern of (**B and C**) highly crystalline rutile and (**E and F**) anatase hybrid nanowires.

N_2 physisorption measurements showed a high surface area of 66 $m^2 \cdot g^{-1}$ for the rutile hybrid nanowires. The hybrids formed porous non-woven networks upon drying (see Figure 2-9 D), which leads to the assumption that the nanowires are still quite flexible. TGA supports the assumption, as it confirmed that the rutile hybrid nanomaterial consists of around 50 wt% soft polymeric material.

In conclusion, we have developed a mild and generally applicable method to mesostructure metal oxides into 1D hybrid nanostructures. The template-directed synthesis of 1D hybrid nanomaterials via cylindrical polyelectrolyte brushes was demonstrated on titania polymorphs, both rutile and anatase, which were selectively mesostructured into hybrid nanowires.

2.5 Individual Contributions to Joint Publications

The results presented in this thesis were obtained in collaboration with others, and have been published or submitted to publication as indicated below. In the following, the contributions of all the co-authors to the different publications are specified. The asterisk denotes the corresponding author(s).

Chapter 3

This work is published in the *Journal of the American Chemical Society* 132, 16587-16592 (2010) under the title:

“**Water-Soluble Organo-Silica Hybrid Nanotubes Templated by Cylindrical Polymer Brushes**”

by Markus Müllner, Jiayin Yuan, Stephan Weiß, Andreas Walther, Melanie Förtsch, Markus Drechsler, and Axel H. E. Müller*

I conducted all experiments and wrote the publication, except that:

- S. Weiß was involved in early experiments during a lab course;
- Walther was involved in discussions;
- M. Förtsch and M. Drechsler performed the cryo-TEM measurements; and
- J. Yuan and A. H. E. Müller were involved in scientific discussions and correcting the publication.

Chapter 4

This work will be submitted under the title:

“**Template-Directed Mild Synthesis of Anatase Hybrid Nanotubes within Cylindrical Core-Shell-Corona Polymer Brushes**”

by Markus Müllner, Thomas Lunkenbein, Martin Schieder, Nobuyoshi Miyajima, Melanie Förtsch, Josef Breu, Frank Caruso,* and Axel H. E. Müller*

I conducted all experiments and wrote the manuscript, except that:

- M. Schieder and T. Lunkenbein both performed SEM and PXRD measurements;
- N. Miyajima performed the HR-TEM measurements;
- M. Förtsch performed the cryo-TEM measurements; and
- J. Breu, F. Caruso and A. H. E. Müller were involved in correcting the manuscript.

Chapter 5

This work has been published in *Chemistry of Materials* under the title:

“**Template-Directed Synthesis of Silica Nanowires and Nanotubes from Cylindrical Core-Shell Polymer Brushes**”

by Markus Müllner, Thomas Lunkenbein, Josef Breu, Frank Caruso,
and Axel H. E. Müller*

I conducted all experiments and wrote the manuscript, except that:

- T. Lunkenbein performed SEM and EDX measurements; and
- J. Breu and F. Caruso were involved in correcting the manuscript.
- A. H. E. Müller was involved in scientific discussions and correcting the manuscript

Chapter 6

This will has been published in *Small* under the title:

“**A Facile Polymer Templating Route Toward High Aspect Ratio Crystalline Titania Nanostructures**”

by Markus Müllner, Thomas Lunkenbein, Nobuyoshi Miyajima, Josef Breu,*
and Axel H. E. Müller*

This is a joint project between the chairs of AC I and MC II.

I conducted all experiments concerning the preparation and the analysis of the polymeric templates. I further assisted in the preparation and the analysis of the nanocrystals and the hybrid materials. I was involved in scientific discussions and wrote the manuscript.

T. Lunkenbein performed most of microscopy experiments and the characterization of the hybrid materials. He further developed the synthesis of the nanocrystals and assisted in the characterization of the sulfonated templates. He was involved in discussions and correcting the manuscript.

Further:

- N. Miyajima performed one of the HR-TEM measurements; and
- J. Breu and A. H. E. Müller were involved in scientific discussions and correcting the manuscript.

References

(1) D. Neugebauer, B. S. Sumerlin, K. Matyjaszewski, B. Goodhart, S. S. Sheiko, *Polymer* **2004**, *45*, 8173.

(2) S. Y. Yu-Su, S. S. Sheiko, H.-i. Lee, W. Jakubowski, A. Nese, K. Matyjaszewski, D. Anokhin, D. A. Ivanov, *Macromolecules* **2009**, *42*, 9008.

(3) J. Yuan, Y. Lu, F. Schacher, T. Lunkenbein, S. Weiss, H. Schmalz, A. H. E. Müller, *Chem. Mater.* **2009**, *21*, 4146.

Chapter 3

Water-Soluble Organo-Silica Hybrid Nanotubes Templated by Cylindrical Polymer Brushes

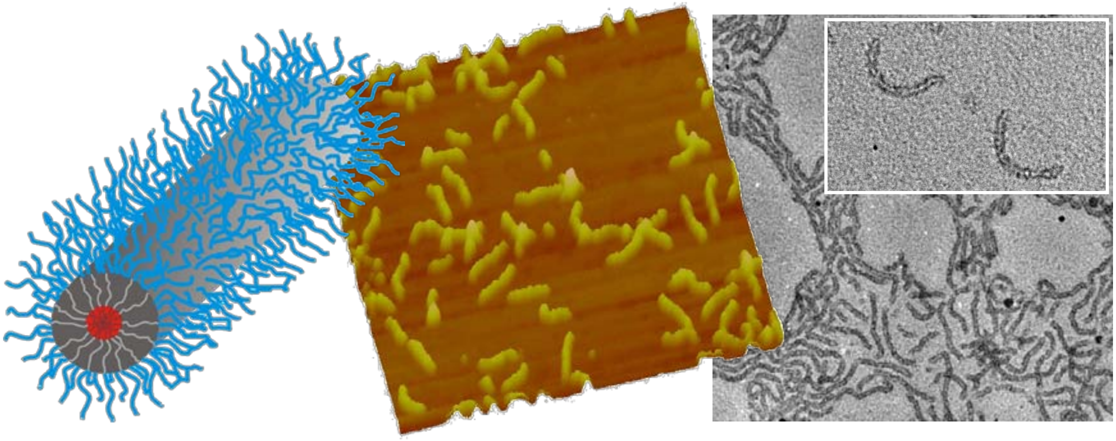

The results of this chapter have been published in the *Journal of the American Chemical Society* as:

"Water-Soluble Organo-Silica Hybrid Nanotubes Templated by Cylindrical Polymer Brushes"

by Markus Müllner, Jiayin Yuan, Stephan Weiß, Andreas Walther, Melanie Förtsch, Markus Drechsler, and Axel H. E. Müller*

Abstract: We report the preparation of water-soluble organo-silica hybrid nanotubes templated by core-shell-corona structured triblock terpolymer cylindrical polymer brushes (CPBs). The CPBs consist of a polymethacrylate backbone, a poly(*tert*-butyl acrylate) (P*t*BA) core, a poly(3-(trimethoxysilyl)propyl acrylate) (PAPTS) shell, and a poly(oligo(ethylene glycol) methacrylate) (POEGMA) corona. They were prepared via the "grafting from" strategy by the combination of two living/controlled polymerization techniques: anionic polymerization for the backbone and atom transfer radical polymerization (ATRP) for the triblock terpolymer side chains. The monomers *t*BA, APTS and OEGMA were consecutively grown from the pendant ATRP initiating groups along the backbone to spatially organize the silica precursor, the trimethoxysilyl groups, into a tubular manner. The synthesized core-shell-corona structured CPBs then served as a unimolecular cylindrical template for the *in-situ* fabrication of water-soluble organo-silica hybrid nanotubes via base-catalyzed condensation of the PAPTS shell block. The formed tubular nanostructures were characterized by transmission electron microscopy (TEM), cryogenic TEM and atomic force microscopy.

Introduction

Cylindrical polymer brushes (CPBs) or “molecular bottlebrushes”, which possess linear side chains or high-generation dendritic side groups densely grafted from a linear main chain, have been the research focus of many polymer chemists and theoreticians over the past decade.[1,2] The interest in this unique hierarchical polymeric architecture arises from the fact that the extended, worm-like chain conformation enables single macromolecular visualization and manipulation, and that particular behavior in solution and bulk has been observed in such macromolecules. So far, three major strategies have been involved in the preparation of CPBs; namely the “grafting through”,[3] “grafting onto”,[4] and “grafting from”[5] strategies. As compared to the first two mechanisms, “grafting from” has drawn more attention as an effective pathway to prepare CPBs of precise dimension and desired functionality. In this approach, a relatively long backbone is first prepared via a living / controlled polymerization technique. This is followed by attaching initiating sites onto each repeating unit along the backbone. Side chains are then grown from these pendant initiating sites, which introduce steric repulsion and lead to stretching of the backbone. Applying the “grafting from” strategy in the field of CPBs has been greatly promoted by the recent progress in living / controlled polymerization techniques, like atom transfer radical polymerization (ATRP),[6,7] nitroxide-mediated radical polymerization[8] and ring-opening polymerization.[9,10] Such techniques have made it possible and convenient to grow uniform side chains with defined chemical structures and compositions. Among them, as a very efficient living / controlled radical polymerization technique, ATRP shows excellent tolerance to many functional groups in monomers, and has been widely employed to graft various side chains from the CPB backbone. Another unique advantage of ATRP when used in the “grafting from” strategy is that block copolymer side chains can be stepwise introduced for the construction of more complex architecture. Based on this technique, CPBs with various architectures have been prepared, including homopolymer brushes,[11,12] core-shell CPBs,[6,13-16] core-shell-corona CPBs,[17,18] hetero-grafted brushes,[19] brush block copolymers,[10,20] star brushes,[21,22] and double-grafted brushes.[23,24] The functional polymerizable monomers in ATRP render CPBs responsive to stimuli such as solvent,[25] temperature,[11,26] light,[27] pH[12] and salts.[12]

The wormlike shape of CPBs has been employed to fabricate inorganic one-dimensional (1D) nanostructures,[28] such as γ-Fe_2O_3,[29] CdS,[30] CdSe,[31] Au,[32] and titania[33] nanowires. Commonly, in a solution approach, the inorganic precursors have been first localized in the cylindrical core area by selectively interacting with the CPB core block. Through chemical reactions occurring only within the core, the precursors have been converted into corresponding functional inorganic nanomaterials, which were spatially organized by the cylindrical template to adopt a wire-like geometry. The CPB shell, free of interaction with the inorganic moieties, protects the formed inorganic nanowires from agglomeration and solubilizes them in solvents. Solubility in water or organic solvents and biocompatibility of the hybrid nanowires can be achieved by the design of the shell block.[33,34] Freestanding, purely inorganic nanowires can be achieved by pyrolytic removal of the polymeric template on a solid substrate. In general, the dimensions of the desired 1D inorganic nanostructure are strictly controlled by the CPBs. For example, the diameter depends on the length of the block in the CPB core, and the length is largely determined by the degree of polymerization of the backbone.[34] We recently reported a novel strategy to form hybrid cylinders with an organo-silica core, where the precursor for the inorganic part is a building unit of the core itself.[34] Organo-silica hybrid nanowires were produced by using poly[(3-acryloxypropyl) trimethoxysilane] (PAPTS) as the core and poly[oligo(ethylene glycol) methacrylate] (POEGMA) as the corona, followed by hydrolytic condensation of the PAPTS core block to form a crosslinked silsesquioxane structure, which could be pyrolized to form pure silica nanowires.[35] Cylindrical or tubular hybrid materials that are not derived from CPBs have been synthesized by using block copolymers as directing agents.[18,36]

So far, only core-shell structured CPBs with diblock copolymer side chains have been chosen as synthetic 1D templates. Herein, we demonstrate the first time that core-shell-corona structured CPBs with triblock terpolymer side chains are employed as an *in-situ* template for the construction of organo-silica hybrid nanotubes, which are soluble in various solvents. Firstly, block terpolymer side-chains of poly(*tert*-butyl acrylate)-*block*-PAPTS-*block*-POEGMA were grown from a poly(2-(2-bromoisobutyryloxy)ethyl methacrylate) (PBIEM) polyinitiator backbone via ATRP. They were then used as a unimolecular cylindrical template for the *in-situ* fabrication of water-soluble organo-silica hybrid nanotubes via condensation of the PAPTS shell block. The formed tubular structures were characterized by transmission electron microscopy (TEM), cryogenic TEM (cryo-TEM) and atomic force microsopy (AFM). Soft tubular nanostructures have also been prepared from small surfactants[37,38] amphiphilic block copolymers[39-43] or multicomponent copolymer cylindrical brushes.[44,45] However, most of these conventional tubular structures are only dynamically stable and can collapse upon a tiny perturbation in the external environment such as a solvent, temperature, concentration, or pH change. In addition, the size and size distribution of assembled structures are usually hard to control. In contrast, due to the living / controlled polymerization techniques employed in the preparation of CPBs, the obtained hybrid tubular structures are uniform in diameter and length. They are stable and tolerant to variations in their environment because the shape and structure of each nanotube is covalently locked.

Experimental Section

Materials. All chemicals were of analytical grade and used as received without further purification, except that (3-acryloxypropyl)trimethoxysilane (APTS) (95%, ABCR) was freshly distilled, and *tert*-butyl acrylate (*t*BA) (98%, Aldrich) and oligo(ethylene glycol) methacrylate (OEGMA) (98%, Aldrich) were filtered through a basic alumina column shortly before each polymerization.

Preparation of core-shell-corona CPB [*t*BA$_{75}$-APTS$_{115}$-OEGMA$_{150}$]$_{3200}$. The poly(macroinitiator) backbone poly(2-(2-bromoisobutyryloxy)ethyl methacrylate) (PBIEM) was prepared by anionic polymerization of 2-(trimethysilyloxy)ethyl methacrylate, acidic cleavage of the trimethylsilyl groups, and an esterification reaction to attach the ATRP initiating sites onto each repeating unit as detailed earlier.[13] The degree of polymerization (DP) of the PBIEM polyinitiator backbone is 3200, and its polydispersity index, determined by gel permeation chromatography (GPC), is 1.14. The synthesis of a P*t*BA homopolymer CPB in anisole was detailed in our previous paper.[13] The initiating efficiency of the PBIEM poly(macroinitiatior) backbone towards *t*BA was determined as 0.65 by cleaving the P*t*BA side chains and determining their molecular weight by GPC.

The ATRP of APTS for the shell block and OEGMA for the corona block was conducted exclusively in benzene in order to suppress the hydrolysis and condensation of the trimethoxysilyl groups in the PAPTS shell block.[34] Typically, in a flask equipped with a septum, CuBr, the poly(macroinitiator), and the monomer (APTS or OEGMA) were added in benzene. The mixture was degassed and stirred until complete dissolution of the poly(macroinitiator) and then heated to 110 °C (in the case of APTS) or 80 °C (in the case of OEGMA). Finally, the degassed ligand, N,N,N',N",N"-pentamethyldiethylenetriamine (PMDETA), was injected to start the polymerization and an initial sample was taken for ^{1}H-NMR measurement. The polymerization was monitored by withdrawing samples for ^{1}H-NMR measurements. When a desired conversion was achieved, the reaction was quenched by cooling the reaction mixture to room temperature and exposing it to air. The reaction mixture was purified by filtration through a basic alumina column, and by ultrafiltration using benzene as the eluent under nitrogen atmosphere.

Preparation of $[(t\mathrm{BA})_{75}\text{-}b\text{-}(\mathrm{SiO}_{1.5})_{115}\text{-}b\text{-}(\mathrm{OEGMA})_{150}]_{3200}$ hybrid organo-silica nanotubes. 400 mg of $[t\mathrm{BA}_{75}\text{-}\mathrm{APTS}_{115}\text{-}\mathrm{OEGMA}_{150}]_{3200}$ core-shell-corona CPBs in 200 ml 1,4-dioxane was mixed with 20 ml of a 25% aqueous solution of ammonia. The reaction mixture was kept under constant stirring at room temperature for 5 days to complete the condensation of the trimethoxysilyl groups. The ammonia was largely removed by rotational evaporation at 30° C and the resulting solution was purified by dialysis against dioxane.

Characterization Methods.

Gel Permeation Chromatography (GPC) in THF was conducted at an elution rate of 1 mL/min using PSS SDVgel columns (300 X 8mm, 5 µm): 10^5, 10^4, 10^3, and 10^2 Å and RI and UV (λ =254 nm) detection. Poly(tert-butyl acrylate) calibration curve was used to calibrate the columns, and toluene was used as an internal standard.

Atomic force microscopy (AFM) images were recorded on a Digital Instruments Dimension 3100 microscope operated in tapping mode. The samples were prepared by dip-coating from dilute solutions (0.02 g/L) of the polymer brush or hybrid nanotubes solution in dioxane or benzene onto a clean silicon wafer or freshly cleaved mica to form a monomolecular film.

Transmission electron microscopy (TEM) images were taken on a Zeiss EM EF-TEM instrument operated at 200 kV. A 5µL droplet of a dilute solution (0.05 g/L) in dioxane or benzene was dropped onto a copper grid (200 mesh) coated with carbon film, followed by blotting the liquid and drying at room temperature for a short time.

Cryogenic transmission electron microscopy (cryo-TEM) was conducted by dropping the aqueous dilute solution (0.1 g/L) on a hydrophilized lacey TEM grid, where most of the liquid was removed with blotting paper, leaving a thin film stretched over the grid holes. The specimens were shock frozen by rapid immersion into liquid ethane and cooled to approximately 90 K by liquid nitrogen in a temperature-controlled freezing unit (Zeiss Cryobox, Zeiss NTS GmbH, Oberkochen, Germany). After the specimens were frozen, the remaining ethane was removed using blotting paper. The specimen was inserted into a cryo-transfer holder (CT3500, Gatan, München, Germany) and transferred to a Zeiss EM922 EF-TEM instrument operated at 200 kV. Cryo-TEM samples from organic solvents, such as THF, were shock frozen in liquid nitrogen, respectively.

Proton nuclear magnetic resonance (^{1}H-NMR) spectra were recorded to determine the monomer conversion on a Bruker AC-300 spectrometer at room temperature in $CDCl_3$.

Results and Discussion

ATRP was employed to graft P*t*BA-*b*-PAPTS-*b*-POEGMA block terpolymer side chains from a PBIEM polyinitiator backbone, along which 3200 ATRP initiating sites were tethered onto each repeating unit.[13] As shown in the general synthetic route in Scheme 3-1, three monomers - namely *tert*-butyl acrylate (*t*BA), (3-acryloxypropyl)trimethoxysilane (APTS) and oligo(ethylene glycol) methacrylate (OEGMA) - were sequentially polymerized in anisole or benzene using CuBr / PMDETA as the catalytic system. Finally, the PAPTS shell block of the obtained core-shell-corona structured CPBs was condensed into a silsesquioxane network in the shell.

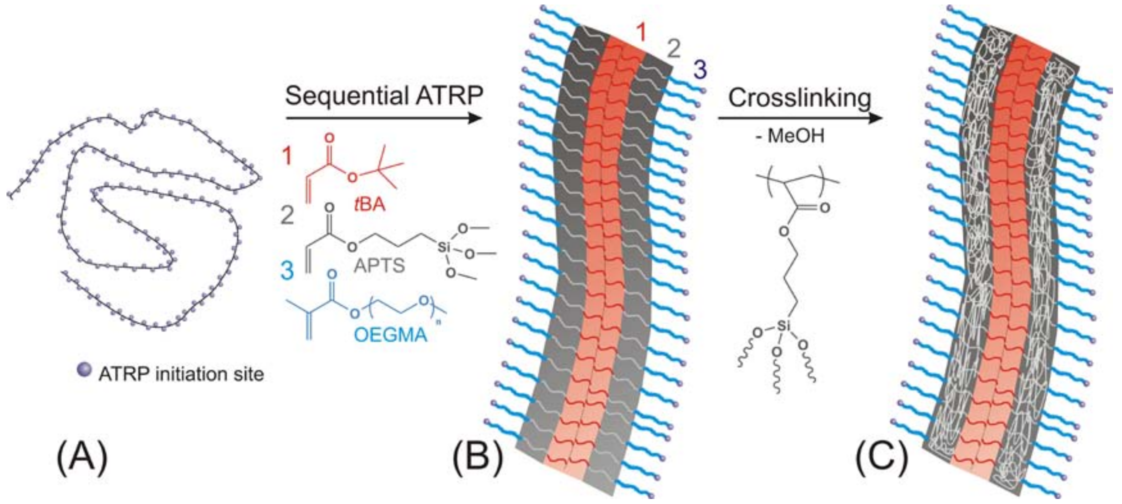

Scheme 3-1. Synthetic route to obtain water-soluble organo-silica hybrid nanotubes templated by core-shell-corona structured CPBs. (**A**) ATRP polyinitiator backbone (PBIEM) with DP ~ 3200; (**B**) core-shell-corona structured CPB [tBA$_{75}$-b-APTS$_x$-b-OEGMA$_y$]$_{3200}$; and (**C**) water-soluble organo-silica hybrid nanotubes [tBA$_{75}$-b-(SiO$_{1.5}$)$_x$-b-OEGMA$_y$]$_{3200}$.

To confirm the successful introduction of each block into the side chains, ^{1}H-NMR spectra were recorded at each block growth step. When *t*BA was polymerized from the PBIEM polyinitiator backbone, the ^{1}H-NMR peaks of PBIEM in Figure 3-1A completely vanished due to their rather low content (< 3%). Instead, the homopolymer CPB [tBA$_{75}$]$_{3200}$ (Figure 3-1B) showed a characteristic sharp peak at 1.44 ppm, assigned to the protons in the *tert*-butyl groups. The P*t*BA homopolymer CPBs were then used as the poly(macroinitiator) for the growth of the PAPTS shell. Figure 3-1C shows the ^{1}H-NMR spectrum of the diblock copolymer CPBs [tBA$_{75}$-b-APTS$_{50}$]$_{3200}$. Besides the peak at 1.44 ppm, another intensive peak appears at ~3.5 ppm, indicating the appearance of trimethoxysilyl groups corresponding to the successful growth of the PAPTS block. In the same manner, the block copolymer CPBs [tBA$_{75}$-b-APTS$_{50}$]$_{3200}$ was used as poly(macroinitiator) for the ATRP of OEGMA. The intensity of the peak at 3.5 ppm (Figure 3-1D/E) is enhanced due to the overlapping of the ethylene proton signals of the oligo(ethylene glycol) moieties and those of the trimethoxysilyl groups.

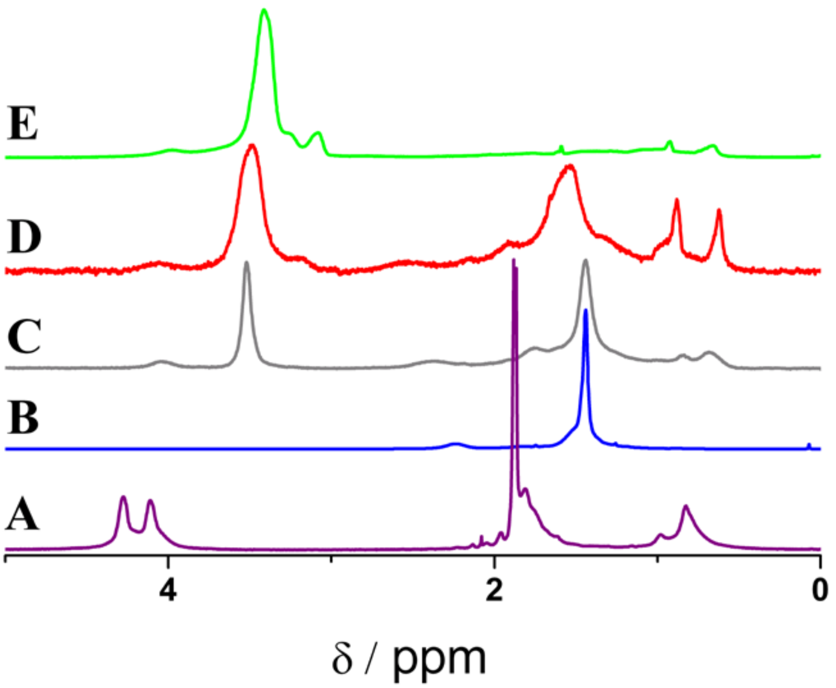

Figure 3-1. ^{1}H-NMR spectra of: (**A**) PBIEM polyinitiator backbone, (**B**) [tBA$_{75}$]$_{3200}$ CPB, (**C**) [tBA$_{75}$-b-APTS$_{50}$]$_{3200}$ CPB, (**D**) [tBA$_{75}$-b-APTS$_{50}$-b-OEGMA$_{30}$]$_{3200}$ CPB, and (**E**) [tBA$_{75}$-b-APTS$_{50}$-b-OEGMA$_{300}$]$_{3200}$ CPB. All samples were measured in $CDCl_3$.

We found the length of the POEGMA block to be very crucial to the success of the synthetic strategy. A short POEGMA corona (DP = 30, ^{1}H-NMR in Figure 3-1D) resulted in an insufficient screening, leading to intermolecular coupling and resulting in large agglomerates that are unstable in solution. Therefore, various terpolymer brushes with a rather long POEGMA corona were synthesized via the "grafting from" approach. After the dialysis of [tBA$_{75}$-b-APTS$_x$-b-OEGMA$_y$]$_{3200}$ from benzene to dioxane, the condensation of the PAPTS shell was carried out by aqueous ammonia. The trimethoxysilyl groups were condensed into a crosslinked silsesquioxane shell. The crosslinked products, [tBA$_{75}$-b-(SiO$_{1.5}$)$_x$-b-OEGMA$_y$]$_{3200}$ organo-silica hybrid nanotubes, are stable in various solvents, like non-polar benzene and toluene, as well as polar methanol and water. Table 3-1 summarizes the synthesized organo-silica hybrid nanotubes and their dimensions in aqueous solution.

Table 3-1. Organo-silica hybrid nanotubes with different dimensions[a] (in nm)

Nanotube composition[b]	Length[c]	Tube diameter[c]	Shell thickness[c,d]
$t\mathrm{BA}_{75}$-b-$(\mathrm{SiO}_{1.5})_{50}$-$b$-$\mathrm{OEGMA}_{300}$	460 ± 120	18 ± 2	~4
$t\mathrm{BA}_{75}$-b-$(\mathrm{SiO}_{1.5})_{115}$-$b$-$\mathrm{OEGMA}_{150}$	330 ± 70	27 ± 3	~10
$t\mathrm{BA}_{75}$-b-$(\mathrm{SiO}_{1.5})_{170}$-$b$-$\mathrm{OEGMA}_{400}$	285 ± 55	33 ± 3	~14

[a] Polymethacrylate backbone with 3200 repeating units. [b] Nanotube composition after crosslinking. [c] Length as evaluated from cryo-TEM measurements, [d] taking into account that the P*t*BA core is always around 8 ± 1 nm.

Molecular visualization via atomic force microscopy (AFM) on mica or silicon wafer has been proven to be a powerful characterization method to verify the successful synthesis and the morphological changes of CPBs.[10,34] Figures 3-2A-I are the AFM images of intermediate and final product CPBs at each synthetic step. Figure 3-2A shows a densely packed monolayer of $[t\mathrm{BA}_{75}]_{3200}$ CPBs with uniform diameter and narrow length distribution. A statistical measurement determines that their average length is 285 ± 74 nm. The cross-section analysis of a single flattened P*t*BA CPB (Figure 3-2B) shows a height in its center of 1.7 nm (Figure 3-2C). It is reported that the repulsion among the dense side chains increases with the side chains length and monomer bulkiness.[1,46,47] Here, by extending the side chains by grafting PAPTS as the shell block, the repulsion between the side chains increases as expected. Figures 3-2D and 3-2E show the AFM images of the diblock copolymer CPBs $[t\mathrm{BA}_{75}$-b-$\mathrm{APTS}_{115}]_{3200}$. The average length is measured to be 375 ± 50 nm, 30% longer than that of the $[t\mathrm{BA}_{75}]_{3200}$ CPBs. The cross-section analysis of the individual CPBs (Figure 3-2F) reveals an increase in the height up to 4.5 nm, ca. 200 % higher than that of $[t\mathrm{BA}_{75}]_{3200}$. In the absence of a corona block, during the condensation step, the diblock copolymer $[t\mathrm{BA}_{75}$-b-$\mathrm{APTS}_{115}]_{3200}$ CPBs undergo both intramolecular and intermolecular crosslinking, which precipitates the CPBs out of solution. Thus a corona block is required to screen the intermolecular coupling before the condensation step and acts as a protective layer. Therefore, a POEGMA block with a DP of 150 was grafted (Figure 3-2G-I) to obtain the final $[t\mathrm{BA}_{75}$-b-APTS_{115}-b-$\mathrm{OEGMA}_{150}]_{3200}$ CPB. The average length slightly increased to 400 ± 50 nm. The cross-section analysis revealed a further increase in height to 8.2 nm. The widths (Figure 3-2 C/F/I) also increased with each polymerization step. However, the worm-like structures appear broader in AFM than in TEM or cryo-TEM measurements due to their spreading on the silicon wafer surface. It is possible to visualize the POEGMA corona with AFM (Figure 3-2G/H), however the values for the width of above 150 nm can only derive from the worms being spread out onto the silicon wafer surface.

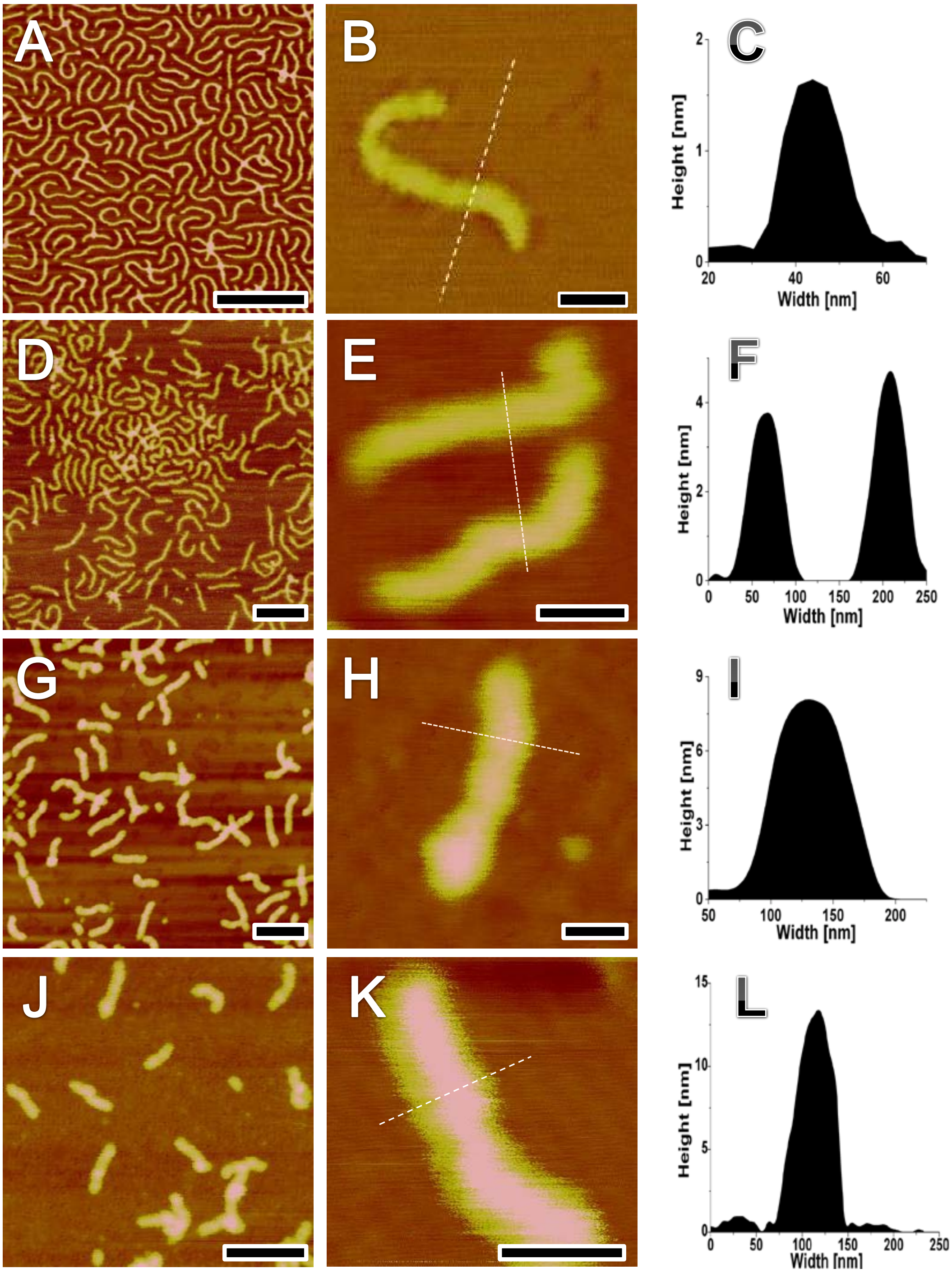

Figure 3-2. Tapping-mode AFM height images (overview and close view) and the corresponding height cross-section analysis of $[t\mathrm{BA}_{75}]_{3200}$ (**A-C**), $[t\mathrm{BA}_{75}\text{-}b\text{-}\mathrm{APTS}_{115}]_{3200}$ (**D-F**), $[t\mathrm{BA}_{75}\text{-}b\text{-}\mathrm{APTS}_{115}\text{-}b\text{-}\mathrm{OEGMA}_{150}]_{3200}$ (**G-I**), and $[t\mathrm{BA}_{75}\text{-}b\text{-}(\mathrm{SiO}_{1,5})_{115}\text{-}b\text{-}\mathrm{OEGMA}_{150}]_{3200}$ (J-L). Z-ranges are 5 (**A**), 8 (**B**), 9 (**D**), 10 (**E**), 15 (**G**), 20 (**H/J**), and 25 nm (**K**), respectively. The scale-bars correspond to 500 nm (**A/D/G/J**) and 100 nm (**B/E/H/K**), respectively.

As mentioned, the crosslinked product, $[(t\mathrm{BA})_{75}\text{-}b\text{-}(\mathrm{SiO}_{1.5})_{115}\text{-}b\text{-}(\mathrm{OEGMA})_{150}]_{3200}$ organo-silica hybrid nanotubes, are stable in various solvents and water. AFM images of the hybrid organo-silica nanotubes are shown in Figure 3-2J/K. The cylindrical morphology was maintained during the complete synthetic route, and actually shaped the silsesquioxane network into a tubular structure. Interestingly, the average length of the crosslinked $[t\mathrm{BA}_{75}\text{-}b\text{-}(\mathrm{SiO}_{1,5})_{115}\text{-}b\text{-}\mathrm{OEGMA}_{150}]_{3200}$ shrinks from 400 ± 50 to 300 ± 60 nm; meanwhile, their height increases further to 13.2 nm (Figure 3-2L), ~60% higher than the precursors (8.2 nm). The longitudinal size contraction and horizontal size expansion result from the intramolecular crosslinking of the side chains. Since more chemical bonds are generated among the side chains in the condensation process, the repulsion force among the side chains is largely compensated. At the same time, both the P*t*BA core and the hybrid silica shell were chemically locked in the CPB center and could not spread over the surface, which enhances the height in the CPB center. Treatment with hydrogen fluoride in THF opens the silsesquioxane network again. Due to the missing crosslinks, the backbone is then able to stretch again. In the case of $[t\mathrm{BA}_{75}\text{-}b\text{-}(\mathrm{SiO}_{1.5})_{170}\text{-}b\text{-}\mathrm{OEGMA}_{400}]_{3200}$, the average length of the backbone increased from 285 nm to above 400 nm (see Supporting Information 3-S3).

As AFM measurements only depict the surface morphology, the intrinsic structure of these hybrid nanotubes was revealed by TEM and cryo-TEM measurements. With TEM characterization, nanotubes appear lighter in the center than at the wall, similar to carbon nanotubes. However, for the hybrid organo-silica nanotubes synthesized here, the core is not empty, but filled partially with P*t*BA polymer. Since the polymer has a weak contrast compared to inorganic or hybrid materials, a tubular structure is thus still expected. In the dry state, the hybrid nanotubes in normal TEM measurements show worm-like morphology (Figure 3-3), indicating that the cylindrical templates work efficiently for the present synthetic strategy. The nanotubes enlarged in Figure 3-3B/C/E appear lighter in the core, as expected. The diameters of the core and of the shell of $[t\mathrm{BA}_{75}\text{-}b\text{-}\mathrm{APTS}_{115}\text{-}b\text{-}\mathrm{OEGMA}_{150}]_{3200}$ in the dry state are 13-17 nm and 33-37 nm. That gives a wall thickness of ~10 nm. For the $[t\mathrm{BA}_{75}\text{-}b\text{-}\mathrm{APTS}_{170}\text{-}b\text{-}\mathrm{OEGMA}_{400}]_{3200}$ nanotubes, the diameter of the core stays around 14-17 nm, where as the total diameter (core and shell) increases to around 45-54 nm. This results in a shell thickness of approximately 15.5 to 18.5 nm (in dry state).

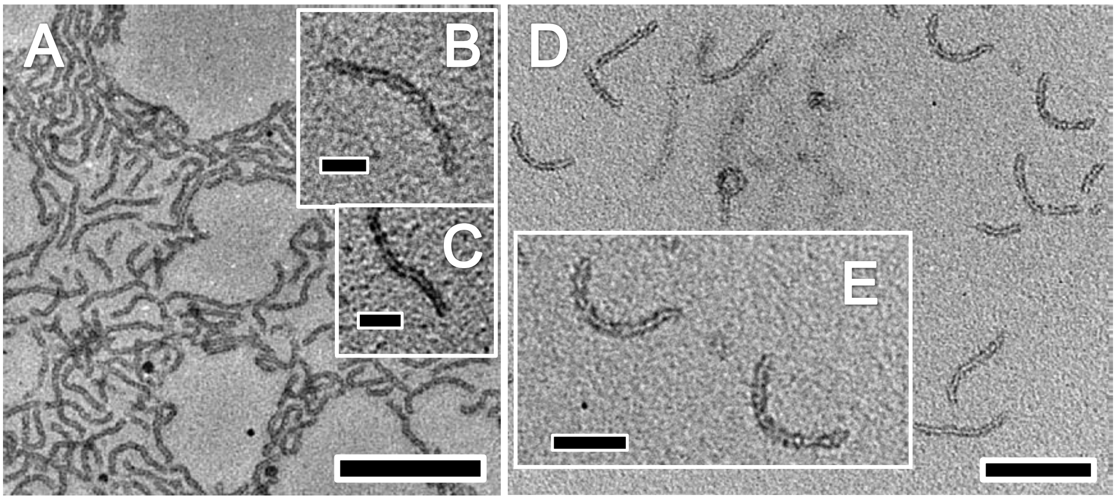

Figure 3-3. TEM characterization of organo-silica nanotubes in THF: non-stained TEM images of [*t*BA$_{75}$-*b*-APTS$_{115}$-*b*-OEGMA$_{150}$]$_{3200}$ (**A**/**B**/**C**), and [*t*BA$_{75}$-*b*-APTS$_{170}$-*b*-OEGMA)$_{400}$]$_{3200}$ (**D**/**E**); (**B**/**C**/**E**) are close-ups of non-stained hybrid nanotubes. The scale-bars are 100 nm (**B**/**C**/**E**) and 200 nm (**A**/**D**), respectively.

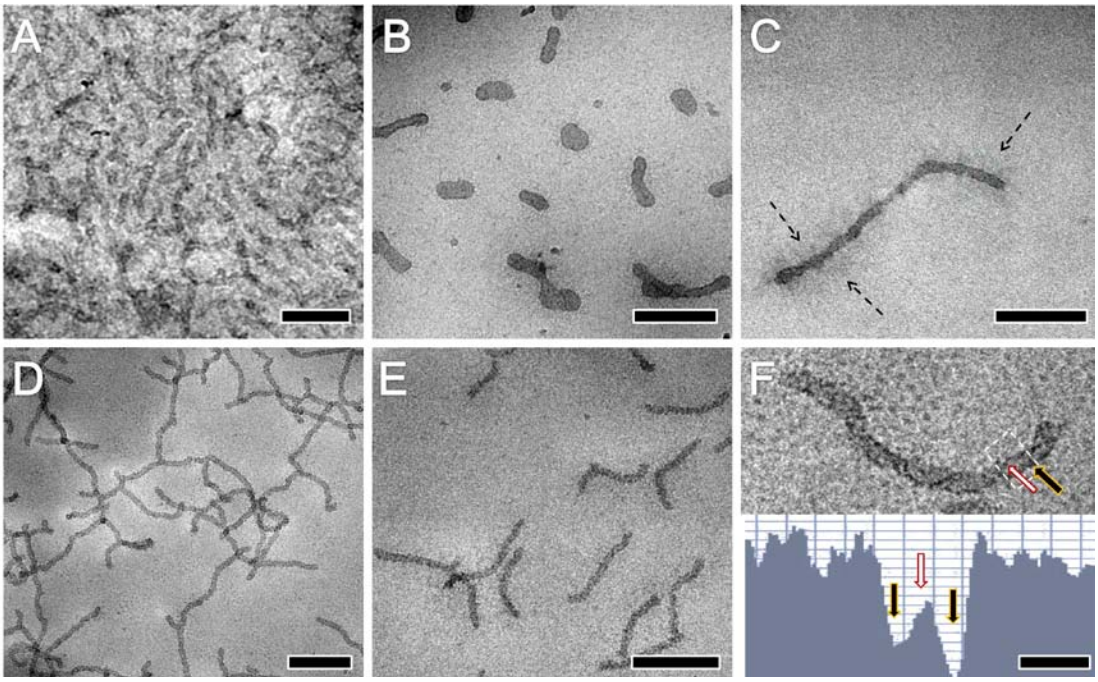

Figure 3-4. Cryo-TEM images of (**A**) non-crosslinked nanotubes [*t*BA$_{75}$-*b*-APTS$_{170}$-*b*-OEGMA$_{400}$]$_{3200}$ in THF; (**B**) non-crosslinked nanotubes [*t*BA$_{75}$-*b*-APTS$_{115}$-*b*-OEGMA$_{150}$]$_{3200}$ in water; (**C**) hybrid nanotube [*t*BA$_{75}$-*b*-(SiO$_{1.5}$)$_{50}$-*b*-OEGMA$_{300}$]$_{3200}$ in water; (**D**) hybrid nanotubes [*t*BA$_{75}$-*b*-(SiO$_{1.5}$)$_{115}$-*b*-OEGMA$_{150}$]$_{3200}$ in water; (**E**) hybrid nanotubes [*t*BA$_{75}$-*b*-(SiO$_{1.5}$)$_{170}$-*b*-OEGMA$_{400}$]$_{3200}$ in water; and (F) a single hybrid nanotube in aqueous solution (the insert is a gray scale analysis of the area shown in image F). The scale-bars represent 200 nm (**A-E**) and 20 nm (**F**), respectively.

As shown above, TEM investigations clearly confirmed the tubular structures. However, the weak contrast of the non-crosslinked organo-silica nanotubes in cryo-TEM measurements in THF made it difficult but possible to depict the tubular structures

(Figure 3-4A). The non-crosslinked nanotubes in aqueous solution were then subjected to cryo-TEM measurements, aiming at detecting the tubular structure in the real solution state (Figures 3-4B and 3-S1 in Supporting Information). Crosslinking was a necessity here, since the tubes broke apart otherwise due to strong repellent forces of the corona (see cryo-TEM images in Figure 3-S2). Figure 3-4 further shows cryo-TEM images of all hybrid nanotubes in water presented in Table 3-1 (Figure 3-4C-E). The dark worms represent the crosslinked shell with a P*t*BA core block in its center. Due to the polymer filling inside the tube, the contrast between the core and the wall is weak. Figure 3-4F shows a single nanotube in water. A grey-scale analysis of [tBA$_{75}$-b-(SiO$_{1.5}$)$_{115}$-b-OEGMA$_{150}$]$_{3200}$ was performed to precisely differentiate the core and the wall (Figure 3-4F). Here, the darkest area is located at the wall (yellow/black arrows); the core (red/white arrow) is clearly lighter than the wall but darker than the background. The diameters of the core and the core and shell of [tBA$_{75}$-b-(SiO$_{1.5}$)$_{115}$-b-OEGMA$_{150}$]$_{3200}$ are determined by the grey scale analysis to be 8 ± 1 nm and 27 ± 3 nm, respectively, again resulting in a shell thickness of ~10 nm. The diameter of roughly 27 nm does not match the height of crosslinked organo-silica tubes (~13 nm) in AFM. Although being crosslinked, the tubes are partially flattened out on the substrate leading to a decreased height and also resulting in a slightly increased width. The corona could not be observed in TEM measurements due to low contrast. Only the cryo-TEM measurement of [tBA$_{75}$-b-(SiO$_{1.5}$)$_{50}$-b-OEGMA$_{300}$]$_{3200}$ gives slight indication of the corona (Figure 3-4C, black dashed arrows).

Conclusions

We successfully demonstrated a synthetic route to water-soluble organo-silica hybrid nanotubes templated by core-shell-corona structured triblock terpolymer cylindrical polymer brushes (CPBs). CPBs with a poly(*tert*-butyl acrylate) (P*t*BA) core, a poly(3-(trimethoxysilyl)propyl acrylate) (PAPTS) shell, and a poly(oligo(ethylene glycol) methacrylate) (POEGMA) corona were prepared via the "grafting-from" strategy by the combination of anionic polymerization and ATRP. The as-synthesized CPBs then acted as a unimolecular cylindrical template for the *in-situ* fabrication of water-soluble organo-silica hybrid nanotubes via condensation of the PAPTS shell middle block to a silsesquioxane network (SiO$_{1.5}$)$_x$. With different monomer feed ratios, it was possible to change the dimensions of the formed nanotubes. Not only can the lengths of the nanotubes can be controlled rather uniformly by the length of the backbone, but also the actual diameter (P*t*BA and PAPTS) as well as the shell thickness (PAPTS) are easy to adjust. The formed tubular nanostructures were confirmed by transmission electron microscopy (TEM), cryogenic TEM and atomic force microscopy (AFM). Deprotection of the P*t*BA core to obtain a polyelectrolyte core and the coordination with nanoparticles will be topic of our following research.

Acknowledgements. This work was supported by the *Deutsche Forschungsgemeinschaft* within the Collaborative Research Center SFB 840.

Supporting Information Available. Cryo-TEM images of non-crosslinked and crosslinked organo-silica nanotubes in aqueous solution and effect of HF treatment in THF. This material is available free of charge via the Internet at http://pubs.acs.org.

References

(1) Sheiko, S. S.; Sumerlin, B. S.; Matyjaszewski, K. *Prog. Polym. Sci.* **2008**, *33*, 759-785.

(2) Zhang, M.; Müller, A. H. E. *J. Polym. Sci. Part A* **2005**, *16*, 3461-3481.

(3) Tsukahara, Y.; Mizuno, K.; Segawa, A.; Yamashita, Y. *Macromolecules* **1989**, *22*, 1546-1552.

(4) Deffieux, A.; Schappacher, M. *Macromolecules* **1999**, *32*, 1797-1802.

(5) Qin, S.; Matyjaszewski, K.; Xu, H.; Sheiko, S. S. *Macromolecules* **2003**, *36*, 605-612.

(6) Cheng, G.; Böker, A.; Zhang, M.; Krausch, G.; Müller, A. H. E. *Macromolecules* **2001**, *34*, 6883-6888.

(7) Beers, K. L.; Gaynor, S. G.; Matyjaszewski, K.; Sheiko, S. S.; Möller, M. *Macromolecules* **1998**, *31*, 9413-9415.

(8) Cheng, C.; Qi, K.; Khoshdel, E.; Wooley, K. L. *J. Am. Chem. Soc.* **2006**, *128*, 6808-6809.

(9) Lee, H.-i.; Jakubowski, W.; Matyjaszewski, K.; Yu, S.; Sheiko, S. S. *Macromolecules* **2006**, *39*, 4983-4989.

(10) Lee, H.-i.; Matyjaszewski, K.; Yu-Su, S.; Sheiko, S. S. *Macromolecules* **2008**, *41*, 6073-6080.

(11) Li, C.; Gunari, N.; Fischer, K.; Janshoff, A.; Schmidt, M. *Angew. Chem. Int. Ed.* **2004**, *43*, 1101-1104.

(12) Xu, Y.; Bolisetty, S.; Drechsler, M.; Fang, B.; Yuan, J.; Ballauff, M.; Müller, A. H. E. *Polymer* **2008**, *49*, 3957-3964.

(13) Zhang, M.; Breiner, T.; Mori, H.; Müller, A. H. E. *Polymer* **2003**, *44*, 1449-1458.

(14) Djalali, R.; Hugenberg, N.; Fischer, K.; Schmidt, M. *Macromol. Rapid Commun.* **1999**, *20*, 444-449.

(15) Börner, H. G.; Beers, K.; Matyjaszewski, K.; Sheiko, S. S.; Möller, M. *Macromolecules* **2001**, *34*, 4375-4383.

(16) Ishizu, K.; Kakinuma, H. *J. Polym. Sci. Part A: Polym. Chem.* **2005**, *43*, 63-70.

(17) Tang, C.; Dufour, B.; Kowalewski, T.; Matyjaszewski, K. *Macromolecules* **2007**, *40*, 6199-6205.

(18) Zhang, K.; Gao, L.; Chen, Y. *Polymer* **2010**, *51*, 2809-2817.

(19) Neugebauer, D.; Zhang, Y.; Pakula, T.; Matyjaszewski, K. *Polymer* **2003**, *44*, 6863-6871.

(20) Ishizu, K.; Satoh, J.; Sogabe, A. *J. Coll. Interf. Sci.* **2004**, *274*, 472-479.

(21) Lee, H.-i.; Boyce, J. R.; Nese, A.; Sheiko, S. S.; Matyjaszewski, K. *Polymer* **2008**, *49*, 5490-5496.

(22) Matyjaszewski, K.; Qin, S.; Boyce, J. R.; Shirvanyants, D.; Sheiko, S. S. *Macromolecules* **2003**, *36*, 1843-1849.

(23) Neugebauer, D.; Zhang, Y.; Pakula, T.; Sheiko, S. S.; Matyjaszewski, K. *Macromolecules* **2003**, *36*, 6746-6755.

(24) Xu, Y.; Becker, H.; Yuan, J.; Burkhardt, M.; Zhang, Y.; Walther, A.; Bolisetty, S.; Ballauff, M.; Müller, A., H. E. *Macromol. Chem. Phys.* **2007**, *208*, 1666-1675.

(25) Fischer, K.; Schmidt, M. *Macromol. Rapid Commun.* **2001**, *22*, 787-791.

(26) Pietrasik, J.; S. Sumerlin, B.; Y. Lee, R.; Matyjaszewski, K. *Macromol. Chem. Phys.* **2007**, *208*, 30-36.

(27) Lee, H.-i.; Pietrasik, J.; Matyjaszewski, K. *Macromolecules* **2006**, *39*, 3914-3920.

(28) Yuan, J.; Müller, A. H. E. *Polymer*, **2010**, *51*, 4015-4036.

(29) Zhang, M.; Estournès, C.; Bietsch, W.; Müller, A. H. E. *Adv. Funct. Mater.* **2004**, *14*, 871-882.

(30) Zhang, M.; Drechsler, M.; Müller, A. H. E. *Chem. Mater.* **2004**, *16*, 537-543.

(31) Yuan, J.; Drechsler, M.; Xu, Y.; Zhang, M.; Müller, A. H. E. *Polymer* **2008**, *49*, 1547-1554.

(32) Djalali, R.; Li, S.-Y.; Schmidt, M. *Macromolecules* **2002**, *35*, 4282-4288.

(33) Yuan, J.; Lu, Y.; Schacher, F.; Lunkenbein, T.; Weiss, S.; Schmalz, H.; Müller, A. H. E. *Chem. Mater.* **2009**, *21*, 4146-4154.

(34) Yuan, J.; Xu, Y.; Walther, A.; Bolisetty, S.; Schumacher, M.; Schmalz, H.; Ballauff, M.; Müller, A. H. E. *Nat. Mater.* **2008**, *7*, 718-722.

(35) Yuan, J.; Schacher, F.; Drechsler, M.; Hanisch, A.; Lu, Y.; Ballauff, M.; Müller, A. H. E. *Chem. Mater.* ***2010***, *22*, 2626-2634.

(36) Jain, A.; Wiesner, U. *Macromolecules* **2004**, *37*, 5665-5670.

(37) Zhai, L.; Herzog, B.; Drechsler, M.; Hoffmann, H. *J. Phys. Chem. B* **2006**, *110*, 17697-17701.

(38) Grabner, D.; Zhai, L.; Talmon, Y.; Schmidt, J.; Freiberger, N.; Glatter, O.; Herzog, B.; Hoffmann, H. *J. Phys. Chem. B* **2008**, *112*, 2901-2908.
(39) Kuo, S.-W.; Lee, H.-F.; Huang, C.-F.; Huang, C.-J.; Chang, F.-C. *J. Polym. Sci. Part A: Polym. Chem.* **2008**, *46*, 3108-3119.
(40) Yan, D.; Zhou, Y.; Hou, J. *Science* **2004**, *303*, 65-67.
(41) Raez, J.; Manners, I.; Winnik, M. A. *J. Am. Chem. Soc.* **2002**, *124*, 10381-10395.
(42) Yu, K.; Eisenberg, A. *Macromolecules* **1998**, *31*, 3509-3518.
(43) Liu, G. *Adv. Polym. Sci.* **2008**, 220, 29-64.
(44) Huang, K.; Rzayev, J. *J. Am. Chem. Soc.* **2009**, *131*, 6880-6885.
(45) Huang, K.; Canterbury, D.P.; Rzayev, J. *Macromolecules* **2010**, *43*, 6632-6638.
(46) Linse, P.; Claesson, P. M. *Macromolecules*, **2009**, *43*, 2076-2083.
(47) Lee, H.-i.; Pietrasik, J.; Sheiko, S. S.; Matyjaszewski, K. *Prog. Polym. Sci.* **2010**, *35*, 24-44.

Supporting Information

S1. Non-Crosslinked Organo-Silica Nanotubes in Water

The tubular structure of the non-crosslinked polymer brushes could be detected in aqueous solution. Cryo-TEM investigations underline the proposed structure of organo-silica nanotubes (see Scheme 3-1). It should be noted that the core diameter in this example exceeds the reported diameter (Table 3-1) by about 3 nm. We assume that shrinking during the crosslinking process and build-up of the silsesquioxane network lead to the observed core diameter of around 8 nm of the crosslinked materials. Further we like to mention that the smaller, not rod-shaped nanoparticles derive from fracturing of the original nanotubes (see S2).

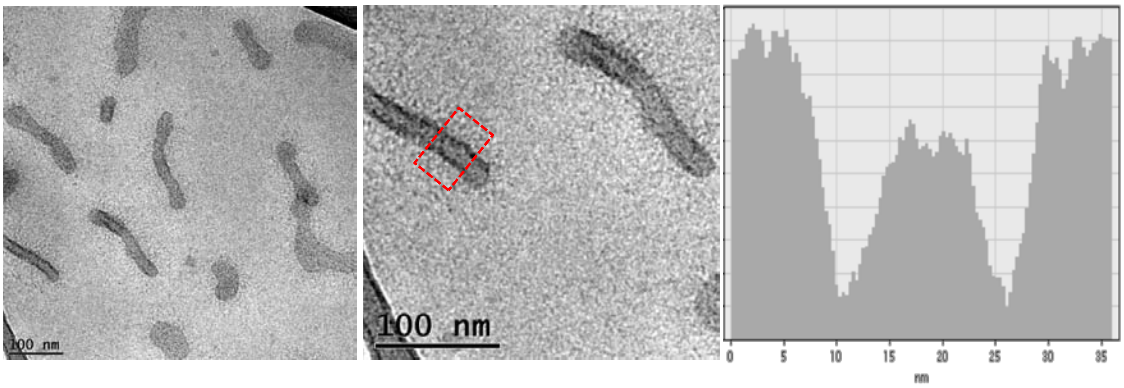

Figure 3-S1. Cryo-TEM images of non-crosslinked [tBA$_{75}$-b-APTS$_{115}$-b-OEGMA$_{150}$]$_{3200}$ in water.

S2. Crosslinking of the APTS shell

Non-crosslinked cylindrical polymer brushes were liable to fractures when in water. We assume that the organo-silica tubes break apart due to high repelling forces and stretching of the side chains in water. More and more spherical objects (Figure 3-S1 A/B) were found next to the pristine polymer brushes (S1 C). After the conversion into organo-silica hybrid nanotubes by crosslinking the APTS shell, the nanotubes were stable enough to not break apart in aqueous solution (see Figure 3-S1 D-F).

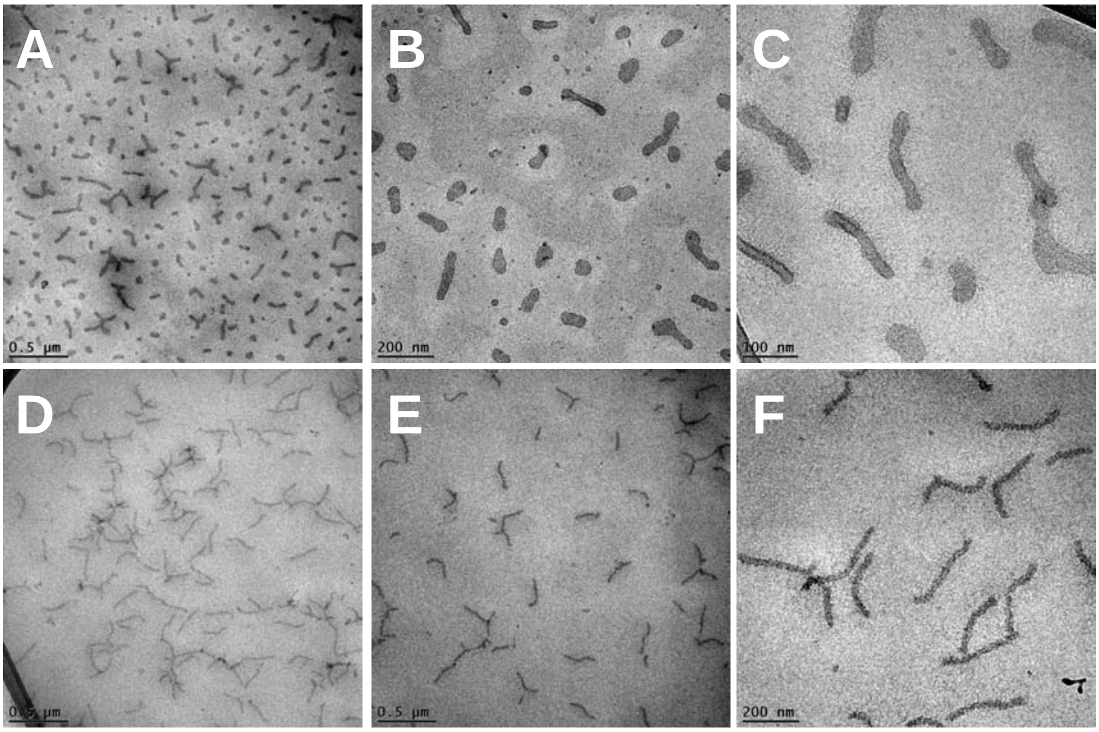

Figure 3-S2. (**A-C**) cryo-TEM images in water of non-crosslinked [tBA$_{75}$-b-APTS$_{115}$-b-OEGMA$_{150}$]$_{3200}$; (**D-F**) cryo-TEM images of crosslinked [tBA$_{75}$-b-(SiO$_{1.5}$)$_{115}$-b-OEGMA$_{150}$]$_{3200}$.

S3. Hydrogen fluoride (HF) treatment

Crosslinked cylindrical polymer brushes were treated with hydrogen fluoride (3 vol%) in THF for one day. After washing with THF, the hybrid nanotubes did not lose their cylindrical shape. HF is known to break Si-O-Si bonds, leading to the decomposition of the silsesquioxane network. However, the Si-C bonds stay unharmed. The remaining silicon provides a good contrast in TEM (see Figure 3-S3) depicting the unharmed cylindrical shape.

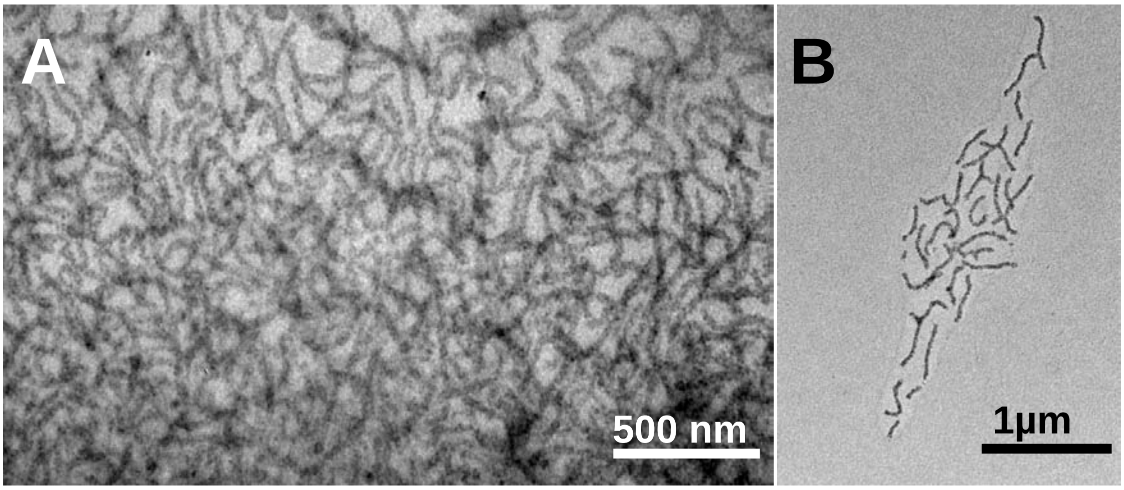

Figure 3-S3. TEM images of HF treated [tBA$_{75}$-b-(SiO$_{1.5}$)$_{170}$-b-OEGMA$_{400}$]$_{3200}$

Chapter 4

Template-Directed Mild Synthesis of Anatase Hybrid Nanotubes within Cylindrical Core-Shell-Corona Polymer Brushes

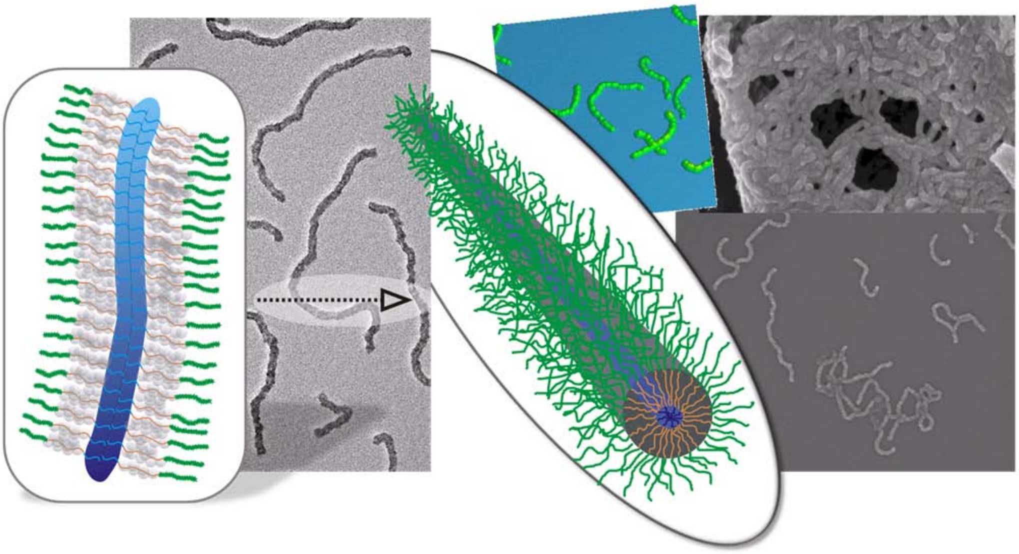

The results of this chapter will be submitted as:

“Template-Directed Mild Synthesis of Anatase Hybrid Nanotubes within Cylindrical Core-Shell-Corona Polymer Brushes”

by Markus Müllner, Thomas Lunkenbein, Martin Schieder, Nobuyoshi Miyajima, Melanie Förtsch, Josef Breu, Frank Caruso,* and Axel H. E. Müller*

Abstract: We demonstrate the synthesis of uniform one-dimensional (1D) titania nanostructures using core-shell-corona cylindrical polymer brushes (CPBs) as soft templates. The CPBs consist of a polymethacrylate backbone with densely grafted poly(*ε*-caprolactone) (PCL) in the core, poly(*2*-(dimethlamino)ethyl methacrylate) (PDMAEMA) in the cationic shell and poly(oligo(ethylene glycol) methyl ether methacrylate) (POEGMA) as the corona. The weak polyelectrolyte shell complexed an oppositely charged titania precursor, namely titanium(IV) bis(ammonium lactate) dihydroxide (TALH), and then acted as a nanoreactor for the hydrolysis and condensation of TALH, resulting in TiO_2. The POEGMA shell provides solubility in aqueous and organic solvents. The hybrid titania nanotubes containing crystalline anatase nanoparticles were characterized by atomic force microscopy (AFM), transmission electron microscopy (TEM) and scanning electrion microscopy (SEM). The phase purity of the crystalline nanostructures was verified by powder X-ray diffractometry (PXRD).

Introduction

One-dimensional (1D) nanostructures have been intensively studied in recent years.[1-4] The ability to precisely produce nanometer-sized materials opens new possibilities in modern science and technology. Their unique size- and shape-dependent properties and their continually expanding application in various research areas have dramatically increased the interest in anisotropic nanostructures, such as rods, wires and tubes.[5-8] Many difficulties associated with the synthesis of 1D nanostructures have been overcome, and it is now possible to precisely fine-tune the dimensions of these nanostructures, as well as control their morphology, phase purity and chemical composition.[9] To date, several strategies have been developed to fabricate organic, hybrid and inorganic 1D nanostructures.[4] They can be synthesized from either vapor, liquid or solid phases by using multiple methods, and using two fundamental steps: nucleation and growth.[5, 10-16] Xia *et al.* highlighted several strategies for “bottom-up” methods as key factors for the fabrication of homogenous 1D inorganic nanostructures.[2] The use of capping agents (such as surfactants)[17-19] or the self-assembly of 0D nanostructures[20, 21] are examples of the promising pathways toward anisotropic nanomaterials. Another elegant route toward 1D nanostructures is the direct use of 1D templates, including organic systems. Cylindrical polymer brushes (CPBs),[4, 22] carbon nanotubes,[23, 24] self-assembled block copolymers[25-27] and biological superstructures[28-30] (viruses or DNA) are examples of templates with pre-existing asymmetric shapes. The main challenges in using template-directed approaches arise with the synthesis and design of the cylindrical template rather than the fabrication of the hybrid material. A promising and uniform 1D template is unimolecular CPBs. These are molecular brushes carrying linear side chains densely grafted from a backbone. They can be synthesized by using “grafting-from”, “grafting-onto” and “grafting-through” strategies.[31] The dense packing of side chains along the polymer backbone causes stretching of the backbone and stiffening of the entire polymer brush. Core-shell-corona structured CPBs – *i.e.*, polymer brushes carrying ABC triblock terpolymers as side chains – have proven to be interesting building blocks and templates. Rzayev and coworkers recently showed molecular transport through polymeric nanotubes prepared from core-shell-corona CPBs.[32]

Through the incompatibility of each side chain block, the polymer brush can be divided into different 1D interior domains, with lengths up to several hundred nanometers. Such structures act as ideal 1D nanoreactors for the synthesis of anisotropic hybrid and inorganic nanostructures. There are a number of studies on using unimolecular soft templates such as CPBs for the fabrication of well-defined anisotropic nanomaterials. Core-shell CPBs have been used for the fabrication of TiO_2,[33] CdS,[34] CdSe[35] and SiO_2[36] hybrid nanowires, as well as core-shell-corona CPBs for the fabrication of silica hybrid nanotubes.[37] All of these nanomaterials have only one compartment of the template, for example the shell or the core, that hosts guest molecules, such as salts or inorganic precursors. These guest molecules can be either loaded into the compartment or already covalently bonded inside the compartment. The loading of inorganic material can be performed via two ways, the *in situ* generation of inorganic material within the template[35, 38] or the loading of presynthesized nanoscopic materials into a template compartment.[25, 38]

Such nanostructuring of inorganic materials has attracted considerable interest, as the resulting materials often exhibit high surface areas and small sizes of the inorganic nanoparticles, which provide them with unique optical, electrical and catalytic properties.[39-42] Nanomaterials of titania (TiO_2) are of particular interest, as it is possible to control their physical and chemical characteristics through synthesis pathways. Consequently, there exists a large variety of applications of TiO_2 nanomaterials in the fields of gas sensing, dielectric ceramics, catalysts, photovoltaic solar cells and pigments.[42-47]

In our previous work, we synthesized TiO_2 nanowires from a bis-hydrophilic core-shell polymer brush $[HEMA_{85}\text{-}OEGMA_{200}]_{3200}$ and titanium tetra(*n*-butoxide), $Ti(OBu)_4$.[33] In that study, $Ti(OBu)_4$ was immobilized into the poly(2-hydroxyethyl methacrylate) (PHEMA) compartment through transalcoholysis and a subsequent hydrolysis step led to uniform TiO_2 nanowires. However, alkoxy-based titania precursors are very labile to hydrolysis, especially in aqueous solution. Mostly they only form amorphous TiO_2 and are then converted into crystalline TiO_2 through additional steps like heat treatment.[33, 48, 49] Although the loading was performed in dioxane, it nevertheless had the side effect that titania nanoparticles were not only complexed in the PHEMA core but also in the shielding POEGMA corona.

Herein, we infiltrated a negatively charged inorganic titania precursor to coordinate exclusively into one of the template brush compartments. We used a core-shell-corona CPB, consisting of a PHEMA backbone with poly(ε-caprolactone) (PCL) as the core, poly[2-(dimethylamino)ethyl methacrylate] (PDMAEMA) as the polycationic shell, and poly(oligo(ethylene gylcol) methyl ether methacrylate) (POEGMA) as the solublizing corona, as a template for the fabrication of anatase nanotubes. The applied polymerization techniques gave excellent control over the synthesis of the template brushes and hence allowed precise adjustment of the diameter of the TiO_2 nanotubes. Using ring-opening polymerization of ε-caprolactone (CL) led to a high grafting efficiency of side chains because the PCL chains have low steric requirements. In addition, they can be degraded by ester hydrolysis. Atom transfer radical polymerization (ATRP) allowed the homogenous and sequential tailoring of the shell and the corona. The use of a charged TiO_2 precursor, titanium(IV) bis(ammonium lactate) dihydroxide (TALH), had two key advantages compared to our previous work. First, TALH guaranteed stability in respect to spontaneous hydrolysis during the loading of the template at ambient temperatures. TALH has already been used to produce titania coatings on silica gels,[50] layered gold nanoparticles[51] and polymeric substrates,[52] and its controlled hydrolysis and condensation at elevated temperatures and different pH values is well studied and documented. Second, the precise and exclusive coordination of TALH into the PDMAEMA shell compartment allowed the fabrication of homogenous TiO_2 nanomaterials. No undesired TiO_2 was found in the corona or in solution.

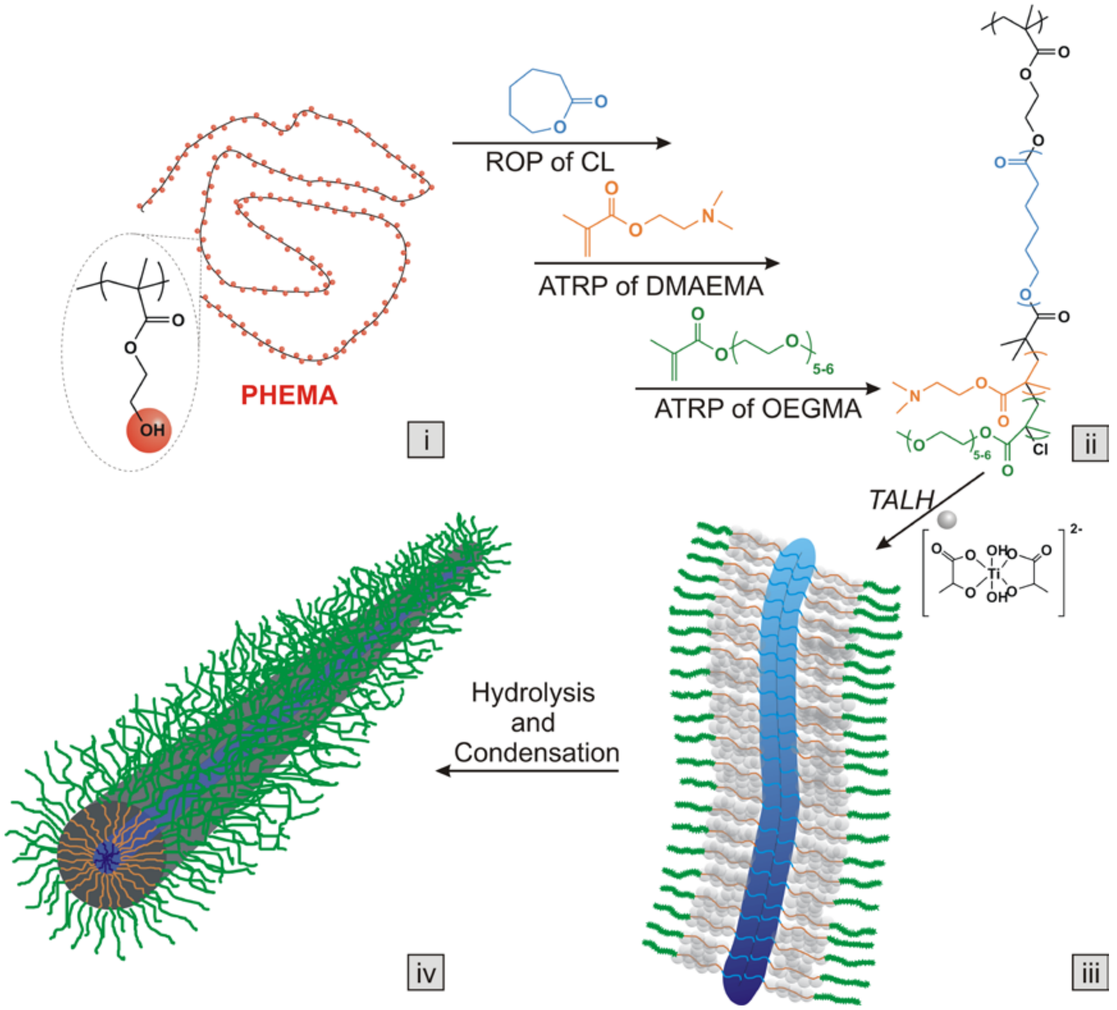

Scheme 4-1. Schematic illustration of the template prepared from PHEMA by the combination of ROP and ATRP to form (**i**) core-shell-corona CPBs (**ii**). Complexation of the titanium salt TALH into the CPBs (**iii**) and its hydrolysis and condensation to form soluble anatase nanotubes (**iv**).

Experimental Section

Materials

All chemicals were of analytical grade and used as received without further purification, except for *2*-(dimethylamino)ethyl methacrylate (Aldrich, 98%) and oligo(ethylene glycol) methyl ether methacrylate (Aldrich, 98%, M_n ~ 300 g·mol^{-1}), which were passed through a silica column prior to polymerization.

Preparation of the polymer brush [PCL-b-PDMAEMA-b-POEGMA]$_x$. The template was synthesized through the combination of anionic, ring opening and ATRP. The stepwise buildup from a polyinitiator backbone to a core-shell cylindrical polymer brush [CL$_{14}$-DMAEMA$_{40}$-OEGMA$_{65}$]$_{7500}$ is explained in detail below.

Synthesis of HEMA$_{7500}$ backbone. The polyinitiator backbone PHEMA was obtained through deprotection of poly(2-(trimethylsiloxy)ethyl methacrylate) (PTMS-HEMA). The PTMS-HEMA backbone was synthesized as previously reported by Mori *et al.*[53] The molecular weight was determined by static light scattering (SLS). The number-average degree of polymerization (DP$_n$) and the polydispersity index (PDI) are 7500 and 1.14, respectively. The deprotection was performed with acetic acid in methanol.

Synthesis of the cylindrical polymer brush [CL$_{14}$]$_{7500}$. PHEMA (80 mg, 0.62 mmol) was dissolved in CL (6 mL, 54.2 mmol) and water traces were distilled off in the presence of benzene. Afterward, the mixture was degassed by bubbling argon for 30 min. The ring-opening polymerization (ROP) of CL was catalyzed by the addition of tin(II) 2-ethylhexanoate (1.5 mg, 3.70 µmol) at 125 °C. The polymerization was allowed to proceed for 11 h, until the mixture became very viscous. The polymerization was quenched by cooling and exposing to air and then diluted with THF and precipitated into cold cyclohexane. The conversion was determined after purification by ^{1}H-NMR by comparing the polymeric CH$_2$-signal at 4.1 ppm and the terminal CH$_2$-signal at 3.65 ppm. The PCL homopolymer brush [CL$_{14}$]$_{7500}$ was precipitated twice into a cold water/methanol mixture (10/90 v/v) and then freeze-dried from dioxane. [CL$_{14}$]$_{7500}$ was then reacted with a 1.5-fold molar excess of 2-bromoisobutyryl bromide and a 2-fold molar excess of triethylamine (TEA) in dry THF to functionalize the PCL brush with ATRP initiating groups. The reaction mixture was stirred for 24 h at room temperature, and then the functionalized polymer was concentrated by solvent evaporation, precipitated in a cold water/methanol mixture (80/20 v/v) and freeze-dried from dioxane.

Synthesis of the cylindrical core-shell polymer brush [CL$_{14}$-DMAEMA$_{40}$]$_{7500}$. [CL$_{14}$]$_{7500}$ (8.0 µmol) was dissolved in 7 mL of anisole and deoxygenated for 10 min in a screw-cap flask sealed with a septum. Then, 0.01 mmol of CuCl was added and argon was bubbled through the mixture for 20 min. Meanwhile, 5 mmol of destabilized DMAEMA, 0.01 mmol of PMDETA and 1 mL of anisole were degassed. The polymerization was started after adding the DMAEMA/PMDETA mixture to the reaction flask at 50 °C. The polymerization was monitored via ^{1}H-NMR and quenched at the desired conversion by cooling it and exposing it to air. The polymer solution was passed through a short silica gel column before it was precipitated into cold cyclohexane. The precipitate was immediately dissolved in ethanol before a second precipitation. The polymer was dissolved in anisole and the excess ethanol was removed by reduced pressure.

Synthesis of the cylindrical core-shell-corona polymer brush $[CL_{14}\text{-}DMAEMA_{40}\text{-}OEGMA_{65}]_{7500}$ (brush 1). $[CL_{14}\text{-}DMAEMA_{40}]_{7500}$ (2.3 µmol) and destabilized OEGMA (1.2 mmol) were dissolved in 5 mL of anisole and deoxygenated for 10 min in a screw-cap flask sealed with a septum. Then, 0.07 mmol of CuCl was added and argon was bubbled through the mixture for 20 min. Meanwhile, 0.7 mmol PMDETA in 0.5 mL anisole was degassed. The polymerization was started after injecting the degassed PMDETA solution to the reaction mixture at 60 °C. The polymerization was monitored via ^{1}H-NMR and quenched at the desired conversion by cooling it and exposing it to air. The polymer solution was passed through a short silica gel column before it was precipitated into cold cylcohexane. The precipitate was dissolved again in acetone and dialyzed into ethanol.

$[CL_{14}\text{-}DMAEMA_{150}\text{-}OEGMA_{240}]_{7500}$ (brush 2) was synthesized in a similar way as above.

Synthesis of anatase hybrid nanotubes. 35 µL of titanium(IV) bis(ammonium lactate) dihydroxide (TALH) solution (contains 0.07 mmol TALH) was added dropwise to 10 mg (contains 0.015 mmol PDMAEMA) of $[CL_{14}\text{-}DMAEMA_{40}\text{-}OEGMA_{65}]_{7500}$ (**brush 1**) ($0.5\ g\cdot L^{-1}$) in an ethanol/water mixture (1:1 v/v). After mixing for about 3 h, the solution was diluted with ethanol and slowly heated to 95 °C. The solution was refluxed over night. The hydrolysis of TALH resulted in the formation of highly crystalline (anatase) TiO_2 nanotubes. The above procedure was the same for $[CL_{14}\text{-}DMAEMA_{150}\text{-}OEGMA_{240}]_{7500}$ (**brush 2**), except that 82 µL of TALH solution (contains 0.17 mmol TALH) was added to fill the PDMAEMA shell.

Characterization

Atomic Force Microscopy (AFM). AFM images were recorded on a Digital Instruments Dimension 3100 microscope operated in tapping mode. The samples were prepared by dip-coating freshly cleaved mica into a dilute solution of polymer brush and ethanol or water to form a monomolecular film.

Transmission Electron Microscopy (TEM). Bright field TEM was performed using a Zeiss CEM 902 electron microscope operated at 80 kV. A droplet of a dilute polymer brush and ethanol solution (0.05 g/L) was dropped onto a copper grid (200 mesh) coated with a carbon film. Liquid was then blotted from the grid and the grid was allowed to dry at room temperature for a short time. HR-TEM was carried out on a Philips CM20FEG TEM operated at 200 kV using lacey TEM grids.

Cryogenic Transmission Electron Microscopy (cryo-TEM). Cryo-TEM was conducted by dropping the dilute polymer brush and water solution (0.1 g/L) on a hydrophilized lacey TEM grid, from which most of the liquid was removed by using blotting paper, leaving a thin film stretched over the grid holes. The specimens were shock frozen by rapid immersion into liquid ethane and cooled to approximately 90 K by liquid nitrogen in a temperature-controlled freezing unit (Zeiss Cryobox, Zeiss NTS GmbH, Oberkochen, Germany). After the specimens were frozen, the remaining ethane was removed using blotting paper. The specimen was inserted into a cryo-transfer holder (CT3500, Gatan, München, Germany) and transferred to a Zeiss EM922 EF-TEM instrument operated at 200 kV.

Static Light Scattering (SLS). SLS measurements were carried out on a Sofica goniometer with He-Ne laser (632.8 nm) at 20 °C in toluene. A Zimm plot was used to evaluate the data. A ScanRef laser interferometer was used to measure the refractive index increment, *dn/dc*, of the polymer solution.

Scanning Electron Microscopy (SEM). SEM analysis was performed using a Zeiss Model 1530 Gemini instrument equipped with a field-emission cathode with a lateral resolution of ∼ 2 nm. The samples were sputtered with platinum for 1 min and then measured on a silica wafer.

Powder X-ray Diffraction (PXRD). The PXRD measurement was performed at 25 °C on a Panalytical XPERT-PRO diffractometer in reflection mode using Cu Kα radiation.

N_2-sorption isotherms. N_2-physisorption was conducted at 77 K on a Quantachrome Autosorb 1 instrument. Prior to the measurements, the samples were degassed at 373 K for 24 h.

Thermogravimetric Analysis (TGA) and calcination. TGA was performed on Netzsch 409C apparatus in air atmosphere, with the temperature ranging from 30 to 650 °C at a heating rate of 10 K min^{-1}. Calcination was done in a tube furnace in air atmosphere at a heating rate of 3 K min^{-1}from 30 °C to 650 °C.

Proton Nuclear Magnetic Resonance (NMR). ^{1}H-NMR spectra were recorded to determine the monomer conversion on a Bruker AC-300 spectrometer at room temperature in $CDCl_3$.

Results and Discussion

Synthesis of the template brushes.

As illustrated in Schemes 4-1 and 4-2, we combined several polymerization techniques to obtain a CPB with defined compartments, which can be used as a soft template for the fabrication of anatase nanotubes. First, PHEMA was used as a polyinitiator backbone for the grafting of CL. PHEMA was produced by anionic polymerization of trimethylsilyl-protected HEMA (TMS-HEMA).[53] Poly(TMS-HEMA) with an number-average molecular weight, M_n, of 1.5 x 10^6 g·mol^{-1} and a polydispersity index, PDI, of 1.14 was achieved. After deprotection with acetic acid, a high molecular weight PHEMA polymer backbone was obtained. PCL homopolymer brushes were synthesized by ring-opening polymerization (ROP) in bulk, using tin(II) 2-ethylhexanoate, $Sn(Oct)_2$, as a catalyst. ROP is an excellent way to increase the grafting density of side chains.[54] In addition it can be degraded by ester hydrolysis. The terminal groups of the PCL brush side chains are hydroxyl groups, which are accessible for esterification with an ATRP initiator. The CH_2-group closest to the terminal OH-group can be used to determine the degree of polymerization (DP_n) by comparing the CH_2-group triplet of the polymeric CH_2-group next to the PCL ester group at 4.1 ppm with that of the terminal OH group at 3.65 ppm (see Supporting Information 4-S1). The ratio is the DP_n of PCL. After reacting 2-bromoisobutyryl bromide with the terminal OH groups of the PCL homopolymer, vinyl monomers could be polymerized via ATRP. We polymerized 2-(dimethylamino)ethyl methacrylate first and then oligo(ethylene glycol) methyl ether methacrylate in two sequential steps from the PCL homopolymer brushes to obtain core-shell-corona CPBs, where PCL, PDMAEMA and POEGMA formed the core, the shell and the corona, respectively. Through the sequential grafting approach, we could readily adjust the dimensions of the PDMAEMA shell and the POEGMA corona (see Table 4-1). The template buildup can also be followed in Scheme 4-2 (A)-(D). The ^{1}H-NMR spectrum of each sequential grafting step is shown in Figure 4-1. Two core-shell-corona CPBs containing the same weight content of PDMAEMA were synthesized: [CL_{14}-

DMAEMA$_{40}$-OEGMA$_{65}$]$_{7500}$ (**brush 1**) and [CL$_{14}$-DMAEMA$_{150}$-OEGMA$_{240}$]$_{7500}$ (**brush 2**) (see Table 4-1).

Figure 4-2A shows the template polymer brush before loading with TALH. The average height was about 1.5 nm. The length was up to 1.3 µm; however, the brush tended to fracture during deposition onto mica due to its rather long length and hydrophilic side chains. Sheiko *et al.* already reported scission of carbon-carbon bonds on substrates.[55]

Table 4-1. Template core-shell-corona CPBs with different diameters[a].

Name	Composition[b]	Shell diameter[c]
Template brush 1	[CL$_{14}$-*b*-DMAEMA$_{40}$-*b*-OEGMA$_{65}$]$_{7500}$	23 ± 2 nm
Template brush 2	[CL$_{14}$-*b*-DMAEMA$_{150}$-*b*-OEGMA$_{240}$]$_{7500}$	39 ± 2 nm

[a] Diameter of the PCL core ~7 nm; brush length < 1.3 µm. [b] As determined by ^{1}H-NMR. [c] After TALH infiltration and hydrolysis (determined by TEM).

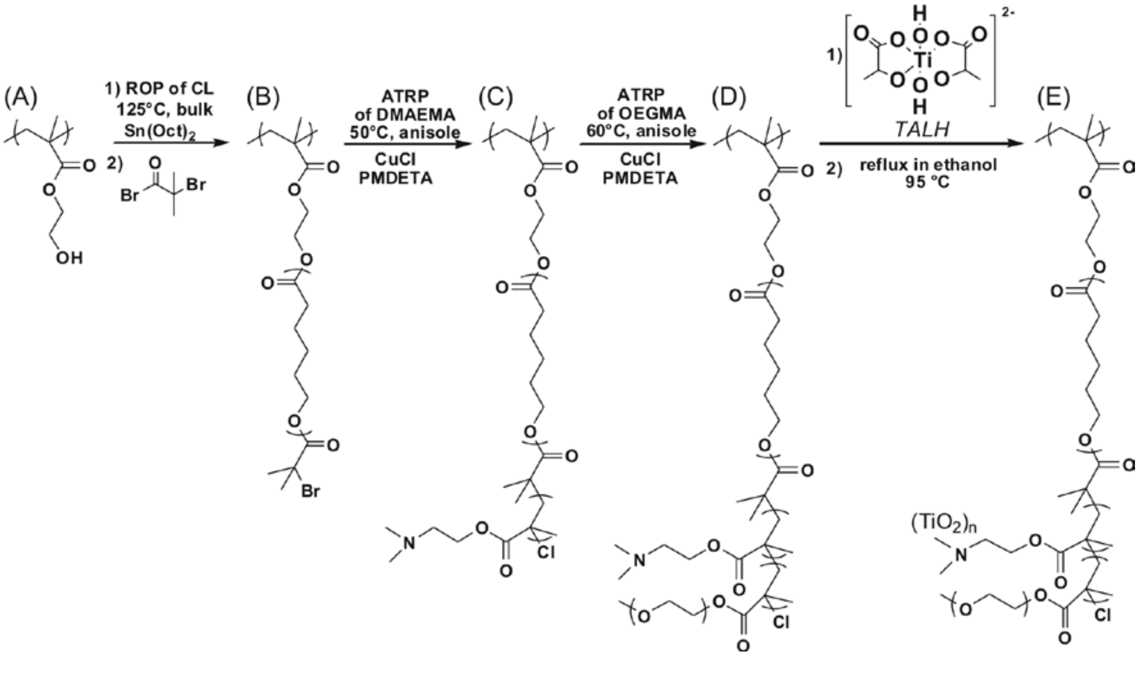

Scheme 4-2. Hybrid brush synthesis via grafting of (**B**) CL, (**C**) DMAEMA and (**D**) OEGMA from (A) a PHEMA backbone. (**E**) The incorporation of TALH into the DMAEMA shell compartment was followed by hydrolysis and formed crystalline anatase.

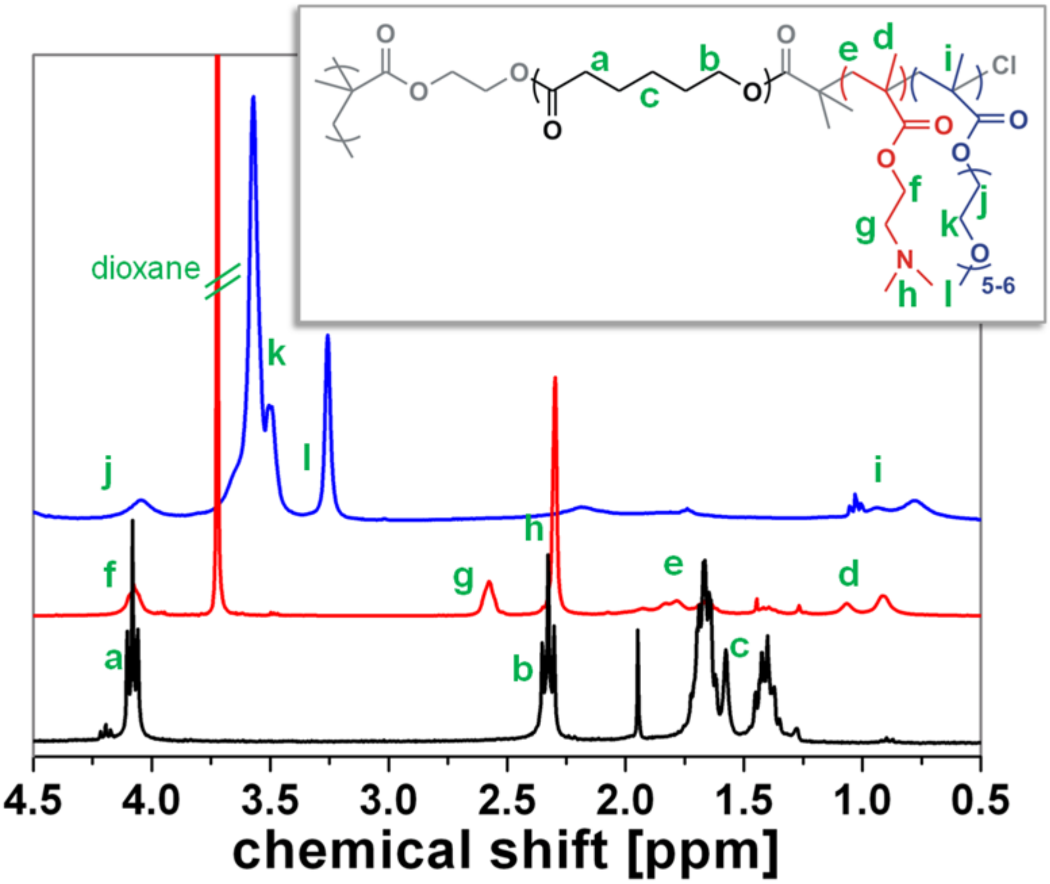

Figure 4-1. ^{1}H-NMR spectra of $[CL_{14}]_{7500}$ (**black line, bottom**) and $[CL_{14}\text{-}DMAEMA_{40}]_{7500}$ (**red line, middle**) in $CDCl_3$, and $[CL_{14}\text{-}DMAEMA_{40}\text{-}OEGMA_{65}]_{7500}$ (**blue line, top**) in D_2O.

Synthesis and characterization of the titania hybrid nanotubes.

The template polymer brush was then used to load TALH into the PDMAEMA shell compartment. By using TALH, we utilized electrostatic interaction for the titania precursor immobilization step instead of the previously used transalcoholysis.[33] Consequently, we achieved exclusive loading of TALH only into the PDMAEMA shell compartment, whereas the POEGMA corona could not complex TALH and therefore remained unloaded. The negatively charged titania precursor interacted exclusively with the partially protonated amino groups of PDMAEMA, forming TALH nanotubes. Furthermore, TALH is stable in aqueous solution at room temperature,[50, 51] compared to other titania precursors, like $Ti(OBu)_4$, which hydrolyze rather rapidly in the presence of water.

The appropriate amount of TALH needed to fill the template brushes was investigated by TEM after different amounts of TALH were added to the template solution. By ensuring the right ratio of TALH to PDMAEMA, the precursor was only located in the shell compartment and no excess precursor was present in solution. Consequently, there is no formation of single titania nanoparticles in solution upon hydrolysis. The advantages of TALH are the controlled hydrolysis and condensation reactions by adjusting both, pH and temperature.[51, 52]

After infiltration and thermal hydrolysis of TALH within the template brush, the chains of the PDMAEMA compartment become rather stretched and hence the average height of the brush as determined by AFM increased about 10-fold to 15 nm, as compared to the pristine unloaded brush template. Figure 4-2B shows an AFM image of the TiO_2 nanotubes. There were no free titania nanoparticles present as the condensation only occurred inside the polymer brush shell. The POEGMA shell was necessary to avoid intermolecular crosslinking upon hybrid formation.

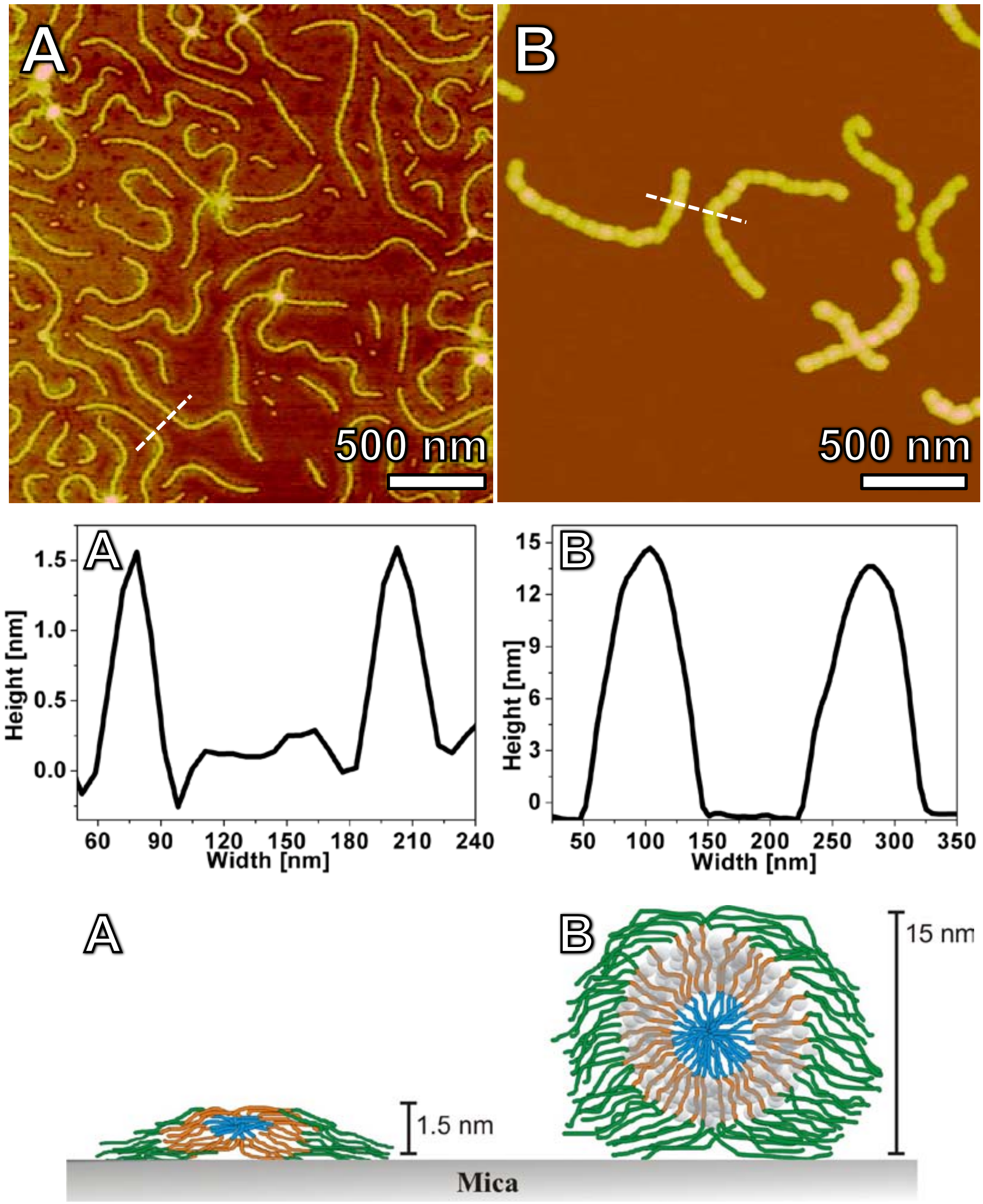

Figure 4-2. AFM height images of (**A**) template brush 1 and (**B**) hydrolyzed TALH infiltrated into hybrid nanotubes, on mica. The cross-sections of the corresponding AFM height images can be found underneath the images. The z-values are (**A**) 6 nm and (**B**) 40 nm.

Figure 4-3 shows TEM micrographs of the TALH-loaded polymer **brush 1** (A, B) and the thermally hydrolyzed and condensed analogues (C, D). In all micrographs, there was no excess TALH/titania nanoparticles visible in the background and the brush templates were homogeneously loaded with TALH/TiO_2. The diameter of the TALH loaded nanotubes was around 28 ± 2 nm. The diameter decreased slightly to 23 ± 2 nm after hydrolysis and condensation. However, the shape and length of the nanotubes remained unchanged. The PCL core of the nanotubes appeared lighter as compared to the TALH/titania containing shell, due to the much lower contrast used (see grey-scale analysis in Figure 4-3B and D). The PCL core remained unchanged during hydrolysis and had a diameter of around 7 nm. The POEGMA corona of the polymer brush (65 and 150 monomer units, respectively) still surrounded the nanotubes and prevented crosslinking between the individual nanotubes. Incidentally, some brushes appear to have merged, e.g. in Figure 4-3D. However, these are drying artifacts.

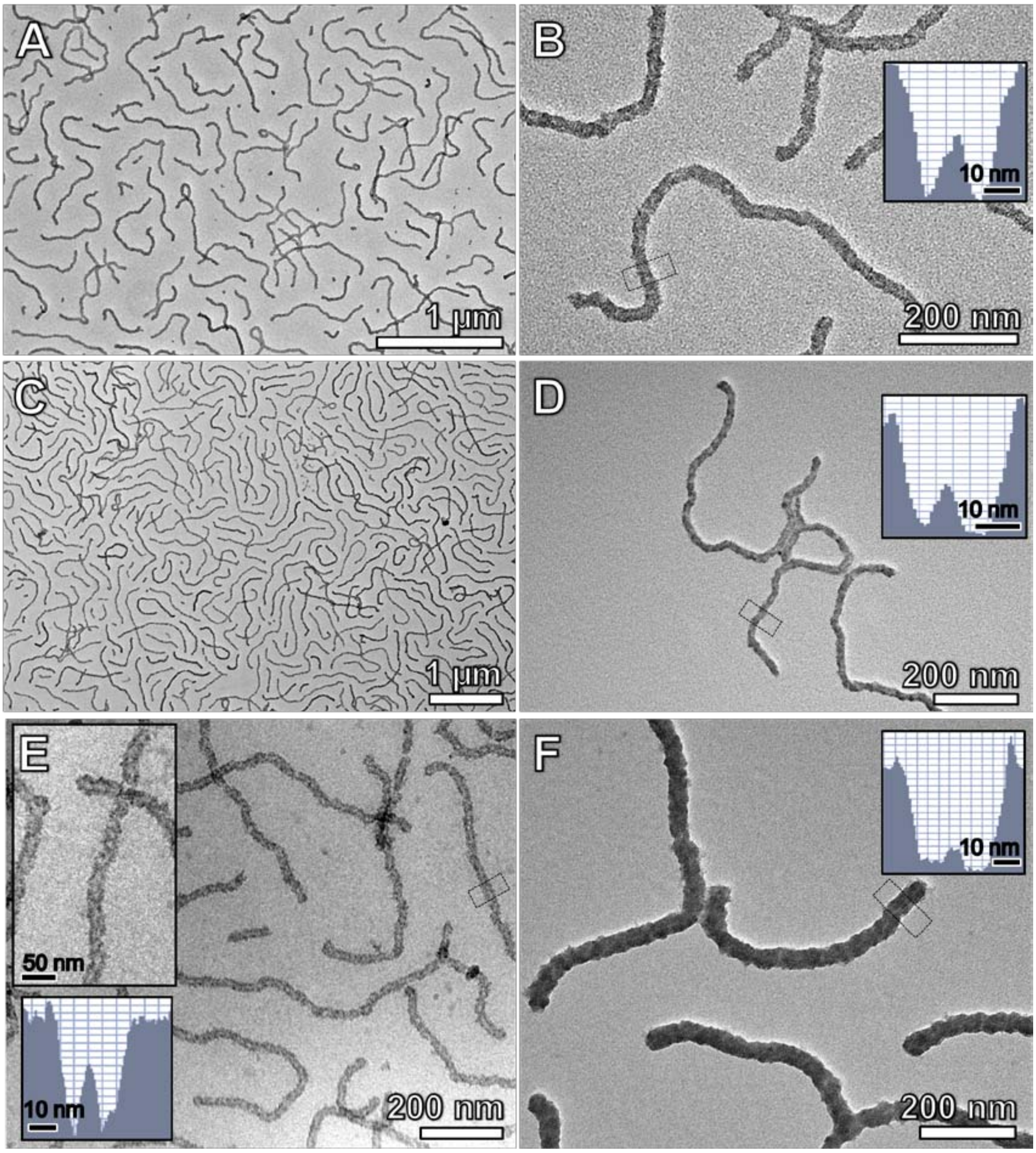

Figure 4-3. (**A, B**) TEM micrographs of TALH loaded core-shell-corona polymer brushes of template brush 1 and (**C, D**) their hydrolyzed crystalline analogues. (**E**) Cryo-TEM micrograph of TALH-loaded template brush 1 in water. (**F**) TEM micrograph of TALH-loaded and hydrolyzed template brush 2. The insets in B, D, E and F show the grey-scale analysis of cross-sections through the respective nanotube.

The POEGMA corona solubilized and stabilized the TiO_2 nanotubes in both organic and aqueous solutions. Cryogenic TEM (cryo-TEM) images highlighted the good dispersibility of TALH nanotubes in water (see Figure 4-3E). The PCL core was again distinguishable due to the lower contrast (see magnification and grey-scale analysis in Figure 4-3E). The POEGMA corona was not visible in the TEM images. The loading into and subsequent hydrolysis of TALH within the **brush 2** led to an increase in thickness to about 39 ± 2 nm due to the larger PDMAEMA shell compartment (see Figure 4-3F).

Several groups have studied the hydrolysis of TALH and demonstrated that it can crystallize to give the anatase polymorph of TiO_2.[52] It is well known that TALH rapidly undergoes hydrolysis at temperatures above 70 °C.[52, 56] It was also shown that the thermal hydrolysis of TALH proceeds smoothly upon step-wise heating.[57] Therefore, we commenced hydrolysis of the TALH-loaded polymer brushes at 60 °C and continued stepwise heating toward 80 °C within 3 hours (raising temperature by 6-7 °C every 30 min). The nanotubes were then refluxed (95 °C) over night in ethanol to ensure complete hydrolysis. Powder X-ray diffractometry (PXRD) of the air-dried TiO_2 nanotubes confirmed the anatase crystal structure (see Figure 4-4B). Peak broadening revealed that the crystalline nanoparticles were quite small. Thus, as might be expected, the hybrid brushes do not represent single crystals of µm dimension but the inorganic walls are rather polycrystalline, composed of many small, tightly aggregated crystallites. Evaluating particle sizes applying the Scherrer formula gave diameters of 3-4 nm which is in good agreement with HR-TEM observations (Figure 4-4A). Moreover, as the crystal lattices are clearly visible, HR-TEM verified that the nanotubes, produced upon hydrolysis, were highly crystalline.

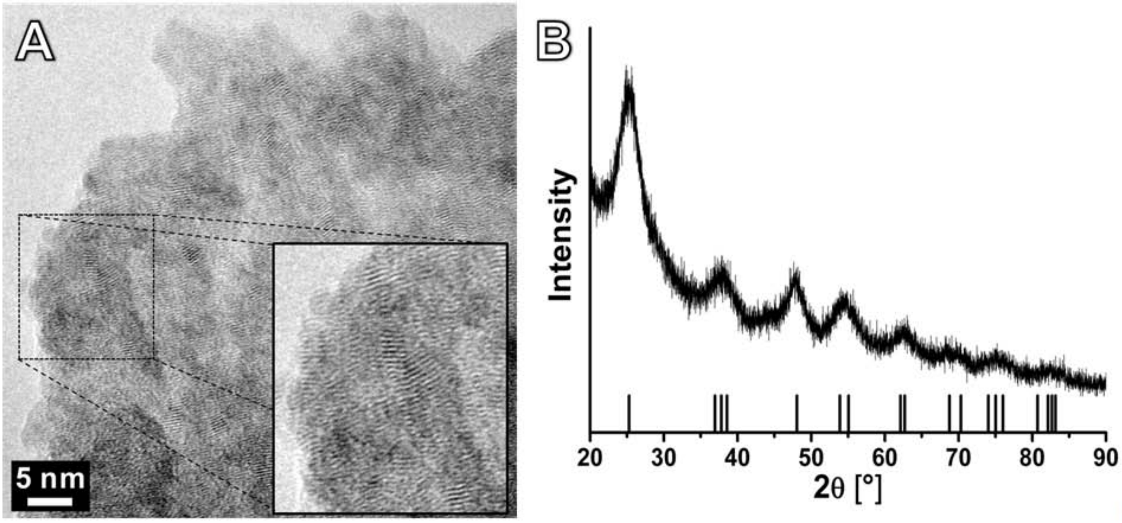

Figure 4-4. (**A**) HR-TEM micrograph of an anatase nanotube from template brush 1. The magnification clearly reveals crystalline areas within the nanotube. (**B**) Powder XRD pattern of hydrolyzed TALH nanotubes. The ticks on the x-axis in (**B**) indicate the expected positions of the anatase reflexes .

Both template brushes 1 and 2 were designed to have an equal weight content of PDMAEMA of around 25 wt% compared to the overall M_n. This made it easier to compare the amount of inorganic material that was incorporated into the PDMAEMA shell. Thermogravimetric analysis (TGA) determined the weight content of TiO_2 in the template brushes with 40 repeating units of DMAEMA to be 39 wt%, whereas the template brushes with 150 repeating units of DMAEMA were able to embed 47 wt% of TiO_2 (Figure 4-5). TGA thereby revealed that longer PDMAEMA chains, as expected, were able to load slightly more TALH into the shell. We assume that with increasing length of polymer brush side chains, the mobility and space of these chains increases as well. Consequently, there is more room for the incorporation of material, which accordingly increases the loading capacity.

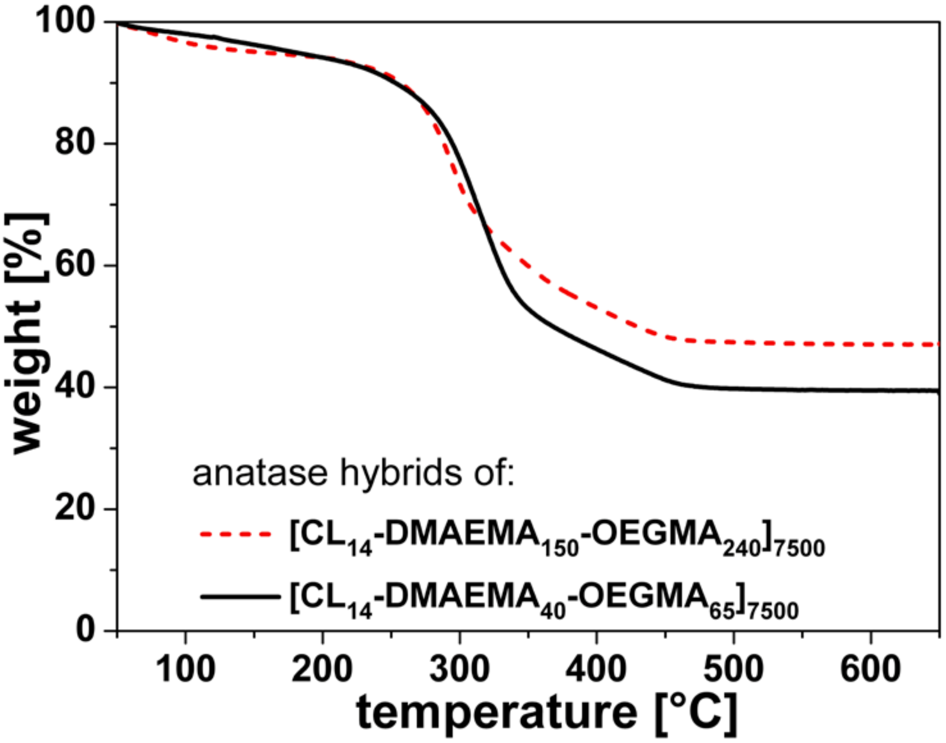

Figure 4-5. TGA of the anatase hybrid nanotubes from template brush 1 (**black solid line**) and template brush 2 (**red dashed line**).

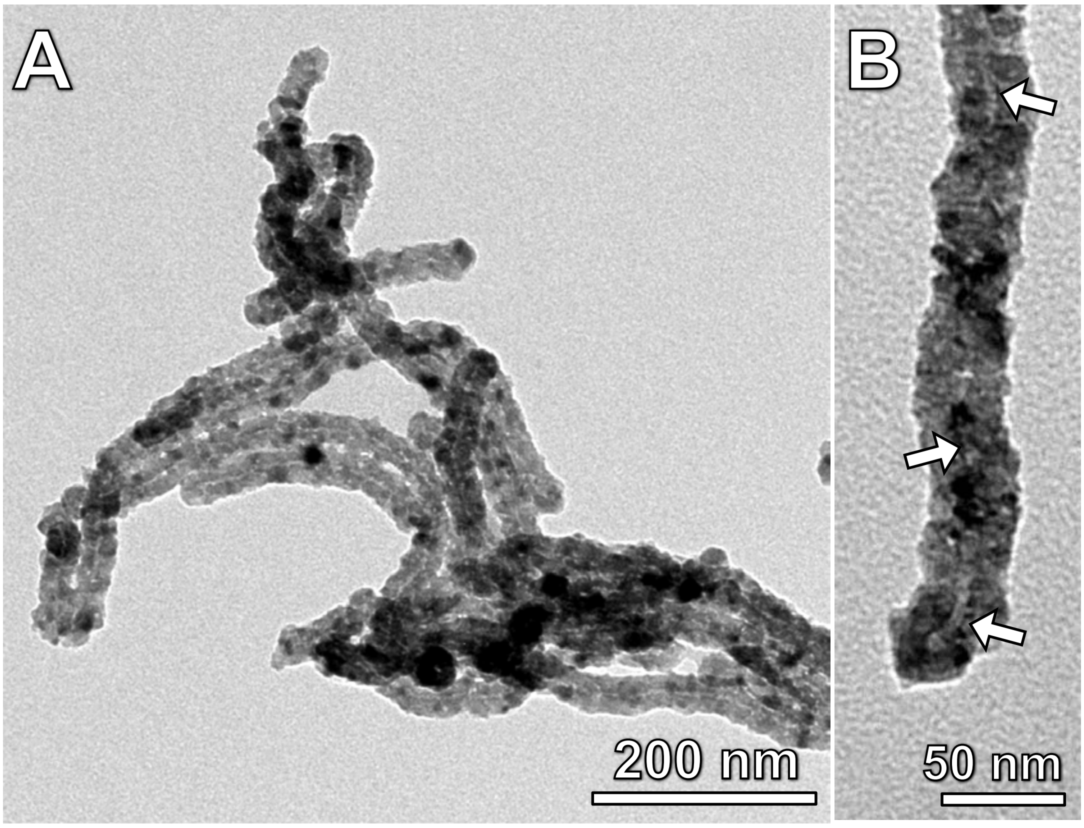

Figure 4-6. (A/B) TEM micrographs of calcined anatase nanotubes. **(B)** The white arrows indicate the tubular structure after calcinations.

Calcination of the anatase hybrid nanomaterial in air resulted in the removale of the template brush which thus resulted in pure anatase nanotubes (Figure 4-6). Additionally, the crystalline nanomaterials were deposited on silicon wafers and investigated with scanning electron microscopy (SEM; Figure 4-7). SEM highlighted, again, the uniformity in thickness of the anatase nanotubes. Highly concentrated dispersions of anatase hybrid nanotubes formed non-woven networks of hybrid nanotubes upon (freeze-)drying (Figure 4-7A–D). Those networks were preserved after calcination in air at 650 °C. Figures 4-7E and 4-7F underlined the high porosity of inorganic nanomaterials obtained by this method. TEM and SEM both revealed that the worm-like structures retained their shape after calcination (see Supporting Information 4-S2). The surface area of the dried hybrid material was 16 $m^{2} \cdot g^{-1}$, as determined by Brunauer-Emmett-Teller analysis of N_2-physisorption isotherms.

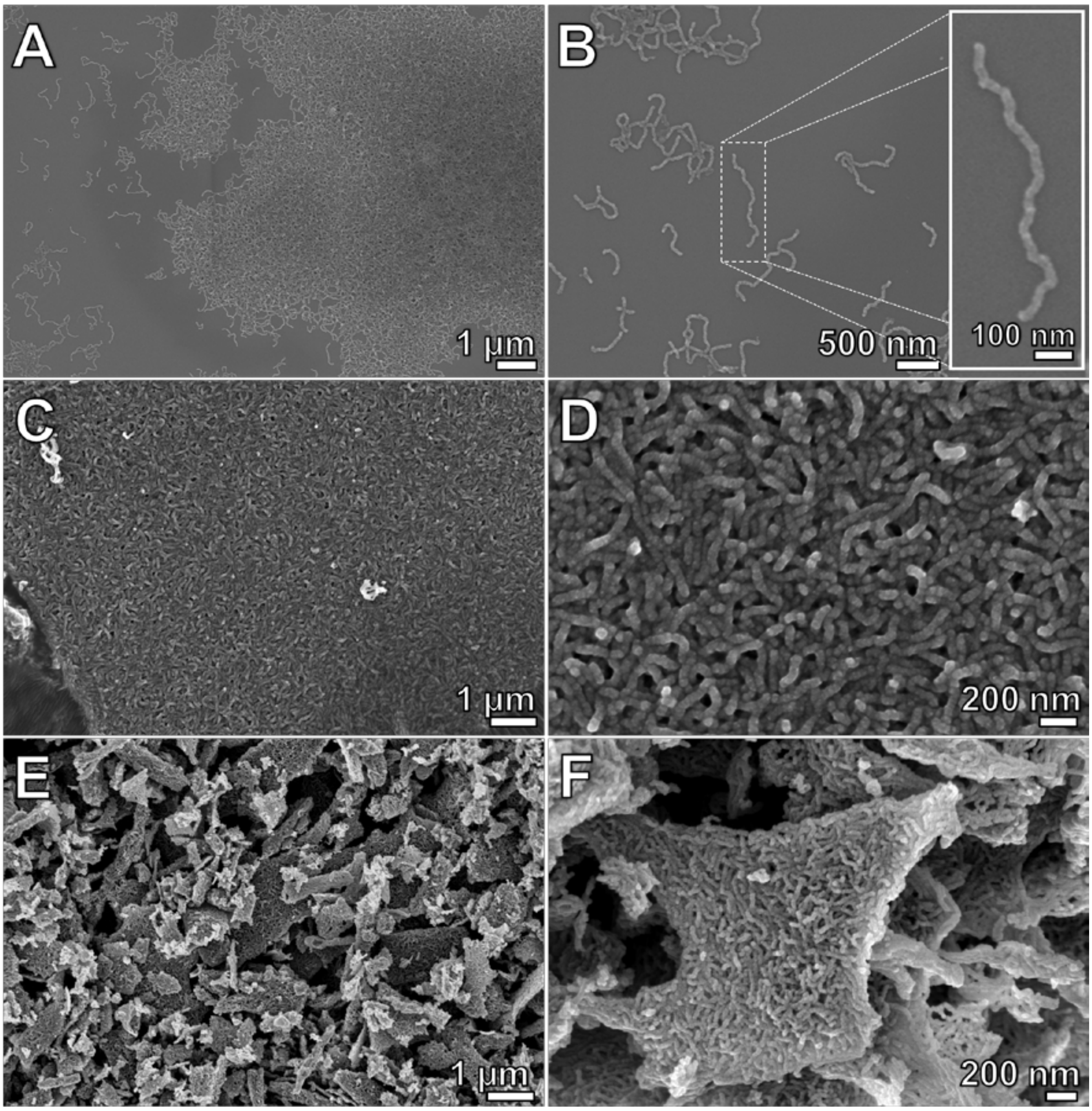

Figure 4-7. SEM images of (**A, B**) as-prepared anatase hybrid nanotubes from template brush 1 (dried from solution), (**C, D**) freeze-dried anatase hybrid nanotubes from template brush 2 at different magnifications, and (**E, F**) freeze-dried anatase hybrid nanotubes from template brush 2 after calcination in an air atmosphere.

Conclusions

Our template-directed approach to hybrid formation allows the synthesis of highly crystalline 1D TiO_2 nanotubes in a mild process at relatively low temperatures (70 °C). The molecular core-shell-corona brushes with a polycationic shell served as ideal 1D nanoreactors for the infiltration of negatively charged molecular titania precursors and guaranteed a homogeneous filling in one dimension. The hydro- and solvophilic corona provides sufficient solubility in various media and prevents crosslinking during hydrolysis and condensation. With this versatile route toward highly crystalline anisotropic TiO_2 nanostructures, it is possible to vary the length and diameter of the hybrids by adjusting the backbone and length of the side chains. The excellent dispersibility in various media makes the 1D anatase hybrids interesting for producing TiO_2 films or networks (Figure 4-7D). Those films should be porous (similar to Figure 4-S2D) after heat treatment. Furthermore, the non-woven mesostructure of the hybrid materials is retained even after calcination. Accordingly, highly crystalline TiO_2 nanomaterials were obtained, which may serve as catalysts, battery materials or in photovoltaic applications.

Acknowledgments. This work was funded by the Collaborative Research Center (SFB) 840 within project A7 and the Australian Research Council under the Discovery Project Scheme. The authors thank Marietta Böhm and Lena Geiling for performing SEC and N_2 physisorption measurements, respectively. We further thank Prof. Andreas Fery (Physical Chemistry II, Universität Bayreuth) for giving us access to the AFM. M. Müllner thanks BayEFG for a scholarship. T. Lunkenbein acknowledges the fellowship provided by the international graduate school of the ENB “Structures, Reactivity and Properties of Metal Oxides”.

Supporting Information Available. NMR of PCL brush (4-S1) and TEM and SEM images of calcined anatase nanostructures (4-S2). This material is available free of charge via the Internet at http://pubs.acs.org.

References

(1) Luan, Z.; Maes, E. M.; van der Heide, P. A. W.; Zhao, D.; Czernuszewicz, R. S.; Kevan, L. *Chem. Mater.* **1999,** 11, (12), 3680-3686.
(2) Xia, Y.; Yang, P.; Sun, Y.; Wu, Y.; Mayers, B.; Gates, B.; Yin, Y.; Kim, F.; Yan, H. *Adv. Mater.* **2003,** 15, (5), 353-389.
(3) Schmidt, V.; Wittemann, J. V.; Senz, S.; Gösele, U. *Adv. Mater.* **2009,** 21, (25-26), 2681-2702.
(4) Yuan, J.; Müller, A. H. E. *Polymer* **2010,** 51, (18), 4015-4036.
(5) Cademartiri, L.; Ozin, G. A. *Adv. Mater.* **2009,** 21, (9), 1013-1020.
(6) Law, M.; Sirbuly, D. J.; Johnson, J. C.; Goldberger, J.; Saykally, R. J.; Yang, P. *Science* **2004,** 305, (5688), 1269-1273.
(7) Johnson, J. C.; Choi, H.-J.; Knutsen, K. P.; Schaller, R. D.; Yang, P.; Saykally, R. J. *Nat. Mater.* **2002,** 1, (2), 106-110.
(8) Law, M.; Goldberger, J.; Yang, P. *Annu. Rev. Mater. Res.* **2004,** 34, 83-122.
(9) Yang, X.; Tang, H.; Cao, K.; Song, H.; Sheng, W.; Wu, Q. *J. Mater. Chem.* 21, (17), 6122-6135.
(10) Banerjee, S.; Dan, A.; Chakravorty, D. *J. Mater. Sci.* **2002,** 37, (20), 4261-4271.
(11) Zhang, Z.; Gekhtman, D.; Dresselhaus, M. S.; Ying, J. Y. *Chem. Mater.* **1999,** 11, 1659-1665
(12) Yuan, J.; Schmalz, H.; Xu, Y.; Miyajima, N.; Drechsler, M.; Möller, M. W.; Schacher, F.; Müller, A. H. E. *Adv. Mater.* **2008,** 20, (5), 947-952.
(13) Jiang, X.; Wang, Y.; Herricks, T.; Xia, Y. *J. Mater. Chem.* **2004,** 14, (4), 695-703.
(14) Pan, Z. W.; Dai, Z. R.; Wang, Z. L. *Science* **2001,** 291, (5510), 1947-1949.
(15) Heath, J. R.; LeGoues, F. K. *Chem. Phys. Lett.* **1993,** 208, (3-4), 263-268.
(16) Trentler, T. J.; Hickman, K. M.; Goel, S. C.; Viano, A. M.; Gibbons, P. C.; Buhro, W. E. *Science* **1995,** 270, (5243), 1791-1794.
(17) Mandal, S.; Müller, A. H. E. *Mater. Chem. Phys.* **2008,** 111, (2-3), 438-443.
(18) Nikoobakht, B.; El-Sayed, M. A. *Chem. Mater.* **2003,** 15, (10), 1957-1962.
(19) Sau, T. K.; Murphy, C. J. *Langmuir* **2004,** 20, (15), 6414-6420.
(20) Korth, B. D.; Keng, P.; Shim, I.; Bowles, S. E.; Tang, C.; Kowalewski, T.; Nebesny, K. W.; Pyun, J. *J. Am. Chem. Soc.* **2006,** 128, (20), 6562-6563.
(21) Nie, Z.; Fava, D.; Kumacheva, E.; Zou, S.; Walker, G. C.; Rubinstein, M. *Nat. Mater.* **2007,** 6, (8), 609-614.
(22) Yuan, J.; Walther, A.; Müller, A. H. E. *Phys. Stat. Sol. B* **2010,** 247, (10), 2436-2450.
(23) Ajayan, P. M.; Stephan, O.; Redlich, P.; Colliex, C., *Nature* **1995,** 375, 564-567.
(24) Jiang, K.; Eitan, A.; Schadler, L. S.; Ajayan, P. M.; Siegel, R. W.; Grobert, N.; Mayne, M.; Reyes-Reyes, M.; Terrones, H.; Terrones, M. *Nano Lett.* **2003,** 3, (3), 275-277.
(25) Yelamanchili, R. S.; Walther, A.; Müller, A. H. E.; Breu, J. *Chem. Commun.* **2008**, (4), 489-491.
(26) Wang, X.-S.; Winnik, M. A.; Manners, I. *Angew. Chem. Int. Ed.* **2004,** 43, (28), 3703-3707.
(27) Yan, X.; Liu, G.; Liu, F.; Tang, B. Z.; Peng, H.; Pakhomov, A. B.; Wong, C. Y. *Angew. Chem. Int. Ed.* **2001,** 40, (19), 3593-3596.
(28) Gu, Q.; Haynie, D. T. *Mater. Lett.* **2008,** 62, (17-18), 3047-3050.
(29) Shenton, W.; Douglas, T.; Young, M.; Stubbs, G.; Mann, S. *Adv. Mater.* **1999,** 11, (3), 253-256.
(30) Dujardin, E.; Peet, C.; Stubbs, G.; Culver, J. N.; Mann, S. *Nano Lett.* **2003,** 3, (3), 413-417.
(31) Zhang, M.; Müller, A. H. E. *J. Polym. Sci. Part A Polym. Chem.* **2005,** 43, (16), 3461-3481.
(32) Huang, K.; Rzayev, J. *J. Am. Chem. Soc.* **2011,** 133, (42), 16726-16729.
(33) Yuan, J.; Lu, Y.; Schacher, F.; Lunkenbein, T.; Weiss, S.; Schmalz, H.; Müller, A. H. E. *Chem. Mater.* **2009,** 21, (18), 4146-4154.
(34) Zhang, M.; Drechsler, M.; Müller, A. H. E. *Chem. Mater.* **2004,** 16, (3), 537-543.
(35) Yuan, J.; Drechsler, M.; Xu, Y.; Zhang, M.; Müller, A. H. E. *Polymer* **2008,** 49, (6), 1547-1554.
(36) Yuan, J.; Xu, Y.; Walther, A.; Bolisetty, S.; Schumacher, M.; Schmalz, H.; Ballauff, M.; Müller, A. H. E. *Nat. Mater.* **2008,** 7, (9), 718-722.
(37) Müllner, M.; Yuan, J.; Weiss, S.; Walther, A.; Förtsch, M.; Drechsler, M.; Müller, A. H. E. *J. Am. Chem. Soc.* **2010,** 132, (46), 16587-16592.
(38) Xu, Y.; Yuan, J.; Fang, B.; Drechsler, M.; Müllner, M.; Bolisetty, S.; Ballauff, M.; Müller, A. H. E. *Adv. Funct. Mater.* **2011,** 20, (23), 4182-4189.

(39) Linsebigler, A. L.; Lu, G.; Yates, J. T. *Chem. Rev.* **1995,** 95, (3), 735-758.

(40) Chiang, Y.-M. *J. Electroceram.* **1997,** 1, (3), 205-209.

(41) Ying, J. Y.; Sun, T. *J. Electroceram.* **1997,** 1, (3), 219-238.

(42) Wold, A. *Chem. Mater.* **1993,** 5, (3), 280-283.

(43) Levy, B. *J.Electroceram.* **1997,** 1, (3), 239-272.

(44) Kavan, L.; Grätzel, M.; Rathousky, J.; Zukalb, A. *J. Electrochem. Soc.* **1996,** 143, (2), 394-400.

(45) Ferroni, M.; Guidi, V.; Martinelli, G.; Faglia, G.; Nelli, P.; Sberveglieri, G. *Nanostruct. Mater.* **1996,** 7, (7), 709-718.

(46) Hoffmann, M. R.; Martin, S. T.; Choi, W.; Bahnemann, D. W. *Chem. Rev.* **1995,** 95, (1), 69-96.

(47) Luo, Z.; Gao, Q.-H. *J.Photochem. Photobiol. A: Chem.* **1992,** 63, (3), 367-375.

(48) Yin, H.; Wada, Y.; Kitamura, T.; Kambe, S.; Murasawa, S.; Mori, H.; Sakata, T.; Yanagida, S. *J. Mater. Chem.* **2001,** 11, (6), 1694-1703.

(49) Wang, C.-C.; Ying, J. Y. *Chem. Mater.* **1999,** 11, (11), 3113-3120.

(50) Hanprasopwattana, A.; Rieker, T.; Sault, A. G.; Datye, A. K. *Catal. Lett.* **1997,** 45, (3), 165-175.

(51) Mayya, K. S.; Gittins, D. I.; Caruso, F. *Chem. Mater.* **2001,** 13, (11), 3833-3836.

(52) Baskaran, S.; Song, L.; Liu, J.; Chen, Y. L.; Graff, G. L. *J. Am. Ceram. Soc.* **1998,** 81, (2), 401-408.

(53) Mori, H.; Wakisaka, O.; Hirao, A.; Nakahama, S. *Macromol. Chem. Phys.* **1994,** 195, (9), 3213-3224.

(54) Yu-Su, S. Y.; Sheiko, S. S.; Lee, H.-i.; Jakubowski, W.; Nese, A.; Matyjaszewski, K.; Anokhin, D.; Ivanov, D. A. *Macromolecules* **2009,** 42, (22), 9008-9017.

(55) Sheiko, S. S.; Sun, F. C.; Randall, A.; Shirvanyants, D.; Rubinstein, M.; Lee, H.-i.; Matyjaszewski, K. *Nature* **2006,** 440, (7081), 191-194.

(56) Möckel, H.; Giersig, M.; Willig, F. *J. Mater. Chem.* **1999,** 9, (12), 3051-3056.

(57) Mayya, K. S.; Gittins, D. I.; Dibaj, A. M.; Caruso, F. *Nano Lett.* **2001,** 1, (12), 727-730.

Supporting Information

4-S1. ^{1}H-NMR of PCL homopolymer brush

NMR was used to determine the degree of polymerization (DP_n) of the PCL side chains. The DP_n was obtained by the ratio of the signal of the terminal CH_2-group at 3.7 ppm to the signal of the respective polymeric group at 4.1 ppm. Upon esterification, the signal at 3.7 ppm shifted completely to 4.2 ppm. This indicated a esterification efficiency. Additionally, a new sigal at 1.9 ppm appeared, which was assigned to the the two methyl groups of the attached ATRP initiator.

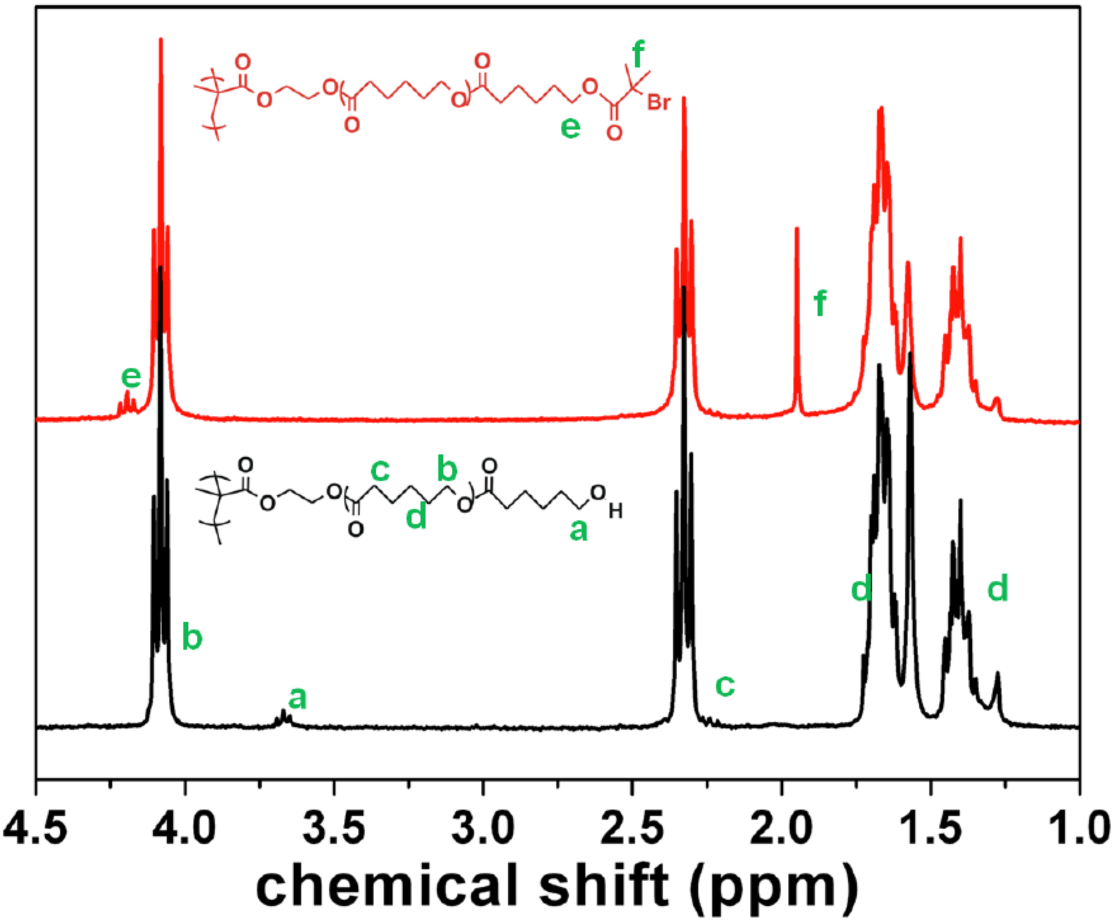

Figure 4-S1. ^{1}H-NMR spectra in $CDCl_3$ of PCL homopolymer brush before (**black, bottom**) and after (**red, top**) esterification.

4-S2. TEM and SEM of calcined anatase hybrid nanotubes.

The cylindrical shape of the hybrid nanotubes was retained after calcination in an air atmosphere. Both TEM and SEM show worm-like nanostructures (see Figure 4-S2). Moreover, the purely inorganic TiO_2 cylinders have a rather rough surface (see the magnification in Figure 4-S2 D).

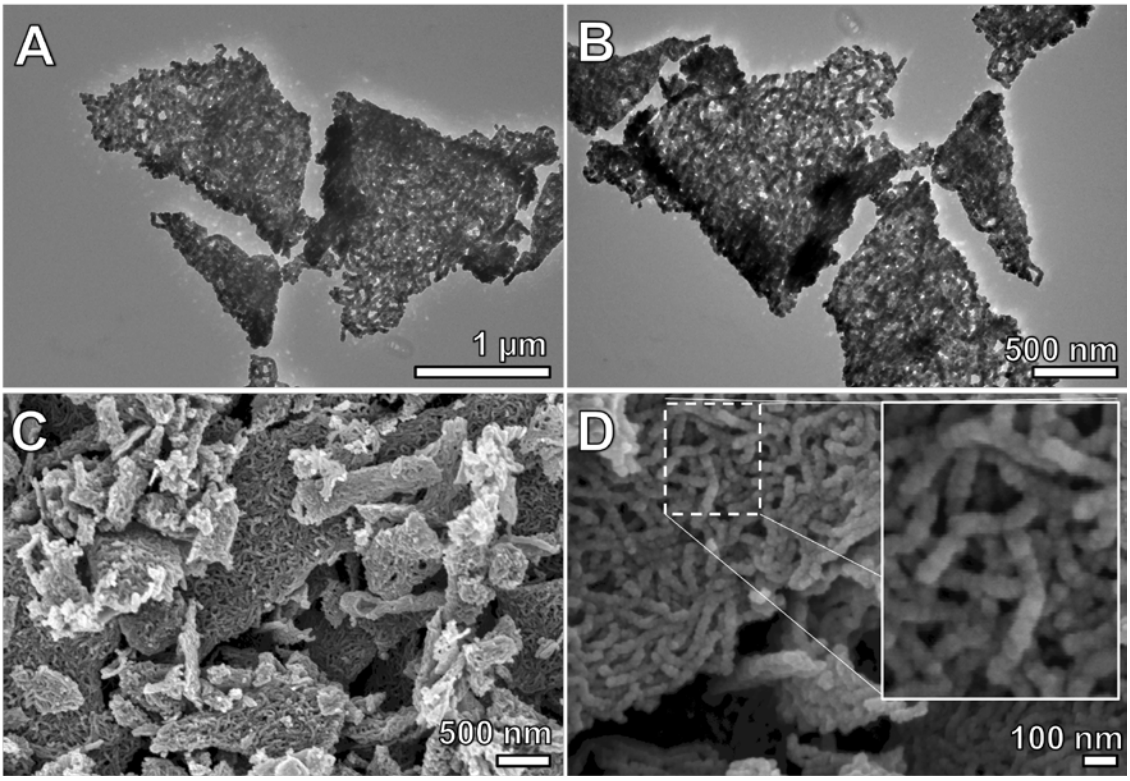

Figure 4-S2. (**A, B**) TEM micrographs and (**C, D**) SEM images of air calcined hybrids from $[CL_{14}$-$DMAEMA_{150}$-$OEGMA_{240}]_{7500}$.

Chapter 5

Template-Directed Synthesis of Silica Nanowires and Nanotubes from Cylindrical Core-Shell Polymer Brushes

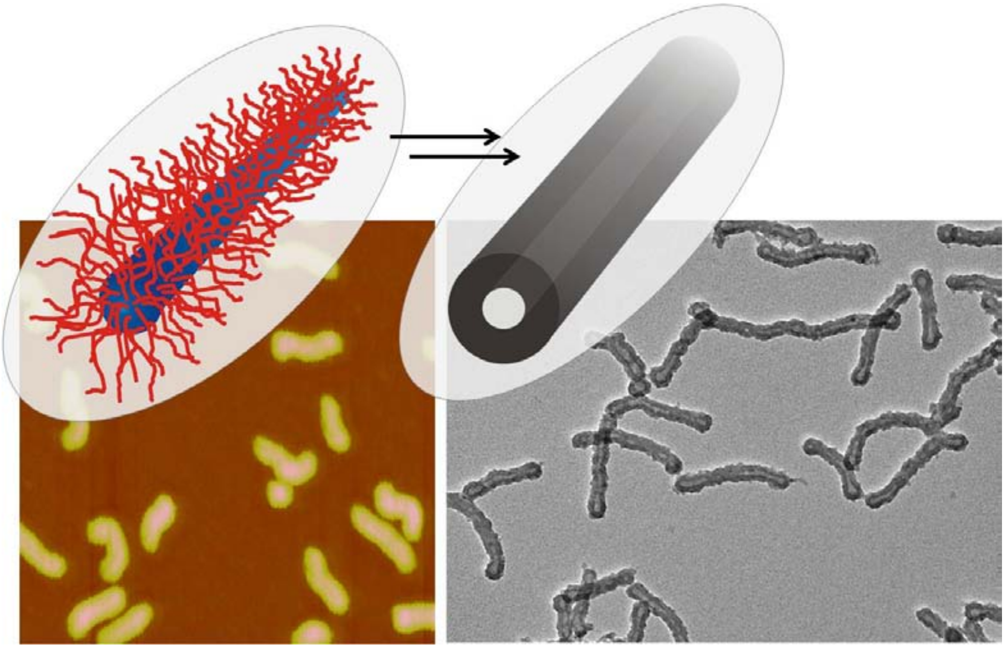

The results of this chapter are published in *Chemistry of Materials* as:

“Template-Directed Synthesis of Silica Nanowires and Nanotubes from Cylindrical Core-Shell Polymer Brushes”

by Markus Müllner, Thomas Lunkenbein, Josef Breu, Frank Caruso,
and Axel H.E. Müller*

Abstract: We report the synthesis and characterization of core-degradable core-shell cylindrical polymer brushes (CPBs) that can be used as a molecular soft template for the fabrication of uniform one-dimensional silica nanostructures with tunable dimensions and morphologies. The silica nanostructures were templated from CPBs consisting of a densely grafted poly(*ε*-caprolactone) core and a poly[2-(dimethylamino)ethyl methacrylate] (PDMAEMA) shell. According to the degree of polymerization of both the backbone and the side chains, silica nanostructures with varying lengths and diameters were obtained. The weak polyelectrolyte shell acted as an ideal nanoreactor for the deposition of silica. Calcination or treatment with an acid of the as-synthesized silica hybrids led to the removal of the core and consequently to hollow silica nanotubes. Calcined nanotubes were microporous and exhibited high pore volumes and specific surface areas. Furthermore, metal salts immobilized within the PDMAEMA shell can be fully embedded into the silica shell. Accessibility of the embedded nanoparticles was demonstrated via the catalysis of the reduction of 4-nitrophenol by sodium borohydride in the presence of nanoparticle-doped silica hybrids.

Introduction

The use of hollow inorganic nanostructures as potential nanoscale reactors has been studied extensively.[1-9] Interior cavities can host reactants or catalysts and shield them from the outer environment. The most studied hollow nanostructures are hollow spheres. However, one-dimensional (1D) inorganic nanostructures, such as tubes, rods and wires, have gained considerable interest due to their high aspect ratio and their potential application in electronic, optical and mechanical devices.[10-12] The unique size- and shape-dependent properties of 1D nanomaterials and their continually expanding applications in various research areas have dramatically increased the interest in anisotropic nanostructures.[13-15] 1D inorganic nanostructures often find use as sensors or in catalysis.[12,16,17] In early research, the exploration of 1D nanomaterials was hampered as the synthesis and control of a distinct geometry at extremely small sizes were difficult.[18] Many 1D nanostructures are built up via templating processes where a suitable template predetermines the shape and size of the hybrid material. It is generally accepted that template-directed syntheses provide a simple, high-through-put, and cost-effective procedure which allows the straightforward production of hybrid material, often in only one step.[12] In general, the applied templates are referred to as either hard or soft. Whereas hard templates are mostly from anodized aluminuim oxide (AAO), soft templates can vary from simple surfactant micelles to more complex templates, such as peptides, carbon nanotubes, viruses, or cylindrical polymer brushes (CPBs).[16,19] CPBs are molecular brushes carrying linear side chains densely grafted from a backbone.[20] The dense packing of side chains along the polymer backbone leads to a streching of the backbone and a stiffening of the entire brush. Various types of CPBs with different structures and chemical compositions have been reported.[20,21] Core-shell or core-shell-corona structured CPBs (that is, polymer brushes carrying di- or triblock copolymers as side chains) have proven to be interesting building blocks in template chemistry. Through the incompatibility of the side chain blocks with each other, the polymer brush can be divided into two or three different concentric compartments, which can be used as unimolecular templates or nanoreactors for the synthesis of 1D organic, hybrid or purely inorganic nanostructures. Core-shell(-corona) CPBs with a degradable core have been used to form uniform tubular nanostructures.[22-24] In addition, a polyelectrolyte core or shell of core-shell CPBs was used to immobilize metal precursors, such as Cd^{2+}, Fe^{2+}/Fe^{3+}, $AuCl_4^-$,

$PtCl_6^-$ and Ti^{4+} ions, and convert the precursors into the corresponding nanoparticles in the core or the shell.[16,25-31] Moreover, CPBs have been used as building blocks for the fabrication of organo-silica hybrid nanotubes and nanowires, where the silica precursor was covalently attached to the template brush.[32,33] In the case of silica nanostructures, many of the abovementioned synthesis routes have been explored.[34-39] Synthetic routes toward silica nanostructures mainly depend on both soft and hard anisotropic templates and involve multiple steps including the introduction of silica.[39] Due to difficulties in obtaining sacrificial 1D templates of high quality and large quantity, the wide use of silica nanostructures, especially nanotubes, has been greatly limited. More specifically, the precise control of the size and aspect ratio, scale-up, and cost minimization during synthesis are a general issue. As a result, a facile synthesis of well-defined and size-tunable silica nanowires and nanotubes on a large scale is highly desirable to fully explore their practical applications. Anisotropic silica-based materials, in particular, are attractive materials due to their chemical inertness, corrosion resistance, and mechanical and thermal stability.

Herein, we use core-shell CPBs, consisting of poly(ε-caprolactone) (PCL) as a core and poly[2-(dimethylamino) ethyl methacrylate] (PDMAEMA) as a polycationic shell, as a template for the fabrication of silica nanowires and nanotubes (Scheme 5-1). The applied polymerization techniques permitted excellent control over the synthesis of the template brushes and allowed precise adjustment of the aspect ratio and morphology of the 1D silica nanostructures. Anionic ring-opening polymerization (ROP) of ε-caprolactone (CL) increased the grafting efficiency and allowed the removal of the core-forming block. The precise production of silica nanomaterials with different lengths and different core and shell diameters was achieved by loading the amine-containing compartment with a silica precursor, namely tetramethyl orthosilicate (TMOS), and the subsequent hydrolysis and condensation. TMOS has already been used for the synthesis of various silica nanostructures.[40-42] Acid treatment or calcination of the PCL-filled nanowires led to hollow silica nanotubes. Furthermore, we loaded the polyelectrolyte shell with metal ions (e.g. $PtCl_4^{2-}$ or $AuCl_4^-$) and embedded the corresponding Pt or Au nanoparticles into the silica shell, giving catalytically active silica nanomaterials.

Scheme 5-1. Synthesis of Template CPBs and their Use in the Template-Directed Synthesis of Silica Hybrid Nanostructures

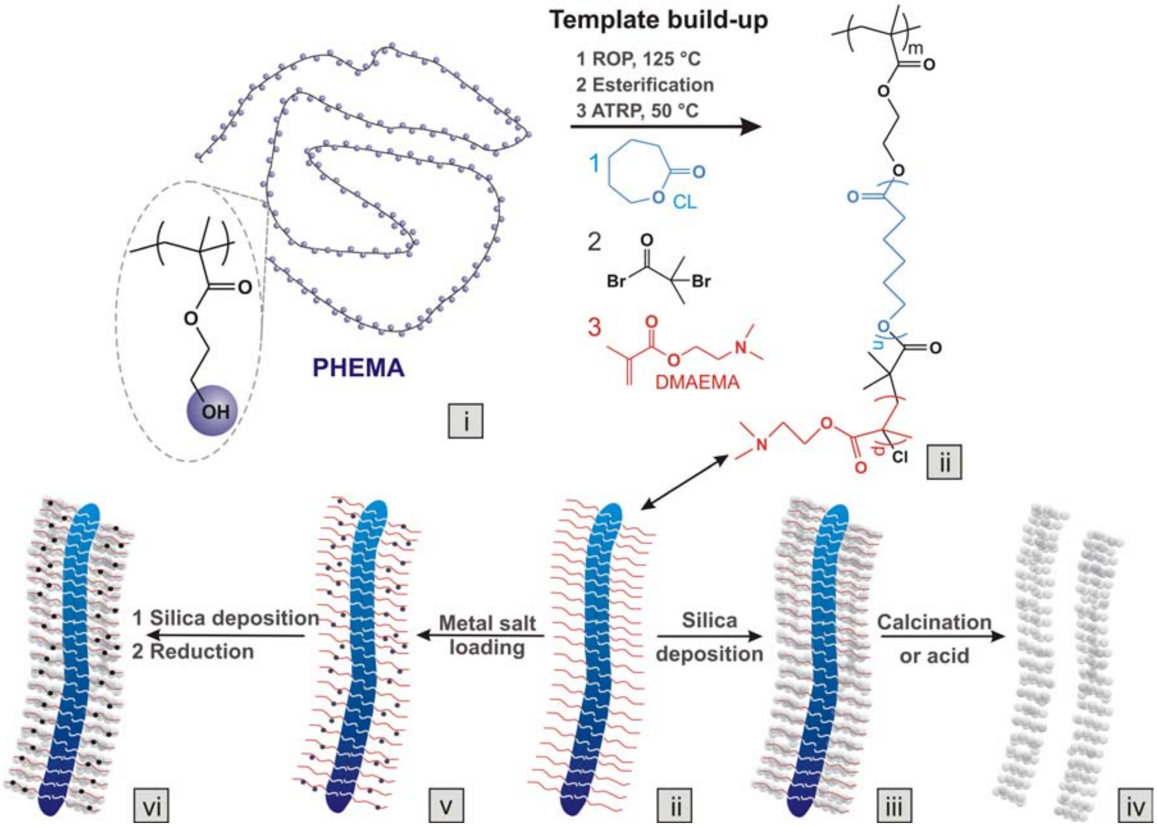

Experimental Section

Materials. All chemicals were of analytical grade and used as received without further purification, except for *2*-(dimethylamino)ethyl methacrylate (Aldrich, 98%), which was passed through a silica column prior to polymerization.

Preparation of the Soft Template Polymer Brush $[CL_nDMAEMA_p]_m$. The template was synthesized through the combination of anionic, ring-opening and atom transfer radical polymerization. Table 5-1 provides an overview of the synthesized polymers and polymer brushes. The stepwise build-up from a polyinitiator backbone to a core-shell CPB is explained in detail below using $[CL_{14}DMAEMA_{43}]_{7500}$ as an example.

Table 5-1. Overview of the Synthesized Polymer Backbones and Polymer Brushes

Polymer composition	M_n [10^6g·mol^{-1}]	M_w/M_n[c]
PHEMA$_{2700}$[a]	0.35[a]	1.05
PHEMA$_{7500}$[a]	0.98[a]	1.14
[CL$_{10}$]$_{2700}$[b]	3.08[b]	1.13
[CL$_{25}$]$_{2700}$[b]	7.70[b]	1.25
[CL$_{14}$]$_{7500}$[b]	12.0[b]	1.40
[CL$_{10}$DMAEMA$_{58}$]$_{2700}$[b]	26.0[b]	-
[CL$_{25}$DMAEMA$_{76}$]$_{2700}$[b]	37.4[b]	-
[CL$_{14}$DMAEMA$_{43}$]$_{7500}$[b]	59.0[b]	-
[CL$_{14}$DMAEMA$_{342}$]$_{7500}$[b]	382[b]	-

[a] Molecular weight as measured by SLS; [b] A determined by ^{1}H-NMR; [c] A determined by SEC in DMAc. The SEC traces of the PCL brushes can be found in the Supporting Information (Fig. S1).

The polyinitiator backbone poly(2-hydroxyethyl methacrylate) (PHEMA) was obtained through the deprotection of poly(2-(trimethylsiloxy)ethyl methacrylate) (PTMS-HEMA). The backbone was synthesized as reported by Mori *et al.*.[43] Two PTMS-HEMA homopolymers with different length were synthesized. The number-average degree of polymerization (DP$_n$) and the polydispersity index (PDI) were 7500 and 1.14 or 2700 and 1.05, respectively. The deprotection of the TMS group was performed with acetic acid in methanol. PHEMA (80 mg, 0.62 mmol) was dissolved in ε-caprolactone (6 mL, 54.2 mmol) and water traces were removed via distillation in the presence of benzene. The mixture was then degassed by bubbling argon for 30 min. The ROP of CL was catalyzed via the addition of tin(II)-ethylhexanoate (1.5 mg, 3.70 µmol) at 125 °C. The polymerization was allowed to proceed for 11 h until the mixture became very viscous. The polymerization was quenched with MeOH, exposed to air and diluted with THF. The conversion was determined after purification with ^{1}H-NMR by comparing the polymeric CH$_2$-signal at 4.1 ppm and the terminal CH$_2$-signal at 3.65 ppm. The PCL homopolymer brush [CL$_{14}$]$_{7500}$ was precipitated twice in a cold water/methanol mixture (10/90 v/v) and then freeze-dried from dioxane. [CL$_{14}$]$_{7500}$ was then reacted with a 1.5 fold molar excess of 2-bromoisobutyryl bromide and a 2 fold molar excess of triethylamine (TEA) in dry THF to functionalize the PCL brush with ATRP initiating groups. The reaction mixture was stirred for 24 h at room temperature, and then the functionalized polymer was concentrated by solvent evaporation, precipitated in a cold water/methanol mixture (80/20 v/v) and freeze-dried from dioxane. $[CL_{14}]_{7500}$ (0.008 mmol) was dissolved in 7 mL anisole and deoxygenated for 10 min in a screw-cap flask sealed with a septum. 0.01 mmol CuCl was then added and argon was continued to be bubbled through the mixture for 20 min. Meanwhile, 5 mmol of destabilized DMAEMA, 0.01 mmol of N,N,N′,N″,N″-pentamethyldiethylenetriamine (PMDETA) and 1 mL of anisole were degassed as well. The polymerization started after adding the DMAEMA/PMDETA mixture to the reaction flask at 50 °C. The polymerization was monitored via ^{1}H-NMR and quenched at the desired conversion by cooling it and exposing it to air. The polymer solution was passed through a silica gel column before it was precipitated into cold cyclohexane. The precipitate was immediately dissolved in ethanol and precipitated a second time. The weight content of the polymer brushes dissolved in ethanol was determined before the solution was dialyzed to water.

Quaternization of $[CL_nDMAEMA_p]_m$. An excess of methyliodide (MeI) was added drop-wise to the core-shell polymer brushes in water. The solution became turbid immediately and was allowed to stir for another 24 h. The viscosity increased significantly during that time. Unreacted MeI was removed under reduced pressure.

Preparation of Silica Hybrid Nanowires. 100µL of tetramethyl orthosilicate (TMOS) was added drop-wise to 2 mL of the cylindrical polymer template in water (0.25 $g \cdot L^{-1}$) at 15 °C under vigorous stirring. The mixture was allowed to stir for 20 min before it was diluted with 6 mL of ethanol. The mixture was then centrifuged at 12 500 rcf for 1 min and washed with ethanol and water, aided by ultrasound.

Preparation of Hollow Silica Nanotubes. The freeze-dried silica hybrids (1 mg) were either mixed with 2M HCl and stirred at 50 °C for three days or calcined as a dry powder in air atmosphere at 650 °C with a heating rate of 10 $K \cdot min^{-1}$.

Preparation of the Platinum-Doped Silica Hybrid Nanowires. 100 µL of an aqueous solution of potassium tetrachloroplatinate (24 $mmol \cdot L^{-1}$) was added drop-wise to 10 mL of the template brush solution (0.25 $g \cdot L^{-1}$) under stirring. After stirring for 1 h, 2 mL of the solution was mixed at 15 °C with TMOS as described above. After washing the platinum-doped hybrid silica nanowires, they were treated with 100 µL of freshly prepared $NaBH_4$ (1 $g \cdot L^{-1}$) solution and mixed for 1 h using ultrasound, before the $NaBH_4$ was washed off using centrifugation.

Preparation of the Gold-Doped Silica Hybrid Nanowires. 100 µL of an aqueous solution of chloroauric acid ($HAuCl_4$) (0.3 wt%) was added drop-wise to 10 mL of the template brush solution (0.25 $g\cdot L^{-1}$) under stirring. After stirring for 1 h, 2 mL of the solution was mixed at 15 °C with TMOS as described above. After washing the gold-doped hybrid silica nanowires, they were treated with 100 µL of freshly prepared $NaBH_4$ (1 $g\cdot L^{-1}$) solution and mixed for 1 h using ultrasound, before the $NaBH_4$ was washed off again.

Reduction of 4-Nitrophenol Catalyzed by Nanoparticle-Doped Silica Hybrid Nanowires. 0.5 mL of $NaBH_4$ solution (60 $mmol\cdot L^{-1}$) was added to 2.5 mL of 4-nitrophenol solution (0.12 $mmol\cdot L^{-1}$) that was contained in a glass cuvette. Then, 0.5 mL of either platinum or gold nanoparticle-doped hybrid nanowires solution (nanowire concentration 0.001 $g\cdot L^{-1}$) was added. Immediately after the addition of the composite particles, ultraviolet (UV) spectra of the sample were taken continuously in the range of 250-500 nm. The rate constants of the reactions were determined by measuring the change in intensity of the peak at 399 nm with time.

Characterization Methods. *Size Exclusion Chromatography (SEC).* SEC in *N, N*-dimethylacetamide (DMAc) with 0.05M lithium bromide was conducted at an elution rate of 0.7 $mL\cdot min^{-1}$ using polyester copolymer network (GRAM) columns (300 × 8 mm, 7 µm): 10^3 and 10^2 Å and RI and UV ($\lambda = 260$ nm) detection. A poly(methyl methacrylate) (PMMA) calibration curve was used to calibrate the columns.

Atomic Force Microscopy (AFM). AFM images were recorded on a Digital Instruments Dimension 3100 microscope operated in tapping mode. The samples were prepared by dip-coating of freshly cleaved mica into a solution of the polymer brush solution diluted in ethanol or water to form a monomolecular film.

Transmission Electron Microscopy (TEM). Bright field TEM was performed using a Zeiss CEM 902 electron microscope operated at 80 kV. A droplet of a solution of the polymer brush solution (0.05 $g\cdot L^{-1}$) in water or ethanol was dropped onto a copper grid (200 mesh) coated with carbon film, followed by blotting the liquid and drying at room temperature for a short time.

Cryogenic Transmission Electron Microscopy (cryo-TEM). Cryo-TEM was conducted by dropping the aqueous dilute solution (0.1 $g\cdot L^{-1}$) on a hydrophilized lacey TEM grid, where most of the liquid was removed with blotting paper, leaving a thin film stretched over the grid holes. The specimens were shock frozen by rapid immersion into liquid ethane and cooled to approximately 90 K by liquid nitrogen in a temperature controlled freezing unit (Zeiss Cryobox, Zeiss NTS GmbH, Oberkochen, Germany). After the specimens were frozen, the remaining ethane was removed using blotting paper. The specimen was inserted into a cryo-transfer holder (CT3500, Gatan, München, Germany) and transferred to a Zeiss EM922 EF-TEM instrument operated at 200 kV.

Scanning Electron Microscopy (SEM) and Energy-Dispersive X-Ray (EDX). SEM and EDX analysis was performed using a Zeiss Model 1530 Gemini instrument equipped with a field-emission cathode with a lateral resolution of ~ 2 nm. The samples were measured on silica wafer and sputtered with platinum for 1 min. In the case of the EDX investigated samples, the samples were centrifuged, dried, not sputtered and directly measured on the plain stud without silica wafer.

Proton Nuclear Magnetic Resonance. ^{1}H-NMR spectra were recorded to determine the monomer conversion on a Bruker AC-300 spectrometer at room temperature in $CDCl_3$.

N_2-physisorption. N_2-physisorption was conducted at 77 K on a Quantachrome Autosorb 1 instrument.Prior to the measurements, the samples were degassed at 403 K for 24 h. The hybrid nanotubes were calcined in a tube furnace in air atmosphere from 30°C to 650 °C (heating rate 10 K min^{-1}). p/p_0 values between 0.01 and 0.06 were taken to determine the specific surface areas. The recommendations of Rouquerol *et al.* regarding the BET equation were followed.[44]

Results and Discussion

Template Synthesis and Characterization. Core-shell CPBs (Scheme 5-1, ii) were used as a template for the fabrication of various 1D silica nanostructures. The polymer brushes were synthesized via the "grafting-from" approach, where side chains are grown from a polyinitiator backbone. Poly(hydroxyethyl methacrylate) (PHEMA) was chosen for the backbone, as it can be used to initiate the anionic ROP of ε- CL. PHEMA was produced via anionic polymerization of TMS-HEMA and a subsequent deprotection step with acetic acid. To obtain different lengths of the later silica hybrids, we synthesized two PHEMA backbones with different molecular weights. The weight-average molecular weight (M_w) for both backbones was determined by static light scattering (SLS; data not shown). Dividing M_w by the respective PDI, obtained from SEC, and the molecular weight of HEMA, resulted in the number-average degree of polymerization (DP_n) of each polymer backbone, namely 2700 ($PHEMA_{2700}$) and 7500 ($PHEMA_{7500}$), respectively. PHEMA was then used for the ROP of CL in bulk. Due to the rather high molecular weights of the polyol backbones, it was complicated to dry the polyinitiator completely and, accordingly, it was difficult to exclude all traces of the water during the polymerization. The presence of water is problematic since it can also act as an initiator for the ROP of CL, leading to non-grafted poly(caprolactone) (PCL). The ROP was catalyzed by tin(II)-ethylhexanoate and is known to have a very high grafting efficiency of above 90%.[45]

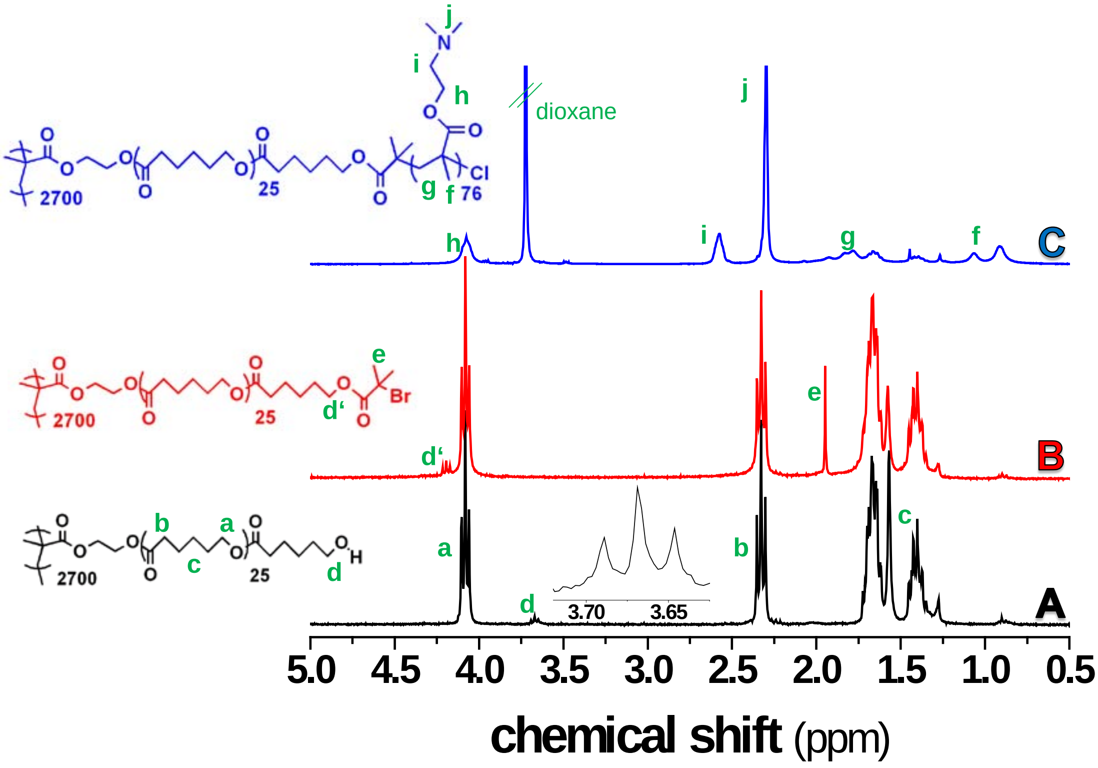

Figure 5-1. ^1H-NMR spectra in $CDCl_3$ of (**A**) the $[CL_{25}]_{2700}$ homopolymer brush, (**B**) the end-group modified PCL brush and (**C**) $[CL_{25}DMAEMA_{76}]_{2700}$.

Before attaching an ATRP initator, the as-synthesized PCL polymer brushes were purified from the homo-PCL by selective precipitation in a THF/cyclohexane mixture. A ^1H-NMR spectrum of the purified PCL homopolymer brushes can be seen in Figure 5-1A. To determine the DP_n of PCL, we compared the ratio of the terminal CH_2-OH-group (d) at 3.65 ppm to the corresponding polymeric CH_2-group (a) at 4.1 ppm. The ratio equals the DP_{PCL}. Upon esterification, the terminal CH_2-group shifts completely lowfield and can be found at 4.25 ppm (d'). This is a clear indication of successful esterification. In addition, a new peak (e) at 1.9 ppm appears, which originates from the two methyl groups of the 2-bromoisobutyrate group (Figure 5-1B). In a final step, 2-(dimethylamino)ethyl methacrylate (DMAEMA) was grafted from the PCL brush to give water-soluble polyelectrolyte CPBs $[CL_nDMAEMA_p]_m$. PDMAEMA was chosen as it is partially charged in water at pH 7. It is also known that cationic polymers can promote localized silica deposition.[40] The conversion of DMAEMA was confirmed by ^{1}H-NMR. Figure 5-1C shows the corresponding spectrum of $[CL_{25}DMAEMA_{76}]_{2700}$ in $CDCl_3$. To determine the efficiency of the grafting of PDMAEMA, the PCL part of the polymer brushes was degraded in 2 M HCl over three days. The turbid brush solution cleared already after several hours, indicating the successful cleavage of the PDMAEMA side chains. The SEC traces (in DMAc, with PDMAEMA calibration) of the cleaved PDMAEMA had a very similar molecular weight compared to the one obtained from ^{1}H-NMR (see Supporting Information, Figure 5-S2). This confirms that the grafting from PCL brushes has $\geq$ 90% efficiency.[45] The increase in grafting density, compared to the grafting from a poly(2-bromoisobutyryloxyethyl methacrylate) (PBIEM) polyinitator (ca. 50-70%),[25,33] is explained by the reduced sterical hindrance of PCL brushes. Grafting from very close to the backbone increases sterical hindrance and hence decreases the grafting efficiency. PCL side chains act as a spacer and therefore increase the grafting efficiency.

Several polymers with different dimensions, with respect to length as well as core and shell diameter, were synthesized and used for the deposition of silica. Four polymer brush compositions are highlighted in Table 5-2.

Table 5-2. 1D Silica Hybrids with Different Dimensions (in nm)

Template composition[a]	Template length[b]	Hybrid length[c]	Core diameter[c]	Silica shell diameter[c]
$[CL_{10}DMAEMA_{58}]_{2700}$	295 ± 20	270 ± 15	5-6	~25
$[CL_{25}DMAEMA_{76}]_{2700}$	265 ± 20	235 ± 20	10-12	~35
$[CL_{14}DMAEMA_{43}]_{7500}$	1250 ± 200	950 ± 350	6-7	~25
$[CL_{14}DMAEMA_{342}]_{7500}$	1250 ± 200	950 ± 350[d]	6-7[e]	~ 85[f]

[a] Determined by ^{1}H-NMR; [b] measured from AFM images of the template brushes; [c] measured from TEM micrographs of the as-synthesized silica hybrids; [d] estimated from TEM micrographs, as it was rather difficult to directly measure the actual length due to the jamming of hairy silica nanostructures; [e] assumed to be the same dimension as with $[CL_{14}DMAEMA_{43}]_{7500}$; [f] taking into account that the core is ~6 nm in diameter.

The template brushes were characterized by AFM. AFM is a powerful tool for the molecular visualization of polymer brushes and their morphological changes. Figure 5-2 shows AFM height images of the core-shell CPBs. The templates were constructed from PHEMA backbones 2700 (A) and 7500 (B), respectively. Figure 5-2B shows very long and curved CPBs. The meandering structure of the adsorbed brushes made it difficult to determine their exact length. In addition, CPBs can undergo scission on substrates[46] which again made the length determination tricky. The height profiles of each template brush in Table 5-2 can be found in the Supporting Information, Figure 5-S3.

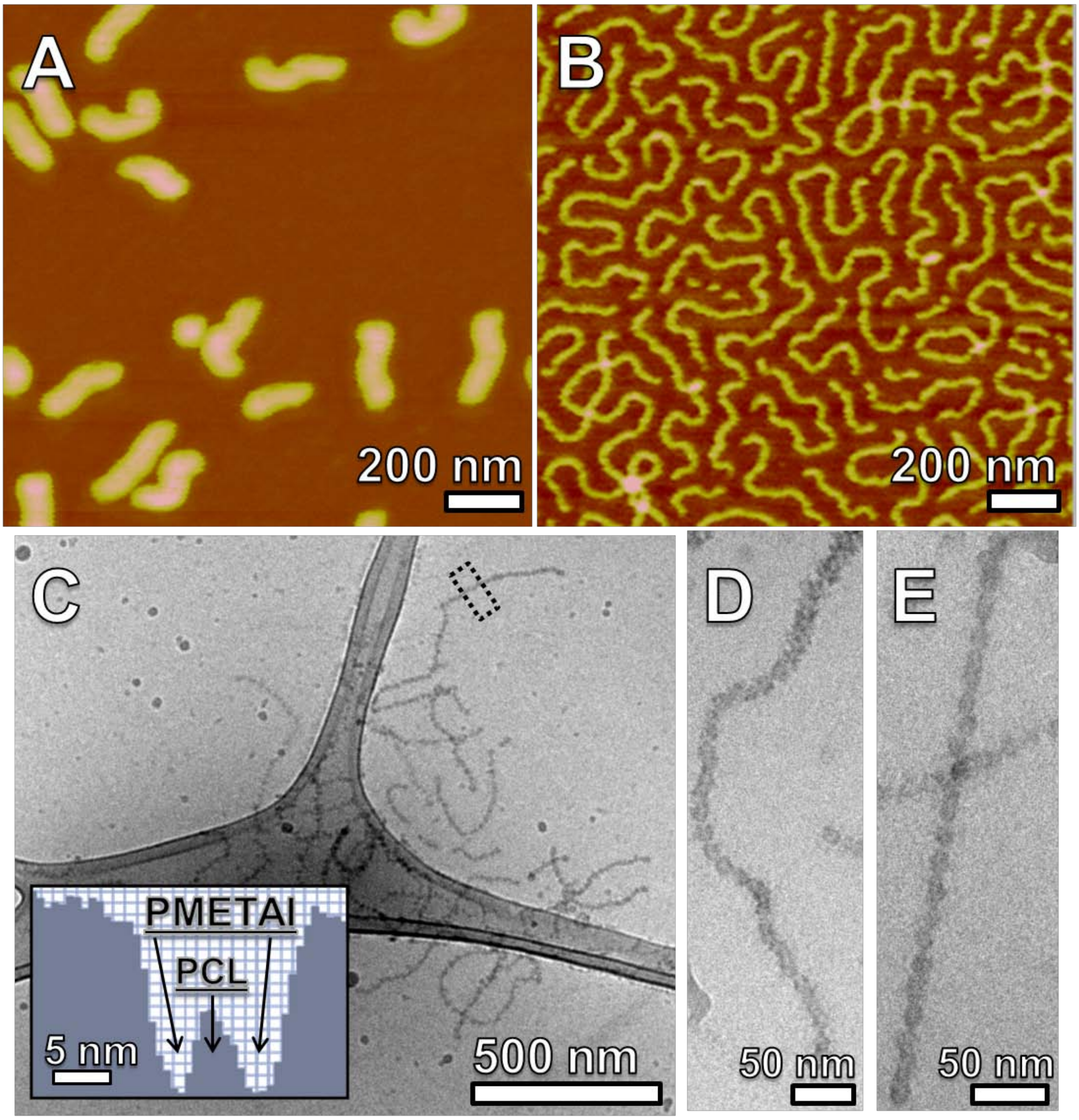

Figure 5-2. AFM height images of (**A**) $[CL_{25}DMAEMA_{76}]_{2700}$ and (**B**) $[CL_{14}DMAEMA_{43}]_{7500}$ on mica. The z-values are 15 nm (**A**) and 3 nm (**B**). (**C**) Cryo-TEM image of quaternized CPBs $[CL_{14}METAI_{43}]_{7500}$ in water, including a grey-scale analysis through one of the quaternized CPBs. (**D, E**) Magnifications of $[CL_{14}METAI_{43}]_{7500}$.

Cryogenic transmission electron microscopy (cryo-TEM) was used to investigate the template brushes in water. The polymer brush shell was quaternized to poly{[2-(methacryloyloxy)ethyl) trimethylammonium iodide} (PMETAI) prior to measurement to increase the contrast of the shell. The PMETAI shell (which contained iodide counterions) appear much darker than the PCL core. The inset in Figure 5-2C shows a grey-scale analysis of a cross-section through a quaternized template brush and verifies the core-shell character of the template brushes. Figures 5-2D, E indicate that the quaternized CPBs exhibited a pearl-necklace morphology in water. This phenomenon is caused by the surface minimization and the subsequent collapse of the hydrophobic PCL core into “pearls” along the backbone.[47] Similar to AFM, we assume that the backbone of long CPBs can break in water.[33] Figure 5-2C reveals that shorter polymer brushes lie alongside longer ones. Quaternized CPBs are assumed to be more liable towards fracturing, as the high osmotic pressure of the counterions forces the side chains to stretch.

Hybrid Formation and Characterization. The deposition of silica into the PDMAEMA shell was performed in water at pH 7 and 15 °C. Tetramethyl orthosilicate (TMOS) was used as a silica precursor, as it undergoes hydrolysis quickly. The addition of TMOS to the template brushes in water led to the incorporation and exclusive growth of silica within the PDMAEMA shell compartment. No crosslinking reactions occurred, as hydrolyzed TMOS precursors migrate into the amine-containing shell and start condensation in the shell.[40-42] Note that PDMAEMA was only quaternized for cryo-TEM, whereas all the hybrids shown in Table 5-2 were produced from non-quaternized template CPBs. Quaternized template brushes preserved their pearl-necklace structure upon hybrid formation and resulted in pearl-necklace silica hybrids (see Supporting Information, Figure 5-S4).

By varying the dimensions of the polymer brush template, we could easily customize the aspect ratio by tuning the length, the core diameter and/or the silica shell diameter. Consequently, aspect ratios between 6 ($[CL_{25}DMAEMA_{76}]_{2700}$) and 50 ($[CL_{14}DMAEMA_{43}]_{7500}$) were achieved by this templating method. Figure 5-3 shows the 1D silica nanostructures described in Table 5-2. The difference in length of the silica nanostructures produced from template brushes with DP of the backbone of 2700 ($[CL_nDMAEMA_m]_{2700}$) (Figure 5-3F, I) is mainly based on the ratio of the hydrophobic core to the hydrophilic shell. A larger hydrophobic core, in case of

$[CL_{25}DMAEMA_{76}]_{2700}$, hinders the stretching of the template brush more efficiently and results in shorter hybrids (see Table 5-2).

As mentioned above, the dimensions of the hybrid can be adjusted by the molecular structure of the template brush. Thus, the core thickness can be controlled by varying the length of the PCL side chains. A DP_{PCL} of around 10, for example, resulted in a core thickness of 5-6 nm, whereas an increase of DP_{PCL} to 25 increased the diameter of the core to around 10-12 nm. In a similar way, the diameter of the silica shell can be increased through longer PDMAEMA side chains. However, very long PDMAEMA side chains led to the growth of rather hairy silica nanowires (Figure 5-2J-L), as compared to the previously discussed wires with smooth silica shells. This inhomogeneous silica shell growth is attributed to the decreased segment density in the outer regions of the polymer brush at longer side chains. Longer side chains then lead to the growth of silica threads or bundles instead of a homogenous silica shell.

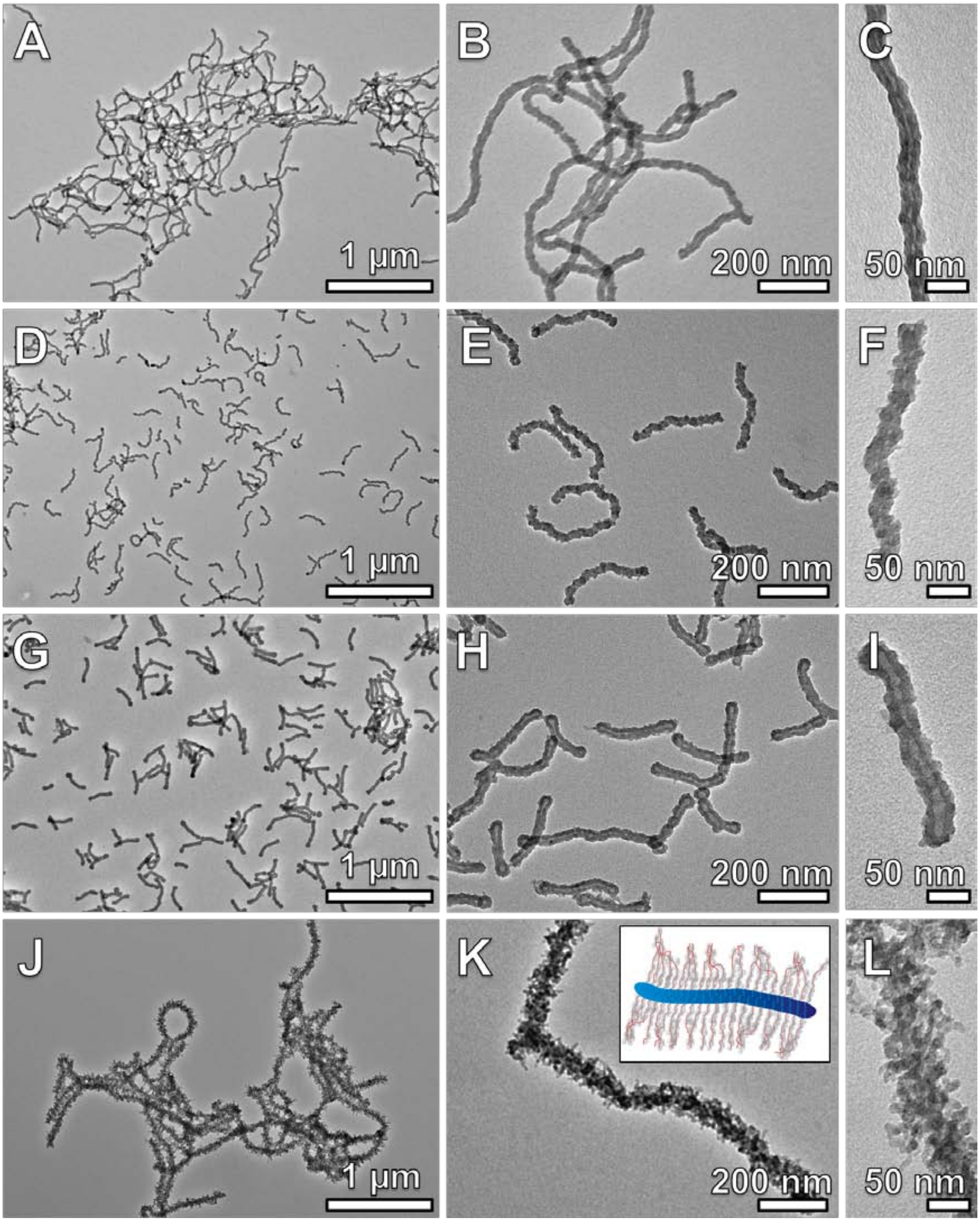

Figure 5-3. TEM micrographs of the as-synthesized silica hybrid nanowires. The silica hybrids were templated from the following polymer brushes: (**A-C**) $[CL_{14}DMAEMA_{43}]_{7500}$, (**D-F**) $[CL_{10}DMAEMA_{58}]_{2700}$, (**G-I**) $[CL_{25}DMAEMA_{76}]_{2700}$ and (**J-L**) $[CL_{14}DMAEMA_{342}]_{7500}$.

Figure 5-4 shows SEM images of the silica hybrid nanowires obtained by drying concentrated solutions. They form hybrid networks with different cavity sizes. The nanowires in Figure 5-4A show smaller cavities than those shown in Figure 5-4B. The difference between those silica hybrids is predominantly in length – the packing of these anisotropic structures becomes denser with decreasing length of the silica nanowires. N_2-

physisorption measurements of the hybrid materials highlight the porosity of the as-synthesized silica nanowires and resulted in specific surface areas of 178 $m^2 \cdot g^{-1}$ ($[CL_{25}DMAEMA_{76}]_{2700}$), 206 $m^2 \cdot g^{-1}$ ($[CL_{14}DMAEMA_{43}]_{7500}$) and 310 $m^2 \cdot g^{-1}$ ($[CL_{14}DMAEMA_{342}]_{7500}$), respectively (Table 5-3 and Supporting Information 5-S5). The aforementioned narrower packing of the shorter silica nanowires can also be observed in the pore size histogram (Figure 5-S6A), where an increased number of mesopores are observed at 25-35 nm. This might be attributed to wedge-shaped mesopores formed by the close packing of the silica nanowires. The longer nanowires did not show such a phenomenon.

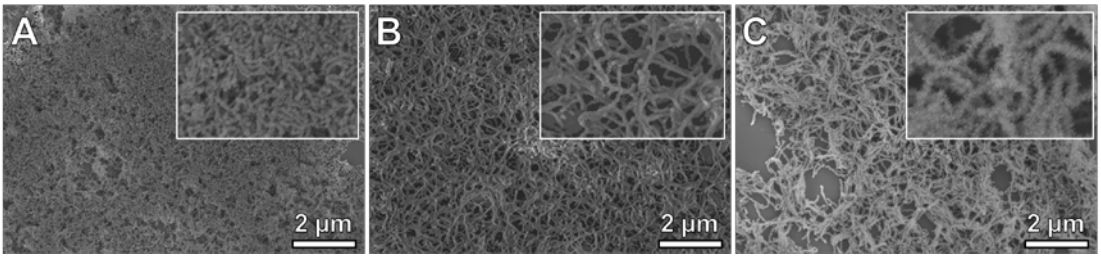

Figure 5-4. SEM images of as-synthesized silica hybrid networks derived from silica nanostructures with different lengths. The silica hybrids were templated from the following polymer brushes: (**A**) $[CL_{25}DMAEMA_{76}]_{2700}$, (**B**) $[CL_{14}DMAEMA_{43}]_{7500}$, and (**C**) $[CL_{14}DMAEMA_{342}]_{7500}$.

The silica hybrid nanostructures from template brushes with core-shell morphology are well dispersible in polar solvents and water. The shorter hybrids (from template brushes $[CL_nDMAEMA_m]_{2700}$) show excellent stability in water and ethanol over several days. In contrast, the longer hybrids precipitate after several hours. To improve the dispersibility of the longer hybrid nanowires, we produced a silica hybrid from a core-shell-corona template brushes (see Supporting Information 5-S6). The introduction of a highly soluble poly(oligo(ethylene glycol) methacrylate) (POEGMA) corona as a third block of the template CPBs, $[CL_{14}DMAEMA_{43}OEGMA_{75}]_{7500}$, aided the hybrids with higher aspect ratio to form dispersions for longer times.

Table 5-3. Surface areas and pore size volumes of as-synthesized nanowires and calcined nanotubes

Template composition[a]	Surface area[b] as-synthesized [$m^2 \cdot g^{-1}$]	Surface area[b] calcined [$m^2 \cdot g^{-1}$]	Micropore volume[c] as-synthesized [$cc \cdot g^{-1}$]	Micropore volume[c] calcined [$cc \cdot g^{-1}$]	Pore volume[d] as-synthesized [$cc \cdot g^{-1}$]	Pore volume[d] calcined [$cc \cdot g^{-1}$]
$[CL_{25}DMAEMA_{76}]_{2700}$	178	639	0.001	0.14	0.63	0.92
$[CL_{14}DMAEMA_{43}]_{7500}$	206	709	0.01	0.16	0.41	0.70
$[CL_{14}DMAEMA_{342}]_{7500}$	310	527	none	0.02	0.99	1.16

[a] Determined by ^{1}H-NMR; [b] determined according to the recommendations of Rouquerol *et al;*[44] regarding the BET equation; [c] only considering pores < 2 nm; [d] considering the total pore volume.

Nanotube Formation. Calcination of the freeze-dried silica hybrid materials in air atmosphere led to the complete removal of polymeric material and produced hollow silica nanotubes (see Figure 5-5). Due to the removal of the polyelectrolyte chains within the silica shell, micropores have been generated (similar to the micropores in SBA-15 materials). Table 5-3 shows the absence of micropores before calcination and highlights the increase of pore volumes in the micropore region, below 2 nm (~50% of the overall pore volume increase of the nanotubes from $[CL_{25}DMAEMA_{76}]_{2700}$ and $[CL_{14}DMAEMA_{43}]_{7500}$ is attributed to micropores). Due to the formation of polymer bundles in case of $[CL_{14}DMAEMA_{342}]_{7500}$ hybrids, no significant micropores were developed upon calcination. Next to the micropores, new mesopores have also been obtained after calcination. Most noticeable are the newly formed mesopores attributed to the former PCL core (see arrows in Figure 5-S6). This demonstrates that the hollow core became accessible through the micropores within the shell. The specific surface areas of the calcined silica nanotubes increased significantly to 639 $m^2 \cdot g^{-1}$ ($[CL_{25}DMAEMA_{76}]_{2700}$) and 709 $m^2 \cdot g^{-1}$ ($[CL_{14}DMAEMA_{43}]_{7500}$) and 527 $m^2 \cdot g^{-1}$ ($[CL_{14}DMAEMA_{342}]_{7500}$), respectively (for pore volume, pore volume distributions and N_2-physisorption measurements, please refer to Table 5-3 and Supporting Information 5-S5). TEM measurements indicated that agglomerates formed during calcination (see Figure 5-5A, D) can be separated by sonication (see Figure 5-5B, E). However, high amplitude ultrasound might cause breakage of the nanotubes. Alternatively, silica nanotubes can be formed at significantly lower temperatures. Acid treatment (2M HCl) of the silica nanostructures for three days at 50 °C did not harm the cylindrical shape.

However, we assume that the core was degraded equally quickly, as in the degradation of the pristine PCL-*b*-PDMAEMA brush and hence resulted in hollow silica nanotubes. TEM and SEM measurements verify the unchanged structure of the nanomaterials after acid treatment (see Figure 5-S8).

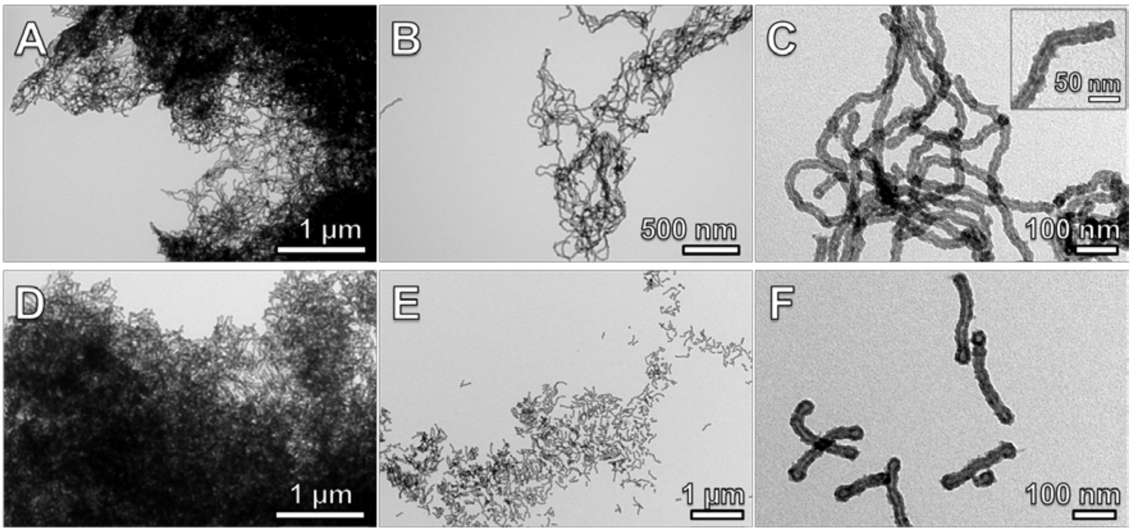

Figure 5-5. TEM micrographs of calcined silica nanotubes templated from (**A-C**) $[CL_{14}DMAEMA_{43}]_{7500}$ and (**D-F**) $[CL_{25}DMAEMA_{76}]_{2700}$. (**A, D**) Agglomerates of silica nanotubes after calcination. (**B, C, E, F**) Separated silica nanotubes after sonication.

Metal-Containing Brushes as Catalysts. To demonstrate the potential of the templated silica nanowires in catalysis applications, we loaded the PDMAEMA shell with metal salts prior to the incorporation of silica. Thus, the addition of TMOS embedded the metal ions (e.g. $[AuCl_4]^-$ or $[PtCl_4]^{2-}$) within the silica shell. Excess salt was removed by ultracentrifugation. The addition of $NaBH_4$ as a reducing agent led to the formation of gold or platinum nanoparticles (NPs). The TEM micrographs in Figure 5-6 confirm the successful incorporation of the nanoparticles and clearly verify the location of the nanoparticles within the silica shell. The size of the nanoparticles was measured via TEM. The average diameter of the platinum and gold nanoparticles is ~ 1.6 nm and ~ 3.5 nm, respectively. Energy-dispersive X-ray measurements confirmed the presence of nanoparticles and showed a gold content of 3 wt% with respect to silicon. For platinum, the content was 4 wt% (see Supporting Information 5-S8).

The reduction of 4-nitrophenol to 4-aminophenol by $NaBH_4$ in the presence of the NP-doped silica nanowires was performed to check their accessibility and catalytic activity. This reaction has been used widely and has become a model reaction for testing the catalytic activity of noble metal nanoparticles.[30,48,49] As shown in the Supporting

Information (Figure 5-S8), the strong UV absorption of 4-nitrophenate ions at 399 nm decreased gradually with time after the addition of nanoparticle-containing hybrid nanowires. Simultaneously, a new peak appeared at 300 nm, which was due to the product 4-aminophenol.[50,51]

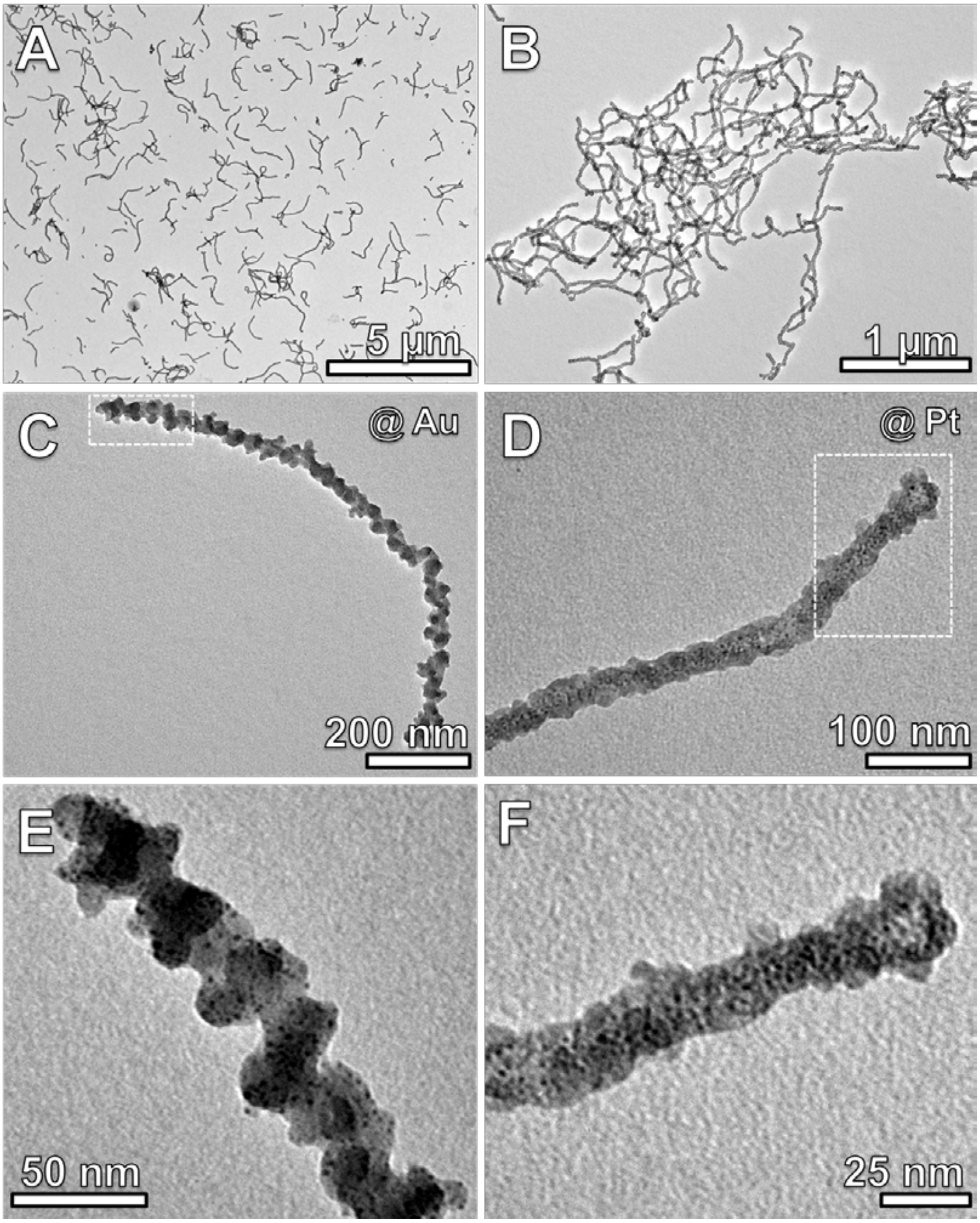

Figure 5-6. TEM micrographs of NP-doped silica hybrid nanowires. Silica hybrid nanowires were filled with (**A, C, E**) Au NPs, or (**B, D, F**) Pt NPs. Magnification of the nanowires shows that they are filled with NPs. The nanowires were templated from $[CL_{14}DMAEMA_{342}]_{7500}$ in the case of Au NPs and from $[CL_{14}DMAEMA_{43}]_{7500}$ in the case of Pt NPs.

Conclusions

The 1D soft template build-up for the fabrication of silica nanowires was realized via the combination of several polymerization techniques that allowed fine-tuning of the dimensions and morphology of the hybrid nanostructures. CPBs proved to be excellent soft templates, as their production is straighforward and cost-effective. Silica deposition into the template shell formed 1D silica hybrid nanowires in a mild procedure in water at ambient temperature. With this versatile route towards anisotropic silica nanostructures, it is possible to not only vary length and diameter, but also to vary the surface morphology by adjusting the shell length. Calcination or treatment with an acid led to the removal of the core and resulted in silica nanotubes with high microporous volumes and high specific surface areas. These materials might be interesting as filter or storage systems. Furthermore, the incorporation of catalytically active nanoparticles was facile and yielded robust catalysts, which can be easily removed from the system after the reaction. Additionally, the incorporation of metallic NPs into silica allows the structures to be used in high temperature applications.[52] These materials might also be interesting in the application of catalytically active filter systems.

Associated content

Supporting Information. SEC traces of PCL brushes (5-S1) and of cleaved PDMAEMA side chains (5-S2); AFM height analysis of template brushes (5-S3); TEM micrographs of silica hybrids from quaternized templates (5-S4), N_2-physisorption measurements and pore volume distributions (5-S5), silica hybrids from core-shell-corona templates (5-S6); silica nanotubes via acid treatment (5-S7); EDX spectra of platinum and gold nanoparticle-doped hybrids (5-S8), and catalytic activity of nanoparticle-doped hybrids (5-S9). This material is available free of charge via the Internet at http://pubs.acs.org."

Acknowledgments

This work was supported by the Deutsche Forschungsgemeinschaft (DFG) within the Collaborative Research Center (SFB) 840 and the Australian Research Council. The authors thank Marietta Böhm and Melanie Förtsch for performing SEC and cryo-TEM measurements, respectively. M. M. acknowledges BayEFG for a scholarship and BayNAT for a fellowship. T. L. thanks the international graduate school of the ENB "Structures, Reactivity and Properties of Metal Oxides" for a fellowship.

REFERENCES

(1) Chen, Z.; Cui, Z.-M.; Niu, F.; Jiang, L.; Song, W.-G. *Chem. Commun.* **2010**, *46*, 6524-6526.

(2) Li, G. L.; Tai, C. A.; Neoh, K. G.; Kang, E. T.; Yang, X. *Polym. Chem.* **2011**, *2*, 1368-1374.

(3) Lou, X. W.; Archer, L. A.; Yang, Z. *Adv. Mater.* **2008**, *20*, 3987-4019.

(4) Caruso, F.; Caruso, R. A.; Möhwald, H. *Science* **1998**, *282*, 1111-1114.

(5) Caruso, F. *Adv. Mater.* **2001**, *13*, 11-22.

(6) Gruber, S.; Gottschlich, A.; Scheel, H.; Aresipathi, C.; Bannat, I.; Zollfrank, C.; Wark, M. *Phys. Stat. Sol. - B* **2010**, *247*, 2401-2411.

(7) Huang, X.; Guo, C.; Zuo, J.; Zheng, N.; Stucky, G. D. *Small* **2009**, *5*, 361-365.

(8) Rahman, M. A.; García-García, F. R.; Hatim, M. D. I.; Kingsbury, B. F. K.; Li, K. *J. Membr. Sci.* **2011**, *368*, 116-123.

(9) Tran-Thi, T.-H.; Dagnelie, R.; Crunaire, S.; Nicole, L. *Chem. Soc. Rev.* **2011**, *40*, 621-639.

(10) Hu, J.; Odom, T. W.; Lieber, C. M. *Acc. Chem. Res.* **1999**, *32*, 435-445.

(11) Cui, Y.; Duan, X.; Hu, J.; Lieber, C. M. *J. Phys. Chem. B* **2000**, *104*, 5213-5216.

(12) Xia, Y.; Yang, P.; Sun, Y.; Wu, Y.; Mayers, B.; Gates, B.; Yin, Y.; Kim, F.; Yan, H. *Adv. Mater.* **2003**, *15*, 353-389.

(13) Cademartiri, L.; Ozin, G. A. *Adv. Mater.* **2009**, *21*, 1013-1020.

(14) Yao, B.; Fleming, D.; Morris, M. A.; Lawrence, S. E. *Chem. Mater.* **2004**, *16*, 4851-4855.

(15) Johnson, J. C.; Choi, H.-J.; Knutsen, K. P.; Schaller, R. D.; Yang, P.; Saykally, R. J. *Nat. Mater.* **2002**, *1*, 106-110.

(16) Yuan, J.; Müller, A. H. E. *Polymer* **2010**, *51*, 4015-4036.

(17) Weber, J.; Singhal, R.; Zekri, S.; Kumar, A. *Int. Mater. Rev.* **2008**, *53*, 235-255.

(18) Yuan, J.; Walther, A.; Müller, A. H. E. *Phys. Stat. Sol. - B* **2010**, *247*, 2436-2450.

(19) Liang, H.-W.; Liu, S.; Yu, S.-H. *Adv. Mater.* **2010**, *22*, 3925-3937.

(20) Zhang, M.; Müller, A. H. E. *J. Polym. Sci. Part A Polym. Chem.* **2005**, *43*, 3461-3481.

(21) Sheiko, S. S.; Sumerlin, B. S.; Matyjaszewski, K. *Prog. Polym.Sci.* **2008**, *33*, 759-785.

(22) Huang, K.; Canterbury, D. P.; Rzayev, J. *Chem. Commun.* **2010**, *46*, 6326-6328.

(23) Huang, K.; Canterbury, D. P.; Rzayev, J. *Macromolecules* **2010**, *43*, 6632-6638.

(24) Huang, K.; Rzayev, J. *J. Am. Chem. Soc.* **2009**, *131*, 6880-6885.

(25) Yuan, J.; Lu, Y.; Schacher, F.; Lunkenbein, T.; Weiss, S.; Schmalz, H.; Müller, A. H. E. *Chem. Mater.* **2009**, *21*, 4146-4154.

(26) Zhang, M.; Estournès, C.; Bietsch, W.; Müller, A. H. E. *Adv. Funct. Mater.* **2004**, *14*, 871-882.

(27) Zhang, M.; Drechsler, M.; Müller, A. H. E. *Chem. Mater.* **2004**, *16*, 537-543.

(28) Yuan, J.; Drechsler, M.; Xu, Y.; Zhang, M.; Müller, A. H. E. *Polymer* **2008**, *49*, 1547-1554.

(29) Djalali, R.; Li, S.-Y.; Schmidt, M. *Macromolecules* **2002**, *35*, 4282-4288.

(30) Yuan, J.; Schacher, F.; Drechsler, M.; Hanisch, A.; Lu, Y.; Ballauff, M.; Müller, A. H. E. *Chem. Mater.* **2010**, *22*, 2626-2634.

(31) Xu, Y.; Yuan, J.; Fang, B.; Drechsler, M.; Müllner, M.; Bolisetty, S.; Ballauff, M.; Müller, A. H. E. *Adv. Funct. Mater.* **2011**, *20*, 4182-4189.

(32) Yuan, J.; Xu, Y.; Walther, A.; Bolisetty, S.; Schumacher, M.; Schmalz, H.; Ballauff, M.; Müller, A. H. E. *Nat. Mater.* **2008**, *7*, 718-722.

(33) Müllner, M.; Yuan, J.; Weiss, S.; Walther, A.; Förtsch, M.; Drechsler, M.; Müller, A. H. E. *J. Am. Chem. Soc.* **2010**, *132*, 16587-16592.

(34) Yang, L.-P.; Zou, P.; Pan, C.-Y. *J. Mater. Chem.* **2009**, *19*, 1843-1849.

(35) Yang, Y.; Suzuki, M.; Owa, S.; Shirai, H.; Hanabusa, K. *J. Mater. Chem.* **2006**, *16*, 1644-1650.

(36) Zhang, Z.; Buitenhuis, J. *Small* **2007**, *3*, 424-428.

(37) Acar, H.; Garifullin, R.; Guler, M. O. *Langmuir* **2011**, *27*, 1079-1084.

(38) Kuijk, A.; van Blaaderen, A.; Imhof, A. *J. Am. Chem. Soc.* **2011**, *133*, 2346-2349.

(39) Gao, C.; Lu, Z.; Yin, Y. *Langmuir* **2011**, *27*, 12201-12208.

(40) Yuan, J.-J.; Mykhaylyk, O. O.; Ryan, A. J.; Armes, S. P. *J. Am. Chem. Soc.* **2007**, *129*, 1717-1723.

(41) Du, J.; Armes, S. P. *Langmuir* **2008**, *24*, 13710-13716.

(42) Li, Y.; Du, J.; Armes, S. P. *Macromol. Rapid Commun.* **2009**, *30*, 464-468.

(43) Mori, H.; Wakisaka, O.; Hirao, A.; Nakahama, S. *Macromol. Chem. Phys.* **1994**, *195*, 3213-3224.

(44) Rouquerol, J.; Llewellyn, P.; Rouquerol, F. *Stud. Surf. Sci. Catal.***2007**, *160*, 49-56.

(45) Yu-Su, S. Y.; Sheiko, S. S.; Lee, H.-i.; Jakubowski, W.; Nese, A.; Matyjaszewski, K.; Anokhin, D.; Ivanov, D. A. *Macromolecules* **2009**, *42*, 9008-9017.

(46) Sheiko, S. S.; Sun, F. C.; Randall, A.; Shirvanyants, D.; Rubinstein, M.; Lee, H.-i.; Matyjaszewski, K. *Nature* **2006**, *440*, 191-194.

(47) Polotsky, A.; Charlaganov, M.; Xu, Y.; Leermakers, F. A. M.; Daoud, M.; Müller, A. H. E.; Dotera, T.; Borisov, O. *Macromolecules* **2008**, *41*, 4020-4028.

(48) Mei, Y.; Lu, Y.; Polzer, F.; Ballauff, M.; Drechsler, M. *Chem. Mater.* **2007**, *19*, 1062-1069.

(49) Lee, J.; Park, J. C.; Song, H. *Adv. Mater.* **2008**, *20*, 1523-1528.

(50) Hayakawa, K.; Yoshimura, T.; Esumi, K. *Langmuir* **2003**, *19*, 5517-5521.

(51) Esumi, K.; Isono, R.; Yoshimura, T. *Langmuir* **2003**, *20*, 237-243.

(52) Joo, S. H.; Park, J. Y.; Tsung, C.-K.; Yamada, Y.; Yang, P.; Somorjai, G. A. *Nat. Mater.* **2009**, *8*, 126-131.

Supporting Information

5-S1. SEC Traces of PCL Homopolymer Brushes

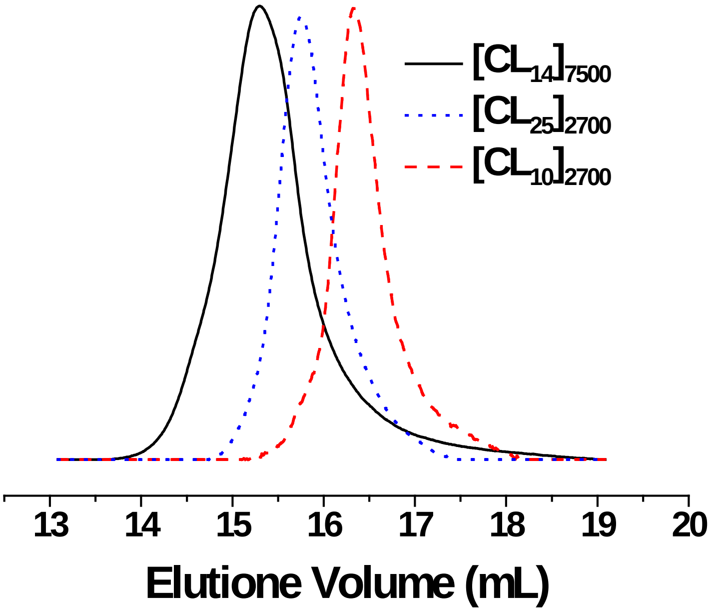

Figure 5-S1. SEC traces in DMAc of the PCL homopolymer brushes.

5-S2. SEC Trace of Cleaved PDMAEMA Grafts

Cleaving of the PDMAEMA side chains of the template brush via acidic ester hydrolysis resulted in a linear homopolymer PDMAEMA with number-average molecular weight (M_n) of 54 x10^3 g·mol^{-1}and a polydispersity index (PDI) of 1.18 (determined via SEC in DMAc and PDMAEMA calibration). According to the conversion measured by ^{1}H-NMR, the M_n was determined to be 49.5 x10^3 g·mol^{-1}. This led to a grafting efficiency of DMAEMA of 91-92%.

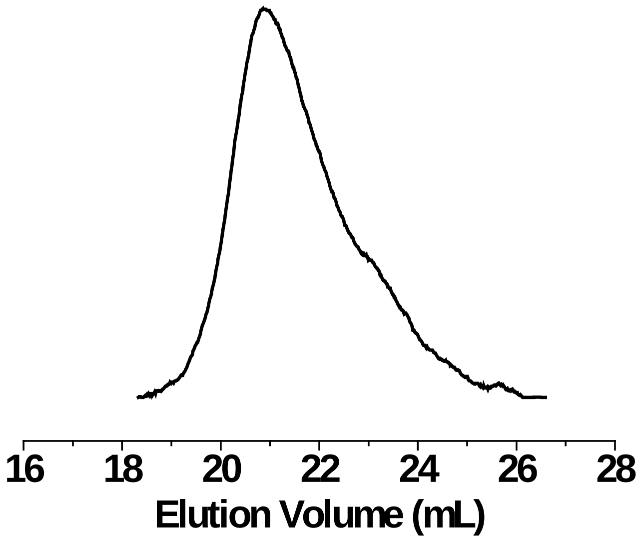

Figure 5-S2. SEC trace in DMAc of $PDMAEMA_{350}$ after cleaving from $[CL_{14}DMAEMA_{350}]_{7500}$ under acidic conditions. SEC was calibrated with PDMAEMA standards.

5-S3. Height Analysis of AFM Images

Cross-sections of the various template brushes listed in Table 5-2 and height profiles of the respective polymer brush (see Figure 5-S3A-D). As already discussed in the manuscript, the length of the polymer brushes is firstly dependent on the degree of polymerization of the backbone. If the backbone of different brushes is identical (see in Figure 5-S3A and B; Figure 5-S3C and D), then the length is dependent on the brush composition. The height in AFM increases when the side chain length increases, as more polymeric material is deposited onto the substrate (compare Figure 5-S3C and D). Despite having a similar overall side chain length, the height in AFM may vary dramatically, as can be seen in Figure 5-S3A and B. This phenomenon is attributed to the different size of the PCL core. As PCL is assumed to prevent direct contact to mica, it will force the core to be completely shielded by PDMAEMA. Due to that fact, the brush with a larger PCL compartment shows an increase in height. In addition, this increase is also based on the segment density of the polymer brush. Due to the very high grafting efficiency, the polymer core is surrounded by a relatively compact PDMAEMA shell, which adds dramatically to the height in AFM (compare cartoons in Figure 5-S3).

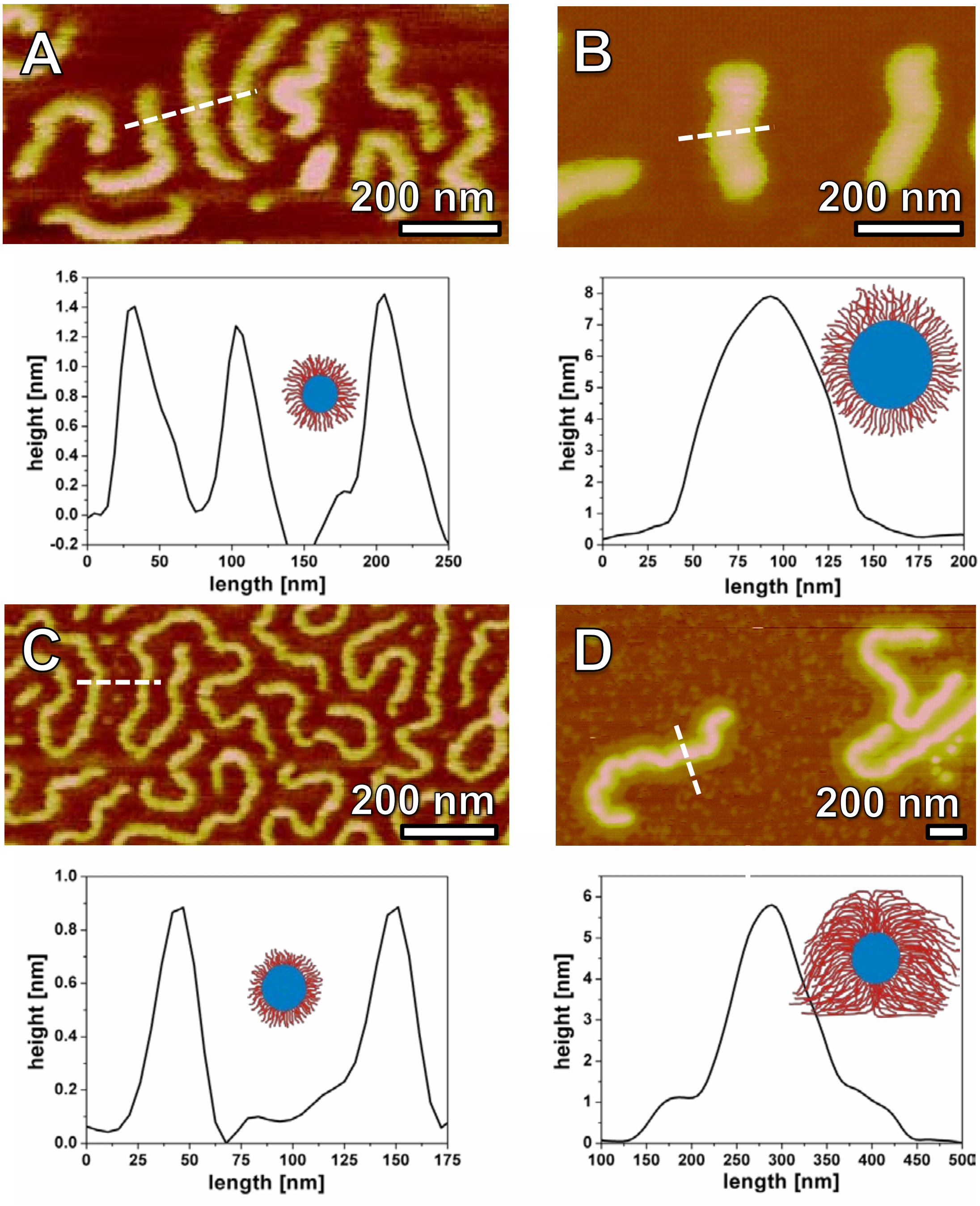

Figure 5-S3. AFM height images of various template brushes and their corresponding height profile (cross-section): (**A**) $[CL_{10}DMAEMA_{58}]_{2700}$, (**B**) $[CL_{25}DMAEMA_{76}]_{2700}$, (**C**) $[CL_{14}DMAEMA_{43}]_{7500}$ and (**D**) $[CL_{14}DMAEMA_{342}]_{7500}$. The z-values are: (**A, C**) 2 nm, (**B**) 15 nm and (**D**) 10 nm.

5-S4. Hybrids from Quaternized Template Brushes

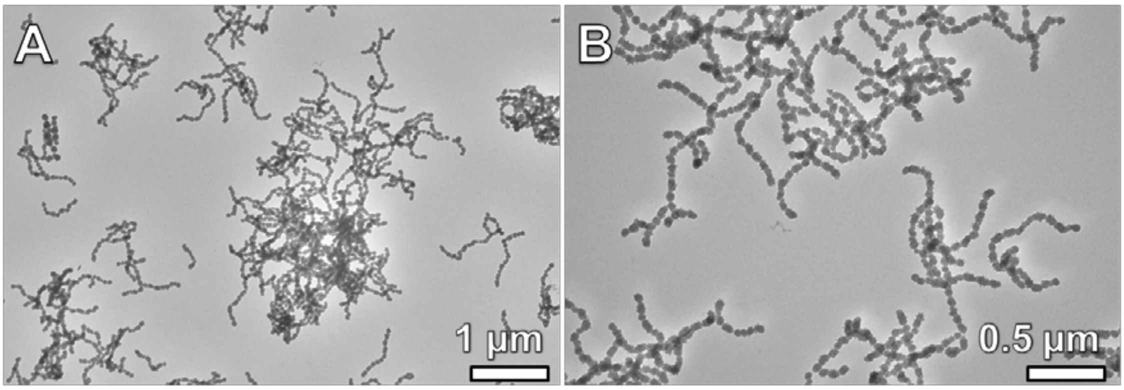

Figure 5-S4. TEM micrographs of silica hybrid template by [CL$_{14}$METAI$_{43}$]$_{7500}$.

S5. N$_2$-physisorption measurements and pore volume distribution

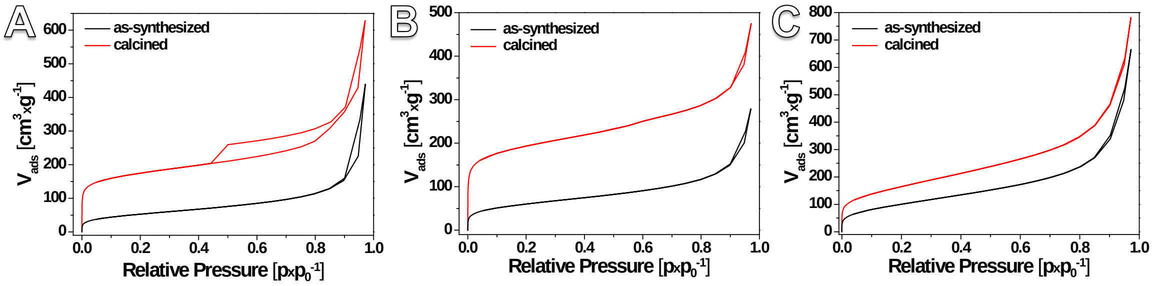

Figure 5-S5. N$_2$-isotherms of as-synthesized (**black line**) and calcined (**red line**) silica nanotubes from template brush **(A)** [CL$_{25}$DMAEMA$_{76}$]$_{2700}$, **(B)** [CL$_{14}$DMAEMA$_{43}$]$_{7500}$ and **(C)** [CL$_{14}$DMAEMA$_{342}$]$_{7500}$.

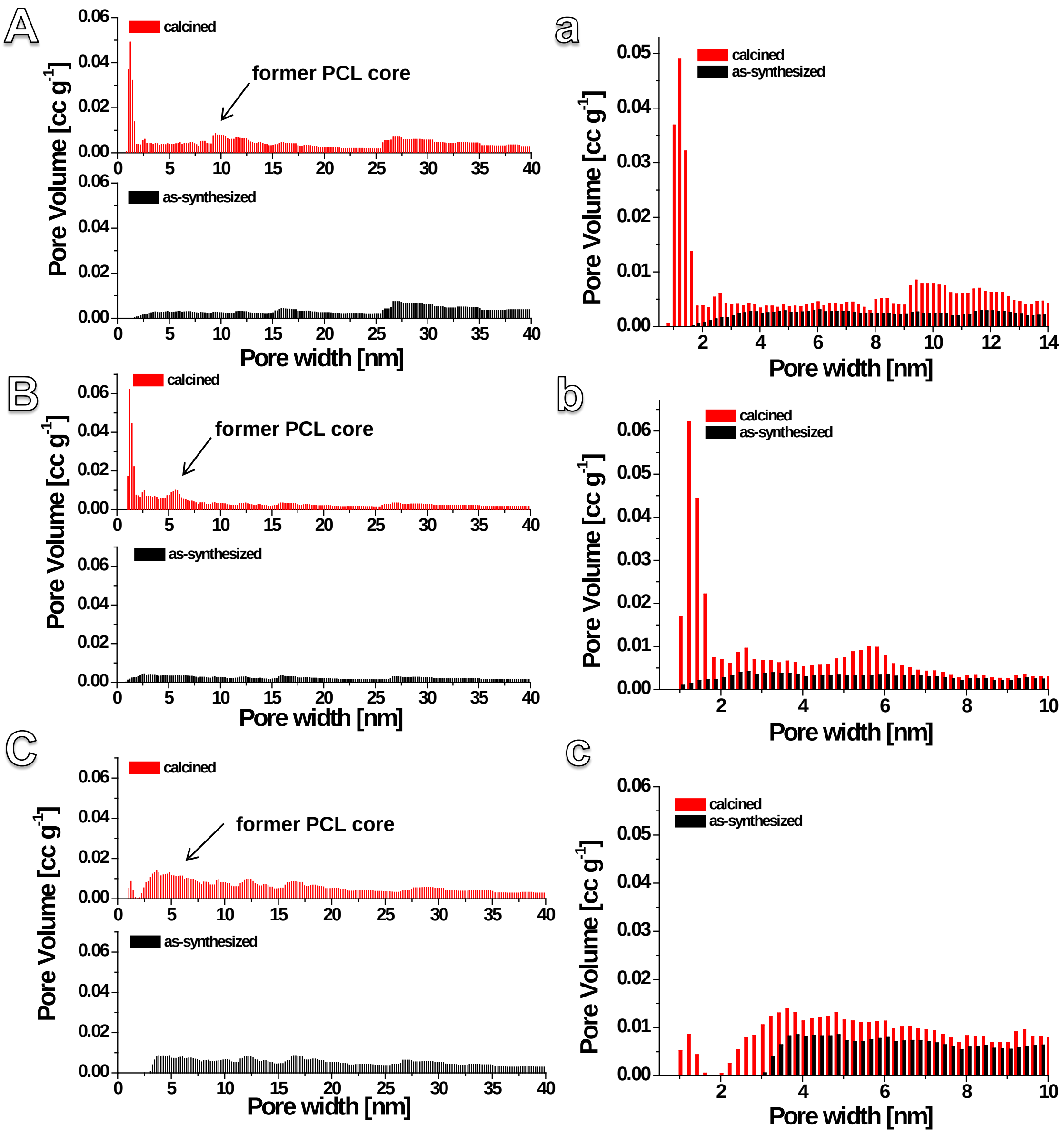

Figure 5-S6. Pore volume distributions of as-synthesized (**black**) and calcined (**red**) silica nanotubes from template brush **(A/a)** $[CL_{25}DMAEMA_{76}]_{2700}$, **(B/b)** $[CL_{14}DMAEMA_{43}]_{7500}$ and **(C/c)** $[CL_{14}DMAEMA_{342}]_{7500}$.

5-S6. Hybrid from Core-Shell-Corona Template Brushes

The use of $[CL_{14}$-*b*-$DMAEMA_{43}$-*b*-$OEGMA_{75}]_{7500}$ polymer brushes as the template for the fabrication of silica nanowires provided the latter hybrid with an additional POEGMA corona. POEGMA increased the dispersibility of the brushes in both polar and non-polar solvents. Figure 5-S7 shows TEM micrographs of the corresponding silica hybrid. The POEGMA corona was not visible in TEM due to low contrast.

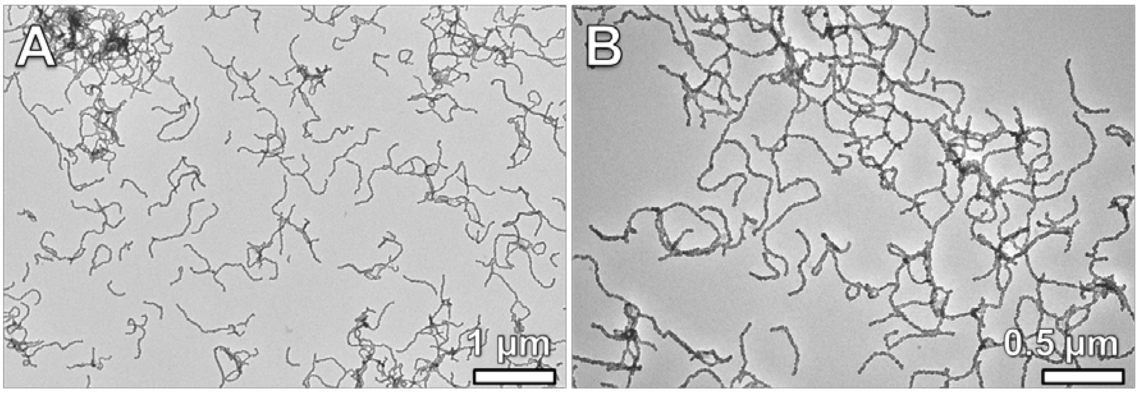

Figure 5-S7. TEM micrographs of 1D silica hybrids templated by core-shell-corona structured brushes $[CL_{14}DMAEMA_{43}OEGMA_{75}]_{7500}$.

5-S7. Nanotubes Through Acid Treatment (SEM and TEM)

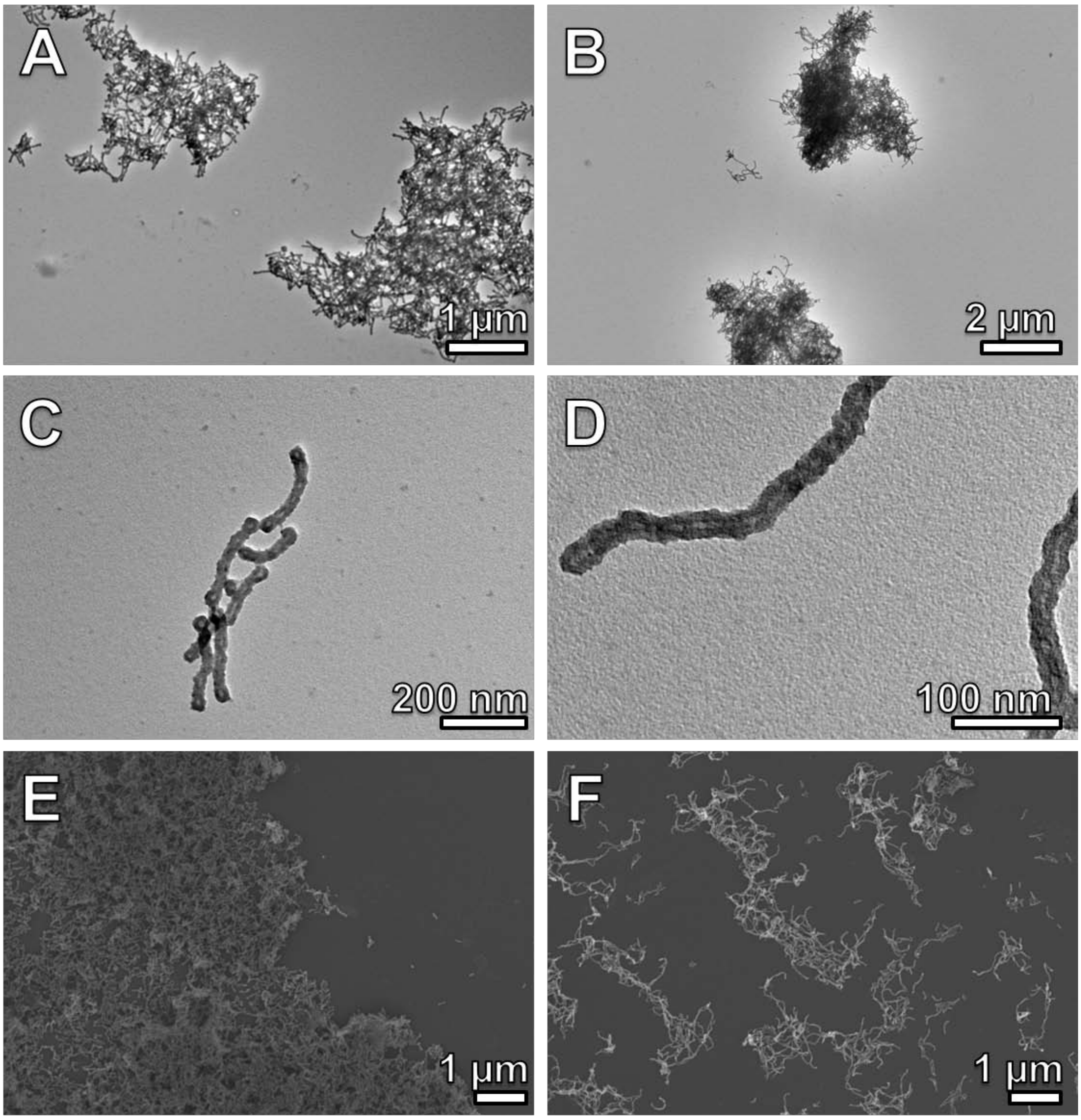

Figure 5-S8. TEM and SEM images of acid treated silica nanotubes templated by $[CL_{25}DMAEMA_{76}]_{2700}$, (**A, C, E**) and $[CL_{14}DMAEMA_{43}]_{7500}$ (**B, D, F**).

5-S8. EDX of Nanoparticle-Containing Silica Hybrids

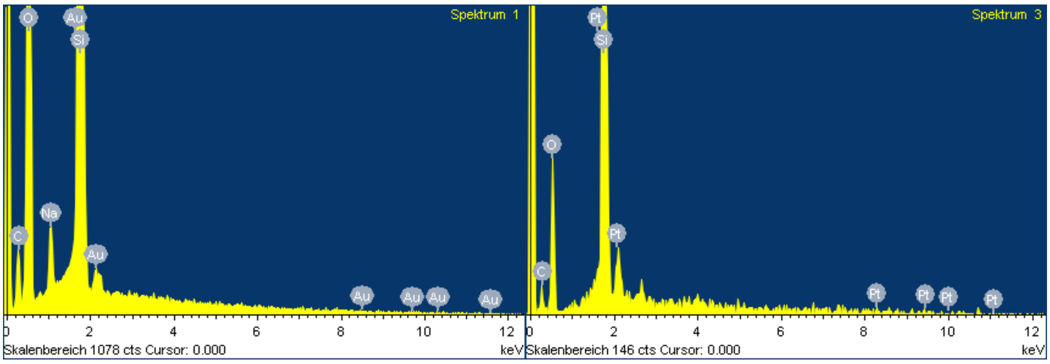

Figure 5-S9. EDX spectra of Au- and Pt-doped silica hybrid nanostructures. Au (**left**) and Pt (**right**).

5-S9. Catalytic Activity

The strong UV absorption of 4-nitrophenate ions at 399 nm decreases gradually with time after the addition of nanoparticle-containing hybrid nanowires. In addition, the concentration of sodium borohydride was adjusted to largely exceed the concentration of 4-nitrophenol. Therefore, in this case, pseudo-first-order kinetics, with regard to the 4-nitrophenol concentrations, could be used to evaluate the catalytic rate. The kinetic plots in Figure 5-S8 show the linear relationship between ln(c/c_0) versus time t from which the apparent rate constant was calculated. The rate constant k_{app} for Au@ $[CL_{14}DMAEMA_{342}]_{7500}$ was 0.023 min^{-1} and 0.007 min^{-1} for Pt@$[CL_{14}DMAEMA_{43}]_{7500}$, respectively.

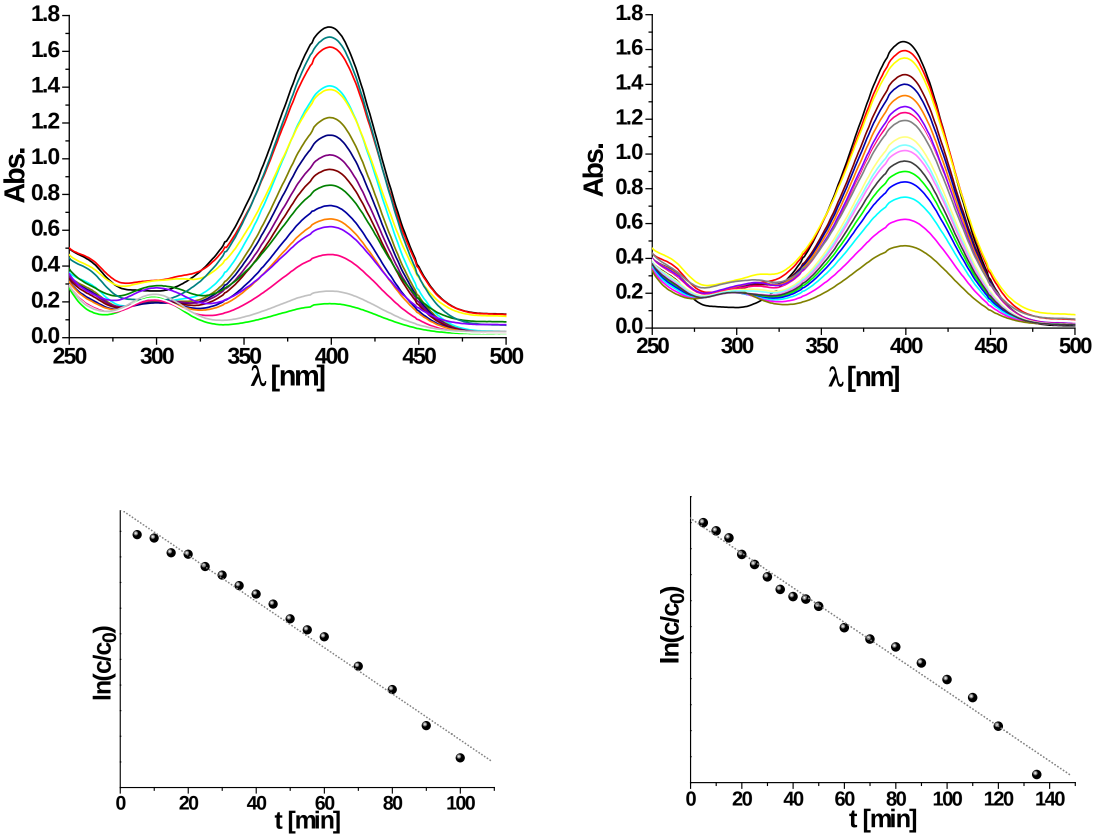

Figure 5-S10. Reduction of 4-nitrophenol to 4-aminophenol via $NaBH_4$ in the presence of Au NP-doped silica nanowires (**left**) or in the presence of Pt NP-doped silica nanowires (**right**). The kinetic plots (**below**) show the linear relationship between ln(c/c_0) vs time.

Chapter 6

A Facile Polymer Templating Route Toward High Aspect Ratio Crystalline Titania Nanostructures

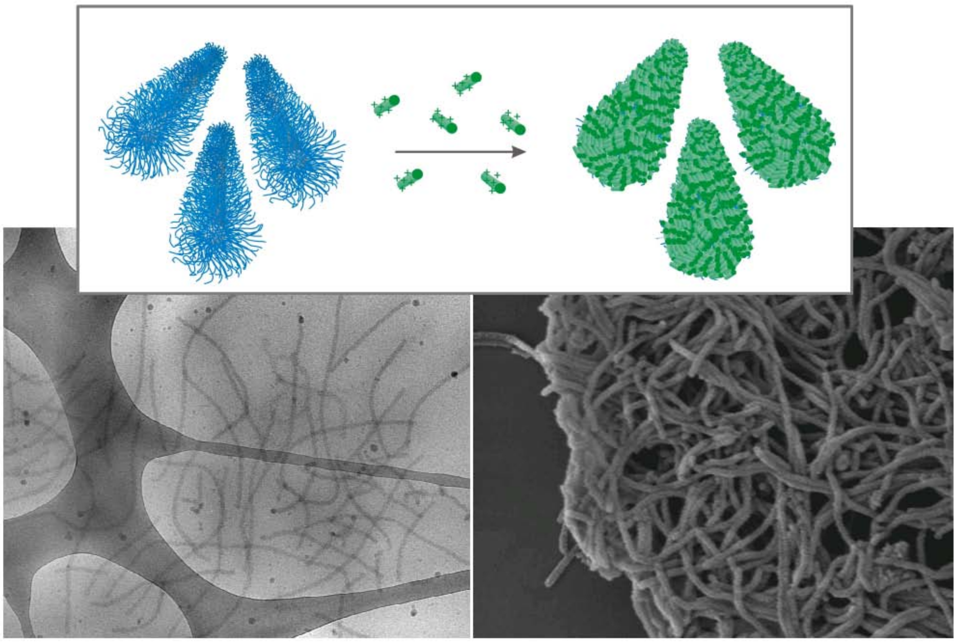

The results of this chapter are published in *Small* as:

“A Facile Polymer Templating Route Toward High Aspect Ratio Crystalline Titania Nanostructures”

by Markus Müllner, Thomas Lunkenbein, Nobuyoshi Miyajima, Josef Breu,*
and Axel H.E. Müller*

Abstract. High aspect ratio rutile and anatase hybrid nanowires are produced *via* a template-directed process using a novel cylindrical polyelectrolyte brush template. Loading the highly negatively charged 1D templates with pre-synthesized TiO_2 nanocrystals, results in the fabrication of soluble crystalline TiO_2 hybrid nanowire.

Introduction

There has been a growing interest in the manipulation of the architecture of materials, which is motivated by application-based objectives in various research areas covering chemistry, biology, physics and materials science. Nanomaterials are promising candidates for solving major problems of nowadays society, such as sustainable energy,[1] information storage,[2] water treatment,[3] etc. Especially one-dimensional (1D) nanostructures of metal oxides, like nanowires or nanotubes, have been under close investigation due to their size-dependent optical and electronical properties, which allow them to be used in catalysis, separation, or photovoltaic applications.[4] Among the many metal oxides used in these fields are the polymorphs of titania (TiO_2). TiO_2 is a semiconductor and well-known for its applications in the field of photocatalysis and photo-electrochemistry due to its excellent optical transmittance and high refractive index.[1a, 5] Crystalline titania (in its anatase and rutile polymorphs) is of considerable interest as it finds further use in sensors and dye-sensitized solar cells.[6] Each polymorph of TiO_2 has different physical properties and, consequently, the ability to control its crystal structure is of great interest.[7]

Several strategies for achieving 1D inorganic nanomaterials have been reported ranging from hydrothermal growth[8] and electrospinning[9] to template chemistry.[4a, 10] Well-defined templates, in particular, allow the fabrication of tailor-made materials with specific shapes and structural properties.[10a, 10b, 11] An important class of organic templates derives from 1D organic structures, in particular cylindrical polymer brushes (CPBs).[10c, 12] CPBs refer to both molecular brushes (having a single macromolecule as backbone) and brushes obtained from block copolymers. Molecular CPBs are synthesized via grafting approaches[13] and give 1D nanoobjects with very uniform length and diameter, which have been used as templates for the synthesis of various 1D hybrid materials, such as CdS,[14] CdSe,[15] Fe_2O_3,[14, 16] SiO_2[17] nanowires and nanotubes.[18] However, when ionic side-chains of a molecular CPB interact with oppositely charged multivalent ions or colloids they are prone to collapse.[19] Earlier attempts to synthesize TiO_2 nanowires based on the interaction of poly(2-hydroxyethyl methacrylate) brushes with $Ti(OBu)_4$ led to amorphous material only.[20] As an alternative to the rather complex molecular brush synthesis and behavior, crosslinking cylindrical bulk morphologies of block copolymers can be applied to form 1D templates with a rigid core.[12b, 21] Organic-inorganic 1D hybrid nanomaterials obtained from CPB templates show many advantages with respect to colloidal stability, functionality, flexibility, and producibility.[10c]

The hybrid formation can occur via two possible ways; the in-situ formation of inorganic material from soluble molecular precursors within the template[15] or the infiltration of pre-synthesized inorganic nanoparticles (colloidal route).[22] In-situ generation of nanoparticles within a 1D template may lead to insufficient or inhomogeneous filling of the template or poor control of nanoparticle size,[15] whereas pre-synthesized nanoparticles can be more easily characterized and homogenously infiltrated leading to better defined hybrid nanostructures.[13, 16]

Within this context, extensive efforts have been devoted to obtain highly crystalline hybrid nanomaterials, as they bear superior properties when compared to amorphous or low crystalline hybrids.[23] However, as-made hybrid materials of TiO_2 are often amorphous and additional high temperature treatment is required to obtain highly crystalline materials[20, 24] which again bears the risk of losing solubility and the hybrid morphology.[23b]

Herein, we demonstrate a novel synthesis concept that can be applied for structuring metal oxides, which we apply to the synthesis of rutile and anatase nanowires with high aspect ratio. To the best of our knowledge, this is the first report on a rigid, water-soluble 1D template that is strongly negatively charged at very low pH. By mildly sulfonating cylindrical polyelectrolyte brushes, obtained from the bulk morphology of polystyrene-*block*-poly(allyl methacrylate) block copolymers, very long and robust organic templates can be produced for the fabrication of anisotropic TiO_2 nanostructures. The phase-pure crystallinity of TiO_2 is adjusted prior to the hybrid formation during production of positively charged colloidal nanocrystals in an aqueous and mild approach. In turn, the hybrid nanostructures are soluble, highly crystalline and produced at low temperatures (60 °C). Additionally, they can serve as precursors for the pyrolytic formation of purely inorganic nanowires. With the presented system, it is possible to realize nanoscale structuring of metal oxides in a facile manner.

Results and Discussion

Synthesis of the 1D Template Brush

Poly(allyl methacrylate) (AMA) was chosen for the crosslinkable and cylinder-forming block, as it is reported that the allyl group undergoes crosslinking in the presence of radicals.[25] Using sequential anionic polymerization, we obtained a well-defined diblock copolymer polystyrene-*block*-poly(allyl methacrylate) (PS-*b*-PAMA). For details see supporting Information, 6-S1 – 6-S4. ^{1}H-NMR, showed the absence of crosslinking (Figure 6-S2). The composition of the diblock copolymer, as determined by a combination of size exclusion chromatography and ^{1}H-NMR, is $PS_{69}PAMA_{31}^{81}$, (subscripts are the weight fractions and the superscript refers to the total number-average molecular weight, M_n, of 81 $kg \cdot mol^{-1}$) with a polydispersity index of 1.06 (Figure 6-S1). The film casting of $PS_{69}PAMA_{31}^{81}$ from toluene resulted in hexagonally packed cylinders of PAMA segments in a PS matrix (see transmission electron microscopy (TEM) images in Figure 6-S3). The diameter of the PAMA cylinders was 22 ± 2 nm, as determined by TEM measurements. The cylindrical morphology was preserved by co-casting 10 wt% of a photoinitiator and crosslinking of the allyl groups by irradiation of the polymer film with UV light for four hours.

After crosslinking, the polymer film was re-dispersed in THF to obtain single cylindrical polymer brushes with a PS corona (see Scheme 6-1,iii). The diameter of the dispersed cylinders was 60-65 nm in the dry state (measured by TEM). The lengths of the cylinders varied from only 200 nm up to 5 µm. The wide length distribution results from the domain size distribution of the cast bulk film. The very long cylinders can be shortened by sonication but we chose not to modify them.

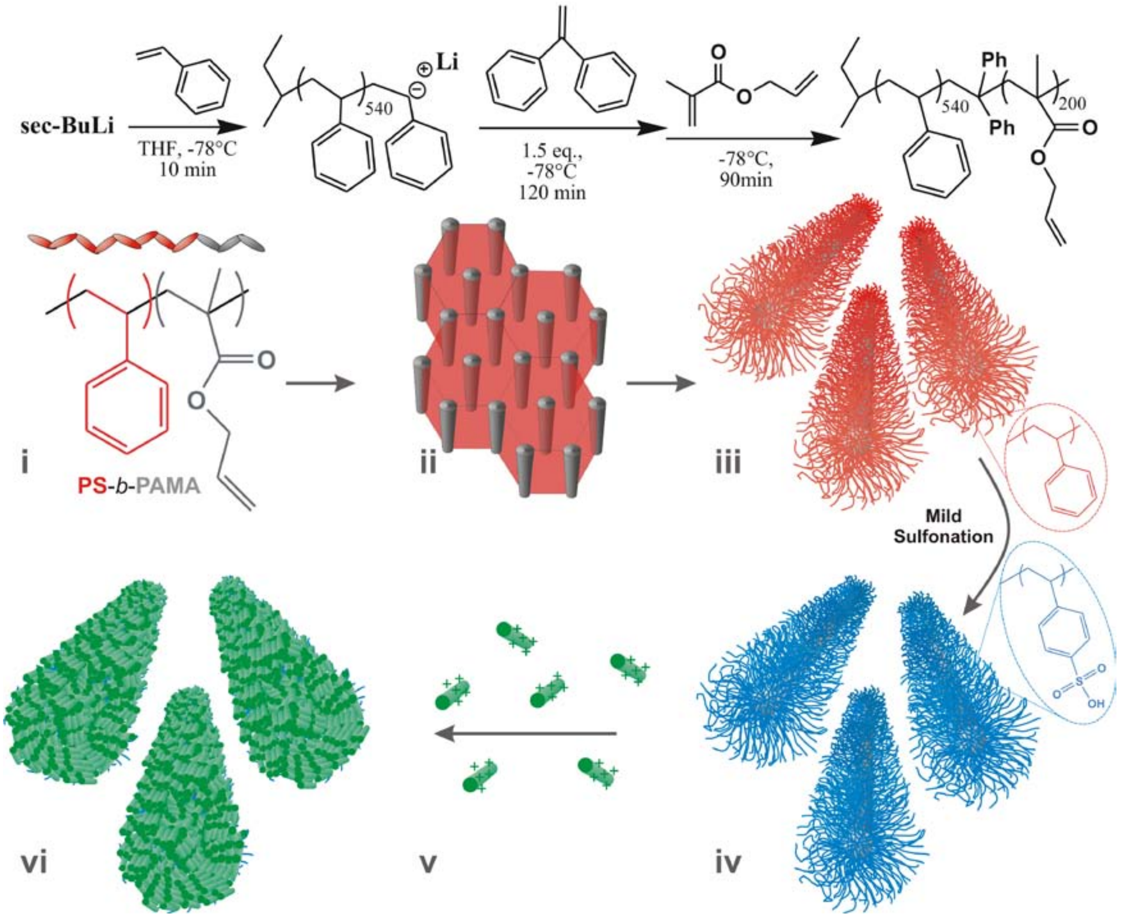

Scheme 6-1: Top: sequential anionic polymerization of polystyrene-*block*-poly(allyl methacrylate) (PS-*b*-PAMA). Below: PS-*b*-PAMA (**i**) microphase-separates into (**ii**) hexagonally packed cylinders. (**iii**) The UV-crosslinked cylindrical polymer brushes with PAMA core and PS corona are redispersed and (**iv**) sulfonated into cylindrical polyelectrolyte brushes with a poly(styrenesulfonic acid) corona. (**v**) Positively charged and pre-synthesized titania nanocrystals are then infiltrated to produce (**vi**) anisotropic metal oxide –polymer brush hybrid nanowires.

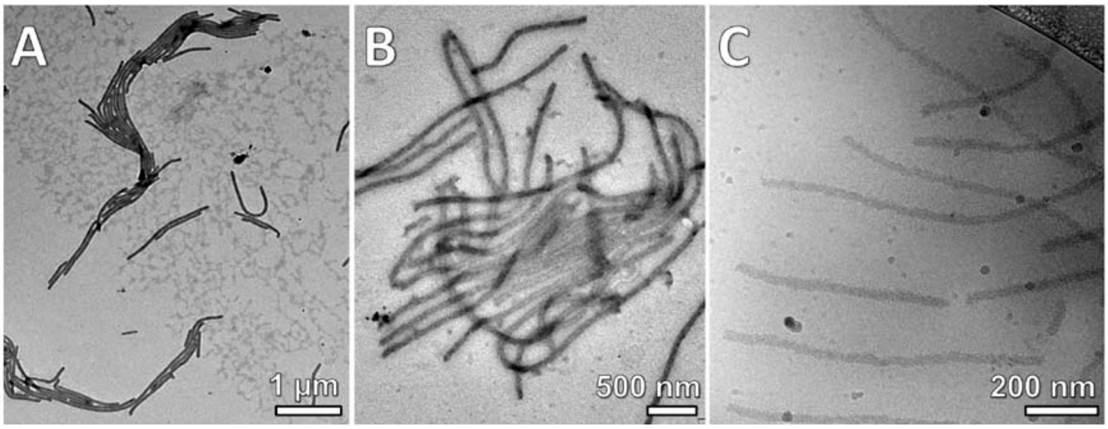

Figure 6-1: TEM micrographs of core-crosslinked cylindrical polymer brushes and their sulfonated analogues: (**A**) RuO_4-stained PS-*b*-PAMA (from THF) and (**B**) PSS-*b*-PAMA (from water). (**C**) Cryo-TEM micrograph of PSS-*b*-PAMA in water.

Next, the PS corona was sulfonated to poly(styrenesulfonic acid) (PSS), which is a strong anionic polyelectrolyte (Scheme 6-1, iv). Mild sulfonation with acetyl sulfonate[26] in dichloroethane led to a degree of sulfonation of 81 % and hence the transformation of most of the PS corona into PSS. After sulfonation, the crosslinked core remained around 25 nm in diameter (see dark cylinders in Figure 6-1C). From the distance of cylinders in cryogenic TEM (cryo-TEM; Figure 6-1C), the length of the PSS side-chains is estimated to be below 100 nm. The PSS side chains consist of 540 monomer units, which leads to a contour length of 135 nm (0.25 nm per monomer unit). The actual length of the polyelectrolyte chains in water is assumed to be quite stretched due to the high charge density and the resulting high osmotic pressure of the dissociated protons. However, it is known that polyelectrolyte chains in aqueous solution are rarely fully extended.[27] The PSS grafts allow excellent dispersion of the polymer brushes in water and guarantee a high and satisfactory amount of negative charges even at low pH values for the infiltration of positively charged TiO_2 nanocrystals.

Note that the block copolymer polystyrene-*block*-polybutadiene, which also produces PS cylinders but with a polybutadiene core, did not survive the mild sulfonation conditions. This phenomenon highlights the superior properties of the PS-*b*-PAMA block copolymer template.

Synthesis of Crystalline TiO_2 Nanocolloids

As for the crystals, both the size and the chemical nature of the surface of the colloid are essential. Therefore, we have developed a modified low-temperature, non-hydrothermal synthesis route for both colloidal rutile and anatase which are only electrostatically stabilized.[22] The titania nanocrystals were synthesized using acidic water as the reaction medium and titanium tetra(*n*-butoxide) as the precursor. Under these conditions, well-defined nanocrystals were obtained under very mild conditions at 60 °C in two hours. The apparent hydrodynamic diameter was ~8 nm for the rutile nanocrystals (Figure 6-2C) and ~14 nm for the anatase ones (Figure 6-S6E). Cryo-TEM images (Figures 6-2A, B) verify the presence of pre-synthesized rutile nanocrystals in water. While the original precursor dispersions were stable, some agglomeration of the nanocrystals occurred due to decreased electrostatic repulsion upon transfer and dilution for the dynamic light scattering (DLS) measurement (see white circle, Figure 6-2B). However, the intensity-weighted hydrodynamic diameter distribution in Figure 6-2C (solid line) overemphasizes the few larger agglomerates. The phase purity of the nanocrystals was confirmed by powder X-ray diffraction (PXRD) (see Figure 6-3A for rutile and Figure 6-S6D for anatase).

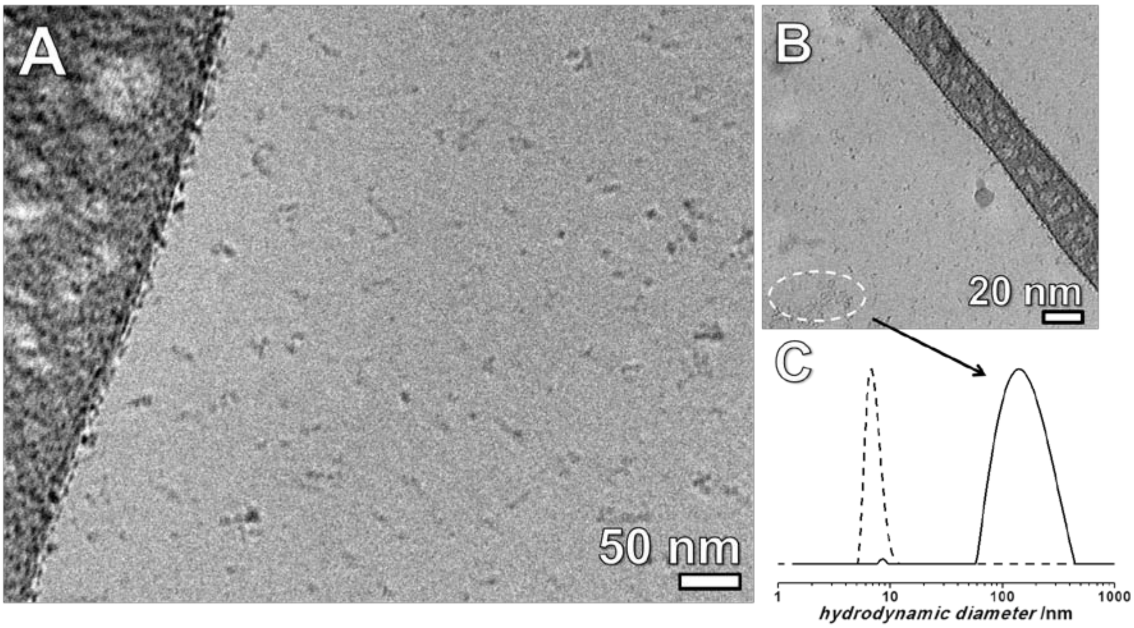

Figure 6-2. (**A, B**) Cryo-TEM micrograph of rutile nanocrystals in water. They can be found aligned at the edge of the lacey grid. (**C**) Hydrodynamic diameter distribution (from DLS) of rutile nanocrystals in acidic water: number-weighted plot (dashed line) and intensity-weighted plot (solid line). Large hydrodynamic diameters derive from the agglomeration of nanocrystals, as can be seen in (**B**) (white circle).

Synthesis of Crystalline 1D TiO_2 Hybrid Nanowires

It is well known that the surface potential of oxides critically depends on pH.[28] Freshly prepared colloidal suspensions of rutile or anatase nanocrystal precursors were used for the TiO_2 hybrid nanowire synthesis. Since titania is quite acidic with a point of zero charge below 5, rutile and anatase only possess a positively charged surface at very low pH values.[22, 28] Contrary to other polyelectrolytes, like poly(meth)acrylic acid, our PSS template still bears a significant negative charge at very low pH values. The resulting strong Coulomb interactions with the PSS polyanions control the supramolecular assembly of the nanocrystals into the corona of the template brushes, leading to crystalline organic-inorganic TiO_2 nanowires. Figure 6-3A shows the PXRD pattern of the as-synthesized rutile composite (top curve). The polymeric template itself is amorphous and only contributes to the background in the PXRD. Therefore, it was subtracted from the PXRD trace. The rutile reflexes seen in the PXRD of the precursors reappear in the pattern of the hybrid material. The same can be found when anatase colloids were used instead of rutile. The corresponding hybrid material exhibits the anatase crystal structure as it was pre-determined by the colloids (Figure 6-S6). Thus, the intercalation of the crystalline TiO_2 colloids into the brush template led to the successful fabrication of soluble hybrid materials with a pre-determined shape, size and crystallinity. The full width of half maximum (FWHM) of the rather broad reflexes in the powder diffraction translate to rather small crystal sizes of infiltrated nanocrystals, as verified by DLS (see precursor hydrodynamic diameter distribution in Figure 6-2C (rutile) and Figure 6-S6E (anatase)).

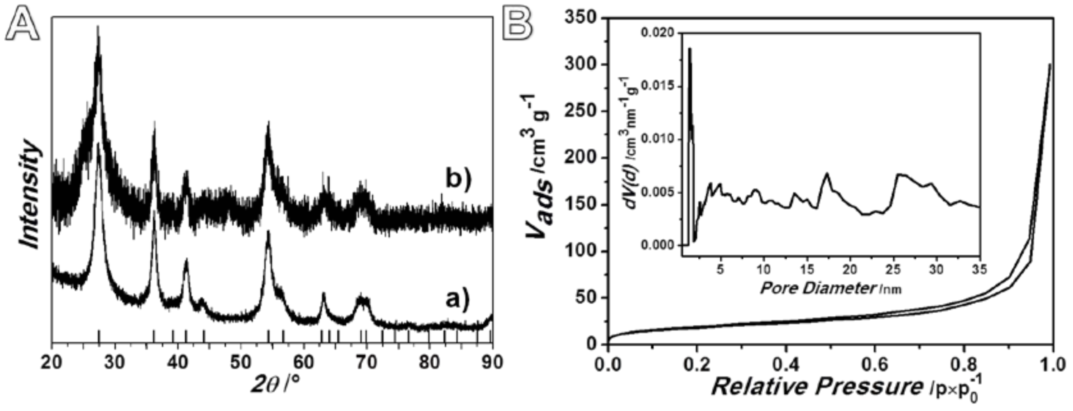

Figure 6-3. (**A**) Powder XRD patterns of a) as-synthesized rutile precursor (**black curve, bottom**) and b) as-synthesized rutile hybrid material (**red curve, top**). The ticks on the x-axis indicate expected rutile reflexes. (**B**) N_2-sorption isotherms of as-synthesized rutile nanowire, including pore diameter distribution.

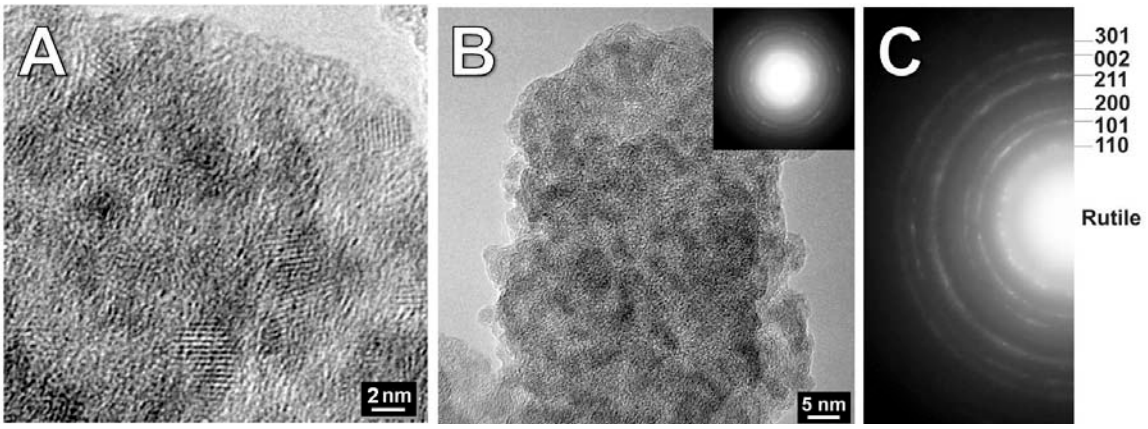

Figure 6-4. (**A, B**) High-ResolutionTEM micrographs of as-synthesized rutile nanostructures and (**C**) the corresponding SAED indexing and verification of rutile crystal structure.

To verify the PXRD pattern and to further underline the crystallinity of the hybrid nanowires, we performed high resolution TEM (HR-TEM) measurements. The HR-TEM micrographs clearly indicate that the inorganic part of the hybrid material is built up through the embedment of crystalline colloids. SAED indexing verified that the embedded colloids exhibit rutile crystal structure (Figure 6-4).

Both TEM (Figure 6-5A–C) and scanning electron microscopy (SEM) images (Figure 6-5D–F) are in line with the proposed mechanism of the hybrid formation. The diameter of the composite nanowires was around 55 nm. This means that the polyelectrolyte corona contracts during the infiltration step due to electrostatic interaction between the polyanion and the positively charged nanocolloids; similar to an interpolyelectrolyte complex (IPEC) formation.[29] In contrast to molecular brushes, it does not collapse. High aspect ratio nanostructured rutile and anatase hybrid materials, which are soluble in polar solvents and water, were produced by this infiltration method (Figure 6-5 and Figure 6-S6). The hybrid nanowires survive harsh ultrasound without fracturing and do not fall apart in salt or at higher pH. The well-dispersed nanowires form non-woven spaghetti-like networks upon drying. Due to the anisotropic shape, the dry composite material provides both a highly porous mesostructure in combination with a comparatively large surface area. The surface area of the dried rutile hybrid material was 66 $m^2 \cdot g^{-1}$, as determined by Brunauer-Emmett-Teller (BET) analysis of N_2-sorption isotherms (Figure 6-3B). Although thermogravimetric analysis (TGA) determines a weight content of TiO_2 of around 50 % (Figure 6-S5) the hybrid material remains highly flexible. The remaining 50% organic material provides a certain ductility to the hybrid.

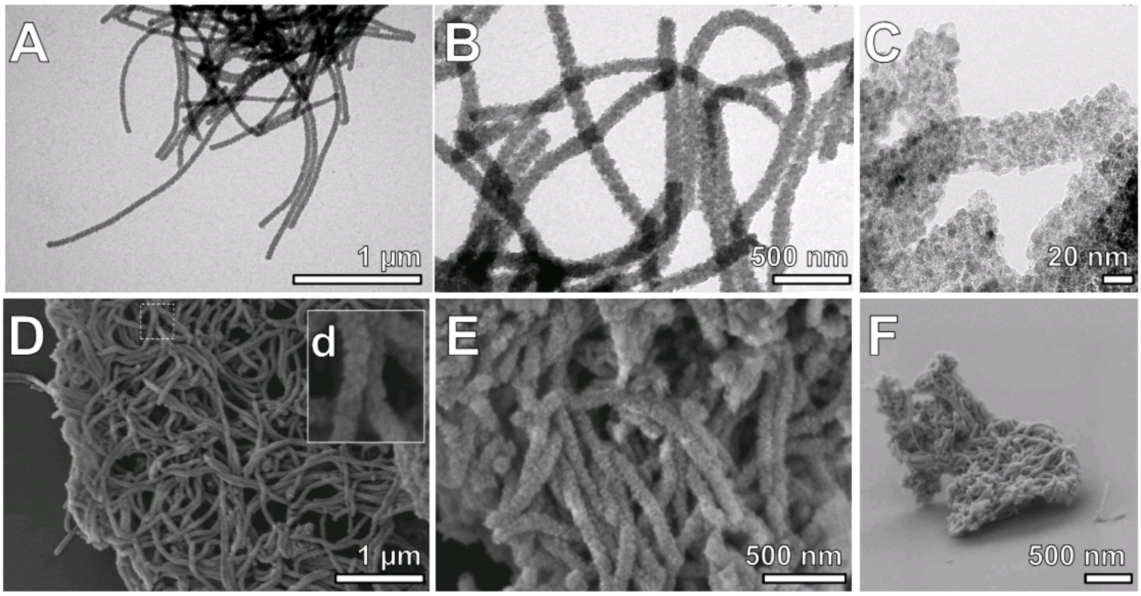

Figure 6-5: (**A-C**) TEM micrographs of as-synthesized anisotropic rutile nanostructures, (**D**) SEM micrographs of as-synthesized rutile nanowires, and (**E, F**) calcined rutile nanowires on a tilted sample stage (75° viewing angle).

After step-wise calcination, first in argon atmosphere and then in air, all polymeric material was destroyed but the cylindrical shape of the former hybrid material was preserved (Figure 6-5E, F).

Conclusions

In conclusion, our mild, template-directed approach produces soluble 1D crystalline TiO_2 nanowires with high aspect ratio and high surface area at rather low temperatures. The nanowires disperse well in polar solvents and arrange into porous non-woven mesostructures with high surface area upon drying, which keep their shape after calcination. Hence, deposition of single TiO_2 nanowires onto substrates or producing well-defined layers is easy. This particular material may give rise to various applications, such as catalytically active filter systems, energy storage devices, or in particular in photovoltaics, as anatase finds wide-spread use in dye-sensitized solar cells.[30] Insufficient contacts between TiO_2 particles in photovoltaic devices still limit the electron transport and hence lower the efficiency of solar cells. On the basis of that fact, we assume that our materials, with their increased aspect ratios and networks structures, might introduce additional electron pathways, when compared to the corresponding spherical materials.

Our novel cylindrical template with PAMA core and PSS corona is unique in two ways: (**i**) it is water-soluble and negatively charged over the full pH range, and (**ii**) due to the crosslinked PAMA core it is rigid enough to prevent collapse upon interaction with the titania nanocrystals.

We are convinced that our colloidal route can be generally used to produce many other anisotropic metal oxide hybrids of any known and desired polymorphic crystal structure, as the only prerequisite is the availability of small and positively charged nanocrystals, where the pH of hybrid formation may be freely adjusted to the particular metal oxide of arbitrary point of zero charge.[28]

Acknowledgments. This work was funded by the Collaborative Research Center (SFB) 840 within project A7. The authors thank M. Böhm and M. Förtsch for performing SEC and cryo-TEM measurements, respectively. We further thank L. Geiling for running the N_2 physisorption measurements, and the Bavarian Geo Institute for giving us access to the HR-TEM instrument. M. Müllner thanks BayEFG for a scholarship. T. Lunkenbein acknowledges the international graduate school of the ENB “Structures, Reactivity and Properties of Metal Oxides” for a fellowship.

Supporting Information Available. Experimental part and methods (6-S1 and 6-S2); SEC (6-S3) and NMR (6-S4) characterization of PS-*b*-PAMA diblock copolymer and TEM micrographs of thin films of the bulk morphology (6-S5); SEM images of argon calcined rutile nanostructures (6-S6), including thermogravimetry analysis (6-S7); and the preparation and characterization of anatase nanostructures (6-S8). This material is available free of charge via the Internet at http://pubs.acs.org.

References

[1] a) M. Grätzel, Nature **2001**, 414, 338; b) B. O'Regan, M. Grätzel, Nature **1991**, 353, 737; c) A. S. Arico, P. Bruce, B. Scrosati, J.-M. Tarascon, W. van Schalkwijk, Nat. Mater. **2005**, 4, 366.

[2] a) G. S. D. Beach, C. Nistor, C. Knutson, M. Tsoi, J. L. Erskine, Nat. Mater. **2005**, 4, 741; b) S. S. P. Parkin, M. Hayashi, L. Thomas, Science **2008**, 320, 190.

[3] a) Q. Li, S. Mahendra, D. Y. Lyon, L. Brunet, M. V. Liga, D. Li, P. J. J. Alvarez, Water Res. **2008**, 42, 4591; b) J.-Y. Bottero, J. Rose, M. R. Wiesner, Integr. Environ. Assess. Manage. **2006**, 2, 391.

[4] a) Y. Xia, P. Yang, Y. Sun, Y. Wu, B. Mayers, B. Gates, Y. Yin, F. Kim, H. Yan, Adv. Mater. **2003**, 15, 353; b) J. Weber, R. Singhal, S. Zekri, A. Kumar, Inter. Mater. Rev. **2008**, 53, 235.

[5] X. Chen, S. S. Mao, Chem. Rev. **2007**, 107, 2891.

[6] a) N. Bahadur, K. Jain, R. Pasricha, Govind, S. Chand, Sensor Actuat- B: Chem. **2010**, 159, 112; b) L. F. O. Furtado, A. D. P. Alexiou, L. Gonçalves, H. E. Toma, K. Araki, Angew. Chem. Int. Ed. **2006**, 45, 3143; c) C. S. Karthikeyan, M. Thelakkat, Inorg. Chim. Acta **2008**, 361, 635; d) J. C. Brendel, Y. Lu, M. Thelakkat, J. Mater. Chem. **2010**, 20, 7255.

[7] a) J. Y. Ying, C. P. Mehnert, M. S. Wong, Angew. Chem. Int. Ed. **1999**, 38, 56; b) D. V. Bavykin, J. M. Friedrich, F. C. Walsh, Adv. Mater. **2006**, 18, 2807.

[8] a) X. Wang, Y. Li, J. Am. Chem. Soc. **2002**, 124, 2880; b) X. Jiaqiang, C. Yuping, C. Daoyong, S. Jianian, Sens. Actuat. B: Chem. **2006**, 113, 526; c) G. Shen, P.-C. Chen, K. Ryu, C. Zhou, J. Mater. Chem. **2009**, 19, 828.

[9] a) P. Viswanathamurthi, N. Bhattarai, H. Y. Kim, D. R. Lee, Nanotechnology **2004**, 15, 320; b) D. Li, Y. Xia, Nano Lett. **2003**, 3, 555; c) H. Dong, D. Wang, G. Sun, J. P. Hinestroza, Chem. Mater. **2008**, 20, 6627.

[10] a) H.-W. Liang, S. Liu, S.-H. Yu, Adv. Mater. **2010**, 22, 3925; b) J. Yuan, A. Walther, A. H. E. Müller, Phys. Stat. Sol. B 2010, 247, 2436; c) J. Yuan, A. H. E. Müller, Polymer **2010**, 51, 4015.

[11] a) P. S. Chinthamanipeta, Q. Lou, D. A. Shipp, ACS Nano **2011**, 5, 450; b) I. Botiz, S. B. Darling, Mater. Today **2010**, 13, 42.

[12] a) M. Antonietti, S. Förtser, Top. Curr. Chem. **2003**, 266, 1; b) R. S. Yelamanchili, A. Walther, A. H. E. Müller, J. Breu, Chem. Commun. **2008**, 489; c) F. H. Schacher, T. Rudolph, M. Drechsler, A. H. E. Müller, Nanoscale **2010**, 3, 288.

[13] M. Zhang, A. H. E. Müller, J. Polym. Sci. Part A: Polym. Chem. **2005**, 43, 3461.

[14] M. Zhang, M. Drechsler, A. H. E. Müller, Chem. Mater. **2004**, 16, 537.

[15] J. Yuan, M. Drechsler, Y. Xu, M. Zhang, A. H. E. Müller, Polymer **2008**, 49, 1547.

[16] Y. Xu, J. Yuan, B. Fang, M. Drechsler, M. Müllner, S. Bolisetty, M. Ballauff, A. H. E. Müller, Adv. Funct. Mater. **2010**, 20, 4182.

[17] a) J. Yuan, Y. Xu, A. Walther, S. Bolisetty, M. Schumacher, H. Schmalz, M. Ballauff, A. H. E. Müller, Nat. Mater. **2008**, 7, 718; b) Y. Xu, J. Yuan, A. H. E. Müller, Polymer **2009**, 50, 5933.

[18] M. Müllner, J. Yuan, S. Weiß, A. Walther, M. Förtsch, M. Drechsler, A. H. E. Müller, J. Am. Chem. Soc. **2010**, 132, 16587.

[19] a) L-T. Yan, Y. Xu, M. Ballauff, A. H. E. Müller, A. Böker, J. Phys. Chem. B **2009**, 113, 5104; b) Y. Xu, S. Bolisetty, M. Drechsler, B. Fang, J. Yuan, L. Harnau, M. Ballauff, A. H. E. Müller, Soft Matter **2009**, 5, 379.

[20] J. Yuan, Y. Lu, F. Schacher, T. Lunkenbein, S. Weiss, H. Schmalz, A. H. E. Müller, Chem. Mater. **2009**, 21, 4146.

[21] a) X. Yan, G. Liu, F. Liu, B. Z. Tang, H. Peng, A. B. Pakhomov, C. Y. Wong, Angew. Chem. Int. Ed. **2001**, 40, 3593; b) Q. Lou, P. S. Chinthamanipeta, D. A. Shipp, Langmuir **2011**, 27, 15206.

[22] R. S. Yelamanchili, Y. Lu, T. Lunkenbein, N. Miyajima, L.-T. Yan, M. Ballauff, J. Breu, Small **2009**, 5, 1326.

[23] a) B. Ohtani, Y. Ogawa, S.-i. Nishimoto, J. Phys. Chem. B **1997**, 101, 3746; b) Lee, M. Christopher Orilall, S. C. Warren, M. Kamperman, F. J. DiSalvo, U. Wiesner, Nat. Mater. **2008**, 7, 222.

[24] a) J. Lee, C. M. Orilall, S. C. Warren, M. Kamperman, F. J. DiSalvo, U. Wiesner, Nat. Mater. **2008**, 7, 222; b) Y. Mao, S. S. Wong, J. Am. Chem. Soc. **2006**, 128, 8217; c) H. Zhang, M. Finnegan, J. F. Banfield, Nano Lett. **2000**, 1, 81.

[25] A. Matsumoto, S. Asai, H. Aota, Macromol. Chem. Phys. **2000**, 201, 2735.

[26] T. Saito, B. D. Mather, P. J. Costanzo, F. L. Beyer, T. E. Long, Macromolecules **2008**, 41, 3503.

[27] M. Balastre, F. Li, P. Schorr, J. Yang, J. W. Mays, M. V. Tirrell Macromolecules, **2002**, 35, 9480.

[28] a) S. Fazio, J. Guzmán, M. T. Colomer, A. Salomoni, R. Moreno, J. Eur. Ceram. Soc. **2008**, 28, 2171; b) M. Kosmulski, J. Colloid Interf. Sci. **2006**, 298, 730.

[29] Y. Xu, O. V. Borisov, M. Ballauff, A. H. E. Müller, Langmuir **2010**, 26, 6919.

[30] a) J. Bandara, K. Willinger, M. Thelakkat, Phys. Chem. Chem. Phys. **2011**, 13, 12906; b) J. T. Park, J. H. Koh, J. A. Seo, J. H. Kim, J. Mater. Chem. **2011**, 21, 1787.

Supporting Information

6-S1. Experimental Part

Materials. *sec*-Butyllithium (1.3 M solution in hexane, Acros) was used without further purification. THF (Fluka) was distilled from CaH_2 and K. Subsequently, the solvent was directly transferred into a glass reactor (Büchi). Styrene (Acros) was stirred over Bu_2Mg for 2 h and afterwards condensed on a vacuum line. Allyl methacrylate (ABCR) was stirred over trioctylaluminium for 40 min and afterwards also condensed on a vacuum line with dynamic vacuum aperture. 1,1-Diphenylethylene (DPE, Aldrich) was distilled from *sec*-butyllithium. The photoinitiator [diphenyl(2,4,6-trimethylbenzoyl)phosphine oxide] (Lucirin TPO®) was provided by BASF. Titanium tetra(*n*-butoxide) (Aldrich), acetic anhydride (Fluka), hydrochloric acid (37% HCl), acetic acid and sulfuric acid (98% H_2SO_4) were used as received.

Synthesis of polystyrene-*block*-poly(allyl methacrylate). PS-*b*-PAMA was synthesized via sequential living anionic polymerization in THF (400 mL) at low temperatures[1] in the presence of alkoxides to stabilize the living chain end. The alkoxides were obtained by reacting 4 mL of *sec*-BuLi with THF at -20 °C and slowly warming to room temperature over night. In the following, styrene (21 g, 0.2 mol) was injected via syringe into the septum-sealed reactor vessel and initiated with *sec*-butyllithium (0.2 mL, 0.28 mmol) at -78 °C. The polymerization was allowed to proceed for 15 min at -78 °C. Before the polymerization of the second block, the polystyrene end chains were end-capped with DPE (0.25 mL, 1.4 mmol) at -78 °C for 1 h in order to attenuate the reactivity of the anions; otherwise, attack of the ester moiety of the allyl methacrylate (AMA) would occur. AMA (9 g, 0.07 mol) was injected via syringe into the reaction vessel and was polymerized for 90 min at -78 °C. Finally the reaction was quenched through the addition of 3 mL of deoxygenated isopropanol. The polymer was then purified by precipitation into cold isopropanol and freeze-dried from dioxane.

Film Casting and Crosslinking. A film of diblock copolymer was cast from toluene with an additional amount of 10 wt% photoinitiator (Lucirin TPO®). After crosslinking, the resulting fixed self-organized structures were re-dissolved in THF by stirring for at least one week. The re-dispersion can be sped up by sonication, which will, however, lead to shorter polymer cylinders. In this way, core-shell cylindrical polymer brushes with a polystyrene corona and a poly(allyl methacrylate) core were produced in a large quantity. The crosslinking procedure did not change the morphology of the bulk structure. Crosslinking of the as-cast polymer film was carried out with a UV-lamp (Hoehnle VG UVAHAND 250 GS with cut-off at 300nm) for 4 h.

Sulfonation of the PS Corona. The PS-*b*-PAMA cylinders (~1 g) were dispersed in dichloroethane (DCE; 50 mL) and deoxygenated by bubbling argon for 15 min. While bubbling, the dispersion was heated to 50°C and 2.5 M of freshly prepared acetyl sulfate solution (10-15 mL) was added slowly. The acetyl sulfate solution was prepared according to literature.[2] The sulfonation process was allowed to proceed for 24 h until a few milliliters of MeOH were added. DCE was distilled off on a rotary evaporator. The sulfonated brushes were washed several times with MilliQ water using a centrifuge, in order for the polymer brushes to be recollected. The degree of sulfonation achieved by this mild method was 81%. This was determined by the elemental analysis of sulfur (theoretical value at 100 % sulfonation of PS to PSS: 13.9 %; experimental value: 11.2 %).

Synthesis of Crystalline TiO_2 Nanocolloids. Rutile was previously produced in the presence of HCl,[3] whereas anatase was already produced in the presence of acetic acid.[4] Herein, the mild synthesis of rutile or anatase nanocrystals was performed in acidic water at 60 °C while continuously stirring by the drop-wise addition of titanium (IV) *n*-butoxide (2 mL) to 5 mL of a 2 M HCl (in case of rutile) or 2M acetic acid (in case of anatase) solution. After 2 h, the stirring was stopped and the required amount of suspension of nanocrystals was taken out via Eppendorf pipette for the hybrid formation.

Synthesis of Crystalline TiO_2 Hybrid Nanowires. A template brush suspension (12 mL, $c = 1\ g\ L^{-1}$) was adjusted to pH 1 by adding 2M HCl. The acidic brush suspension was then added drop-wise to 160 µL of the as-prepared rutile crystal suspension in a glass vial under stirring (60 °C). For the fabrication of anatase hybrid nanowires, the same template brush suspension (pH 1) was added drop-wise to 180 µL of the anatase crystal suspension. However, it is not possible to reach pH 1 with acetic acid; consequently, the pH of the anatase colloid suspension was adjusted to pH 1 by adding 2M H_2SO_4 prior to the addition of the template brushes.

In both cases, the hybrid formation was stopped after 2h of stirring at 60 °C. Immediately, the resulting hybrid materials were centrifuged and washed several times with water and methanol until they were dried in air or freeze-dried from water. The dry hybrid materials were then used for further characterization and experiments.

6-S2. Methods

Transmission Electron Microscopy (TEM). Ultrathin (30-80 nm) samples for TEM were cut from the as-cast and crosslinked polymer films with a Reichert-Jung Ultracut E equipped with a diamond knife. TEM micrographs were taken on a Zeiss CEM 902 operating at 80 kV. In order to enhance the electron density of the poly(allyl methacrylate) phase, the samples were stained with OsO_4. For TEM samples coming from solution, a droplet of a dilute solution (0.05 g L^{-1}) of THF or water was dropped onto a copper grid (200 mesh) coated with carbon film. The liquid was then blotted and the sample allowed to dry at room temperature for a short time. In the case of water, the copper grid was treated with plasma for about 15 sec in order to enhance the wetting. High resolution TEM (HR-TEM) was carried out on a Philips CM20FEG TEM operated at 200 kV using lacey TEM grids.

Cryogenic Transmission Electron Microscopy (Cryo-TEM). Cryo-TEM was conducted by dropping the aqueous dilute solution on a hydrophilized lacey TEM grid, where most of the liquid was removed with blotting paper, leaving a thin film stretched over the grid holes. The specimens were shock frozen by rapid immersion into liquid ethane and cooled to approximately 90 K by liquid nitrogen in a temperature controlled freezing unit (Zeiss Cryobox, Zeiss NTS GmbH, Oberkochen, Germany). After the specimens were frozen, the remaining ethane was removed using blotting paper. The specimen was inserted into a cryo-transfer holder (CT3500, Gatan, München, Germany) and transferred to a Zeiss EM922 EF-TEM instrument operated at 200 kV.

Scanning Electron Microscopy (SEM). SEM images were taken from a high resolution scanning electron microscope (LEO 1530 FESEM) with field emission cathode. A magnification in the range from 20x to 900000x can be achieved. All samples were investigated from a silicon wafer and sputtered with platinum prior to measurement.

Molecular Characterization of the Block Copolymer. Size exclusion chromatography (SEC) with THF as eluent was performed on an apparatus equipped with PSS SDVgel columns (30 x 8 mm, 5 mm particle size) with 10^5, 10^4, 10^3, and 10^2 Å pore sizes using RI and UV detection (λ = 254 nm) at a flow rate of 1.0 mL/min. The calibration was based on polystyrene standards and toluene was used as an internal standard. Proton nuclear magnetic resonance (^{1}H-NMR) spectra were recorded on a Bruker AC-300 spectrometer at room temperature in $CDCl_3$ in order to determine the polymer composition. The molecular weight of PAMA was calculated from the number-average molecular weight, M_n, of the PS precursor obtained by THF-SEC and the ratio of characteristic NMR signals.

Composite Characterization. Powder X-ray diffraction (PXRD) measurements were performed at 25 °C on a Panalytical XPERT-PRO diffractometer in reflection mode using CuKα radiation. N_2 physisorption was conducted at 77 K on a Quantachrome Autosorb 1 instrument. Prior to the measurements, the samples were degassed at 403 K for 24 h. Calcination was done in a tube furnace. First, the sample was calcined within a nitrogen atmosphere at a heating rate of 3 K min^{-1}from 30 °C to 650 °C. The heating procedure was sectioned into three parts: from 30 °C to 300 °C (3 K min^{-1}), isotherm at 300 °C for 5 h, and then from 300 °C to 650 °C (3 K min^{-1}). The material was again calcined in air at a heating rate of 3K/min from 30 °C to 550 °C.

6-S3. SEC of $PS_{69}PAMA_{31}^{81}$ Diblock Copolymer

SEC measurements were performed to determine the molecular weight distribution of the PS precursor and the diblock copolymer. SEC was calibrated with PS standards, which allowed the precise determination of the number-average molecular weight (M_n) of the PS block. Polydispersity indices were 1.02 (PS) and 1.06 (PS_{540}-*b*-$PAMA_{200}$).

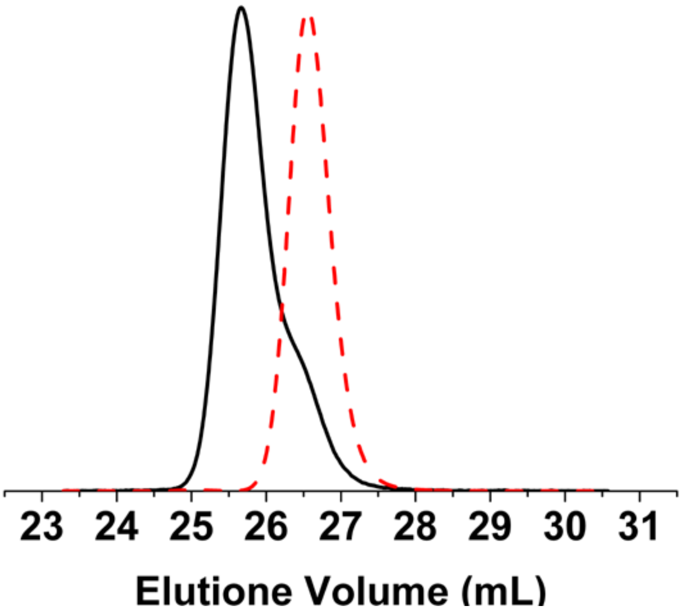

Figure 6-S1. SEC traces of PS homopolymer (**red dashed line**) and $PS_{69}PAMA_{31}^{81}$ diblock copolymer (**black solid line**).

6-S4. ^{1}H-NMR of $PS_{69}PAMA_{31}^{81}$

A ^{1}H-NMR measurement in $CDCl_3$ was performed to determine the compositions of the diblock copolymer. Knowing the M_n of the PS block from SEC, the characteristic PS peaks at around 7 ppm were compared to the characteristic signals of the PAMA block. Figure 6-S2 shows the attribution of the respective protons of the diblock copolymer. Comparison of the two allyl protons (Figure 6-S2(b)) at 5.4 ppm with the two protons at 4.5 ppm (Figure 6-S2(d)) gave a ratio of 1:1 and thus revealed that the allyl bond was indeed not affected by anionic polymerization.

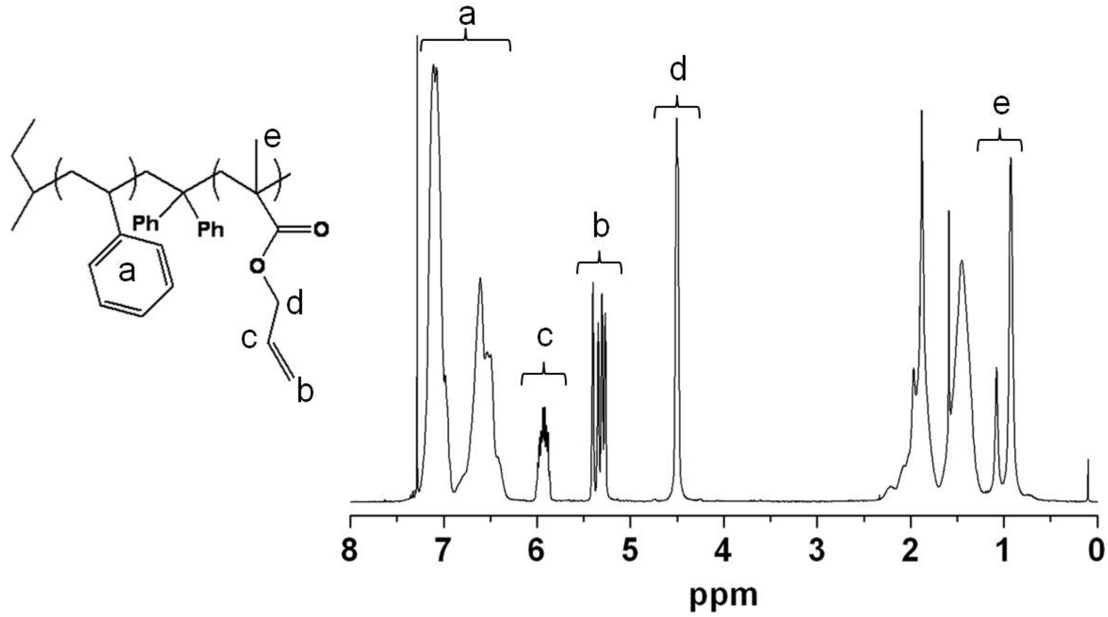

Figure 6-S2. ^{1}H-NMR spectra of diblock copolymer $PS_{69}PAMA_{31}^{81}$ in $CDCl_3$.

6-S5. Bulk Morphology

Thin cut films of non-crosslinked polymer films revealed hexagonally packed PAMA cylinders in a PS matrix. After co-casting a photo-crosslinker and crosslinking under UV light, the micrographs remained unchanged.

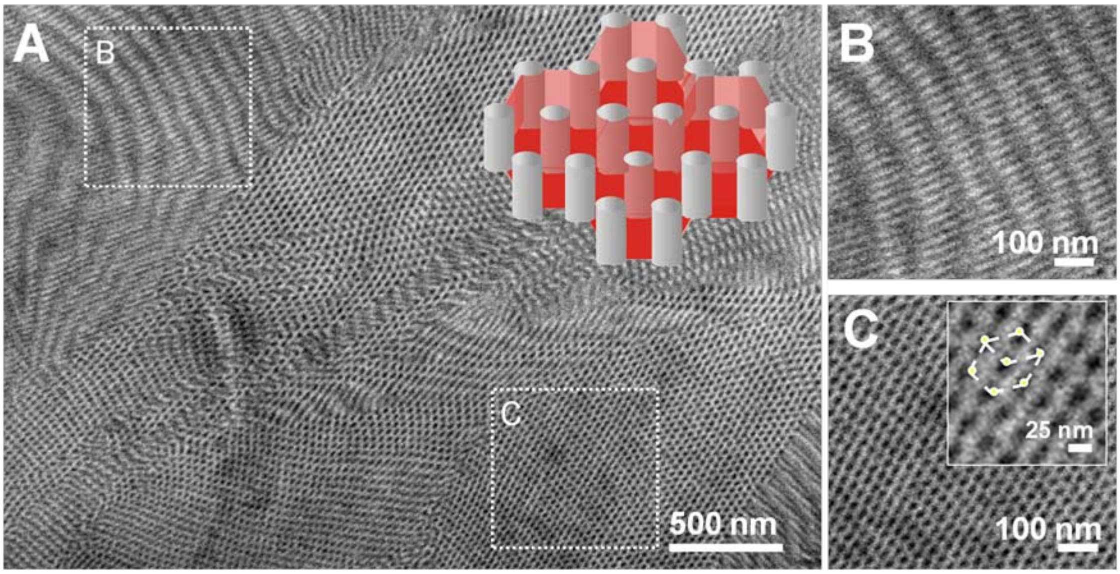

Figure 6-S3. (**A**) TEM micrograph of $PS_{69}PAMA_{31}$[81] cast film from toluene. (**B**) and (**C**) are magnifications of the insets in (**A**) and highlight the lying and standing PAMA cylinders, respectively. The double-bond containing cylinders were stained with OsO_4 to increase contrast.

6-S6. SEM of Argon Calcined Rutile Nanowires

SEM of argon calcined rutile nanowires highlights the porosity and stability of calcined rutile nanowires. The images clearly show the anisotropic shape of the rutile nanostructures (Figures 6-S4A/B). Through sample stage tilting, it was possible to further underline the intact worm-like structures (Figures 6-S4C/D).

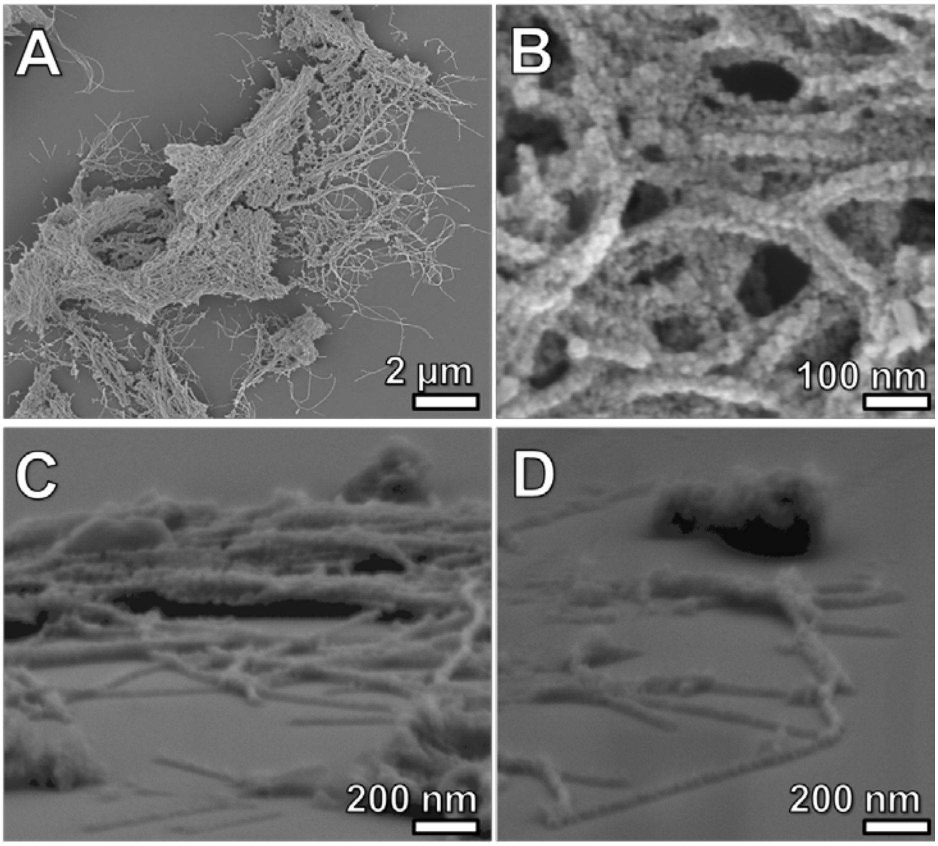

Figure 6-S4. (**A/B**) SEM images of argon calcined rutile nanostructures at different magnifications and (**C/D**) with tilted sample stage (75° angle of view).

6-S7. Thermogravimetric Analysis of Rutile Nanostructures

Thermogravimetric analysis (TGA) of rutile nanostructures revealed the inorganic TiO_2 content of the hybrid material. Calcination from 30 °C to 650 °C at a heating rate of 10 K min^{-1} and a subsequent isotherm for 2 h at 650 °C removed 51 % of organic material and only left TiO_2 behind. The composition of the hybrid materials is consequently around 50:50 in weight content.

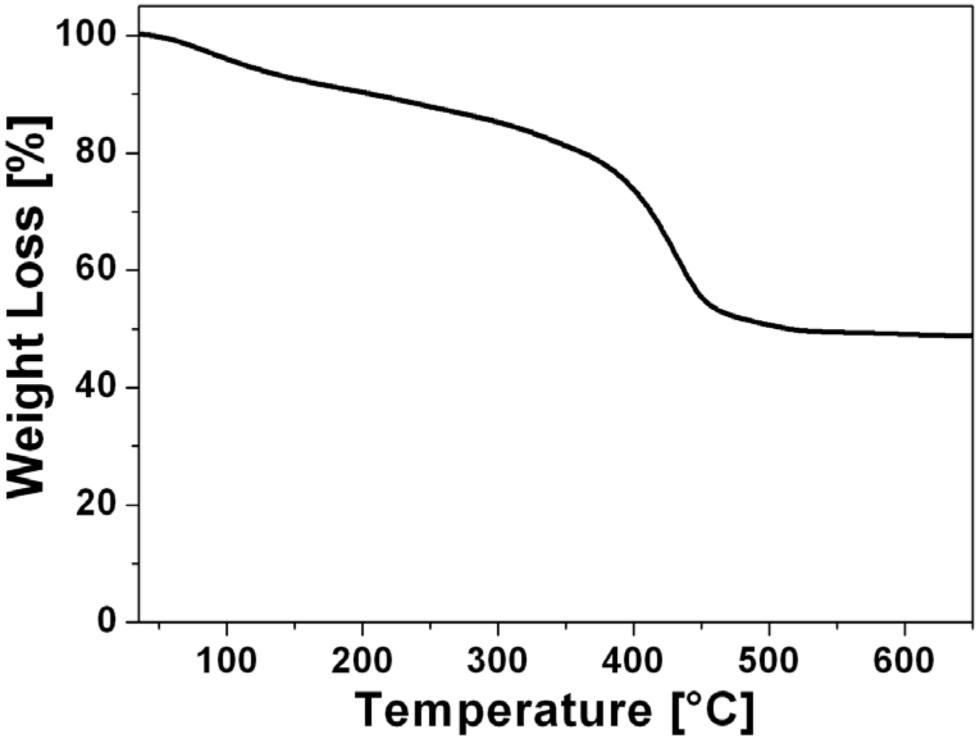

Figure 6-S5. TGA measurement of rutile nanostructures in air.

6-S8. Crystalline Anatase Nanowires from Pre-synthesized Crystalline Anatase Colloids

We also applied the colloidal route to produce crystalline anatase nanostructures. Similar to the synthesis of crystalline rutile nanocrystals, crystalline nanocolloids of anatase were successfully synthesized prior to hybrid formation. It is reported that titanium tetra(*n*-butoxide) forms anatase crystals with acetic acid.[4] Therefore, we synthesized these colloids in 2M acetic acid. Phase purity of the anatase colloids was determined by PXRD (see the black bottom curve in Figure 6-S6D). The size of anatase nanocrystals was measured by DLS in 2M HCl in order to supply sufficient surface charge. Nanocolloids with an apparent hydrodynamic diameter of around 14 nm were observed. The large signal at around 110 nm is attributed to the agglomeration of nanocolloids. As larger object scatter more light, the signal at around 100 nm is greatly enhanced in the intensity-weighted DLS plot (Figure 6-S6E).

After infiltration of the oppositely charged anatase nanocrystals into the template brush corona at pH 1, crystalline nanowires with a high aspect ratio were obtained (Figure 6-S6A). When compared to the rutile nanostructures in the main manuscript, these nanostructures look quite identical. However, these nanostructures differ in crystallinity, as it is possible to adjust the crystal structure through the infiltrated nanocrystals. Consequently, when anatase nanocolloids were used, the corresponding hybrid material consisted of crystals of the same polymorph as the nanocolloids, as can be seen and verified by PXRD (see red top curve in Figure 6-S6D). The HR-TEM micrographs in Figure 6-S6B/C show the crystal lattices of as-prepared anatase hybrid nanowires.

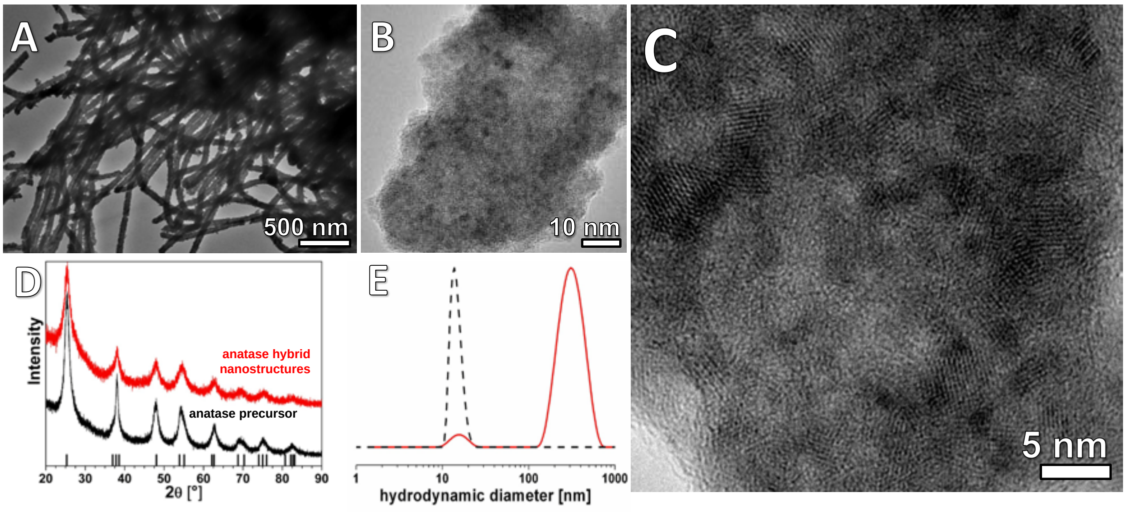

Figure 6-S6. (**A**) TEM micrograph of as-synthesized anatase hybrid nanowires. (**B**/**C**) HR-TEM micrographs of as-synthesized anatase hybrid nanowire. (**D**) PXRD pattern of anatase nanocrystals (**black bottom pattern**) and as-synthesized anatase hybrid nanostructures (**red top pattern**). The ticks on the x-axis indicate all anatase reflexes. (**E**) DLS measurement of anatase nanocrystals in 2M HCl: number-weighted plot (**black dashed line**) and unweighted plot (**red solid line**).

References

[1] F. Schacher, M. Müllner, H. Schmalz, A. H. E. Müller, *Macromol. Chem. Phys.* **2009**, *210*, 256.

[2] T. Saito, B. D. Mather, P. J. Costanzo, F. L. Beyer, T. E. Long, *Macromolecules* **2008**, *41*, 3503.

[3] R. S. Yelamanchili, Y. Lu, T. Lunkenbein, N. Miyajima, L.-T. Yan, M. Ballauff, J. Breu, *Small* **2009**, *5*, 1326.

[4] S. Li, G. Ye, G. Chen, *J. Phys. Chem. C* **2009**, *113*, 4031.

List of Publications

9. **Müllner, M.**; Lunkenbein, T.; Schieder, M.; Miyajima, N.; Breu, J.; Caruso, F.; Müller A.H.E.: Template-Directed Mild Synthesis of Anatase Nanotubes within Cylindrical Core-Shell-Corona Polymer Brushes, **2012**, to be submitted

8. **Müllner, M.**; Lunkenbein, T.; Miyajima, N.; Breu, J.; Müller A.H.E.: A Facile Polymer Templating Route Toward High Aspect Ratio Crystalline Titania Nanostructures, *Small* **2012**, accepted

7. **Müllner, M.**; Lunkenbein, T.; Breu J.; Caruso, F.; Müller A.H.E.: Template-Directed Synthesis of Silica Nanowires and Nanotubes from Cylindrical Core-Shell Polymer Brushes, *Chem. Mater.* **2012**, DOI: 10.1021/cm300312g

6. Xu, Y.; Yuan, J.; Fang, B.; Drechsler, M.; **Müllner, M.**; Bolisetty, S.; Ballauff, M.; Müller, A.H.E.: Hybrids of Magnetic Nanoparticles with Double-Hydrophilic Core/Shell Cylindrical Polymer Brushes and Their Alignment in a Magnetic Field, *Adv. Funct. Mater.* **2011**, *20*, 4182. DOI: 10.1002/adfm.201000769

5. **Müllner, M.**; Yuan, J.; Weiß, S.; Walther, A.; Förtsch, M.; Drechsler, M.; Müller, A.H.E.: Water-Soluble Organo-Silica Hybrid Nanotubes Templated by Cylindrical Polymer Brushes, *J. Am. Chem. Soc.* **2010**, *132*, 16587. DOI: 10.1021/ja107132j

4. **Müllner, M.**; Schallon, A.; Walther, A.; Freitag, R.; Müller, A.H.E.: Clickable, Biocompatible and Fluorescent Hybrid Nanoparticles for Intracellular Delivery and Optical Imaging, *Polym. Prepr. (Am. Chem. Soc., Div. Polym. Chem.)* **2010**, *51*, 630.

3. Müller, A.H.E.; Betthausen, E.; **Müllner, M.**; Schacher, F.H.; Synatschke, C.V.; Walther, A.; Wolf, A.: Self-Organized Nanostructures from New Block co- and Terpolymers, *Polym. Prepr. (Am. Chem. Soc., Div. Polym. Chem.)* **2010**, *51*, 308.

2. **Müllner, M.**; Schallon, A.; Walther, A.; Freitag, R.; Müller, A.H.E.: Clickable, Biocompatible, and Fluorescent Hybrid Nanoparticles for Intracellular Delivery and Optical Imaging, *Biomacromolecules* **2010**, *11*, 390. DOI: 10.1021/bm901099p

1. Schacher, F.H.; **Müllner, M.**; Schmalz, H.; Müller, A.H.E.: New Block Copolymers with Poly(*N*,*N*-dimethylaminoethyl methacrylate) as a Double Stimuli-Responsive Block, *Macromol. Chem. Phys.* **2009**, *210*, 256. DOI: 10.1002/macp.200800557

Acknowledgements

Working towards a PhD degree is not a path taken by a single person, but a journey with many contributors and collaborations. Therefore, I would like to thank all of the people I was fortunate to meet and work with during my thesis and time in Bayreuth.

First and foremost, I would like to thank Prof. Axel H. E. Müller. Not only was he my mentor within the graduate school, but he helped me choose polymer science as the direction I want to pursue for my future. His inspiring attitude and reputation in the field motivated me to join his department, and I am very thankful that he offered me the opportunity to undertake research within his group. I am sincerely grateful for our friendly and helpful discussions throughout my thesis and the multiple opportunities to present our research to national and international audiences at several conferences. I also want to thank Prof. Müller for allowing me to undertake research abroad. I owe him a debt of gratitude for his confidence in letting me foster my interest in chemistry by developing projects with as little control as necessary.

Special thanks also go to Prof. Josef Breu and Prof. Andreas Fery, who were my other mentors within the graduate school. I thank them for all the time spent in discussions and helping me correct my manuscripts.

I would also like to especially thank Thomas Lunkenbein who has been involved in joint projects and has helped me develop and characterize new nanomaterials.

Most of all, I have to thank the entire MC^2 crew. This group is definitely magical. I consider it the best work environment because, as André Gröschel once said, it is a “big living community”. I have enjoyed coming to work every day. The after work drinks and the many evenings spent in the coffee room or barbequing will truly make me miss the people and this place a lot. The MC^2 atmosphere made time pass quickly, but also successfully, and a lot of that is due to our helpful technical assistants who have helped me with all kinds of analytical issues. Therefore, a big thanks to Melanie Förtsch, Marietta Böhm, Annika Pfaffenberger, Annette Krökel, Dane Blasser, Sabine Wunder, Susanne Edinger and Rockser Jeannine. In addition, I thank Gaby Oliver very much for all her patience with us and for all her help with any and all administrative matters.

Many thanks also go to the present and former members of the MC^2 team, who made my time in Bayreuth remarkable and one that will always be etched in my mind. I would also like to thank many other people outside of MC^2 that I have met and worked with during my time here. So in, no particular order, thank you André Gröschel, André Pfaff, Jiayin Yuan, Andreas Hanisch, Alexander Schmalz, Sandrine Tea, Shohei Ida, Alexander (Sascha) Yakimansky, Christopher Synatschke, Joachim Schmelz, Stephan Weiß, Thomas Ruhland, Alexander Majweski, Andreas Walther, Anja Goldmann, Youyong Xu, Felix Schacher, Markus Drechsler, Eva Betthausen, Francesca Bennet, Marina Krekhova, Kerstin Küspert, Tina Löbling, Ramón Novoa-Carballal, Lourdes Pastor-Pérez, Holger

Schmalz, Andrea Wolf, Zhicheng Zheng, Markus Burkhardt, Stefan Döhler, Annika Eckardt, Bing Fang, Pierre-Eric Millard, Anuj Mittal, Karina Möller, Sergey Nosov, Daniela Pirner, Felix Plamper, Stefan Reinicke, Markus Retsch, Manuela Schumacher, Ainhoa Tolentino Chivite, Hans-Joachim Voigtländer, Markus Ruppel, Michael Witt, Marko Schmidt, Daniel Kunz, Florian Wieberger, Florian Richter, Andreas Ringk, Patrick Feicht, Martin Schieder, Katja Willinger and many more ...

I would also like to thank the undergraduate students - Christian Bartz, Fabian Pooch, Christoph Steinlein, Jasmin Schmid and Hubertus Burchhardt - who have worked on several projects with me. I have benefited from their helping hands and reliable work.

For the duration of four months, I had the opportunity to perform research at The University of Melbourne with the Department of Chemical and Biomolecular Engineering within the Nanostructured Interfaces and Materials Group. Many thanks go to Prof. Frank Caruso, Angus Johnston, Georgina Such, James Best, Sarah Dodds, Henk Dam, Jiwei Cui, Kang Liang, Philipp Senn, Blaise Tardy, Martin van Koeverden, Denison Chang, Rona Chandrawati, Yan Yan, Yajun Wang, Emma van der Gaag, Hannah Lomas, Marc Riemer, Marloes Kamphuis and Olga Shimoni. I had an incredible and memorable time in Australia and was able to gain great insights into new topics.

I thank the Bayreuth graduate school (BayNAT) for a membership within the PhD program “Polymer Science”. For financial support, I thank the Deutsche Forschungsgemeinschaft (DFG) within the Collaborative Research Center SFB 840. I am also thankful to the Bavarian State for having provided me with a scholarship through the BayEFG.

Most importantly, I thank my family, my parents, my grandparents, my brothers and my girlfriend Iva for their overwhelming support over the years. I deeply thank you for everything you did for me because otherwise I would not be where I am today. I especially thank you Iva for all your love, patience and encouragement, and apologize for all the hours of chemistry talks you had to endure ;)

Erklärung

Die vorliegende Arbeit wurde von mir selbstsändig verfasst und ich habe dabei keine anderen als die angegebenen Hilfsmittel und Quellen benutzt.

Ferner habe ich nicht versucht, anderweitig mit oder ohne Erfolg eine Dissertation einzureichen oder mich der Doktorprüfung zu unterziehen.

Bayreuth, den 01.02.2012

Markus Müllner